INEEL/EXT-01-00183
Revision 1

Dry Cask Storage Characterization Project-Phase I: CASTOR V/21 Cask Opening And Examination

W. C. Bare
L. D. Torgerson

August 2001

Idaho National Engineering and Environmental Laboratory
Bechtel BWXT Idaho, LLC

INEEL/EXT-01-00183
Revision 1

Dry Cask Storage Characterization Project – Phase 1: CASTOR V/21 Cask Opening And Examination

W. C. Bare
L. D. Torgerson

August 2001

Idaho National Engineering and Environmental Laboratory

Idaho Falls, Idaho 83415

Prepared for the
U.S. Department of Energy
Assistant Secretary
Under DOE Idaho Operations Office
Contract DE-AC07-99ID13727

ABSTRACT

This report documents visual examination and testing conducted in 1999 and early 2000 at the Idaho National Engineering and Environmental Laboratory (INEEL) on a Gesellschaft für Nuklear Service (GNS) CASTOR V/21 pressurized water reactor (PWR) spent fuel dry storage cask. The purpose of the examination and testing is to develop a technical basis for renewal of licenses and Certificates of Compliance for dry storage systems for spent nuclear fuel and high-level waste at independent spent fuel storage installation sites. The examination and testing was conducted to assess the condition of the cask internal and external surfaces, cask contents consisting of 21 Westinghouse PWR spent fuel assemblies from Dominion's (formerly named Virginia Power) Surry Power Station and cask concrete storage pad. The assemblies have been continuously stored in the CASTOR cask since 1985. Cask exterior surface and selected fuel assembly temperatures, and cask surface gamma and neutron dose rates were measured. Cask external/internal surfaces, fuel basket components including accessible weldments, fuel assembly exteriors, and primary lid seals were visually examined. Selected fuel rods were removed from one fuel assembly, visually examined, and then shipped to Argonne National Laboratory for nondestructive, destructive, and mechanical examination. Cask interior crud samples and helium cover gas samples were collected and analyzed. The results of the examination and testing indicate the concrete storage pad, CASTOR V/21 cask, and cask contents exhibited sound structural and seal integrity and that long-term storage has not caused detectable degradation of the spent fuel cladding or the release of gaseous fission products between 1985 and 1999.

CONTENTS

FIGURES

TABLES

EXECUTIVE SUMMARY

To augment the technical basis for renewals of licenses and Certificates of Compliance for dry storage systems for spent nuclear fuel and high-level waste at independent spent fuel storage installation sites, a dry cask storage system, the CASTOR-V/21, was examined and tested after it had undergone an extended period of service. This report presents the results of visual examination and testing conducted in 1999 and early 2000 on a Gesellschaft für Nuklear Service (GNS) CASTOR V/21 pressurized water reactor (PWR) spent fuel storage cask located at the Idaho National Engineering and Environmental Laboratory (INEEL). The examination and testing evaluated the condition and integrity of the exterior and interior surfaces of the CASTOR V/21 cask and its contents consisting of 21 Westinghouse 15 × 15, PWR spent fuel assemblies from Dominion's (formerly named Virginia Power) Surry Power Station) and the concrete spent fuel storage pad after a 14-year storage duration. Performance of activities was conducted under a standard order agreement between the U.S. Nuclear Regulatory Commission, Office of Nuclear Regulatory Research (NRC-RES) and the U.S. Department of Energy (DOE), Idaho Field Office, the INEEL operated by Bechtel BWXT Idaho. The project (Dry Cask Storage Characterization) was jointly funded by Nuclear Regulatory Commission-RES, Electric Power Research Institute (EPRI), DOE-Office of Civilian Radioactive Waste Management (RW), and DOE-Office of Environmental Management (EM) to examine the spent fuel and cask in dry storage at the INEEL. Examination and testing, including video and photographic scans, were performed at the INEEL Test Area North (TAN) Hot Shop facility and consisted of pretest preparations, performance testing, and post-test activities.

Pretest preparations included conducting cask-external examination, measurement of cask exterior surface temperature, extraction of helium cover gas samples and analysis, and handling and transport of the cask from the concrete storage pad to the TAN Hot Shop. Performance examination and testing included cask remote primary lid removal, remote indirect visual examination of cask internals, primary lid seals, 21 PWR spent fuel assemblies, and measurement of selected fuel assembly temperatures. Interior crud samples were taken, and cask surface gamma and neutron dose rates were measured. Selected fuel rods were removed from one fuel assembly, visually examined, and shipped to Argonne National Laboratory West for nondestructive, destructive, and mechanical examination. Post examination and test activities included examination and removal of one fuel assembly from the TAN Hot Cell and reinstallation in the CASTOR V/21, examination of the primary lid and cask sealing surfaces, installation of new primary lid seals, primary lid installation, refill of cask with fresh helium, leak testing of primary lid seals, and extraction of helium cover gas samples and analysis.

The CASTOR-V/21 PWR spent fuel storage cask consists of a nodular cast-iron body. The cast-body material was found to be in very good condition and continues to provide effective gamma shielding. The cask is 4.9 m (16 ft) high and 2.4 m (8 ft) in diameter and weighs approximately 112 tons when loaded with PWR spent fuel. Two concentric rows of polyethylene rods incorporated in the cask wall continues to provide the required level of neutron shielding. The external surface consists of heat transfer fins oriented

circumferentially around the cask surface. The fuel basket within the cask is configured to hold 21 PWR spent fuel assemblies and is constructed of stainless steel and borated stainless steel for criticality control. The Surry spent fuel assemblies are of a standard Westinghouse 15 × 15 rod design. The cask is closed with a primary lid having both elastomer and metallic O-rings to seal the cask cavity from the environment. A secondary lid, used in commercial applications, was not used in this testing program (Section 1.3.4).

Based on 1985 pretest ORIGEN2 predictions, fuel assembly decay heat generation rates totaled approximately 28 kW at the start of testing and 27 kW at the end of testing in 1985. In 1985, thirteen of the twenty-one fuel assemblies had decay heat rates near 1 kW; the remaining eight assemblies had decay heat rates of approximately 1.8 kW. The 1999 measured temperature of the exterior cask surface ranged from 103°F (39°C) to 141°F (61°C) (ambient temperature 91.2°F [32.9°C]). The hottest of selected fuel assemblies measured 309°F (154°C). This compares to 109°F (43°C) to 221°F (105°C) on the exterior cask surface, and a peak internal cask guide tube temperature of 676°F (358°C) measured in 1985 with a nitrogen backfill, with lid in place and cask in the vertical orientation (EPRI NP-4887).

Examination and Testing Findings

Based on the 1999 examination and testing results, there was no evidence of cask, shielding, or fuel rod degradation during long-term (14 years) storage that would affect cask performance or fuel integrity. There was no evidence of exterior or interior cask deterioration during storage period, nor were there any signs of seal or shielding failure. The fuel was intact, and there were no indications of any significant cladding creep or rod bow. There was some crud adherent to the rods, but no crud appears to have fallen into either the spacers or cask bottom. The crud is not a result of the fuel or cladding oxidation during dry storage, but rather the results of oxidation of steel components by the coolant in reactor operations. However, fifteen of sixteen stitch welds (Appendix B) in the triangular air channels at the perimeter of the basket were found to be cracked. These welds attached the basket borated stainless partition plates to the basket barrel. Based on the cask testing performed in 1985 (EPRI NP-4887 report), it was concluded that applicable triangular air channels were not examined back in 1985, and the defective stitch welds cracked during high temperature testing cycles and test configurations that the cask experienced during the 1985 testing campaign rather than during the long-term storage period. These welds in their current condition do not affect required cask performance parameters.

ACKNOWLEDGMENTS

The Dry Cask Storage Characterization Project personnel would like to express our appreciation to those that helped make this project successful and to those that contributed to this report.

Our thanks to Roger Kenneally, Charles Interrante, and Louise Lund of the Nuclear Regulatory Commission, Tom Brookmire of Dominion, and John Kessler and Albert Machiels from the Electric Power Research Institute for their technical guidance, reviews, and support during the performance of this project.

Our thanks to Peter Dirkmaat and David Koelsch of the U.S. Department of Energy, Idaho Operations Office, for their contributions and support of the project.

Our thanks to Bruce Hilton, Michael Billone, and Robert Einziger of the Argonne National Laboratory for their technical guidance and their assistance in shipping the Surry fuel.

Our thanks to Matthias Ebner at the Idaho National Engineering and Environmental Laboratory (INEEL) for providing technical input and preparation of this report.

Our thanks to the personnel at the INEEL Test Area North for their dedication and work performance, which allows this report to be possible. These personnel include Lyle Albertson, Jimmy Spells, Kevin Streeper, Ilene Harrell, John Cummings, John Hansen, Jake Green, and Doug Illum.

Our thanks to Jim Dobbins for his exceptional work with the design and fabrication of the equipment for boring and pulling spent fuel rods and to James Rivera for his support with camera systems that allowed the video inspections to be completed.

Our thanks to the Quality Assurance inspectors Lonnie Gilson and Jim Dowalo, to Daryl Lopez for his design efforts and to Richard Deaton and Raymond Mitchell for fabrication of needed equipment.

Our thanks to Paul Ruhter, INEEL Dosimetry, who with Rick Sorenson selected appropriate radiation monitoring and reporting methods to allow gamma/neutron assessments to be made.

We would also like to thank Tom Bridges for his support with the Transport Plan for movement of fuel rods to Argonne National Laboratory, Gary Koyama for budget support, Claude Kimball and Baird McNaught for project management efforts, Brent Satterthwaite for cask transportation support, Chris Morgan for photo and video service support, Jan Montgomery for technical editing support, and Louise Judy for text processing support.

Our thanks to Dinesh Gupta of the DOE Office of Environmental Management, and David Stahl and Joe Price of the DOE Office of Civilian Radioactive Waste Management, for their technical guidance and financial contribution to this project.

ACRONYMS

ANL-E	Argonne National Laboratory-East
ANL-W	Argonne National Laboratory-West
CASTOR	Cast Iron Cask for Storage and Transport of Radioactive Material
DOE	U.S. Department of Energy
EDS	Energy Dispersive Spectrometry
EM	Office of Environmental Management
EPRI	Electric Power Research Institute
INEEL	Idaho National Engineering and Environmental Laboratory
INTEC	Idaho Nuclear Technology and Engineering Center
LLNL	Lawrence Livermore National Laboratory
LTSM	Long-Term Storage Monitoring (Program)
NRC	U.S. Nuclear Regulatory Commission
PNNL	Pacific Northwest National Laboratory
RES	Office of Nuclear Regulatory Research
RW	Office of Civilian Radioactive Waste Management
SEM	Scanning Electron Microscope
SFB	Spent Fuel Behavior (Study)
TAN	Test Area North
TED	track etch dosimeter
TLD	thermoluminescent dosimeter

Dry Cask Storage Characterization Project—Phase 1: Cask Opening and Examination

1. INTRODUCTION

1.1 Regulations

Most nuclear power plants in the United States were not originally designed with a storage capacity for the spent fuel generated over the operating life by their reactors. Utilities originally planned for spent fuel to remain in the spent fuel pool for a few years after discharge and then to be sent to a reprocessing facility. Because reprocessing has been eliminated, and no other option for spent fuel disposition currently exists, utilities expanded the storage capacity of their spent fuel pools by using high-density storage racks. This has been a short-term solution with many utilities having reached, or soon will reach, their spent fuel pool storage capacity (Fisher and Howe 1998). Utilities have developed independent spent fuel storage installations as a means of expanding their spent fuel storage capacity on an interim basis until the geologic repository is available to accept spent fuel for permanent storage.

The U.S. Nuclear Regulatory Commission (NRC) promulgated 10 CFR Part 72 (Title 10 1999) for the independent storage of spent nuclear fuel and high-level radioactive waste outside reactor spent fuel pools. Part 72 currently limits the license term for an independent spent fuel storage installation to 20 years from the date of issuance. In preparation for possible license renewal, the NRC, Office of Nuclear Material and Safeguards, Spent Fuel Project Office is developing the technical basis for renewals of licenses and Certificates of Compliance for dry storage systems for spent nuclear fuel and high-level radioactive waste at independent spent fuel storage installation sites. These renewals would cover periods from 20 to 100 years and would require development of a technical basis for ensuring continued safe performance under the extended service conditions. An analysis of past performance of selected components of these systems is required as part of that technical basis. The components include the spent fuel and all structures, systems, and other components with functions important to safety. The safety functions, which apply for normal, off-normal, and accident conditions, are as follows: maintain subcriticality, maintain confinement, ensure that radiation rates and doses to workers and the public do not exceed acceptable levels and remain as low as reasonably achievable, maintain retrievability, and ensure heat removal as needed to meet the safety requirements.

1.2 Objectives and Scope

In the mid-1980s, the U.S. Department of Energy (DOE) procured three prototype dry storage casks for testing at the Idaho National Engineering and Environmental Laboratory (INEEL): MC-10, TN-24P, and CASTOR V/21. The primary purpose of the test was to benchmark thermal and radiological codes and to determine the thermal and radiological characteristics of the three casks. The CASTOR V/21 cask was loaded with irradiated assemblies from the Surry Nuclear Power Plant and then tested in a series of configurations using a variety of fill gases. Because the tests were not intended to be fundamental fuel behavior tests, the fuel prior to the tests had undergone only minimal characterization consisting of visual examination of the outside of the assemblies and ultrasonic examination to ensure no breached rods would be included. During the tests, the temperature at various locations was monitored, and the cover gas was periodically analyzed to determine if any leaking rods had developed. None were found. The details of these tests have been reported in a number of documents.

In 1999, a project was jointly funded by NRC-Office of Nuclear Regulatory Research (RES), Electric Power Research Institute (EPRI), DOE-Office of Civilian Radioactive Waste Management (RW), and DOE-Office of Environmental Management (EM) to examine the Surry spent fuel in dry storage at the INEEL. This project is intended to provided confirmatory data to be used by licensees submitting an

application (no later than 2004 for the first licensee) for continuing dry storage beyond 20 years and by the NRC staff in their technical licensing reviews. The objectives of the Dry Cask Storage Characterization Project are to:

1. Obtain data to confirm the predicted long-term integrity of dry storage cask systems and spent nuclear fuel under dry storage conditions

2. Provide data to augment the technical bases and criteria for evaluating the safety of spent fuel storage and transportation systems, and for extending dry cask storage licenses.

Phase 1 of the overall program involved moving the CASTORV/21 dry storage cask from the INEEL Test Area North (TAN) storage area to the INEEL TAN Hot Shop facility; extracting helium cover gas samples and analysis; obtaining temperature readings of the cask exteriors; performing a radiation survey; performing video and photographic inspection of the cask exterior and interior surfaces; examining cask primary lid seals, fuel assembly exteriors and selected fuel rods; and returning the cask to storage. The specific tasks executed in the project are as follows:

Task 1.1—Equipment: Design, fabricate, and purchase of material, equipment, and fixtures necessary to (1) move the cask; (2) remove and replace fuel assemblies; (3) remove fuel rods from one selected assembly; and (4) videotape and photograph the external and internal surfaces of the cask, fuel assemblies, and fuel rods.

Task 1.2—Procedures and Training: Develop procedures, obtain required reviews and approvals, perform needed training, and other pertinent activities associated with (1) movement of the cask, (2) removal of the designated fuel assemblies or canisters, (3) removal of fuel rods, (4) returning the fuel assemblies or canisters to the cask, and (5) returning the cask to storage.

Task 1.3—Hot Shop/Cell Rental: Use the TAN Hot Shop and Hot Cell and TAN operations oversight.

Task 1.4—Inspection of Cask and Internals: Activities include (1) temperature readings of the cask exterior; (2) radiation survey; (3) video and photographic inspections of the cask exterior and interior, seal, and storage pad; (4) video and photographic inspections of sixteen fuel assemblies in general and five assemblies in detail and twelve fuel rods selected from one fuel assembly; (5) obtain crud and smear samples; and (6) temporary storage of the fuel rods until transported to ANL for Phase 2 evaluations.

Task 1.5—Transportation: Transport the fuel rods to Argonne National Laboratory-West (ANL-W) and crud and smear samples to the Idaho Nuclear Technology and Engineering Center (INTEC) for analysis. Return the fuel rod pieces and other material (e.g., crud samples) to the TAN facilities for permanent storage.

Phase 2 of the program, to be reported by others in the future, involves nondestructive, destructive, and mechanical examinations of dry-stored spent nuclear fuel elements. This will provide quantitative and qualitative information concerning the integrity of the fuel. Examples of the type of information that will be obtained include: in situ creep; percentage of fission gas release, internal rod pressure; oxide thickness, hydride morphology and orientation, residual cladding thickness, cladding microstructure; hydrogen content; creep rates, breakaway temperature; tensile strengths; and ductility. These tasks will take place at either ANL-W or ANL-East (ANL-E). The Phase 2 task interface between TAN and ANL-W at the INEEL are activities at ANL-W associated with the transportation of the fuel rods from the TAN facilities at the INEEL to ANL-W, the fuel rod segments from ANL-W to ANL-E, and the return of the fuel rod pieces and other material from ANL-W and ANL-E to the TAN facilities for storage.

1.3 CASTOR-V/21 Cask Description

1.3.1 Cask Body

The cask body is a one piece cylindrical structure composed of ductile cast iron in nodular graphite form. This material exhibits good strength and ductility, as well as providing effective gamma shielding. The overall external dimensions of the cask body are 4886 mm (16 ft) high and 2385 mm (8 ft) in diameter (Figure 1-1). The external surface has 73 heat transfer fins that run circumferentially around the cask and is coated with epoxy paint for corrosion protection and ease of decontamination.

The cask body wall, excluding fins, is 380 mm (15 in.) thick. Incorporated within the wall of the body are polyethylene moderator rods to provide neutron shielding. Two concentric rows of these 60-mm (2.3-in.) nominal diameter rods are distributed around the cask perimeter (Figure 1-2). Two lifting trunnions are bolted on each end of the cask body.

The diameter of the inner cavity is 1527 mm (5 ft), and the overall inner cavity length is 4152 mm (163 in.). Precision-machined surfaces are provided at the open end of the cask cavity for positive gasket sealing, and bolt holes are included at these locations to secure the two cask lids. The interior cavity surfaces, including sealing surfaces, have a galvanic-applied nickel plating.

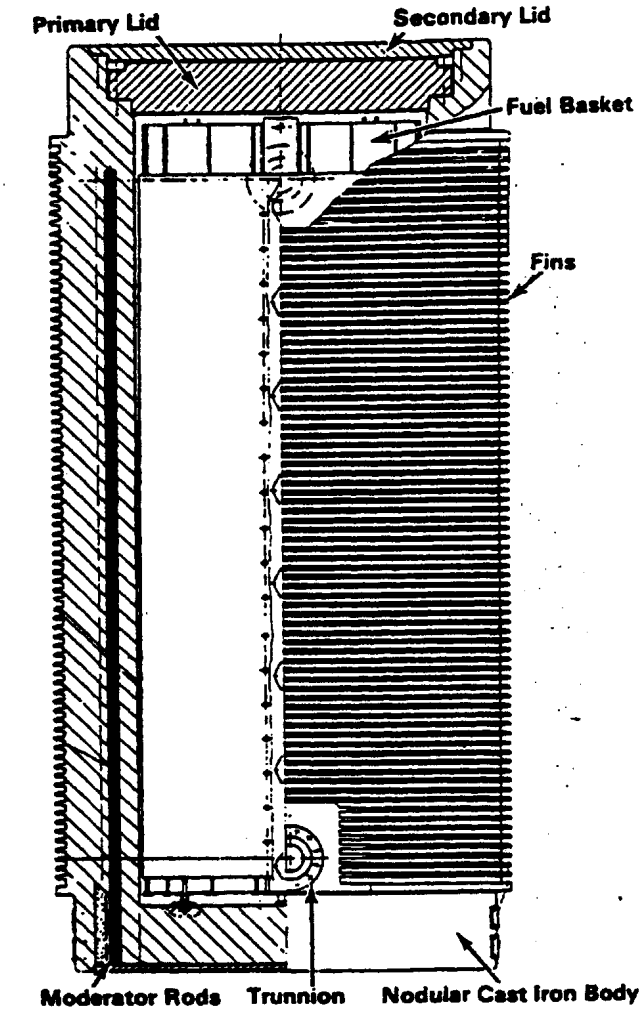

Figure 1-1. CASTOR-V/21 PWR spent fuel storage cask. (From EPRI NP-4887. Permission to use this copyrighted material is granted by EPRI.)

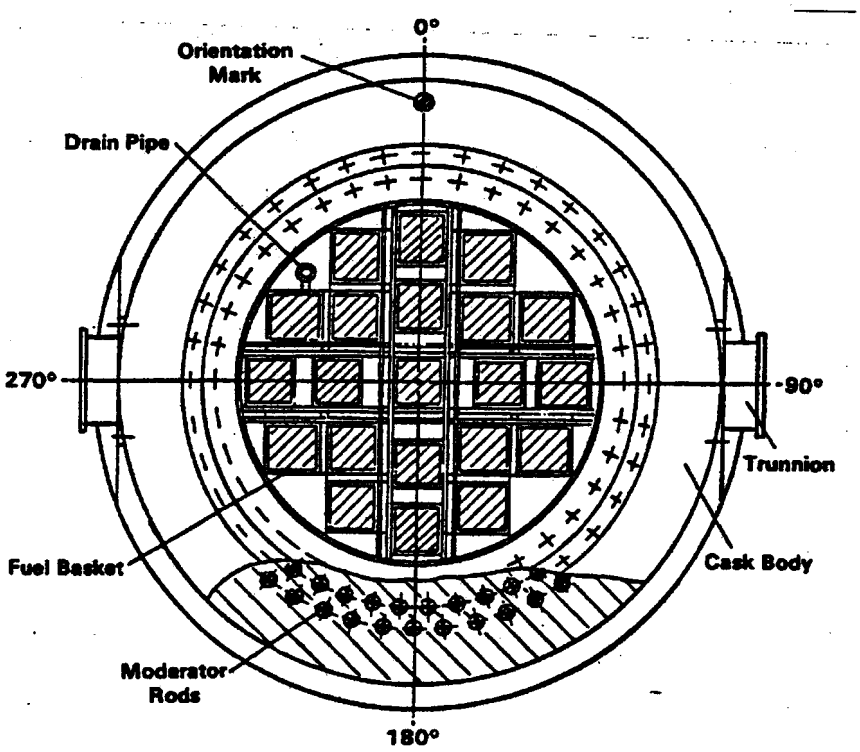

Figure 1-2. CASTOR-V/21 cask cross section. (From EPRI NP-4887. Permission to use this copyrighted material is granted by EPRI.)

1.3.2 Spent Fuel Basket

The spent fuel basket (Figure 1-2) is a cylindrical structure of welded stainless steel plate and borated stainless steel plate, having a boron content of approximately 1% for criticality control. The basket comprises an array of 21 square fuel tubes/channels that provide structural support and positive positioning of the fuel assemblies. The basket overall height is 4110 mm (13.5 ft) including the four 130-mm-diameter (5-in.) pedestals that support the basket and fuel weight on the bottom of the cask cavity. The basket outside diameter of 1524 mm (5 ft) fits tightly in the cask cavity inner diameter of 1527 mm (5 ft). The depth of each fuel tube is 4050 mm (13.3 ft). A spacing of 74 mm (3 in.) is present between the top of the basket cavity and the underside of the primary lid, thus accommodating a fuel assembly length of 4124 mm (162 in.) and supporting convection heat transfer. The final assembly results in a clearance of approximately 60 mm (2.3 in.) between the top of the fuel assemblies and the bottom of the primary lid, for a reference fuel assembly of 4064 mm (160 in.).

The basket layout results in inter-fuel tube spaces that act as flux traps for criticality control and channels to support free convection heat transfer. The basket design ensures a subcritical configuration under worst-case conditions, and the basket structure physically protects the fuel under normal and accident conditions.

A pipe with an inner diameter of 42 mm (1.6 in.) and a lead-in funnel at the top are welded to the side of a fuel tube near the outer circumference of the basket. The pipe location corresponds to a penetration in the primary lid and the low side of the slope in the cask cavity bottom. The pipe provides a path for a flanged pipe used to fill and drain the cask.

1.3.3 Primary Lid

A stainless steel primary lid, 1785 mm (6 ft) in diameter and 290 mm (12 in.) thick, is provided (Figure 1-3). Forty-four bolt holes are machined near the lid perimeter to secure the lid to the cask body. Two grooves machined around the lid underside, inside the bolt circle, are provided for O-ring seals (Figure 1-4). The inner groove accepts a metal "C" shaped O-ring, which serves as the first barrier between stored fuel and the environment. The outer grove accepts an elastomer O-ring. A 10-mm-diameter (0.4-in.) penetration through the lid provides access to the annulus between the two seals to perform post-assembly leak testing. This penetration is plugged when not in use.

Three penetrations through the lid are provided for various cask operations. A 35-mm-diameter (1.4-in.) straight-through penetration is used for water fill/drain operations. This penetration is located near the perimeter of the lid and is normally sealed with two flanges equipped with elastomer O-rings. This location corresponds to the pipe attached to the fuel basket. The other two penetrations, spaced next to each other and covered by a single flange, are also located near the lid perimeter, but 180 degrees from the fill/drain penetration. The through-lid penetration at this location is equipped with a quick-disconnect fitting used for vacuum drying and backfilling with gas. The second penetration at this location leads to the lower edge of the lid. Although not needed for the CASTOR-V/21, this penetration could be used for leak-testing an optional third lid gasket. This penetration is sealed by a gasketed seal plug in addition to the top cover flange.

The primary lid used during 1985 testing was not a standard lid and has 10 additional penetrations for fuel assembly guide tube instrumentation (thermocouple [TC] lances). The pattern of the 10 fuel assembly instrumentation penetrations was selected to measure radial temperature profiles across the basket in the spent fuel assemblies.

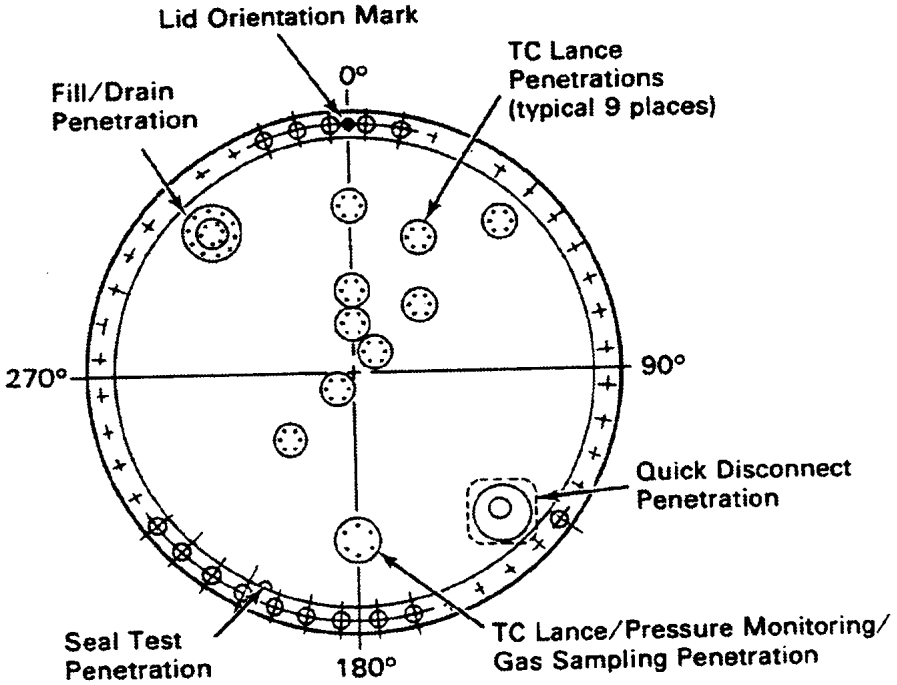

Figure 1-3. CASTOR V/21 primary lid. (From EPRI NP-4887. Permission to use this copyrighted material is granted by EPRI.)

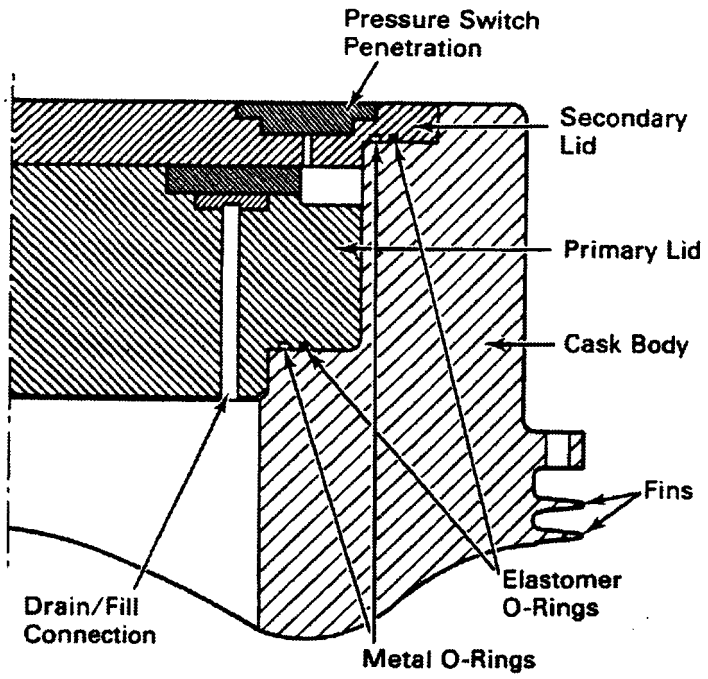

Figure 1-4. CASTOR V/21 cask lid system. (From EPRI NP-4887. Permission to use this copyrighted material is granted by EPRI.)

1.3.4 Secondary Lid

The Secondary Lid, used in commercial application, was not used during the 1985 CASTOR V/21 cask performance test or the long term storage monitoring program conducted during 1994 through 1999, because of interference with fuel assembly instrument leads and the repeated removal and handling of the secondary lid for gas sampling activities. The following functional description of the Secondary Lid is provided for completeness. The stainless steel secondary lid is 2007 mm (79 in.) in diameter and 90 mm (3.5 in.) thick (Figure 1-4). Forty-eight bolt holes are machined near the lid perimeter to secure the lid to the cask body. Two concentric grooves located inside the bolt circle on the underside are provided for a metal O-ring/elastomer O-ring sealing system of the same design as that used on the primary lid. Three normally sealed penetrations are provided for various cask operations (Figure 1-4). A 10-mm-diameter (0.4-in.) penetration through the lid provides access to the annulus between the two seals for post-assembly seal testing. A gasketed seal plug is used to close this penetration.

A second penetration is equipped with a quick-disconnect fitting, which is used for vacuum drying and gas backfilling of the primary/secondary inter-lid space. A 130-mm-diameter (5-in.) cover plate and gasket secured by six 12-mm (0.5-in.) bolts is in place when this penetration is not used. The third penetration provides a pressure sensing port between the inner-lid space and a pressure switch mounted in the secondary lid. The pressure switch is the primary component of the cask seal monitoring system. Due to the secondary lid not being used dose rates discussed in Section 3 were obtained on the primary lid exterior surface. Addition of the secondary lid will greatly reduce measured gamma dose rate values.

2. INSPECTIONS AND TESTS

The following inspections and tests are described in this section:

- Long-term surveillance of the concrete pad upon which the casks rest. Objective: look for any degradation of the concrete pad.
- Cask exterior visual inspection. Objective: look for any visual indications of degradation.
- Cask lid bolts. Objective: look for degradation such as rust.
- Cask lid seals. Objective: look for signs of corrosion, wear, or scoring of the seals that may lead to loss of the pressure boundary.
- Cask interior and basket inspections. Objectives: look for signs of corrosion, presence of crud spalled from fuel assemblies; gouging; and integrity of basket welds.
- Fuel assembly visual inspections. Objectives: look for signs of additional corrosion or other cladding degradation; determine if assemblies have bowed or otherwise corroded that may cause difficulty removing the assemblies from the cask.

2.1 Long-Term Spent Fuel Storage Pad

2.1.1 Description of Pad

Facilities were constructed in 1985 directly to the west of TAN-607, adjacent to the rail track that exits the TAN Hot Shop, for the long-term surveillance of several dry storage casks. The facilities consisted of a concrete pad for the dry storage casks and a data acquisition building. The facilities originally include a weather station that was part of the 1985 thermal testing program and was removed from service between 1990 and 1991.

The concrete pad was designed to hold several spent fuel storage casks (Figure 2-1). Analysis for pad loading show that the concrete slab can support the weight of ten 102,454 kilograms (225,400-pound) casks arranged in two rows and spaced 1.52 meters (5 ft) apart and located 1.52 meters (5 ft) from the edge of the slab. The size of the pad is approximately 28.7 m (94 ft 4 in.) long by 12.1 m (39 ft 8 in.) wide. The pad consists of 0.61-m (2-ft) thickness of concrete on top of a minimum of 30 cm (12 in.) of compacted subbase of pit run gravel. The concrete was reinforced with two mats of #6 steel reinforcement bar spaced 18 cm (7 in.) on center (each way); the mats were each embedded 10 cm (4 in.) below and above the top and bottom surfaces of the pad, respectively. The concrete was covered and kept wet during the first 7 days of the curing period to ensure maximum strength and durability. The design strength of the concrete was 28 MPa (4000 psi); the 28-day post-cure compression strength averaged 30 MPa (4400 psi).

Although it was designed to hold several storage casks, the pad held four dry storage casks, including the CASTOR V/21. The CASTOR V/21 cask was located approximately 13.9 m (45 ft 6 in.) from the west edge and 4.3 m (14 ft) from the north edge of the pad (Figure 2-1).

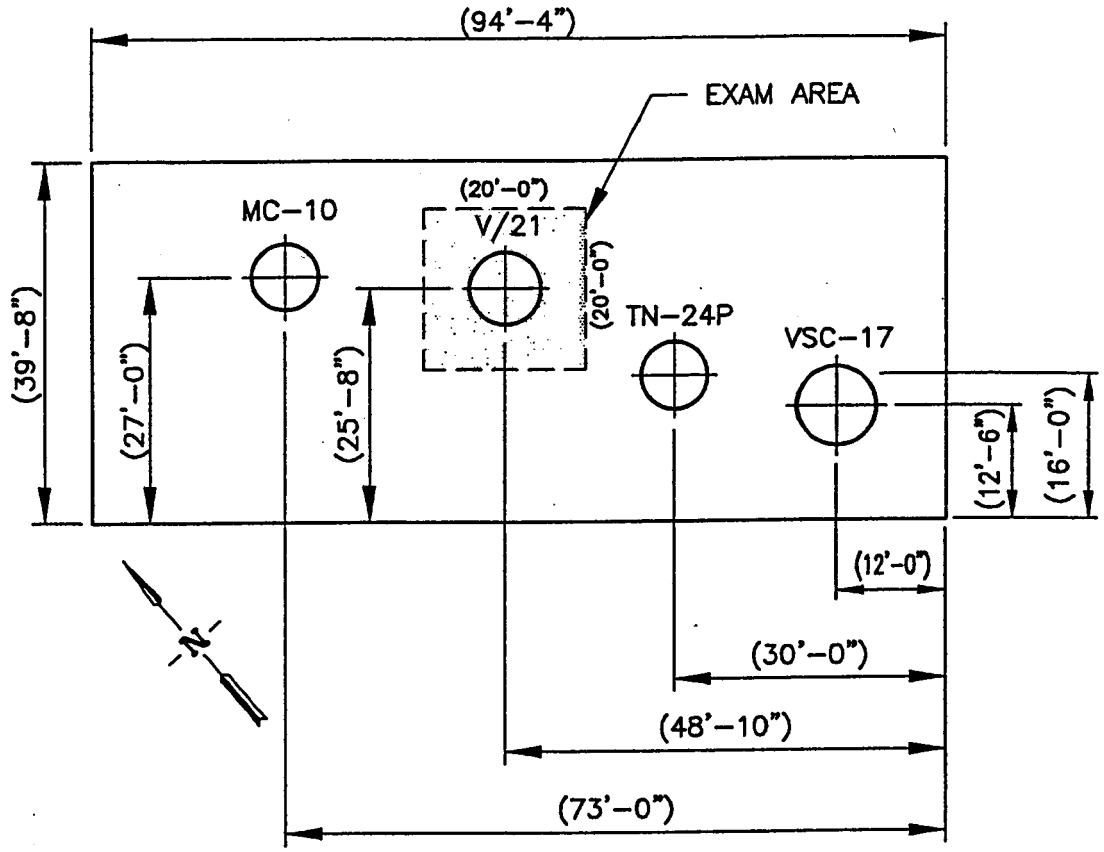

V/21
96"Ø O.D.
LOADED WEIGHT: 225, 419 LB
FULLY LOADED WITH 21
WESTINGHOUSE PWR 15X15
INTACT FUEL ASSEMBLES

TN–24P
90"Ø O.D.
LOADED WEIGHT: 177, 728 LB
PARTIALLY LOADED WITH 7
CONSOLIDATION FUEL CANISTERS
EACH CONTAINING THE RODS
FROM 2 WESTINGHOUSE PWR
FUEL ASSEMBLES 15X15
24 SPACES AVAILABLE IN CASK

MC–10
88"Ø O.D.
LOADED WEIGHT: 214, 102 LB
PARTIALLY LOADED WITH 18
WESTINGHOUSE PWR 15X15
INTACT FUEL ASSEMBLES
CASK WILL HOLD 24

VSC–17
105"Ø O.D.
LOADED WEIGHT: 210, 926 LB
FULLY LOADED WITH 17
CONSOLIDATION FUEL CANISTERS
EACH CONTAINING THE RODS
FROM 2 WESTINGHOUSE PWR
FUEL ASSEMBLES 15X15

Figure 2-1. Location of fuel storage casks on spent fuel storage pad TAN/TSF-791.

2.1.2 Pad Inspection

The evaluation of the integrity of the 15-year-old storage pad consisted of the testing of the structural soundness of the surface of the concrete and a visual assessment of the physical condition of the concrete surface, particularly at and immediately around the cask location.

The structural soundness of the concrete was determined by ASTM test standard C805-94 (Test Method for Rebound Number of Hardened Concrete, also known as the Swiss hammer test). The Swiss hammer test was performed on the concrete surface in 9 places in a 37.2 m (122 ft) area centered on the placement of the CASTOR V/21 cask, of which 5 places were selected in the area under the cask. The nine test results (Figure 2-2), which ranged from 28 MPa (4050 psi) to 41 MPa (5900 psi), averaged at 33 MPa (4800 psi) and demonstrated that the structural integrity of the concrete pad still meets or exceeds the 28 MPa (4050 psi) design strength of the concrete.

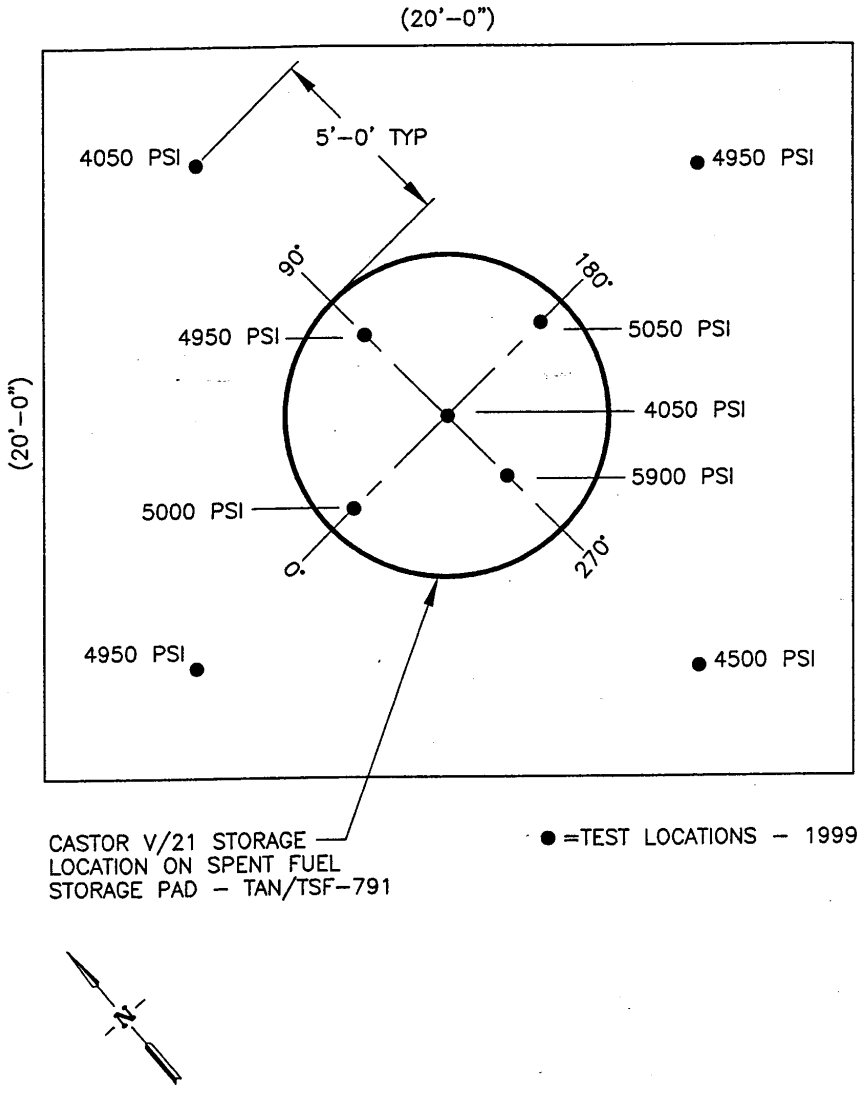

Figure 2-2. Rebound hammer test locations at CASTOR V/21 storage pad location.

The pad was also visually inspected for evidence of degradation and structural failure. The surface of the whole pad did not exhibit any evidence of structural failure of the concrete, such as open cracks or cracks with displacements in elevation of the surface. The surface of the concrete did not exhibit any evidence of spallation of the surface, exposed aggregate, or aggregate pop-out from the surface. The surface was solid and exhibited only minor wear and environmental weathering, well within the extent of weathering expected for the cold and windy climate of Idaho. The broom-finished unpainted surface exhibited only a network of faint, fine surface shrinkage cracks (Figure 2-3), less than 0.8 mm (1/32 in.) wide and of superficial depth, and a few rust stains under the cask from lightly rusted bolts on the cask. Similar cracks were prevalent across the entire surface of the pad, and were not associated with the cask locations. Tests with a straight taught line across the 6.1 m × 6.1 m (20 × 20 ft) grid indicated that there was no sag or vertical displacement in the concrete associated with the crack network; measurements with a straight edge and the taught line indicated only localized variations in the elevation of the concrete that were less than 3.2 mm (1/8 in.). The localized variations in elevation were not associated with the location of the cask and were most likely an artifact of the screeding and finishing when the concrete was originally poured.

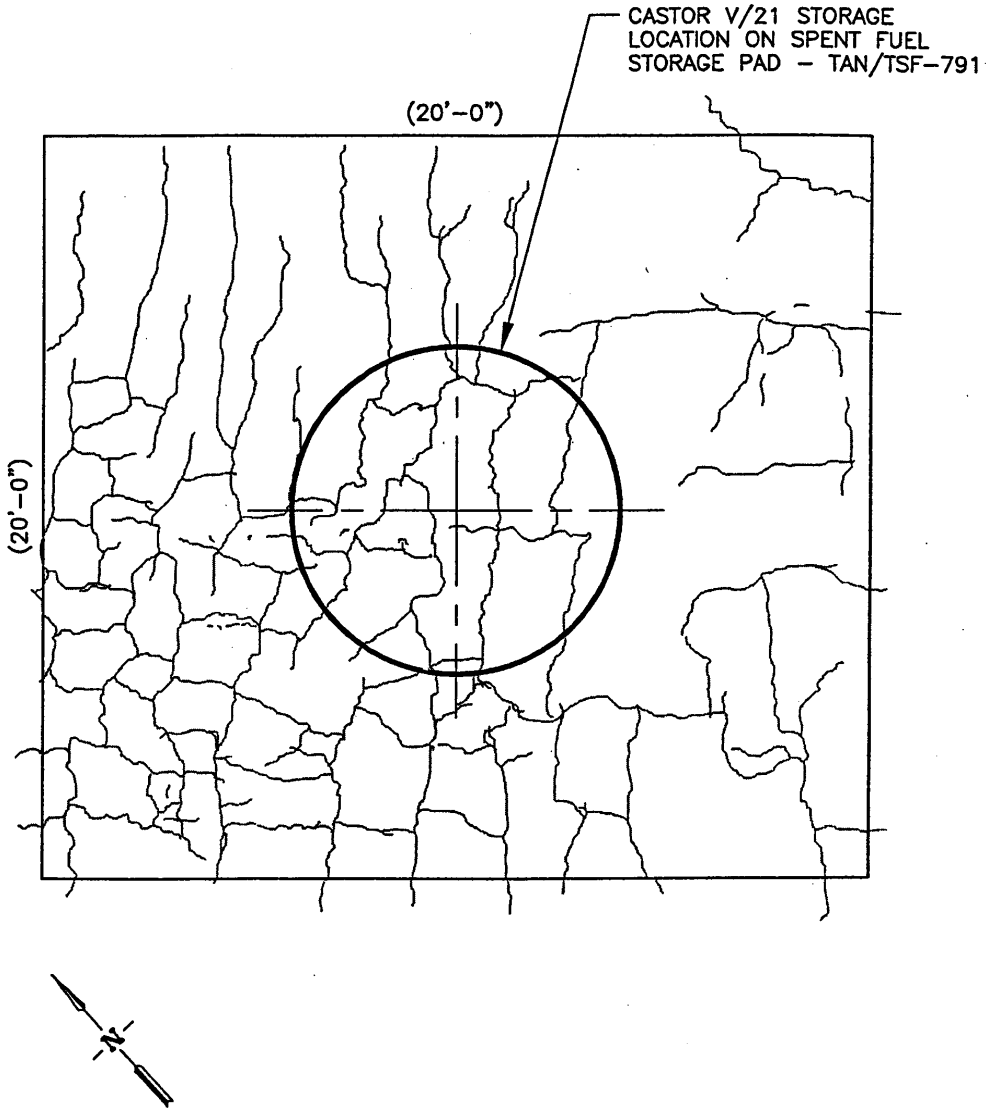

Figure 2-3. Shrink crack indication of CASTOR V/21 concrete pad storage area.

2.2 Cask Exterior

The cask exterior (Figure 1-1) consists of the cask cooling fins painted with epoxy paint, upper and lower exposed portions of the cask body painted with epoxy paint, upper and lower lifting trunnions, bottom cover plate, and an auxiliary top weather cover. These items have been exposed to all seasonal outside weather conditions for the past 14 years. The Primary Lid (Figure 1-4) was protected by the auxiliary top weather cover from weather conditions.

The entire cask exterior surface of items described above were video examined and supplemented by direct visual examination for any evidence of degradation. The resolution and color rendition of the cam recorder was checked with a resolution chart (with alphabet characters ranging in height from 0.063 in. to 0.10 in.) and a Kodak color resolution chart. The observed conditions are:

- The cask cooling fins contained small superficial corroded areas where the epoxy paint had been chipped and peeled due to possible combination of improper mixing or application of paint, or interface with cask handling equipment. At two separate fin locations on the outside fin edge were gouged as a result of cask movement activities. The operational performance or structural integrity of the fins are not impacted by the gouges.

- The upper and lower exposed portions of the cask body and upper and lower lifting trunnions and bolts contained minor superficial rust areas resulting from exposure to outside weather conditions and contact with dissimilar metals and cask handling equipment.

- The cask bottom cover plate that interfaces with the concrete spent fuel storage pad during storage contained minor discoloration from exposure to rain and snow water, surface scratches from cask movement activities, superficial rust areas around the circumference of the cover plate, and cask body interface. There was evidence of heavy corrosion deposits on one of the plate recessed attachment bolts at the cask 180-degree position as shown in Figure 2-4. Removal of the corrosion deposits from the affected area supplemented with visual examination showed bolt head pitting and surface irregularities as presented in Figure 2-5. Based on the condition and function of the bolt, the bolt and surrounding area was coated with moisture resistant sealant and retained for service. The cause of the heavy corrosion deposits appeared to be from long-term exposure to moisture resulting from wet weather conditions and condensation possibly being generated on the top side of the cover plate and resulting excess water passing through the bolt thread path.

The primary lid was removed using an overhead crane. The operation was sensitive because of the tight clearance between the lid and the cask. The torque values on the bolts were not recorded during their removal.

2.3 Cask Lid Bolts

The cask is sealed by the inner primary lid. The outer secondary lid was not installed or used during the long-term storage monitoring program for reasons described in Section 2.2. The primary lid is secured with 44 bolts. The 44 bolts of the primary lid were individually inspected visually for their physical condition, specifically for evidence of cracks, pitting corrosion, general corrosion, thread damage, and any discoloration. The exposed portion of the bolt heads of the 44 bolts were examined prior to removal and the entire bolt surface after removal. Included in the examination was the exposed portion of the primary lid penetration flange bolts.

All bolts were in satisfactory condition. The exposed portion of all bolt heads were found to be in very good condition. None of the primary lid bolts as shown in Figures 2-6 and 2-7 had any indications of

Figure 2-4. Cask bottom cover plate bolt corrosion.

Figure 2-5. Cask bottom cover plate bolt after corrosion removal.

Figure 2-6. Typical cask primary lid bolt after removal.

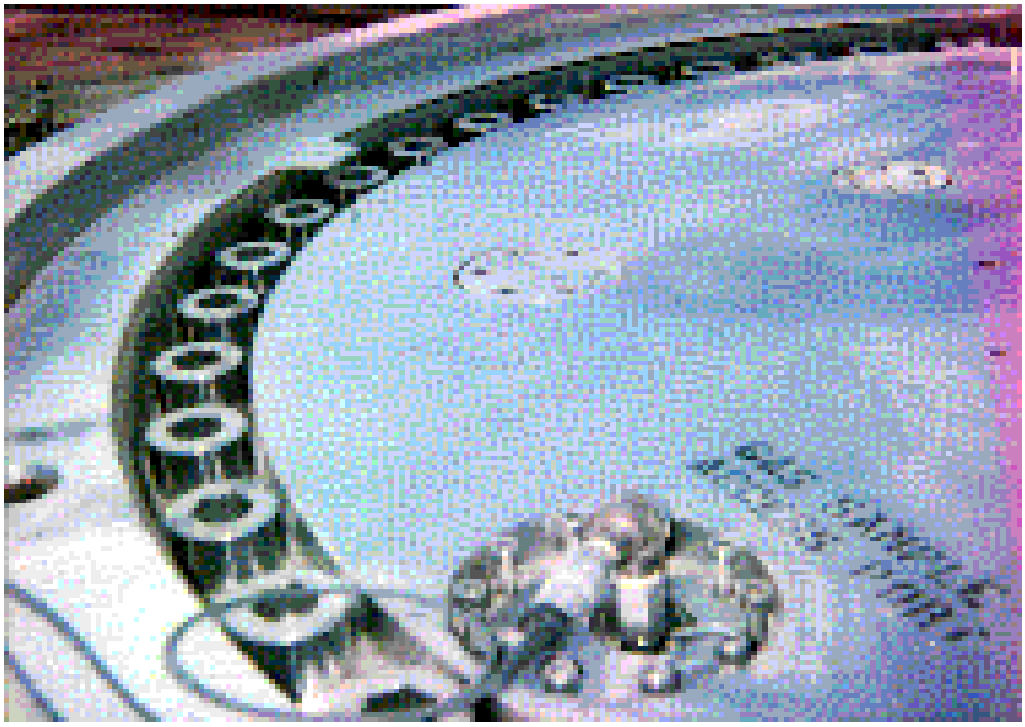

Figure 2-7. Cask primary lid bolts prior to removal.

pitting or general corrosion, cracks, thread damage, discoloration, or any defects or indications of potential failure. All bolts had a deposit of graphitic thread lubrication over the threaded area of the shaft. Nine of the bolts also had a residue of a light gray/white material on the threads that resembled tape residue, and a residue of a red compound, probably a thread compound.

The lid was removed using an overhead crane. The operation was sensitive because of the tight clearance between the lid and the cask. The procedure for opening the V/21 cask was checked and torque values on the bolts were not recorded for opening the cask.

2.4 Cask Lid Seals

The CASTOR V/21 primary lid is sealed by a metal and an elastomer O-ring housed in separate O-ring grooves. The O-rings of the primary lid were inspected immediately after opening of the cask and after replacement of the O-rings. The objectives of the inspection were to evaluate the condition of the seals for potential degradation due to:

- Oxidation of the elastomer and metal seals; thermal degradation of the elastomer seal
- Embrittlement or hardening, including cracking, crazing, and evidence of loss of elasticity or ductility
- Physical damage to the seals, such as scratches across the seal surfaces, dents, and seal deformation.

2.4.1 Description of the Seals

The metal O-ring seals are, 1600 mm (5.25 ft) outside diameter × 1580.2 mm (5.19 ft) inside diameter× 9.9 mm (0.39 in.) cross section diameter, Helicoflex type HN 200, manufactured from the following materials:

- Outside lining: aluminum
- Inside lining: 304 L or 316 L stainless steel
- Spring: Nimonic or Inconel.

The elastomer O-ring seals are, 1580 mm (5.19 ft) outside diameter × 1560.2 mm (5.12 ft) inside diameter × 9.9 mm (0.39 in.) cross section diameter, EPDM type 50049-2.2, supplied by the Helicoflex Company, Columbia, SC

2.5 Remote Inspection

The O-rings of the primary lid were inspected by remote video camera immediately after the opening of the cask and by direct visual examination after replacement of the O-rings prior to resealing the cask. The initial remote camera inspection occurred on September 8, 1999, when the primary lid was first opened. The O-rings on the primary lid were reinspected by remote camera on September 20, 1999. Obviously, the remote camera inspection of the seals (before removal from lid) permitted the inspection only of the compression surface contacting the cask, rather than the whole surface of the seal. The remote inspection used three video cameras mounted on work stand (work platform) at 120 degree intervals around the top perimeter of the cask.

The resolution and color rendition of the cameras were checked daily with a resolution chart (with alphabet characters ranging in height from 0.063 in. to 0.10 in.) and a Kodak color resolution chart. The magnification and resolution of the remote cameras were sufficient to discern fine defects; in the initial inspection immediately upon opening the cask, we were able to identify clearly a long fine hair (presumably human hair) that was looped across the two O-rings of the primary lid. The O-rings were also inspected by direct visual examination on March 28, 2000, after they were removed from the primary lid for a complete examination of the whole surface of the seals.

The O-rings in the primary lid were in excellent condition. The remote visual inspection immediately upon opening the cask and removal of the primary lid indicated that the elastomer and the metal O-rings were free of breaks, cracks, crazing, delamination, pull-outs, oxidation, or other evidence of degradation of the O-rings.

The compression area of each seal was in excellent condition with no visible damage to the seating (compression) area of the O-ring seal. The only defect that was visible by remote camera was an imperfect splice joint in the elastomer O-ring. The compression sealing area of the metal O-ring was quite reflective, glinting in the natural illumination in the hot shop and indicating that no corrosion or excessive oxidation had occurred. The compression area of the metal O-ring was textured due to the impression of the machining marks from the mating metal seal surface of the cask body. The metal compression surface did not show any evidence of breaks, scratches, dents, distortion, or corrosion.

The O-rings, particularly the elastomer, did exhibit random, crisply delineated patches of light surface discoloration, which appeared gray against the black color of the elastomer. These patches were often associated with similar areas of light discoloration on the metal flange of the lid, especially in the bolt circle area of the flange. In several areas on the bolt circle of the lid flange, the discoloration patches formed particularly thick surface films and had partially peeled. From the peeled sections, it was obvious that the discolored areas were polymeric films and most likely are deposits of excess antigalling and antiseize compounds used on the lid bolts. Slight amounts of the antiseize compound were also evident on the land of the flange between the two O-ring grooves. The compound may be responsible for the random particles of “dirt” on the sides and a few dark discolorations or “smudges” on the metal O-ring compression surface.

The discolorations on the compression surface of the metal O-ring were usually associated with similar gray discoloration on the elastomer seal and with deposits/films of material on the metal flange of the bolt circle. It seems possible that excess fluid antiseize compound may have run off the lid bolts onto the solid sealing surface of the cask body and wicked onto the elastomer and the metal O-rings before the bolts and the lid were torqued down.

The O-rings were reinspected by remote video approximately two weeks after the initial inspection. In the interim, the primary lid was removed and replaced daily (without bolting) on the cask as part of the fuel and cask inspection process. On the second remote inspection, the condition of the O-rings was unchanged, except that the metal O-ring exhibited a few pin-point indentations. The indentations were typically less than 1 mm (0.04 in.) in dimension in the compression area of the seal. Quite likely these pin-point indentations were the consequence of small amounts of grit on the cask body seal surface, deposited there by the seal protector or by air currents. A swab collected a small but visible amount of grime from the seal surface on the cask body.

The precision-machined seal seat of the cask body was in excellent condition. The surface of the seat was clean, brightly reflective, and free of corrosion, scratches, cracks, dents, or other forms of degradation that could affect the quality of the seal. However, the surface was lightly coated with a thin film whose optical density varied and seemed to be associated with patches of excess thread lubricant in the bolt circle area. Except for occasional small dense spots, the film was generally faint and difficult to

define. However, two continuous, concentric bright circular lines were discernable on the seal seat, equivalent to the imprint of the O-ring seals, where the film was absent.

2.5.1 Direct Visual Inspection

Finally, the O-ring seals were examined by direct visual inspection after they were replaced with new O-rings prior to resealing the cask. The whole surface of the seals, including the edges, was examined.

The elastomer was still firmly resilient in consistency, flexible, and limber, with no evidence of embrittlement, stiffness, or depolymerization. Bending, pulling, twisting, and coiling the elastomer into a 30 cm (12 in.) diameter coil did not cause fracture or stress failure. There was no physical evidence of delamination or pullout of material, spallation, or chalking. The black elastomer surface exhibited a satin matte sheen and was free of breaks, cuts, scratches, cracks, or craze defects. There was no evidence of oxidation or physical degradation of the elastomer. The crushed dimensional configuration taken along a segment of the elastomer O-ring after removal (14 years of service) is presented in Figure 2-8.

The elastomer O-ring was fabricated with a 45-degree scarf splice joint. As was noted in the remote camera inspections, the splice joint was slightly misaligned and partially open; the glue did not completely fill the gaps in the joint as shown in the Figures 2-9 and 2-10. However, the joint still had good strength and could not be pulled apart manually.

The elastomer exhibited numerous sharply defined gray patches on all surfaces. These patches were not associated with surface relief or differences in flexibility, resiliency, or firmness of the polymer and had a graphitic sheen, suggesting that they are probably caused by excess antiseize lubricant that was used on the lid bolts. These graphitic patches were much more numerous on the back side of the elastomer, which contacted the seat of the O-ring groove in the lid, suggesting that the antiseize lubricant was used as an aid to hold the seal in place during lid assembly.

The metal O-ring was also in good condition and was still ductile, as indicated by a few slight kinks, bends, and fresh surface scratches imparted by handling during removal from the lid. The metal showed no evidence of gross embrittlement such as cracks either in the body of the seal or at the handling defects. In general, the metal surface exhibited a metallic luster and showed no evidence of corrosion or extensive oxidation. The flattened contact surfaces bore the imprint of the machine marks of the O-ring groove and the mating seal surface of the cask body. The crushed dimensional configuration taken along a segment of the metal O-ring after removal (14 years of service) is presented in Figure 2-11.

The top surface of the metal O-ring, which was in contact with the seat of the O-ring groove, did not have any defects except for a few fresh (unoxidized) shallow scratches that have been attributed to handling damage during removal from the lid. The bottom surface as shown in Figure 2-12, which was in contact with the seal surface of the cask body, exhibited approximately 20 small pin-point indentations into the surface. The indentations were typically less than 1 mm (0.04 in.)in lateral dimension and did not appear to puncture the thickness of the metal O-ring. Because these were not spotted in the initial remote camera inspection, these features are being attributed to compression damage from environmental grit on the seal surface of the cask body. The grit was probably transfer from the bottom of the seal protector to the seal area during the fuel examination operations.

2.5.2 Observations and Results

On the metal seal there was observed:

- Several pinpoint indentations, some on sealing surface; typically <0.5 mm dia, probably <0.5 mm deep

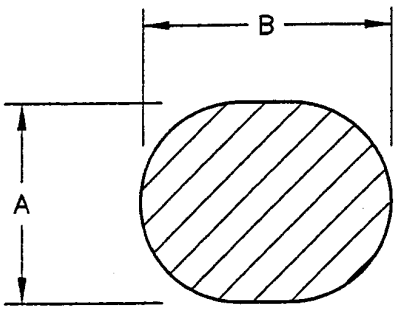

LOC.	DIMENSION A MEAS.	DIMENSION B MEAS.
2"	0.336"	0.427"
4"	0.338"	0.422"
6"	0.337"	0.423"
8"	0.340"	0.421"
10"	0.340"	0.421"
12"	0.338"	0.421"
14"	0.342"	0.420"
16"	0.340"	0.420"
AVERAGE:	0.339"	0.422"
Ø:	0.002"	0.002"

Figure 2-8. Primary lid elastomer O-ring crushed dimensional configuration.

Figure 2-9. Elastomer O-ring splice joint configuration.

Figure 2-10. Elastomer O-ring splice joint configuration.

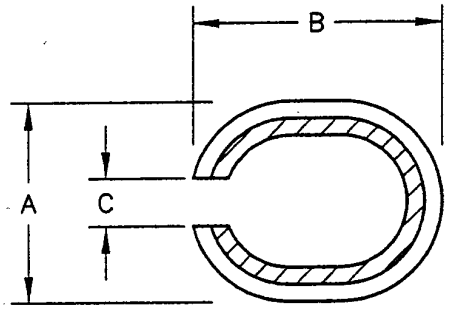

LOC.	DIMENSION A MEAS.	DIMENSION B MEAS.	DIMENSION C MEAS.
2"	0.355"	0.445"	0.085"
4"	0.352"	0.445"	0.080"
6"	0.354"	0.446"	0.065"
8"	0.353"	0.450	0.081"
10"	0.355"	0.452"	0.086"
12"	0.353"	0.454"	0.095"
14"	0.353"	0.456"	0.088"
16"	0.354"	0.450"	0.074"
18"	0.354"	0.454"	0.073"
AVERAGE:	0.354"	0.450"	0.081"
σ:	0.001"	0.004"	0.009"

Figure 2-11. Primary lid metal O-ring crushed dimensional configuration.

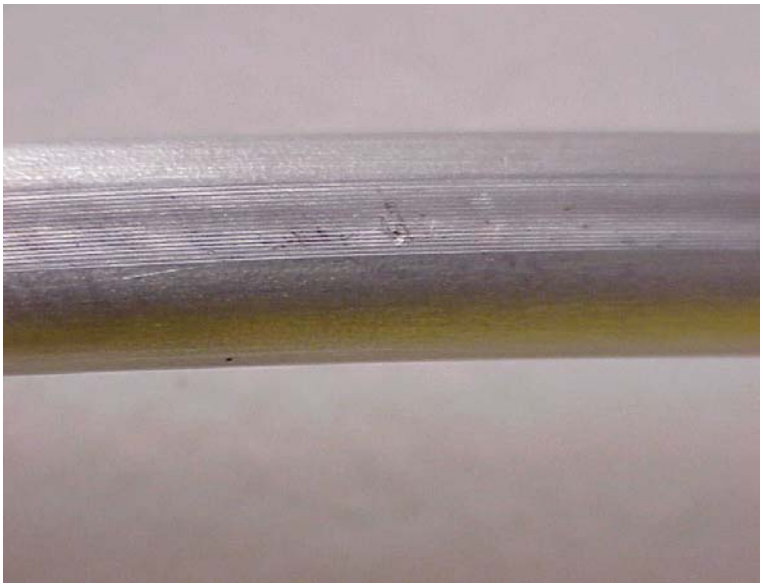

Figures 2-12. Primary lid metal O-ring.

- Several light scratches, a few across the sealing surface; most have metal glint in scratch root, indicating fresh scratches
- No evidence of significant general corrosion, pitting corrosion, stains
- Sealing surface defined by the impression of the machining marks from the seal surface on cask
- No evidence of significant oxidation or spallation of these fine line features
- No deformation of the individual line impressions despite numerous cycles of lid removal/replacement during fuel inspection.

2.6 Cask Interior

The CASTOR V/21 cask is a one-piece cylinder manufactured from ductile cast iron in nodular graphitic form. The external dimensions of the cask body is 4886 mm (16 ft) high and 2385 mm (8 ft) external diameter. The internal diameter is 1527 mm (5 ft), and the cavity depth is 4152 mm (13 ft 7 in.). The internal surfaces of the cask, including the sealing surfaces, were galvanically coated with nickel plating.

The fuel basket is a cylindrical barrel that is partitioned into an array of 21 square fuel tubes in a quadrant layout. The basket is fabricated from welded stainless steel and borated stainless steel plate for criticality control; the borated steel contains approximately 1% boron. Each fuel tube is separated from the adjacent tube by channels that act as flux traps for criticality control and as channels for convective heat transfer. The basket has an outer diameter of 1524 mm (5 ft) and a gross depth of 4110 mm (13.5 ft), including the four 130 mm (5 in.) diameter pedestals at the bottom of the basket. The basket barrel fits snugly within the cask with a clearance of only 3 mm (0.12 in.) total and 74 mm (3 in.) between the bottom of the primary lid and the top of the basket.

The objectives of examination of the cask interior were to inspect the exposed, accessible internal surfaces of the cask structure for evidence of the cask and basket degradation caused by long-term

storage. For the cask cavity, the visual inspection focused on evidence of corrosion and crack formation in the sidewalls and the bottom of the cask, particularly in the bottom corner. It also focused on the failure of the nickel coating by blistering, delamination, corrosion, or discoloration. For the fuel basket, the inspection focused on evidence of new cracks in welds or in walls of fuel tubes,[a] propogation of existing cracks in welds, corrosion and discoloration of fuel tube walls, and accumulations of oxide particles on bottom support brackets and at the bottom of the cask in each fuel tube.

2.6.1 Method of Inspection

Most of the cask inner wall and bottom was not accessible to visual inspection due to the size and tightly fitting characteristics of the basket. At the top of the cask, only approximately 8 cm (3 in.) of sidewall were exposed above the top of the basket and the rebate below the seal area of the cask body (i.e., the sidewall area between the top of the basket and the bottom of the lid), the 5 cm (2-in.) step of the rebate, and approximately 25 cm (10 in.) of sidewall between the primary and secondary seal seats. The floor of the cask was accessible only through the 21 fuel tubes. The bottom corner and 2–5 cm (1–2 in.) height of cask sidewall was partially accessible through a few of the larger flux traps (only = 9 cm [3.5 in.] at the widest) at the periphery of the basket.

The inspection of the inner wall at the top of the cask was performed by remotely using three video cameras mounted on work stand (work platform) at 120° intervals around the top perimeter of the cask. The floor and the bottom corner of the cask were examined with a radiation-tolerant miniature (pencil) camera and light mounted at the end of a 4.5 m (15 ft) pole. The pencil camera head was a cylindrical unit approximately 1.3 cm (0.5 in.) in diameter and 6.4 cm (2.5 in.) long. As with the video cameras, the pencil camera resolution was checked daily with the resolution and color charts.

Because of the tight clearances for access to the bottom corner and sidewall of the cask, the examination was attempted initially with a borescope, but failed because of the narrow field of view, short working distance, short depth of field, and poor dynamic response of the borescope camera.

2.6.2 Interior Cask Sidewall

The upper exposed area of the inner sidewall of the cask was in very good condition as shown in Figure 2-13. The galvanically applied nickel coating was still intact and did not show any evidence of blistering, peeling, cracking, delamination, or corrosion.

The nickel-plated sidewall was free of significant defects. However, a few isolated minor, superficial features or imperfections were visible in the visual inspection; these appeared to be light scuff and faint scrape marks that were most likely created during the initial installation of the basket in the cask. Adjacent to fuel tube D3 (at the 270° mark with respect to the 0° orientation mark as shown in Figure 2-16), the sidewall had an imperfection that initial inspection identified as a blister or dimple. However, close examination of the illumination shadows indicated that the feature was a shallow depression (dimple) about 2 cm (0.8 in.) in diameter and probably only approximately a millimeter deep, with the nickel coating still intact. The visible surface of the sidewall also had several isolated, randomly oriented superficial lines that could be surface deposits (from abrasion by a softer material) or superficial scrapes. These features are quite faint, with no discernible vertical dimensions, burrs, ridged edges, or plow marks that usually are associated with scratches that penetrate coatings or gall a surface.

a. Cracks were formed in some of the basket welds during the initial thermal testing conducted in 1985 (prior to long-term storage). The intent here is to determine if new cracks may have formed during long-term storage.

Figure 2-13. Cask wall at top—typical surface condition.

Considering the tight fit of the basket within the cask body, the nickel coating on the upper sidewall shows little evidence of damage due to insertion of the basket. The only discernible feature that might constitute significant coating damage was a black mark on the sidewall at the level of and coincident with the corner of fuel tube D3. However, the black surface mark appeared to be superficial, and did not have any burrs or dimensional relief indicative of substantial abrasion damage, corrosion product formation, or cracks. While the feature is coincident in location with the corner of fuel tube D3, it cannot be the result of abrasion by the corner of the fuel tube (by vibration from cask handling), for the fuel tube is separated from the wall by the thickness of the steel barrel plate comprising the outer rim of the basket. Instead, this feature may be the result of abrasion during insertion of the tightly fitting basket into the cask or from vertical thermal expansion of the tightly fitting basket barrel wall during the 1985 thermal tests. The upper sidewall has several similar, less distinct blemishes that could be construed as light scuffing or abrasion of the nickel coating from contact during the insertion of the basket into the cask body. These features consist of black 'scuffs' and spots on the nickel surface, as if the nickel plating was lightly abraded from the high points of the rough as-machined surface of the cask body. These features have no discernible relief, implying negligible superficial damage at worst, and have no evidence of more than possibly superficial surface corrosion as might have occurred prior to sealing the cask in 1985. Furthermore, there was no evidence of delamination and peeling of the nickel layer around these features or of subsurface corrosion or blistering in the areas surrounding the features, which could be the expected effect from a corrosive, oxidizing environment.

2.6.3 Interior Cask Bottom and Bottom Sidewall

The cask bottom and bottom sidewall could be inspected only to a limited extent by access through the 21 fuel tubes and the eight channels at the perimeter of the basket. Access via the remaining flux traps was prevented by the tight dimensions of the traps and the structural gussets and spacers in the cavities of the traps. In addition, the inspection of the whole area of the cask floor was hampered by the small clearance (3.8 cm [1.5 in.]) between the bottom of the basket and the cask floor.

The floor of the cask was of roughly grained as-cast texture, overcoated with the nickel plating. The floor of the cask turned smoothly up into the sidewall, so that the first centimeter or two of sidewall was also generally of rough as-cast texture. The sidewall above the bottom corner radius was smoother than the floor as if it had been machined to remove the as-cast texture prior to nickel plating.

The nickel plating on the floor and bottom sidewall was generally clean and quite reflective despite the as-cast texture as shown in Figures 2-14, 2-15, and Appendix F. There was no evidence of any corrosion, cracks, or flaws in the nickel plating, such as blistering or delamination in the floor, corner or sidewall of the cask. In general, the bottom sidewall was quite clean and reflective, particularly those areas that were machined prior to nickel plating. There were, however, isolated areas that appeared to be covered with light-colored spots of material that were not reflective and had no relief. These patches appeared to be mineral spots (Appendix F, Figure F-12), as if deposited from residual water in the cask (as from evaporation of residual plating solution or rinse water). These flat, light-colored spots did not appear to contain much material as they had no relief (depth); neighboring areas were free of these deposits. They did not appear to be caused by corrosion or oxidation, nor was the integrity or adherence of the nickel plating affected by them.

Small grains of debris were thinly scattered over most of the cask floor as shown in Figure 2-14 and Appendix F. The debris ranged from sandlike particles of submillimeter to several millimeter size to long slivers of material several millimeters in length. These generally appeared to have been deposited after the nickel plating of the surface, because the larger particles were dark in color and not reflective. Similar material had accumulated on the horizontal bars at the bottom of each fuel tube on which the fuel assemblies rested. Much of the sand-like debris probably consists of welding slag or grinding swarf from the basket. However, some of the debris appeared to consist of slivers of metal. The slivers may be slivers of stainless steel gouged from the fuel tube walls by insertion and extraction of the fuel assemblies, because the fuel tube walls exhibited much evidence of scraping by the fuel assemblies.

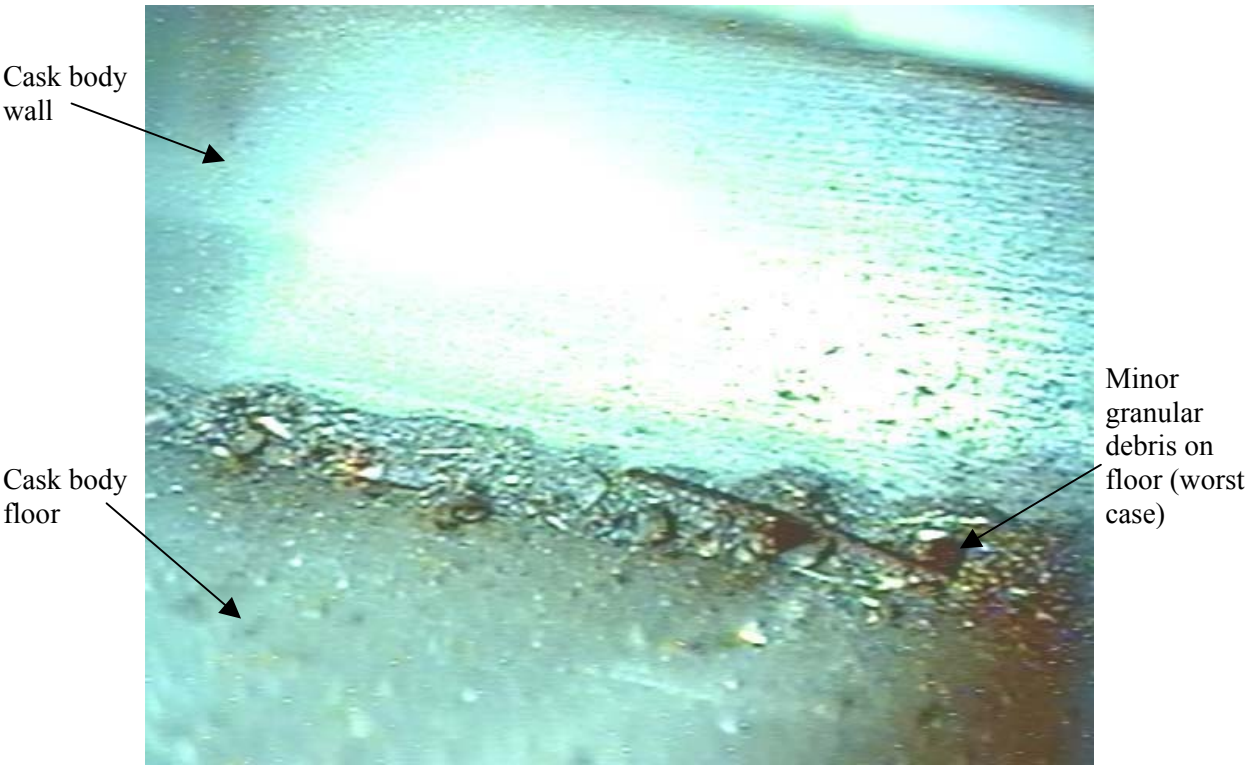

Figure 2-14. Cask floor and wall below fuel tube C8—reflective surfaces free of corrosion.

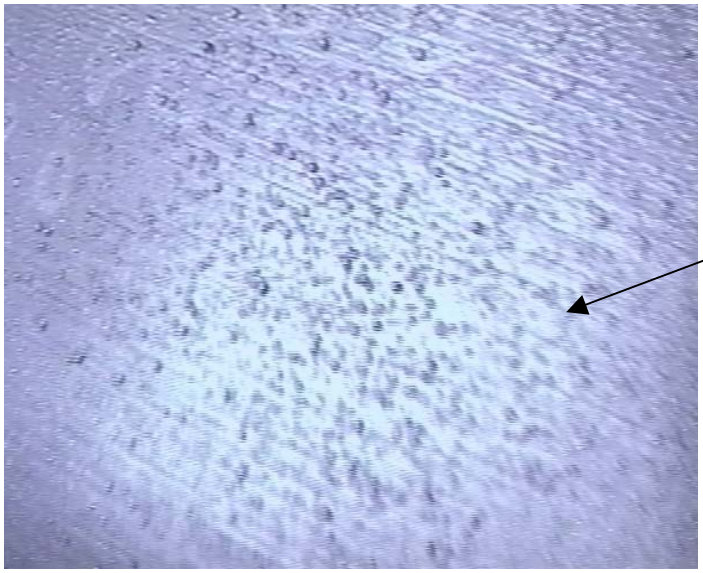

Figure 2-15. Cask wall below and between fuel tube A7 and A8—reflective surface free of corrosion—typical of cask wall condition without mineral stains.

Samples of the particulate debris on the cask floor were retrieved with tape swabs. The locations of the samples are summarized in Table 2.1.

The visual inspection, scanning electronic microscope (SEM), and energy dispersive spectrometry (EDS) results suggest that the visible grains are primarily steel slivers or steel oxide particles from the steel fuel basket. The slivers appeared to be the result of scraping or abrasion of the steel fuel tube walls by the fuel assemblies during past insertions and extractions. The walls of the fuel tubes have long, straight, deep axial (vertical) scratches that are consistent with abrasion by the fuel assembly components during insertion or removal. Moreover, the roots of those scratches glint in the camera lighting, indicating that the scratches are relatively unoxidized and not a characteristic of the mill finish of the plate steel. The larger oxide particles appeared to be residual pieces of welding slag that were dislodged from the basket; the smaller particles of oxide and steel are probably grinding residue dislodged from the basket.

The radiation/chemical analysis of the crud samples were analyzed at the INTEC in November 1999. Samples include those taken from fuel assemblies and the bottom of the cask interior. The test for "iron-phase" was completed and was not conclusive due to the insufficient amount of loose material for sample analysis.

All of the samples show low levels of radioactivity, primarily due to the presence of Co-60, a component of crud. The other common radioisotopes associated with crud were below detection limits for the test. In addition, Cs-137, one of the primary gamma-emitting fission products, was also below detection limits. The gamma analyses suggest that the debris on the floor of the cask may contain some crud particles. Because the crud constituents other than Co-60 were below detection limits, the mass of crud contamination is small and probably consistent with the limited amount of crud that might have been scraped off the fuel assemblies during insertion into and extraction from the fuel tubes.

2.7 Fuel Assembly Basket

The accessible portions of the fuel assembly basket inside the cask were inspected visually, using the three remote video cameras positioned around the top rim of the cask and the pencil camera used to inspect the internal cask floor and exposed portion of the cask wall. The fuel basket was examined for

Table 2-1. Characterization of the particulate debris retrieved from the cask floor. Location of the samples were taken from the CASTOR V/21 cask for characterization.

Sample Number	Method of Sampling[a]	Location of Sample Material (see Figure 2-16)
V/21-1	Tape pad on rod (1)	Cask floor at fuel tube Al
V/21-3	Tape pad on rod	Cask floor at fuel tube C5
V/21-10	Tape pad on rod	Cask floor at fuel tube D5
V/21-12	Tape pad on rod	Cask floor at fuel tube D6
V/21-14	Tape pad on rod	Cask floor at fuel tube A4
V/21-15	Tape pad on rod	Control, exposed to Hot Shop ambient environment and manipulated like samples
V/21-16	Tape pad on rod	Control, exposed to Hot Shop ambient environment and manipulated like samples
V/21-17	Tape pad on rod	Cask floor between fuel tube C8 and barrel wall
V/21-18	Tape pad on rod	Cask floor between fuel tube D8 and barrel wall

a. For retrieval of small granular debris from the bottom of the cask, white nuclear grade duct tape was fastened to a flat foam pad mounted to the end of a 4.6 m (15 ft) steel rod.

evidence of further corrosion of the plate surface, the welds and associated heat-affected zone, the junction between stainless steel and borated stainless, and contact points between the stainless steel structure and the zircaloy fuel assembly structure, such as on the steel brackets at the bottom of each fuel tube that support the weight of the fuel assemblies. In addition, the welds in the basket structure were inspected for failure, both for propagation of the cracks in the known broken welds (prior to long-term storage) and for initiation of new cracks in other welds that may have occurred during long-term storage.

2.7.1 Basket Condition

Only the surfaces of the basket directly accessible to the video and pencil cameras were inspected. The basket was inspected while in place within the cask. The extremely tight diametral clearance between the basket and cask wall (3 mm) prevented the unloading and extraction of the basket from the cask. The top surfaces of the basket were inspected by the three video cameras mounted around the top of the cask. With the fuel assemblies removed, the interior surfaces of the 21 fuel tubes (Appendix D) and eight ungussetted air channels were inspected with the pencil camera system. The interior surfaces of the flux traps and the triangular air spaces at the perimeter of the basket could not be inspected with the pencil camera. These air spaces were obstructed by welded spacers and gussets or were too narrow to permit insertion of the pencil camera.

The fuel basket was in good condition, comparable with the surface condition noted in the 1985. (EPRI NP-4887). In fact, some of the images of the tops of the basket in the 1985 video tapes looked worse (more oxide scale) that in the 1999 inspections, an effect attributed to the difference in lighting conditions. The basket structure showed no evidence of corrosion beyond the mill surface finish and the heat tarnish in the heat-affected zones of the welds. The fabricator of the basket had left the mill surface finish on the steel plate components of the basket. No attempt had been made to remove the native oxide, stencils, construction layout marks, or environmental stains on the as-supplied steel stock.

Therefore, most of the surfaces of the basket structure had a light-gray nonreflective surface as well as superficial oxide tarnish in the region of many of the welds. However, some of the interior surfaces of

the fuel tubes bore the marks of spot (rotary) surface grinding that 'skinned' the flat surfaces and original fabrication layout markings. These ground surfaces were still brightly reflective under the camera illumination and markings were still legible, indicating that neither significant air oxidation nor corrosion had occurred since the fabrication of the basket as shown in Appendix D (Figure D-20 and D-25). There was no evidence of corrosion due to incompatibility between the stainless steel and the borated steel, nor was there evidence of corrosion or degradation at the contact between the stainless steel 304 bottom nozzle of the fuel assemblies and the bottom support plates in the fuel tubes. No cracks or similar degradation was seen in the steel plate components, except for some of the welds as noted below.

2.7.2 Basket Welds

The 1985 inspection of the basket after the completion of the heat transfer performance tests identified eight broken welds in the top of the basket (EPRI NP-4887). The affected welds are identified as welds 1 through 8 in Figure 2-16. The welds cracked as a consequence of the stresses created by the differential thermal expansion of the tightly fitting basket within the cask during the tests (EPRI NP-4887). An objective of the 1999 inspections was to reexamine the affected welds for any changes in configuration and to examine other accessible welds in the basket structure for cracks or corrosion. Unfortunately, the stitch welds of the structure are located in the flux trap and spacer channels, not inside the 21 fuel tubes. Therefore, the only accessible welds were the welds visible at the top of the basket and a few others. The present condition of these welds are as shown in Appendix G.

The eight known existing broken welds appeared to be the same as in the 1985 inspection. The four welds in the corners of the central fuel tube A1 (cracks 4, 5, 6 and 7 in Figure 2-16) all involved welds of stainless steel to borated stainless steel, whereas the four welds joining the fuel tubes in clusters A8/A5/A6, B6/B5/B8, C8/C5/C6, and D6/D5/D8 (Cracks 1, 2, 3, and 8 in Figure 2-16) involved only stainless steel. The 1999 inspection confirmed that five welds were broken clear through, and three had substantial cracks that propagated partially through the top stitch weld. The narrowness of the flux traps and the supports within blocked the views of the stitch welds below the top welds from the top-side video cameras, and prevented the insertion of the pencil camera assembly. Therefore, the condition of those welds could not be determined. The top stitch welds throughout the top of the basket were inspected as well as the welds of the top-most struts within the flux traps. Except for the eight known cracked welds, the remaining welds appear to be in good condition and free of cracks.

The stitch welds in the triangular air channels at the inside perimeter of the basket barrel (Figure 2-16, crack locations 9 through 16) were examined with the pencil camera system. The gusset- and strut-free channels were just large enough to permit insertion of the pencil camera for viewing the stitch welds attaching the fuel basket borated stainless steel partition plates to the stainless steel basket barrel. There were two stitch welds approximately three inches long located in each air channel, one at the top and one at the bottom.

The inspections found that all eight of the bottom stitch welds were cracked and seven of the eight top welds. The weld free of cracks was the top weld at location 12 as shown in Figure 2-16. The top weld at location 13 was only partially cracked at the bottom (1/4 in. long) including several fine lateral cracks. A typical view of the remaining cracked stitch welds with full length longitudinal center line cracks are as shown in Figure 2-17 and 2-18. A view of all stitch welds examined in the triangular air channels are as shown in Appendix B.

Additional cracks in basket welds (as shown in Figure 2-19.) were associated with stainless/borated steel junctions welds in fuel tubes.

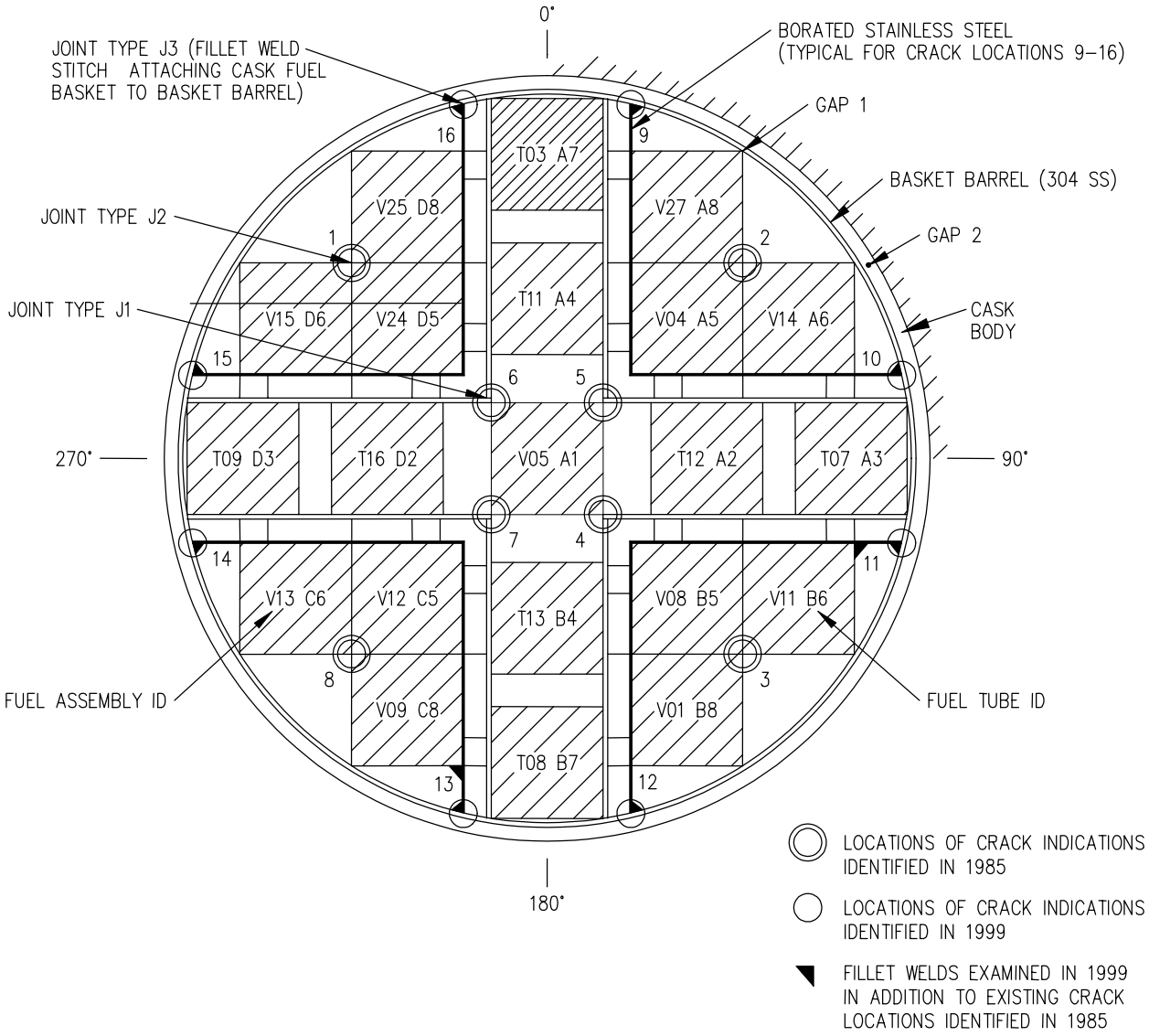

Figure 2-16. CASTOR-V/21 basket crack indication locations and fuel tube arrangement.

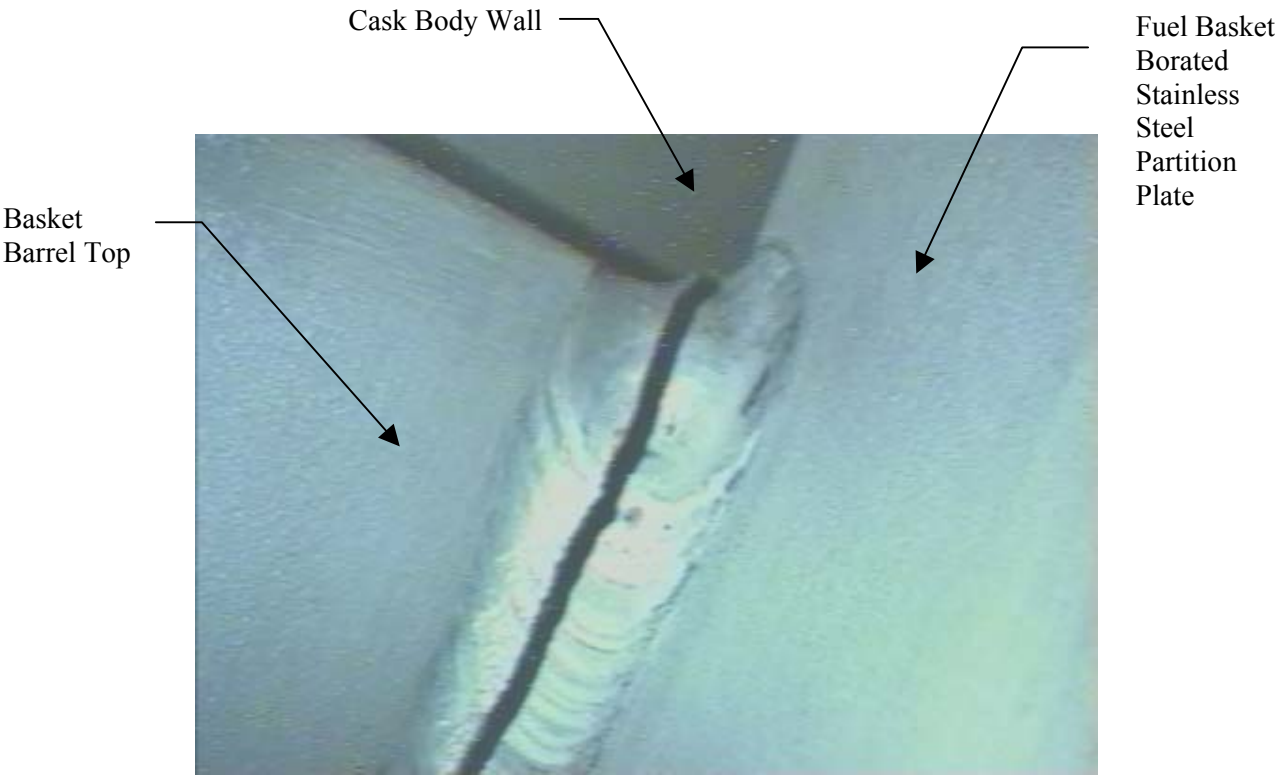

Figure 2-17. Typical top stitch weld crack at location 14 identified in Figure 2-16.

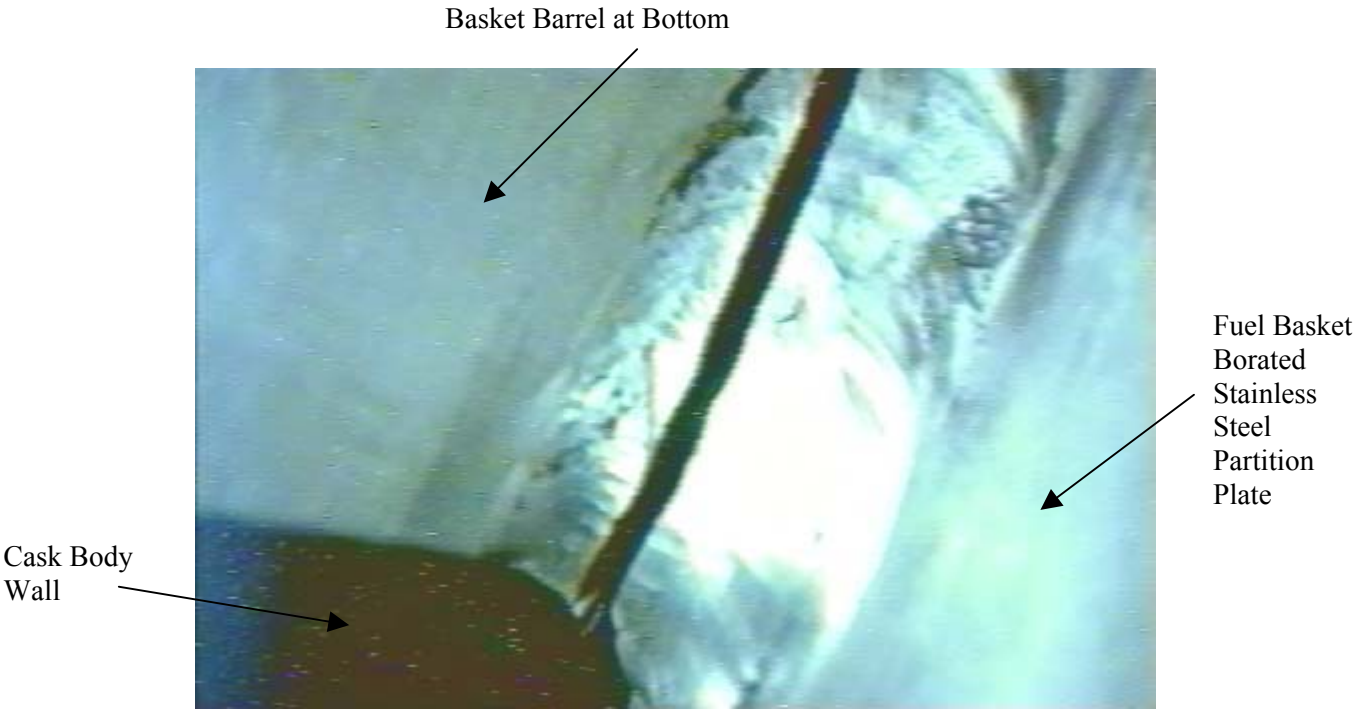

Figure 2-18. Typical bottom stitch weld crack at location 14 identified in Figure 2-16.

Figure 2-19. Crack in basket weld below weld crack 4 (120 degree side) identified in Figure 2-13.

The stitch welds in the triangular air channels appear to be nonstructural welds and were only intended to add additional stability for holding the fuel basket in place during 1985 fuel loading and vertical and horizontal thermal testing. The 1985 cask heat transfer performance testing (EPRI NP-4887) thermal analysis, concluded that the tightly fitted fuel basket expanded and came in contact with the basket barrel and the fuel barrel came in contact with the inner wall of the cask. The results of the thermal analysis indicated that thermal stresses in the weld joints at the eight crack locations identified in 1985 were well above yield stresses measured during tensile testing of applicable weld samples. Based on these results and speculations, it appears that all new cracks identified in 1999 occurred during the 1985 thermal testing. Further, it is concluded the cracks are not relevant to normal long-term storage and presents no adverse safety implications on the cask or components to perform their safety related function.

2.8 Fuel Assemblies

2.8.1 Purpose of the Inspection

The inspection searched for visual evidence of change in the structure and integrity of the fuel assemblies after 14 years of dry storage. The primary characteristics examined were: changes in corrosion and crud deposits on nozzles, grid spacers, rod cladding; loose or lightly adherent corrosion product or crud; evidence of spallation or flaking; physical degradation or damage to nozzles, grid spacers, fuel rods; cracks, bowing of rods, or distortion.

2.8.2 Method of Inspection and Lifting Force Measurements

The visual inspection requires the removal of the fuel assembly from the basket (Figures 2-20 and 2.21).

Table 2-2 provides the fuel assembly weight and the force required to start lifting each assembly out of the V/21 cask. The lifting force measurements indicate little sticking of the assemblies during removal, suggesting that no significant bowing of the assemblies or development of corrosion products causing adherence to the cask floor occurred.

Once the assembly was lifted out of cask basket, the inspectors identified the assembly serial number and its orientation with respect to basket. They checked the relative uniformity of fuel rod lengths by clearance between tops of rods and top nozzle, then scanned the four sides using the three remotely operated cameras. Each scan permitted a clear-through view between the fuel rod array. After the visual inspection, the fuel assembly was returned to its original fuel tube in the cask, maintaining the original orientation.

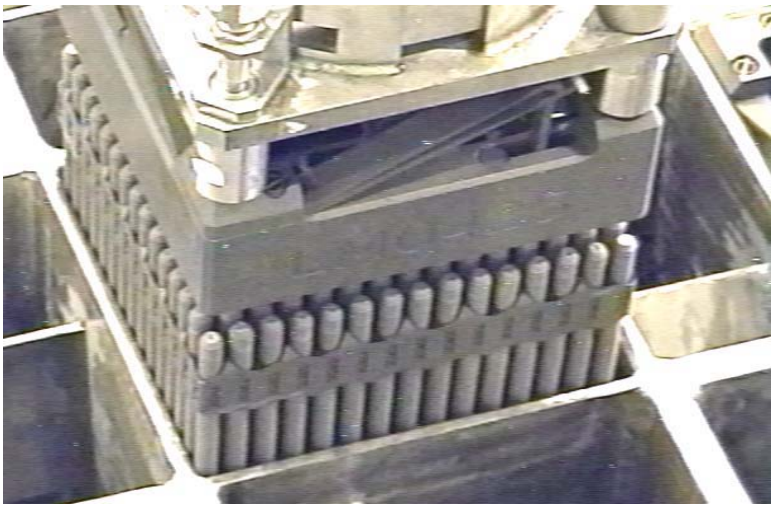

Figure 2-20. Fuel assembly being lifted out of the basket for visual examination.

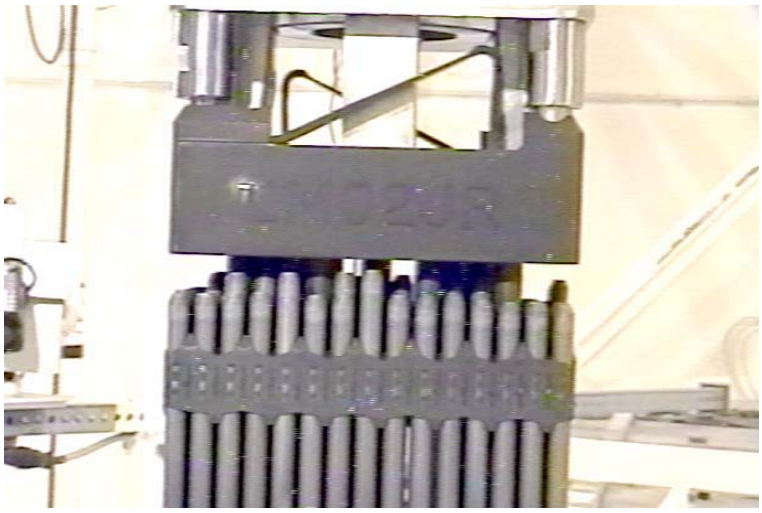

Figure 2-21. Fuel assembly T11 attached to lifting grapple for visual examination.

Table 2-2. Fuel assembly examination sequence and lift force measurements.

Fuel Assembly ID	Inspection Sequence	Selected for Closer Examination	Grapple + Fuel wt		Force to Start Lifting	
			(lb)	(kg)	(lb)	(kg)
VO5	1	YES	1414.5	642.9	1436	652.7
TO3	2		1421	645.9	1472	669.1
V27	3		1419	642.7	1457	662.3
V04	4		1419	642.7	1439	654.1
V14	5		1415	643.2	1446	657.3
T07	6		1419	642.7	1434	651.8
T12	7		1415	643.2	1442	655.5
V08	8		1412	641.8	1431	650.5
V11	9		1407	639.5	1421	645.9
V01	10		1415	643.2	1433	651.4
T08	11		1410	640.9	1431	650.5
V09	12		1412	641.8	1440	654.5
V12	13	YES	1403	637.7	1420	645.5
V13	14		1417	644.1	1442	655.5
T09	15		1410	640.9	1428	649.1
T16	16		1413	642.3	1441	655.0
V24	17	YES	1410	640.9	1430	650.0
V15	18	YES	1408	640.0	1433	651.4
V25	19		1413	642.3	1426	648.2
T13	20		1412	641.8	1427	648.6
T11	21	YES	1410	640.9	1420	645.5

Once the fuel assembly was removed, the entire length of the four external surfaces were inspected by three remotely operated video cameras with zoom capabilities. Specification requirements for camera resolution was 2.6 mm (0.105 inches), maximum lower case character height, actual was demonstrated as better than 1.5 mm (0.060 inches). Appendix C shows an example of the condition of the assemblies.

2.8.3 Fuel Rod Length Variation

The uniformity of the gaps between the tops of the fuel rods and the top nozzle was evaluated for all fuel assemblies. This information was required to evaluate the potential for interference by the fuel rods in drilling the top nozzle for fuel rod extraction. In all of the fuel assemblies, the gap varied considerably, by as much as 0.5 inch (1.2 cm).

The variations in rod length did not show any recognizable pattern, except that the rods within the array, near the center of the assembly, often appeared to be slightly longer on the average than the rods at the periphery of the array. In the outer peripheral rows, the rod length varied sharply from one rod to the

next, with no discernible pattern. The variation in the gap was previously ascribed to uneven fuel rod growth during irradiation (EPRI 4887).

2.8.4 Fuel Rod Bowing

The fuel rods in the fuel assemblies did not exhibit any detectable deformation except for slight localized bowing in the fuel rod sections between spacer grids. The extent of bowing was relatively small, amounting to less than a 50% deviation from the nominal 0.141 inch (3.58 mm) space between rods, based on a nominal rod pitch and diameter of 0.563 inches (14.30 mm) and 0.422 inches (10.72 mm), respectively. The views through the spaces between the fuel rods rows in the arrays indicated that the fuel rods within the arrays were also generally straight and without significant bowing or deformation.

2.8.5 Cladding Failure

The cask fill gas has been monitored for the last 14 years for gaseous fission product release, as evidence of cladding failure. No fission products have been found in the cask backfill gas samples (as presented in Section 4), indicating good integrity of the rod cladding. In the 1999 inspection, the surfaces of the rods were examined directly for cracks, cladding defects, general corrosion, and pitting corrosion as indications of established or incipient failure of the cladding. The inspections found no evidence of cracks, cladding damage or defects, general corrosion, pitting corrosion, or other indicators of established or incipient failure of the cladding.

2.8.6 Crud Coating

The oxide coatings on the visible rods were remarkably similar from rod to rod and assembly to assembly. The top nozzle, the exposed spacer grids surfaces, and the upper portions of the rods (above the third spacer grid) had a thin, uniform coating of light-colored adherent oxide (light gray to light tan/brown in the ambient lighting of the Hot Shop). Generally, below the third spacer grid (numbered from the top of the assembly), the oxide coating became increasingly mottled in appearance, with increasing areal fractions of dark gray oxide patches mixed with the light brown oxide. The gray mottling usually peaked on the rod surfaces near the fifth or sixth spacer grid (numbered from the top). The mottling was most pronounced on the rod surfaces just above the spacer grids, and often was the dominant oxide.

The 1985 examinations ascribed the uniform light gray/brown oxide coating on the upper portion of the fuel assembly to crud deposits (EPRI 4887). Although characterization attempts on the crud were not successful, it is likely that the crud is composed of Fe_3O_4, and probably the $Ni_xFe_{3-x}O_4$ spinel that is typical of PWR systems. The axial gradation of oxide uniformity (judged by oxide color), with greater color uniformity at the top of the assembly, suggests a slightly thicker accumulation of light tan/brown crud on the upper surfaces, with thinning of the crud in the lower sections. It is possible that the gray mottling that was usually prominent above the fifth and sixth spacer grids may represent an area of very thin crud deposition, that the dark gray mottled phase consists of exposed substoichiometic ZrO_x (which, unlike the white stoichiometric ZrO_2, is dark gray or black in color). However, this identification is speculative, since the color of PWR crud is dependent on reactor conditions, and can vary from light colors to gray/black (Sandoval et al., 1988). It is highly unlikely that the mottling is due to spallation of a lighter-colored surface coating, with exposure of an underlying dark-colored oxide. Mottled oxide structures have been reported previously on PWR fuel (Sandoval et al., 1988). Furthermore, the mottled oxide structure was never associated with any visual evidence of spallation, flaking, or surface relief in these inspections, nor was there any evidence of accumulated spalled material on the upper surface of the bottom nozzle, the upper surfaces of the fuel tube brackets on which the assemblies rested, or on the bottom floor of the cask.

Most of the fuel rods in all of the assemblies exhibited two faint white rings of material just above and below the bottom weld that sealed the bottom end plug to the cladding. The rings were typically thin

and narrow, on the order of 0.05-0.1 inches wide. The most pronounced of these features is shown in Figure C-59 of Appendix C, which shows some rods with typical white rings, as well as one rod with one of the most pronounced oxide rings seen in the inspections (fuel assembly V-25, LM040H) Similar features were not seen on the upper ends of the rods, nor were these features observed on the individual rods that were extracted from fuel assembly T11. This suggests that these features, if real, are very thin and their detection is sensitive to the lighting conditions. Since the two white rings correspond to the heat-affected zone of the bottom weld, they may consist of stoichiometric ZrO_2, which can form as a white, discontinuous and non-adherent oxide. The formation of the non-adherent stoichiometric oxide is usually associated with low levels (parts per million) of contaminants, such as nitrogen or carbon, in the zircaloy (Berry, 1971). Because these features were so faint, they were probably present in the 1985 tests but not detected in the visual inspections, and were not considered significant in the 1999 inspections.

The only difference between the 1985 and the 1999 inspections was one of color perception; the 1985 examination reported the oxide as a 'typical orange/reddish crud' (EPRI 4887) whereas in 1999 the oxide appeared light tan/brown and light gray, depending on the viewing angle (i.e., the lighting conditions). The uniform light-colored oxide coating on the upper surfaces of the fuel assemblies and the mottled coatings on the lower portions seen in 1999 were similar in appearance to the video-taped images acquired in the 1985 inspections. As in the 1985 inspections, the oxide coatings on the fuel assemblies were thin and very tightly adherent. There was no evidence of growth of oxide scale on the top or bottom nozzle, the grid spacers, and the cladding. The wear marks on the surfaces of the grid spacers (from abrasion during extraction of the fuel assembly) indicated that the oxide coating was still very thin and tightly adherent. The edges of the rods were crisply-defined, with no evidence of loosely adherent material. In addition, the upper surfaces of the bottom nozzle did not have any accumulations of spalled or loose material. There was no visual evidence that the dry storage period had caused a change in the oxide coatings, either with respect to thickness, oxide structure (surface patterns), or the adherent nature of the oxide. The tiny amount of crud that was collected was still tightly adherent after 14 years, and consisted of a few grains a few microns in size. Too little material was collected to obtain quantitative values for ^{60}Co.

2.8.7 Fuel Rod Removal and Examination

At the conclusion of the examination of the fuel assemblies, fuel assembly T11was selected for extraction of 12 individual fuel rods for visual examination and shipment to the Argonne National Laboratory for nondestructive, destructive, and mechanical examinations. Fuel assembly T11, located in fuel tube A4 (see Figure 2-16), was selected on the basis of maximum burnup and decay heating. The entire surface of each of the 12 individual fuel rods was visually inspected for the condition of the cladding including cracks, pitting, corrosion, bowing, imperfection, discoloration, stains and general surface deterioration.

The tops of the fuel rods were accessed by cutting a 3 inch diameter hole through the top fuel assembly nozzle, centered on the fuel rod array, using a portable hole saw as shown in Figure E-1 of Appendix E.

The fuel rods selected and removed are as shown in Figure 2-22. To withdraw the individual fuel rods, a rod puller grapple and load cell were attached to the top end of the rod. The rods were pulled from the assembly with the in-cell remote manipulators, taking care that the load limits were not exceeded. The applied pull force required to extract each rod from the assembly was approximately 35 to 45 pounds mass (15.9 to 20.5 kg) to dislodge each rod from the grid spacers; thereafter the applied force quickly dropped to 20 to 25 pounds (9.1 to 11.4 kg) for the duration the extraction. The fuel rods were pulled individually into a horizontal aluminum alloy channel tray for visual examination. After the visual examination, each fuel rod was transferred to the shipping container (Appendix E, Figure E-13)

The twelve fuel rods were free of physical damage, except for long, continuous longitudinal scratches in the cladding from initial installation into the fuel assembly (Figure 2-23, 2-24 and Appendix E). The longitudial scratches were old scratches, for the roots of the scratches were thinly coated with oxide (crud). Several of the rods had many (6-12) parallel longitudinal scratches running most of the rod length; none of the scratches had perforated the cladding and are not caused by creep failure. There was no evidence on any of the rods of extensive corrosion, pitting, or creep failure.

While the cladding of all fuel rods exhibited numerous longitudinal, continuous scratches due to the initial installation into the fuel assembly, the extractions created only a few new scratches in the cladding surfaces. The new scratches did not break through the cladding. The relative ease of extraction, which caused less distress to the cladding than the original assembly operation, indicated that the cladding had not experienced any significant radial creep in any of the fuel rods, nor any significant reaction with the inconel spacers.

Each rod was covered with a thin but uniform coating of oxide. The oxide coating seemed to comprise two layers, a light tan and a red-brown layer with sharp delineations between them, especially in the vicinity of the spacer grids (Figure 2-23 & Appendix E). These rods, drawn from within the bundle, appeared to have a more uniform oxide coating than the peripheral rods in the array. In general, the oxide layers appeared to be very thin and tenacious. On the upper portions of the rods, the incident lighting reflected diffusely from the thin oxide, imparting a pearly or vitreous satin sheen to the surfaces.

The dark gray mottled oxide structure that was so characteristic in the lower portions of the peripheral rods in the array was limited to a few inches of rod length, generally only on areas covered by the fifth and sixth spacer grid. As with the peripheral rods, these rods also exhibited the very thin white bands of oxide above and below the weld on the bottom end caps of the rods (Appendix C, Figure C-13).

The oxide layers were tightly adherent to the surface of the rods. The adhesion was tested with a steel wire brush and a steel spatula scraper. Neither tool was able to remove detectable amounts of oxide or to change the surface appearance of the rod. Only with application of considerable force and with considerable flexing of the spatula blade was the oxide layer broken and a small amount of oxide removed.

All of the fuel rods exhibited small spots (≤0.060 inches [1.6 mm] diameter), often occurring in sets of two, with similar sets of spots spaced 90 degree azimuthally around the rod. These features corresponded to the positions of the spacer grids and are assumed to be the contact points between the spacer grid springs and the cladding. These features were not pinholes or pitting corrosion, for several of these black spots gleamed with reflected light when oriented appropriately. The contact points were usually associated with the long longitudinal old scratches in the cladding surface and frequently were the termination of an old scratch.

The assemblies were in a generally good condition, which had not changed since the 1985 inspection. The general visual survey revealed a dark gray oxide layer under ambient cell lights, and light tan by video. The inspection found no increase in the oxide layer thickness. There was no formation of a loose oxide scale or particles between the fuel rods of the grid spacers or on the bottom nozzles. A general view of fuel assemblies is shown in Appendix C.

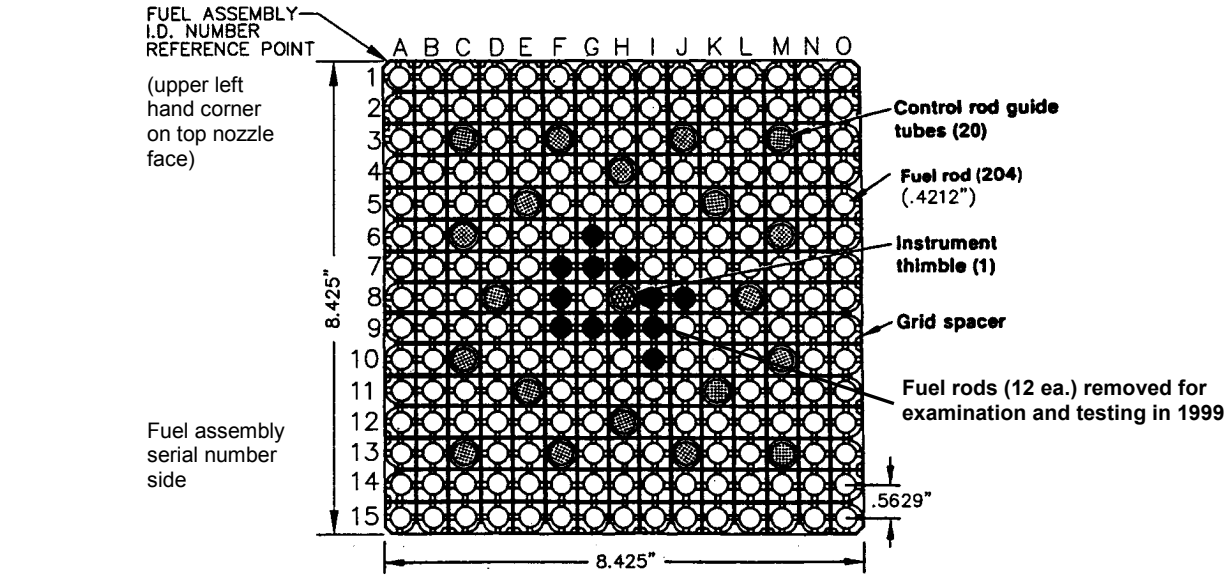

Cross Section

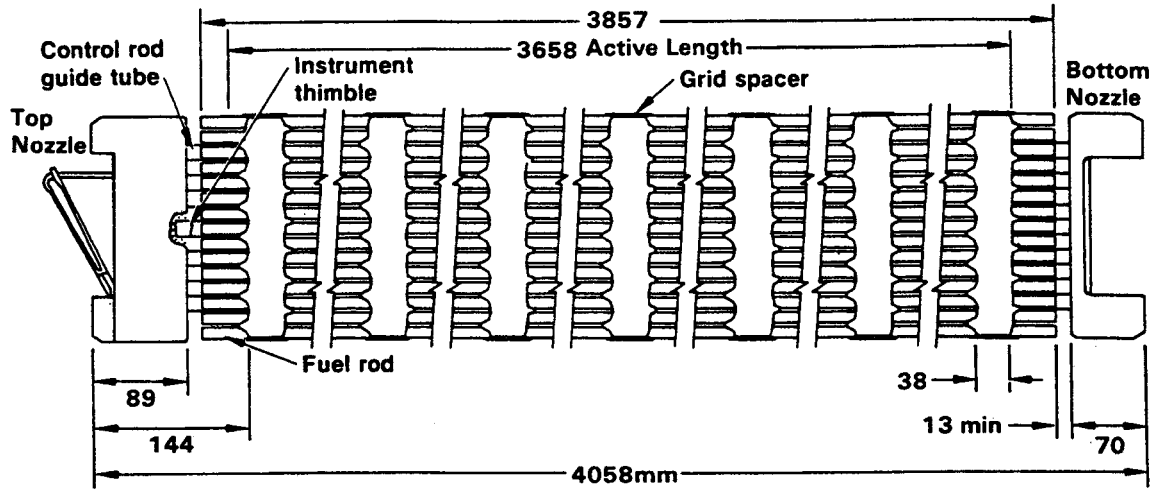

Figure 2-22. Surry 15 × 15 PWR Fuel Assembly T11, Serial number LM02JR.

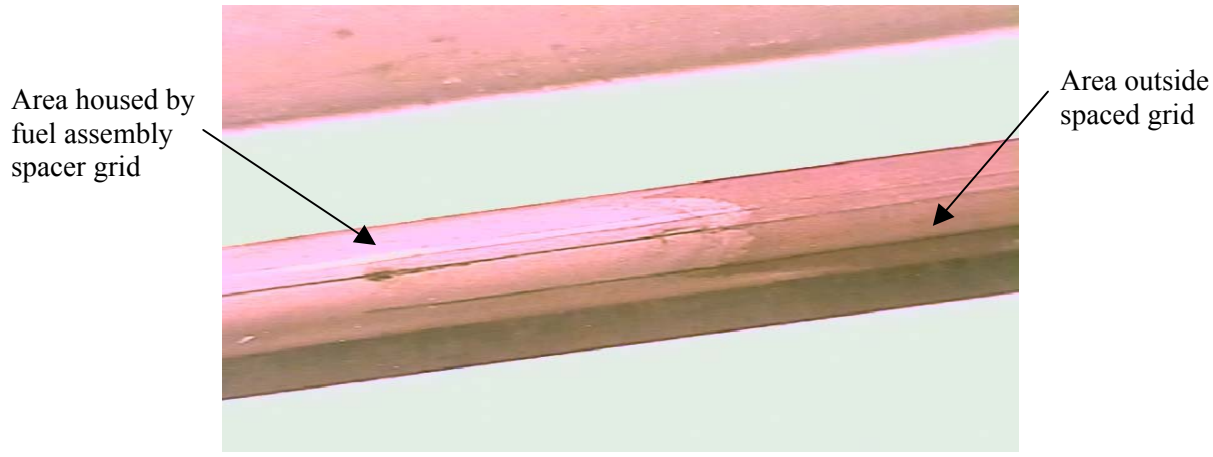

Figure 2-23. Close up of Fuel rod removed from fuel assembly T11 position 7H identified in Figure 2-22.

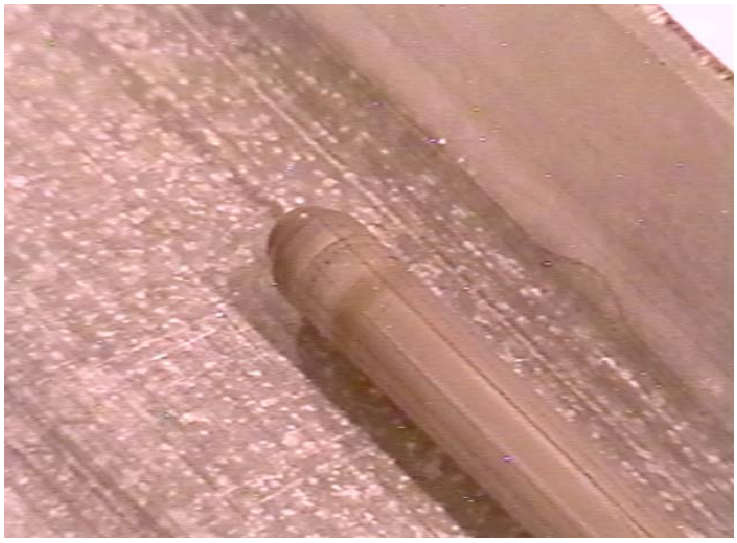

Figure 2-24. Fuel rod removed from fuel assembly T11 position 8I identified in Figure 2-22.

2.9 Cask Temperatures

Storage systems must be designed to allow ready retrieval of spent fuel from the monitored retrievable storage installation (10 CFR Part 72). The spent fuel cladding must be protected against degradation by thermally activated processes by keeping the storage temperature down. Spent fuel storage or handling systems must be designed with a passive heat-removal capacity without active cooling systems. The conditions in the second dry cask storage period will be less severe than in the first storage period because the decay heat decreases with time. The decreasing decay heat requires less heat removal capacity during the extended licensing period.

2.9.1 Internal Temperature

The thermocouple lance system used in 1985 was no longer available for the tests in 1999. Thus, the temperatures inside the cask had to be measured with the lid off. Therefore, the internal temperature measurements obtained during the 1999 testing would only provide a general indication of temperatures inside the cask.

Internal temperatures were recorded on September 29, 1999, between approximately 4 pm and 5 pm. The cask lid was removed every workday morning at approximately 7:30–8 am, and by procedure, it was replaced nightly at the end of the day's activities (generally between 7 and 9:30 pm). When these temperature measurements started, the lid had been off the cask for approximately 8 hours.

The bolts were removed from the primary lid on September 7, 1999, and the primary lid was first removed on September 8, 1999. Between September 8 and 29, the lid had been open generally 5 days per week and about 10 hours per day, with at least 8 hours of convective cooling on that day. The gradual convective cooling was achieved during the working days prior to that measurement. Therefore, the contents would have cooled considerably.

The temperature was measured with a Type J thermocouple inserted into the control rod guide tube. It was expected that the upper portions of the fuel assembly would exhibit the highest temperatures due to convection. To approximate the best position, the temperature in V05 (fuel tube A1, Figure 2-16) were quickly measured at three positions:

- After 12 minutes, 0.6 m (2 ft) below the top nozzle, 152.1°C (305.8°F)
- After 5 minutes, 1.5 m (5 ft) below the top nozzle, <140°C (284°F)
- After 10 minutes, 0.3 m (1 ft) below the top nozzle, 146.5°C (295.7°F).

Within 10 minutes or so, the temperatures equilibrated to within 0.1°C/min (0.2°F/min) rise; the temperature readings were recorded for at least the last 5 minutes of equilibration. The final readings at 10 minutes (12 minute for VO5), measured approximately 0.6 m (2 ft) beneath the top nozzle, were as follows in Table 2-3.

Readings at 1-min intervals indicated that the equilibration was close to completion at 10 min; the final true equilibration temperature might be at most 2°–3°C (5 degrees Fahrenheit) higher.

Table 2-3. Internal temperature.

Assembly ID	Fuel Tube ID	Temperature
V05	A1(center of basket)	152.1ºC (305.8°F)
T11	A4 (between center and outer tubes)	154.6ºC (310.3°F)
T03	A7 (outer tube, at 0º mark on cask)	122.8ºC (253.0°F)

The hottest zone in the hottest of the three measured assemblies was 154°C (309°F) at the end of 10 minutes equilibration, when the rate of rise was still 0.1°C/min (0.2 °F/min). A plot of the data indicated that the temperature would eventually equilibrate between 155 and 160°C (311 and 320°F).

It must be emphasized that these results pertain only to the conditions at the time of measurement and represent an estimate of the maximum temperature of the assembly. It was considered as satisfactory that the air temperatures were well below 200°C (392°F) to allow the use of aluminum for the laydown fixture used to transport the fuel assembly from the hot shop to the hot cell. More rigorous measurements of the actual rod surface temperatures to get a better assessment of the impact on using aluminum for the laydown fixture were not executed. It was assumed that fuel assembly T11 with its high burn up was thermally the hottest or at least representative of the hottest assemblies It is nevertheless true that with the cask lid in place, the final equilibrium temperature will be higher than the value recorded and reported.

2.9.2 External Surface Temperature

Measurements of the external surface temperature of the cask were taken by portable pyrometry. The temperatures were recorded on August 2, 1999, at approximately 4:30 pm. The results are summarized in Table 2-4 along with the 1985 measurements.

As expected for the reduced decay heat, the surface temperatures of the cask were substantially cooler (by approximately 10°C [50°F]) in 1999 than in 1985. In addition, the 1999 readings qualitatively track the 1985 readings quite well. The 1999 data show less scatter in the various azimuthal readings at a given elevation and describe a flatter temperature profile than the 1985 data. These data are summarized in Figure 2-25.

Table 2-4. External temperature data for CASTOR V/21 Cask.

		Temperature 1999		Temperature 1985		
No.	Elevation[a] (mm) @ Azimuth[b]	°F	°C	°F	°C	Location
1	175@0°	103.9	39.9	148.2	64.6	Cask side[d,e]
2	460@353°	105.2	40.7	154.9	68.3	Cask side[d,e]
3	1148@0°	107.7	42.1	167.9	75.5	Cask side[d,e]
4	1130@0°	110.9	43.8	161.0	71.7	Cask side[d,e]
5	2348@0°	118.9	48.3	178.8	81.6	Cask side[d,e]
6	2330@0°	113.6	45.3	166.6	74.8	Cask side[d,e]
7	3148@0°	119.3	48.5	179.0	81.7	Cask side[d,e]
8	3130@0°	115.4	46.3	166.4	74.7	Cask side[d,e]
9	3898@0°	117.9	48.8	172.5	78.1	Cask side[d,e]
10	4380@0°	116.4	46.9	169.7	76.5	Cask side[d,e]
11	4621@0°	115.1	46.2	169.8	76.6	Cask side[d,e]
12	1148@45°	110.6	43.7	161.7	72.1	Cask side[d,e]
13	2348@45°	117.5	47.5	172.7	78.2	Cask side[d,e]
14	3898@45°	117.7	47.6	174.5	79.2	Cask side[d,e]

Table 2-4. (continued).

No.	Elevation[a] (mm) @ Azimuth[b]	Temperature 1999 °F	Temperature 1999 °C	Temperature 1985 °F	Temperature 1985 °C	Location
15	1148@180°	111.4	44.1	168.4	75.8	Cask side[d,e]
16	2348@180°	118.5	48.1	184.2	84.6	Cask side[d,e]
17	2330@180°	114.0	45.6	175.1	79.5	Cask side[d,e]
18	3880@180°	120.3	49.1	178.8	81.6	Cask side[d,e]
19	2348@225°	117.8	47.7	173.3	78.5	Cask side[d,e]
20	3898@225°	118.5	48.1	199.9	93.3	Cask side[d,e]
21	1148@270°	112.3	44.6	160.1	71.2	Cask side[d,e]
22	2348@270°	119.2	48.4	178.5	81.4	Cask side[d,e]
23	3898@270°	117.4	47.4	174.2	79.0	Cask side[d,e]
	Radius[c] (mm) @ azimuth[b]					
24	487@0°	131.3	55.2	207.5	97.5	Cask top[d,e]
25	1100@0°	113.0	45.0	165.3	74.1	Cask top[d,e]
26	487@90°	133.9	56.6	217.2	102.9	Cask top[d,e]
27	1100@90°	115.6	46.4	166.1	74.5	Cask top[d,e]
28	Center	141.0	60.6	221.5	105.3	Cask top[d,e]
29	1100@180°	113.9	45.5	109.5	43.1	Cask top[d,e]
	Radius[c] (mm) @ azimuth[b]					
30	487@0°	—	—	76.8	24.9	Cask bottom[d,e]
31	1100@0°	—	—	79.7	26.5	Cask bottom[d,e]
32	487@90°	—	—	—	—	Cask bottom[d,e]
33	1100@90°	—	—	—	—	Cask bottom[d,e]
34	Center	—	—	—	—	Cask bottom[d,e]
35	1100@180°	—	—	—	—	Cask bottom[d,e]
36	Ambient Temperature	91.2°F	32.9	82.7°F	28.2	

a. From exterior bottom of cask.
b. From 0º orientation mark. Figure 2-16.
c. From cask centerline.
d. Cask orientation vertical with helium backfill.
e. Exterior cask surface.

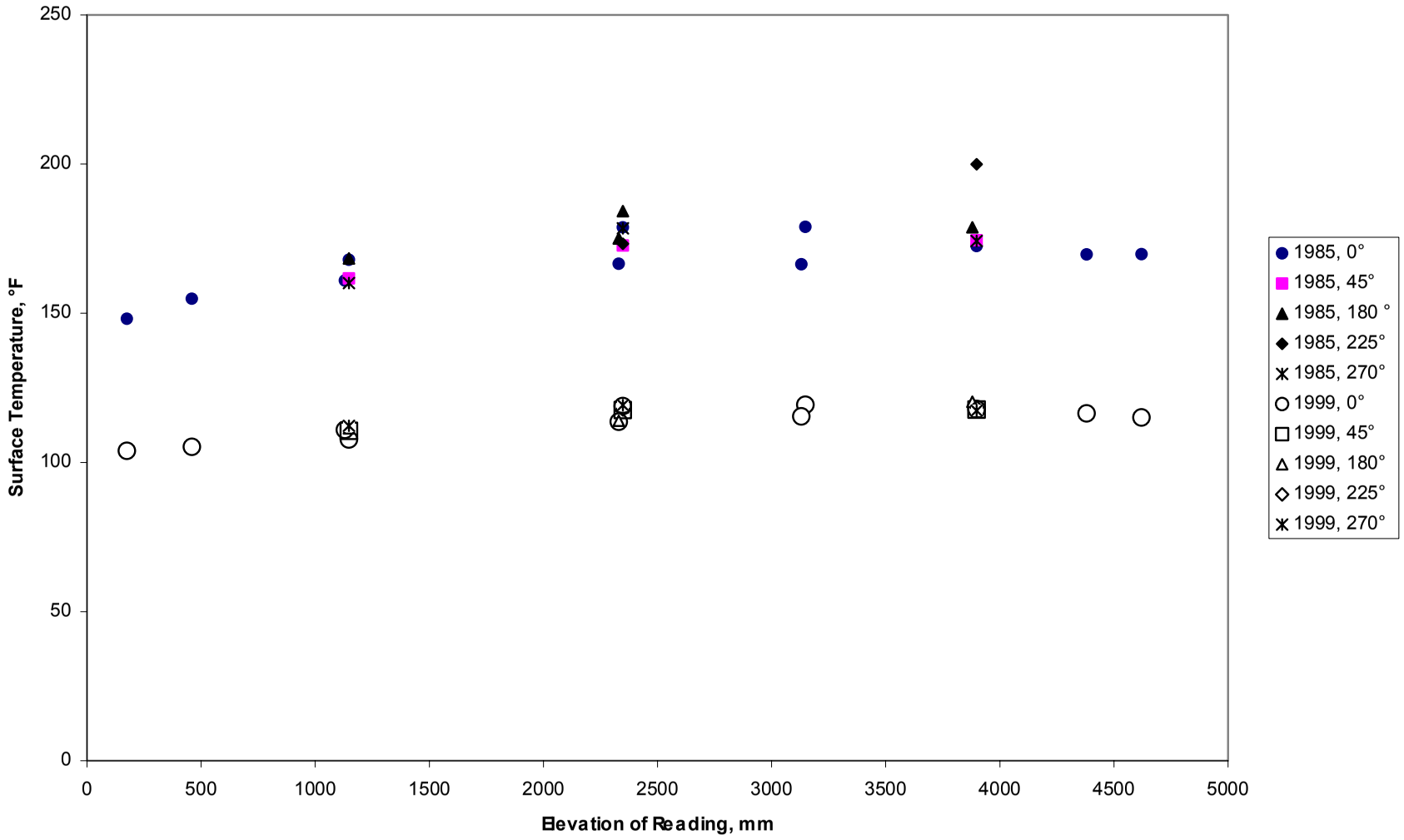

Figure 2-25. Surface temperatures of the CASTOR V/21 Cask.

3. RADIATION SURVEY

3.1 Objectives

Radiation shielding and confinement features that are sufficient to meet all necessary requirements of 10 CFR Part 72 must be maintained as long as the spent fuel is to be stored. Because the radioactive and thermal source terms are decreasing, a dry storage cask that met the requirements for the first license period will also meet those for the second license period provided that material alterations have not led to unexpected behavior or decreased capabilities of factors important to safety.

A radiation survey was conducted in 2001 to evaluate the performance of the cask shielding for neutron and gamma radiation at the sidewall, top and bottom surfaces of the cask. The dose rate readings were compared to the 1985 measurements to evaluate the performance of the cask shielding.

3.2 Methods of Measurement

In the 1985 EPRI study (EPRI NP-4887), gamma doses were measured at 69 locations on the surface of the cask with lithium fluoride (LiF) thermoluminescent dosimeters (TLDs). Neutron doses were measured with track etch dosimeters (TEDs), which consisted of allyl diglycol polycarbonate containing Cr-39 and were fabricated specifically for this test. Average dose rate values were generated by normalizing to exposure time.

Portable hand-held survey instruments were also used in the 1985 surveys to measure both gamma and neutron dose rates at some of the same locations as the TLD and TED readings. However, the coverage with portable instruments was not as complete as with TLD and TED measurements. The gamma dose rate measurements were made with two ion chamber instruments, an Eberline RO-3A (INEL) and an Eberline RO-3B (PNL). The 1985 neutron dose rate measurements were made using an Eberline PRN-4 and a SNOOPY instrument. Both instruments had BF_3 detectors with polyethylene moderators; the Eberline PRN-4 had a 9-inch diameter moderator sphere (INEL) and the SNOOPY had an 8.5-inch moderator cylinder (PNL) (EPRI NP-4887). The results of these measurements were presented in detail in EPRI NP-4887 and summarized in Appendix A.

Similar measurements were obtained in May 2001 at the same locations as the 1985 readings, as detailed in Appendix H. The 1985 and 2001 readings were obtained on the side wall at intervals on two vertical lines spaced at the 45 and 90-degree azimuths with respect to the 0-degree cask reference, as well as on the 45 and 90-degree radius of the lid and bottom of the cask. The locations of the readings on the cask are shown in Figures 3-1 and 3-2. An additional 39 gamma dose rate measurements were made in 2001 to determine the uniformity of the shielding around the circumference of the cask at several elevations. These additional readings were obtained at 30-degree increments circumferentially at the 4400 mm, 4298 mm, and 2701 mm elevations, as measured from the bottom of the cask. The locations of the 2001 measurements are detailed in Appendix H, and the results are given in Appendix A.

The 2001 readings were made with environmental TLDs and an Eberline RO-20 for the gamma dose rates, and an Eberline E-600/NRD digital portable meter for the neutron dose rates. The environmental TLDs consist of LiF and a magnesium copper phosphate phospor. The Eberline RO-20 is an air-filled ion chamber instrument, comparable to the RO-3A used in 1985. The RO-20 was calibrated against a Cs-137 source to an accuracy of ±5% (at 2 standard deviations); the accuracy in field operation is considered to be no better than ±10% and is more likely ±20%. The digital Eberline E-600 meter was fitted with an Eberline Neutron rem Detector (NRD), which consists of a BF_3 detector tube and a 9-inch polyethylene sphere. The accuracy was calibrated against a Cf-252 source to within ±10% (at 2 standard deviations); the accuracy in field operation is considered to be no better than ±30%. The neutron response of Eberline NRD decreases nonlinearly with decreasing neutron energy, and is approximately

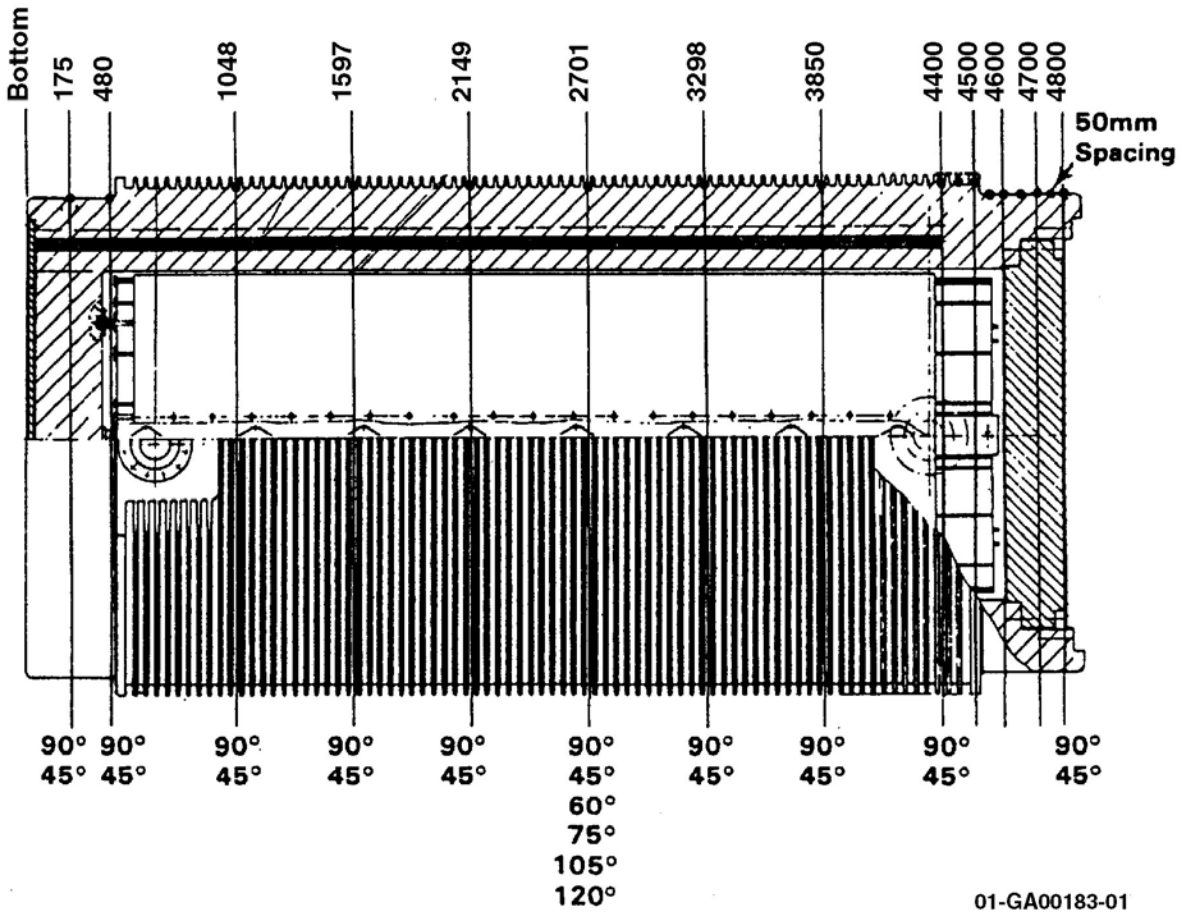

Figure 3-1. Vertical location of the gamma and neutron dose rate readings on the sidewall of the CASTOR V/21 cask. Locations of the readings at the 45 and 90-degree azimuths are given as elevation (in millimeters) from the bottom of the cask. The bottom of the cask in the figure is on the left.

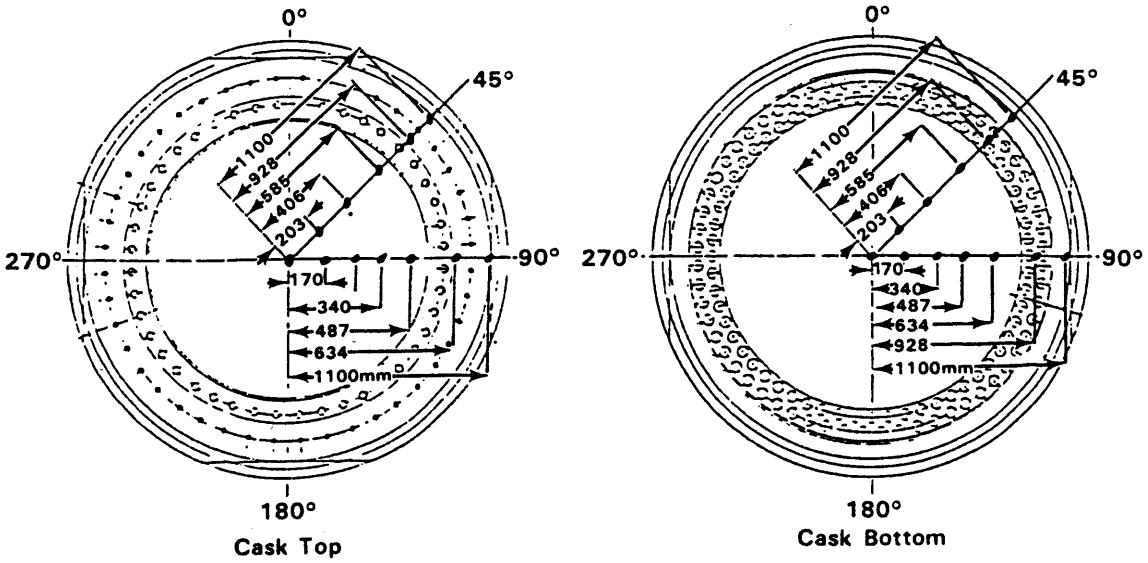

Figure 3-2. Radial locations of the gamma and neutron dose rate readings on the top and bottom surfaces of the cask. Locations of the readings are given as radial displacement (in millimeters) from the center on the 45 and 90-degree azimuths.

3 rem/n/cm^2 at 150 keV (the approximate energy of the unmoderated neutrons of the spent fuel [EPRI NP-4887]) and 0.7 rem/n/cm^2 for thermal neutrons. The sensitivity of the neutron instrumentation used for the 1985 measurements was not included in the EPRI NP-4887 report and is unknown at this time.

The 2001 neutron dose measurements were not attempted with TEDs, because the 1985 TED configuration could not be duplicated at the INEEL. An attempt was made to measure the neutron dose with Cr39 TEDs supplied by ICN Worldwide Dosimetry Service, Inc. However, these TEDs significantly underestimated the neutron dose equivalent because the ICN TED was not sensitive to neutron energies less than 250 keV, the range of neutron energies measured for the cask in 1985. (EPRI NP-4887)

For the sidewall contact readings, the TLD dosimeters were held by an external frame at the appropriate elevations, with the TLDs in contact with the cask cooling fins (i.e., positioned between the frame and the cask wall). The TLD dosimeters for the cask bottom were placed in precut cavities in two thicknesses of plywood placed under the cask. The dosimeters for the top of the cask were suspended from a frame above the primary lid; as in the 1985 measurements, the secondary lid was not in place when the measurements were made in 2001. Unfortunately, high winds dislodged some of the suspended TLDs during the course of the exposure, dropping the dosimeters onto the primary lid and scrambling their sequence. Although they were reattached to the frame 12 to 15 hours later (after discovery of the situation), they yielded inconsistent results. Therefore, the analyses of dose rates on the cask top relied only on the RO-20 readings. Except for the readings on the cask top, the TLD and RO-20 gamma readings compared favorably.

3.3 Observations

In general, the gamma dose rates in 2001 were substantially lower than the 1985 measurements, as was expected from decay considerations. Peak sidewall gamma dose readings were less than 12 mR/hr, substantially less than the peak gamma rate of 140 mR/hr that was observed in 1985. The peak readings on the cask sidewall occurred at locations corresponding to the position of the top and bottom flow nozzles of the fuel assemblies within the cask. The gamma dose rates for the active fuel region were less than 2 mR/hr. The gamma dose rates for the top and bottom surfaces of the cask peaked in the center, at approximately 10 and 7 mR/hr, respectively.

Within the uncertainties of the measurements and differences in the responses of the 1985 and 2001 instruments, the 1985 and 2001 neutron dose measurements resulted in reasonably similar readings, with sidewall readings peaking at approximately 15 mrem/hr. The sidewall neutron dose rate peaks occurred at the same sidewall elevation in the 2001 and 1985 measurements and corresponded to the top of the polyethylene rods in the cask wall. The neutron dose rates at the top and bottom surfaces peaked at the center at approximately 45 and 55 mrem/hr, respectively. Within the uncertainty in the measurement, the 2001 neutron dose rate readings were comparable to the 1985 readings.

The gamma and neutron dose rate profiles showed no evidence of failure or degradation of the shielding.

3.3.1 Gamma Contributors

In 1985, the gamma energy spectrum of the radiation from the cask sidewall, top, and bottom surfaces was analyzed by germanium spectrometry. Spectral analysis identified the source radionuclides for the gamma radiation at the cask surfaces as ^{60}Co, ^{144}Ce/Pr, ^{137}Cs, ^{134}Cs, and ^{154}Eu. The relative intensity distribution of the various gammas from these radionuclides was not given. However, from the gamma spectra, ^{60}Co and ^{144}Ce/Pr were identified as the primary components to the radiation at the top and bottom of the cask, and ^{144}Ce/Pr as the primary component on the sidewall. The dominance of ^{60}Co at the top and bottom was due to the activation of the stainless steel flow nozzles on the ends of the fuel

assemblies. The remaining radionuclides, including the ^{144}Ce/Pr, are fission products present in the spent fuel.(EPRI NP-4887)

Because of the decay time and the relatively short half-lives of some of these radionuclides, the spectrum of contributors to the 2001 dose rate readings was expected to shift significantly from the 1985 spectrum, and the 2001 dose rate readings were expected to be substantially lower than the 1985 readings. Table 3-1 summarizes the decay-normalized gamma intensity of these radionuclides in 2001, assuming a 16-year decay time. The decay adjustments indicate that the primary contributors in 1985 to the gamma dose rate at the external surfaces of the cask were substantially reduced by 2001. The gamma contribution from ^{60}Co in 2001 is expected to be only approximately 10% of the 1985 levels, and the ^{144}Ce/^{144}Pr has effectively decayed away and no longer contributes to the dose rate at the external surfaces of the cask.

Table 3-1. Decay-normalized gamma intensity from radionuclides identified as major contributors to the gamma dose rate in 1985, assuming a 16-year decay time.

Radionuclide	Half-life[a]	Decay-Adjusted Normalized Intensity in 2001
^{60}Co	5.271 y	0.12
^{144}Ce/^{144}Pr	284.6 d/17.28 m	6.7×10^{-7}
^{137}Cs	30.17 y	0.69
^{134}Cs	2.065 y	4.7×10^{-3}
^{154}Eu	8.59 y	0.28

a. F. W. Walker, J. R. Parrington, and F. Feiner, Nuclides and Isotopes, Fourteenth Edition, General Electric Company, San Jose, CA, 1989.

3.3.2 Gamma Dose Rates on the Sides of the Cask

The gamma dose rates were acquired in 2001 at the same locations as the 1985 readings. The gamma results for 2001 and 1985 are summarized in Appendix A. As shown graphically in Figure 3-3, the 2001 gamma dose rate profiles for the 45 and 90-degree azimuths on the sidewall are qualitatively similar to the corresponding 1985 profiles, and show distinct gamma dose rate peaks near the bottom (480 mm elevation) and top areas (≈4400 mm elevation) of the side wall. The peaks correspond to the locations of the bottom and top flow nozzles of the PWR assemblies within the cask and are presumed to be due to ^{60}Co in the steel flow nozzles EPRI NP-4887, GNS Drawing 49001-E-01, GNS CASTOR SAR Figures 7.3-5 and 7.3-6).

The peak gamma dose rate (TLD) values decreased more than 90% from the 1985 values in agreement with the above decay-based projection. At the 480-mm elevation at the 45 and 90-degree azimuths, the peak dose rate dropped from 140 and 125 mR/hr in 1985 to 4.4 and 8.1 mR/hr, respectively, in 2001. At the 4400-mm elevation, the peak dose rates decreased from 118 and 134 (for the 45 and 90-degree azimuths) in 1985 to 8 and 11.1 mR/hr, respectively, in 2001. Similarly, the readings in the active fuel zone, corresponding to elevations of 1048 through 3850 mm, decreased approximately 95%, from 36.0 mR/hr (1 σ = 4.05) and 30.5 mR/hr (1 σ = 19.4) in 1985 to 1.32 (1 σ = 0.19) and 2.25 mR/hr (1 σ = 1.17) for the for the 45 and 90-degree azimuths, respectively, in 2001.

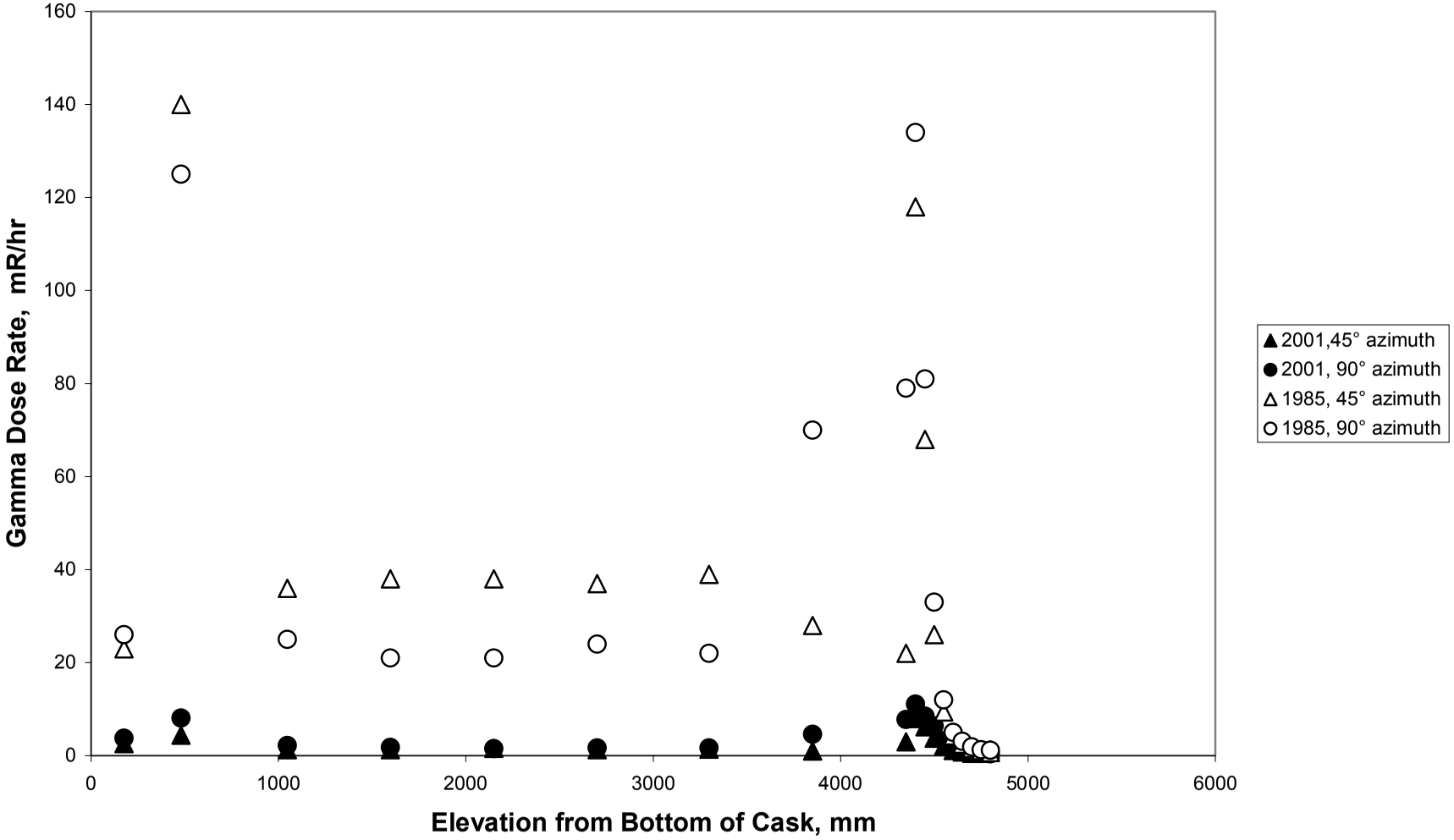

Figure 3-3. Comparison of the 2001 and 1985 gamma dose rates on the cask sidewall at the 45 and 90-degree azimuths.

The 1985 gamma data in Figure 3-3 show a slight difference in the gamma profiles for the 45 and 90-dgree azimuths, primarily in the shoulder below the peak at 4400 mm in the 90-degree profile. The shoulder in the 90-degree profile was reproduced in the 2001 gamma dose rate measurements, as shown in Figure 3-4. The shoulder at 3850–4400-mm elevation of the 90-degree profile may be a consequence of the decreased shielding due to the flat milled seat at that location for the upper, bolt-on trunnion. As can be seen from the error bars in Figure 3-4, the dose rate peaks at each end show some differences in intensity between the two azimuths that may be statistically different, with slightly higher readings at the 90-degree azimuth, and is probably due to the proximity of three fuel assemblies to the cask wall at this azimuth. There is no significant difference in the two azimuthal sets of readings in the active fuel zone of the cask (1048 through 3850 mm).

In 2001, 39 additional gamma dose readings were acquired at three sidewall elevations around the full circumference of the cask to determine the circumferential and axial uniformity of the cask shielding. These readings were taken at 30-degree intervals at the 4400, 4298, and 2701-mm elevations. The full circumference readings are summarized in Appendix A and in Figure 3-5, along with 45–120-degree sector readings at other elevations. The gamma data show a distinct but short-range axial non-uniformity in dose rates comparable to the profiles shown in Figures 3-3 and 3-4. The highest gamma dose rate readings occurred at 4400-mm elevation, with readings that varied circumferentially from approximately 10 to 25 mR/hr. These high readings are due to the ^{60}Co in the upper flow nozzle of the fuel assemblies. The readings at 4298-mm and 2701-mm elevation are substantially lower, generally less than 2 mR/hr. However, the readings at the 4400 and 4298-mm elevations exhibited some azimuthal variations. The set of readings at 4400 mm exhibited peaks at 0, 90, 180, and 270-degree azimuth, while the readings at 4298 mm exhibited two peaks at 90 and 270-degree azimuth. These readings correspond to locations with three fuel assemblies in close proximity to the cask wall.

3.3.3 Neutron Dose Rates on the Sides of the Cask

The neutron dose rate profiles for the cask sidewall in 1985 and 2001 are shown in Figure 3-6. The neutron dose rate data for both 1985 and 2001 show considerable scatter due to the measurement uncertainty of ±30%. Because of the extremely long decay half-life of the fissile radionuclides in the fuel, the neutron dose rates for 1985 and 2001 should be comparable within the uncertainty of the measurements. The maximum neutron dose rates in 1985 and 2001 are comparable at approximately 16 mrem/hr. However, as indicated by Figure 3-6 and the summary in Table 3-2, much of the 2001 neutron dose rate data for the active fuel zone are approximately half the 1985 values. It is unlikely that the lower values in 2001 pertain to changes in shielding; the difference most likely is due to the use of two different methods for neutron dosimetry. The lower readings in 2001 were obtained with the Eberline E-600/NRD and suggest a lower response sensitivity to thermalized neutrons than the TED used in 1985. This possibility is suggested by the shape of the 2001 profile in Figure 3-5 in which the E-600/NRD readings are lower than the TED in the polyethylene-shielded fuel zone, yet comparable to the TED readings at elevations above 4400 mm, above the polyethylene rods within the cask wall. The manufacturer's response curve shows a decreasing sensitivity with decreasing neutron energy, from approximately 3 rem/n/cm^2 at 150 keV to 0.7 rem/n/cm^2 at 1 eV (Eberline). Depending on the extent of thermalization of the neutrons by the polyethylene shield rods, the E-600/NRD response for the neutrons from polyethylene-shielded zone of the side wall could easily be only 50% of the response for the less moderated neutrons above the polyethylene shield.

The 2001 data in Figure 3-6 do not show any increase in the neutron dose rate readings for sidewall elevations below 4400 mm, which corresponds to the top of the polyethylene shielding rods. This indicates that major degradation or slumping of the polyethylene shielding rods has not occurred.

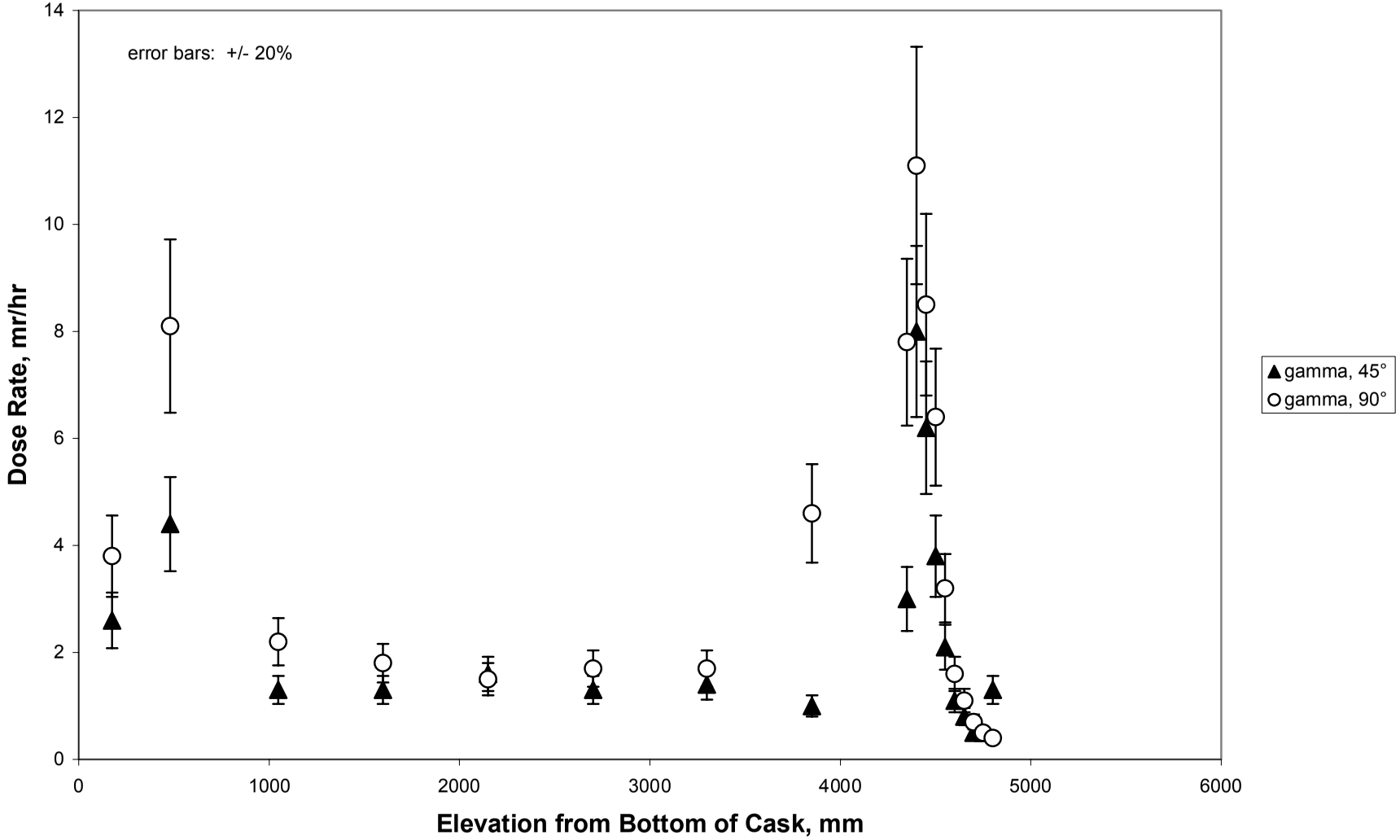

Figure 3-4. Gamma dose rates in 2001 as a function of elevation for the 45 and 90-degree azimuths on the sidewall of the cask. The dose rate profiles for the two azimuths appear to differ slightly at the ends of the cask.

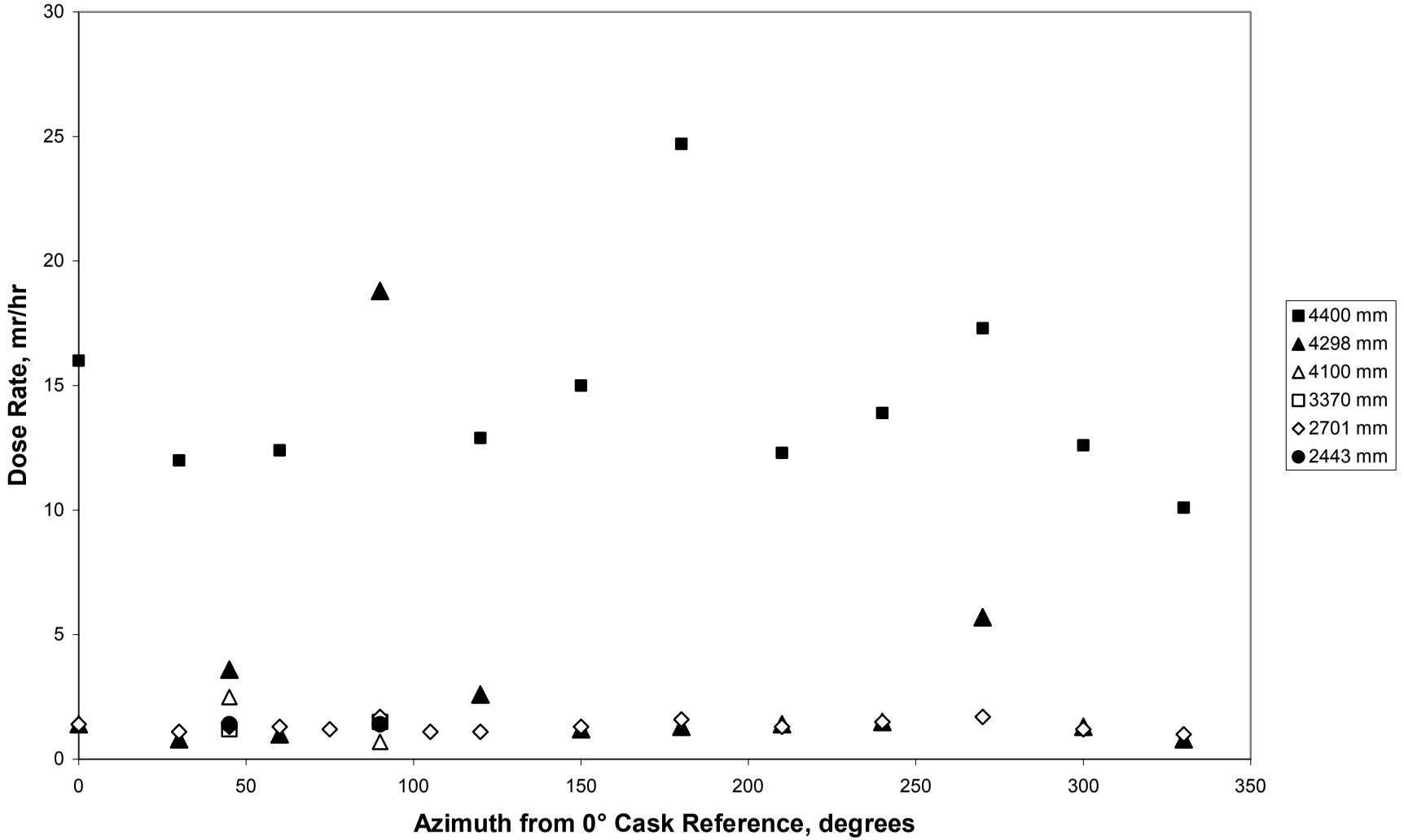

Figure 3-5. Circumferential profiles of gamma dose rates on the cask sidewall, acquired in 2001 as a function of azimuth and elevation. Readings were taken at the 4400, 4298, and 2701-mm elevations in 30-degree increments around the entire cask circumference.

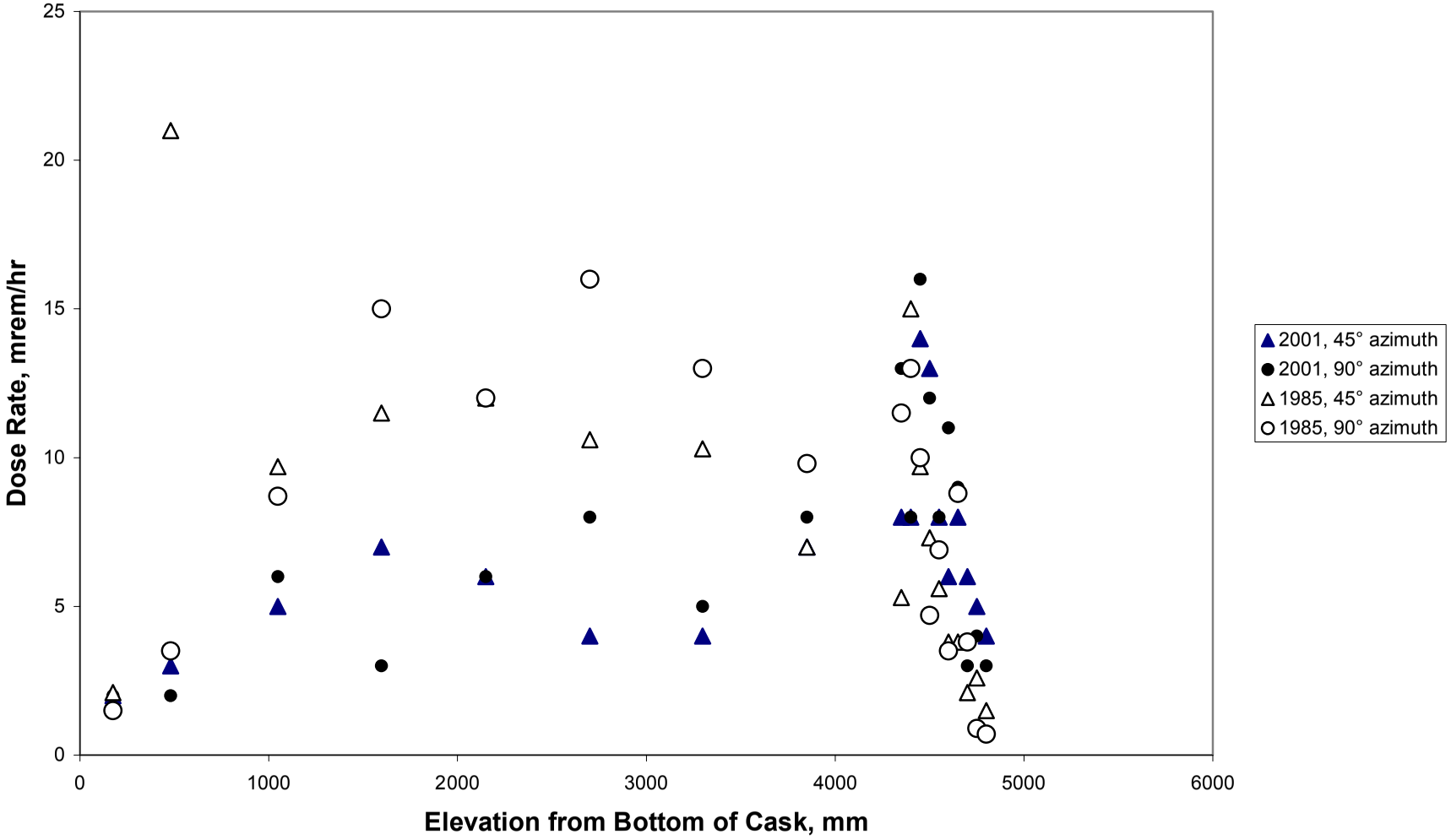

Figure 3-6. Comparison of the neutron dose rates measured in 1985 and 2001 on the cask sidewall at the 45 and 90-degree azimuths.

Table 3-2. Maximum and average neutron dose rates for the 1985 and 2001 cask sidewall readings.

	1985 Neutron Dose Rates		2001 Neutron Dose Rates	
	45° Azimuth	90° Azimuth	45° Azimuth	90° Azimuth
Maximum Reading, mrem/hr	15	16	14	16
Average of Full Profile (1 σ), mrem/hr	7.83 (5.17)	7.96 (4.95)	6.56 (3.11)	7.06 (4.05)
Average over Fuel Zone (1 σ), mrem/hr	10.18 (1.77)	12.42 (2.85)	5.5 (1.38)	6.0 (1.90)

In 2001, 39 additional neutron dose readings were acquired at three sidewall elevations around the full circumference of the cask to determine the circumferential and axial uniformity of the cask shielding. The readings were obtained at the same locations as the circumferential gamma readings discussed above. The results for the neutron dosimetry are given in Appendix A and in Figure 3-7. The average circumferential readings at 4400, 4298, and 2701 mm are 11.3 mrem/hr (σ = 2.8 mrem/hr), 9.9 mrem/hr (σ = 1.8 mrem/hr), and 6.5 mrem/hr (σ = 1.6 mrem/hr) respectively. The readings at 4400 and 4298-mm elevation appear to be statistically identical and are in good agreement with the neutron dose rate data generated in 1985 as shown in Figure 3-8. The lower average at 2701 mm is most likely a function of the response curve of the NRD unit.

At each elevation, the circumferential readings show substantial scatter that is consistent with the uncertainty in the measurements (±30%). While the circumferential readings at 4298 and 2701-mm elevation appear to have similar profiles, the similarity is most likely a statistical artifact. There is no obvious trend in the circumferential readings that would indicate problems with the uniformity or integrity of the shielding. The range of neutron dose rates in these tests is consistent with the other neutron dose rate values obtained 2001 and 1985.

In 1985, neutron dose rate readings were made at 1-degree intervals from 72 to 77-degree azimuth (with respect to the 0-degree cask reference) at the 2149-mm elevation of the sidewall of the cask. The purpose of the original readings was to test for local nonuniformity of shielding due to the circumferential spacing of the cylindrical polyethylene shielding rods in the cask wall. At the time, no significant nonuniformity in neutron dose rate was observed. The test was repeated in 2001; the results are summarized in Figure 3-9 along with the 1985 results. Again, no significant nonuniformity was found in 2001. The measured neutron dose rates varied from 5 to 7 mrem/hr. However, as shown in Figure 3-9, the azimuthal profile of the 2001 neutron dose readings appears to duplicate the minor variations in the 1985 gamma and neutron dose rate profiles. The data do indicate that the stacking configuration of the polyethylene rods at this location has not changed between 1985 and 2001, and the effectiveness of the shielding has not diminished.

3.3.4 Gamma Dose Rates on the Top and Bottom Surfaces of the Cask

The gamma dose rate data for the top and bottom surfaces of the cask are summarized in Appendix A. Figures 3-10 and 3-11 graphically compare the gamma dose rate readings for the 45 and 90-degree azimuths in both the 1985 and the 2001 tests. The 2001 gamma dose rate values in the fuel region are approximately 15–20% of the corresponding 1985 values, consistent with ^{60}Co decay considerations. (Both the 1985 and 2001 measurements were taken with the secondary lid removed from the cask.) As shown by Figures 3-10 and 3-11, the dose rate profiles are fairly flat, with no spikes. The data for the 45 and 90-degree azimuths for the top and bottom are in very good agreement, within the uncertainty of the measurement.

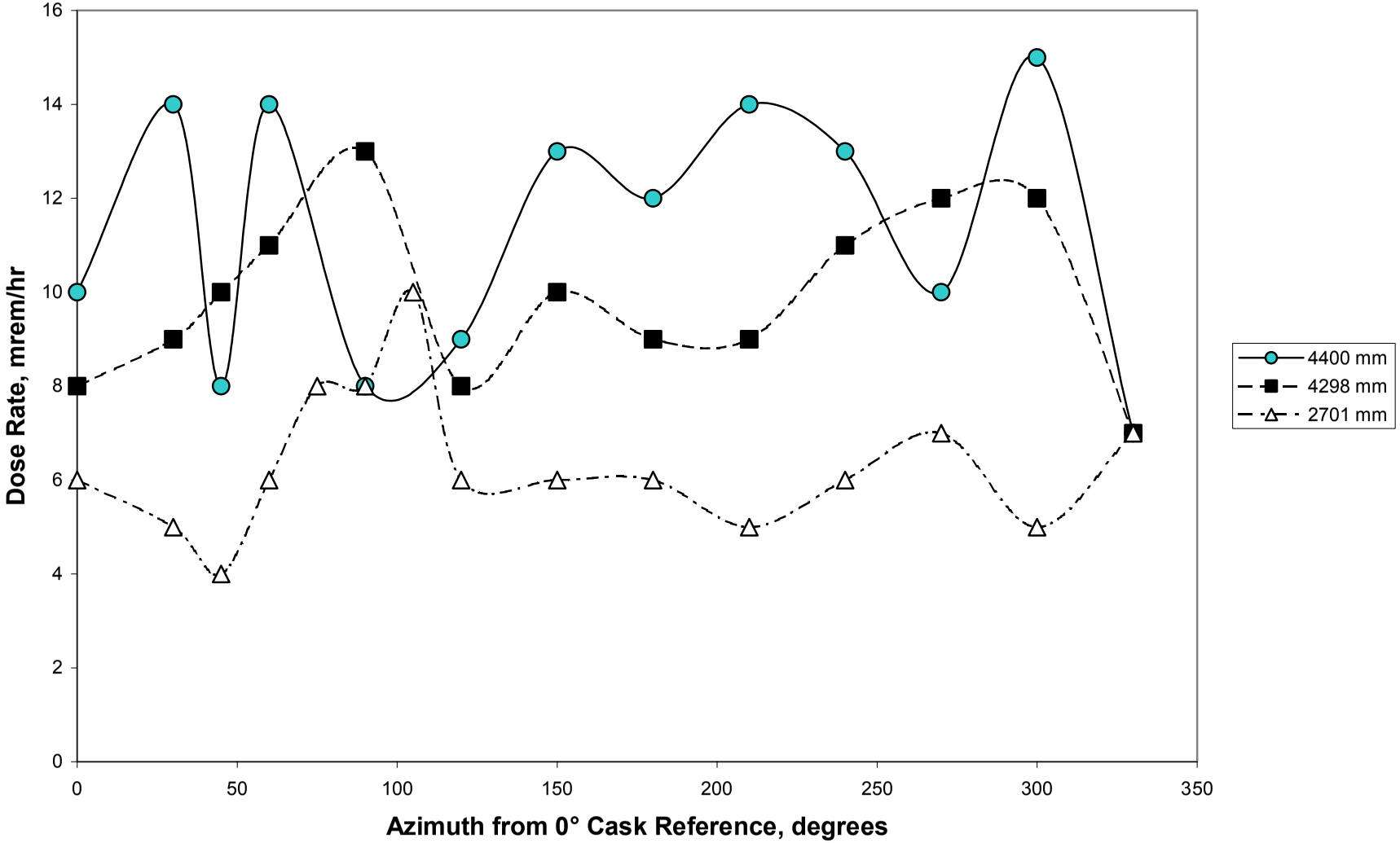

Figure 3-7. Circumferential profiles of neutron dose rates on the cask sidewall, acquired in 2001 as a function of azimuth and elevation. Readings were taken at the 4400, 4298, and 2701-mm elevations in 30-degree increments around the entire cask circumference.

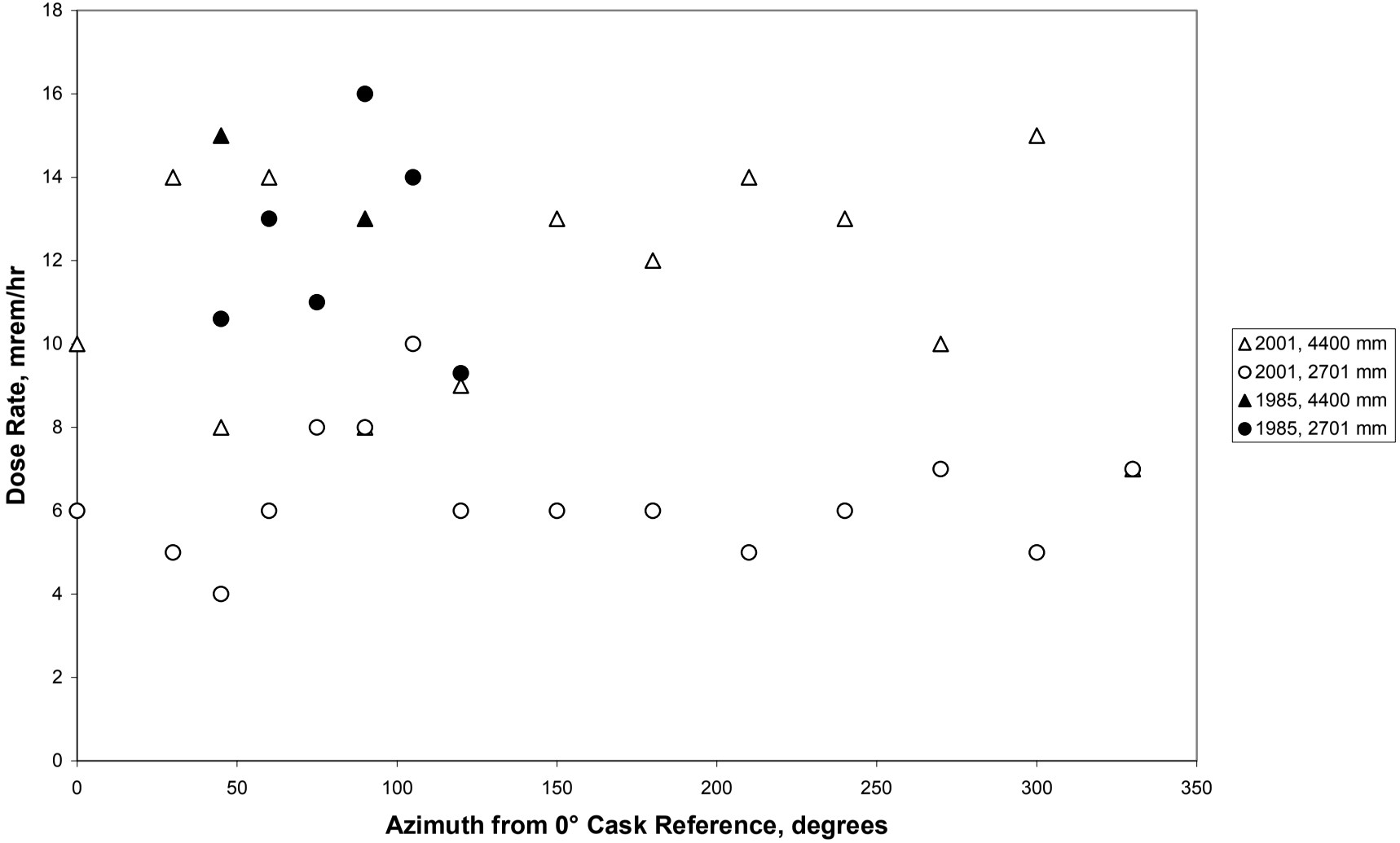

Figure 3-8. Comparison of the 1985 and 2001 neutron dose rates as a function of azimuth and elevation. Although the 1985 neutron dosimetry is limited to the 45–120-degree sector, the 2001 circumferential data compare favorably.

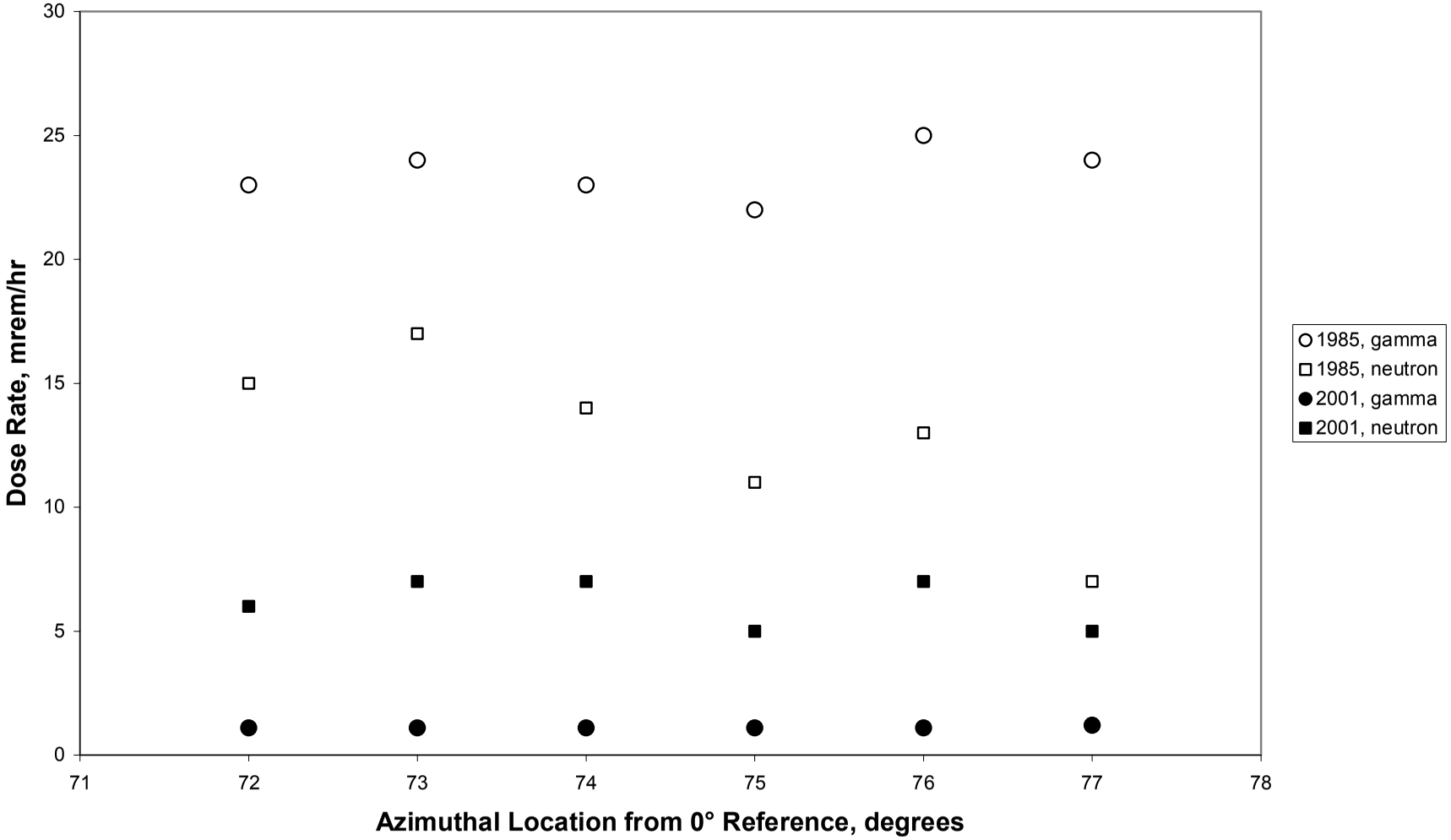

Figure 3-9. Local variations is shielding due to the stacking configuration of the cylindrical polyethylene rods. Plot compares the 1985 and the 2001 data for gamma and neutron radiation.

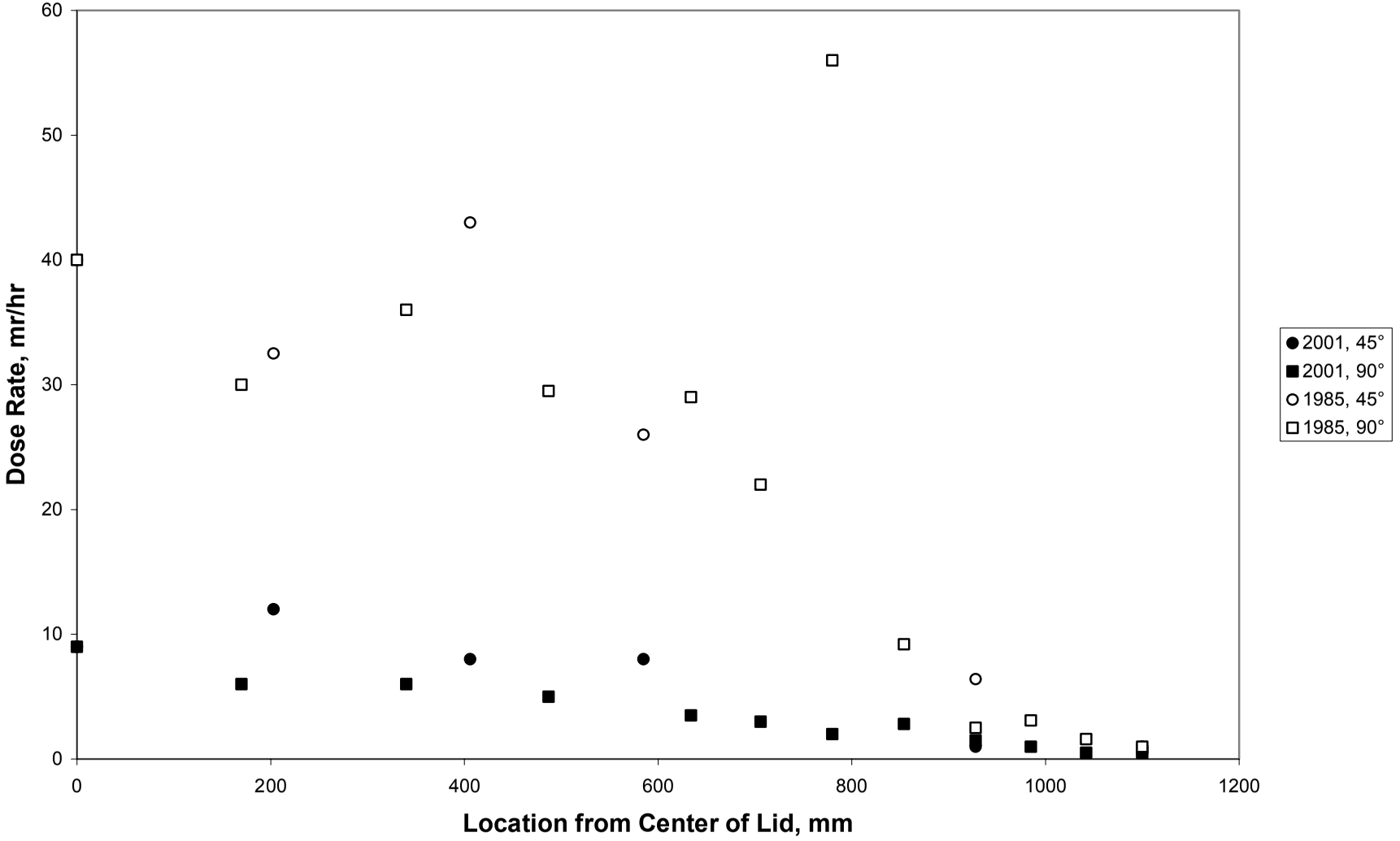

Figure 3-10. Radial gamma dose rate profile on the top surface of the cask. The plot compares the 2001 and 1985 readings at the 45 and 90-degree azimuths.

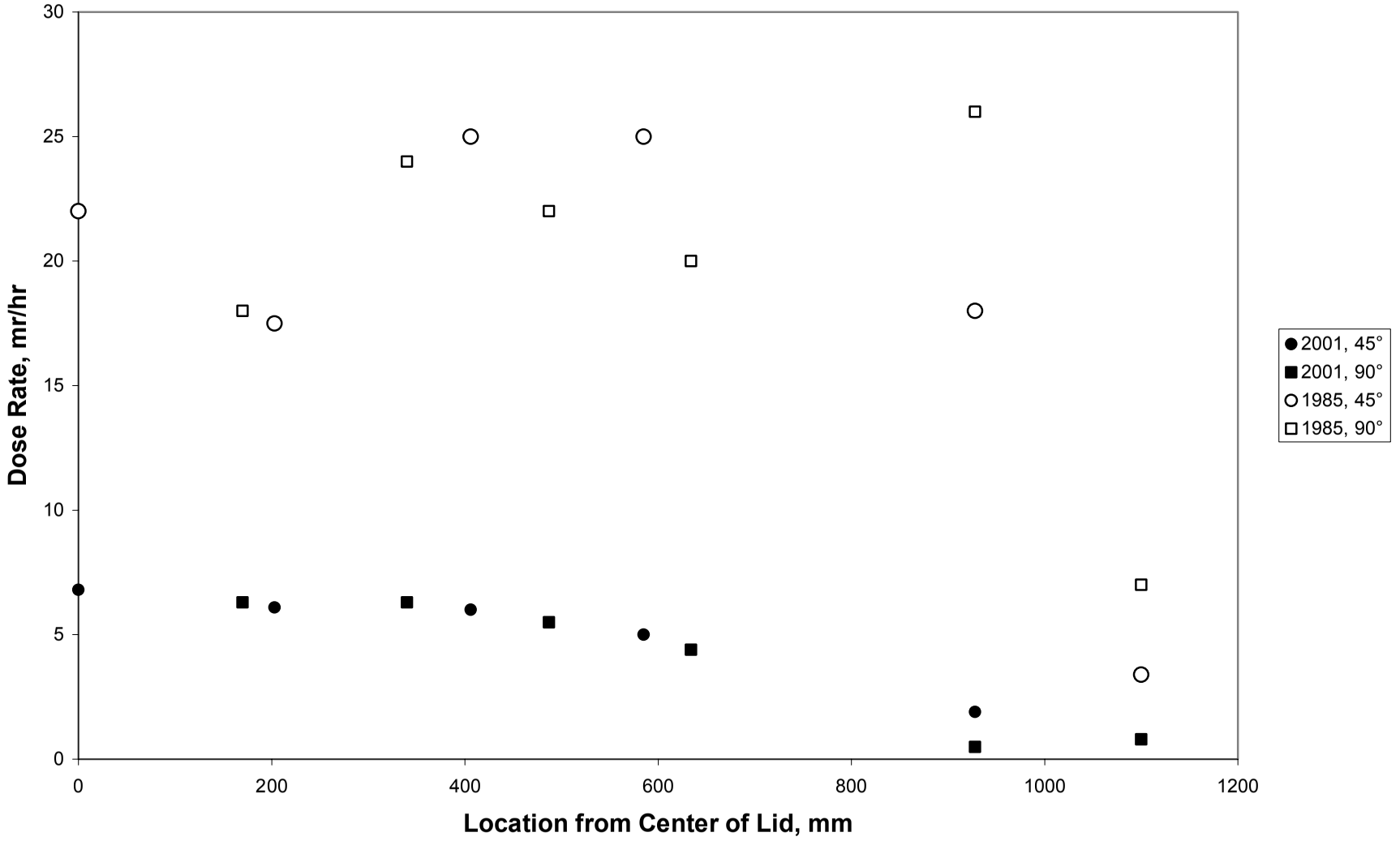

Figure 3-11. Radial gamma dose rate profile on the bottom surface of the cask. The plot compares the 2001 and 1985 readings at the 45 and 90-degree azimuths.

Figures 3-12 and 3-13 compare the 2001 and 1985 neutron dose rate data for the top and bottom surfaces of the cask. As shown in Figure 3-12, the 2001 and 1985 neutron dose rates for the cask top are identical both in profile shape and in magnitude. As in the 1985 measurements, the neutron dose rate peaks near the center of the cask lid at approximately 45 mrem/hr.

Figure 3-13 compares the neutron dose rate data for the bottom of the cask from the 2001 and 1985 tests. Unlike the top surface, the 2001 neutron dose rates are consistently higher than the corresponding 1985 data. Within the radius of the fueled area, the 2001 neutron dose rates are approximately twice as high as the 1985 values; the difference is even greater beyond the fueled area. The 2001 neutron dose rates at the 90-degree azimuth ranged from 53 mrem/hr near the center to 24 mrem/hr at the outer edge; whereas the 1985 readings ranged from 31 to 1.6 mrem/hr, respectively. In addition, unlike the top surface readings, the 45-degree azimuth readings are consistently lower than the readings at the 90-degree azimuth. The 45-degree azimuth readings in 2001 ranged from approximately 55 mrem/hr in the center to 12 mrem/hr at the outer edge. By comparison, the 1985 neutron dose rates at the 45-degree azimuth ranged from 41 to 3 mrem/hr.

The disparity in the 1985 and 2001 readings may be in part an artifact of the difference in the cask orientation in 1985 and 2001 and the proximity of the detector to structures that thermalize and scatter neutrons. In 1985, the dose rate measurements were made with the cask in a horizontal orientation resting on a rail car in the TAN Warm Shop. Floors and structures that could thermalize and scatter or reflect neutrons back to the detector were many feet from the cask bottom and from the detector. In 2001, the measurements were made with the cask upright on the storage pad. The cask was hoisted approximately 43 to 48 cm (17 to 19 inches) above the concrete pad for access to the bottom of the cask. This also put the detector relatively close to the concrete surface. The proximity of the concrete surface allows it to thermalize neutrons and/or backscatter the neutrons to the detector. For the same neutron source, the neutron dose rates measured in the configuration on the pad could be 40 to 50% higher due to the backscatter than the dose rates measured on the bottom of a horizontal cask in the Warm Shop. The scattering process may have also broadened the neutron field, increasing the apparent dose rate at the periphery of the bottom surface.

3.3.5 Conclusion

The 1985 radiation measurements demonstrated that the shielding performance of the CASTOR V/21 cask exceeded the design goal of less than 200 mrem/hr activity at the external surface of the cask. The 2001 radiation measurements have demonstrated that the shielding performance of the cask has not degraded since 1985.

The 2001 dose rate data supports the conclusion that gamma dose rates have decreased since 1985, as would be expected due to radioactive decay. Because of differences in cask configuration and location, some of the 2001 neutron dose measurements appear higher than those taken in 1985. This is caused by backscatter from the concrete pad. There is no obvious evidence of degradation in the performance of the gamma or neutron shielding between 1985 and 2001 that calls into question the long-term ability of the cask to maintain adequate shielding.

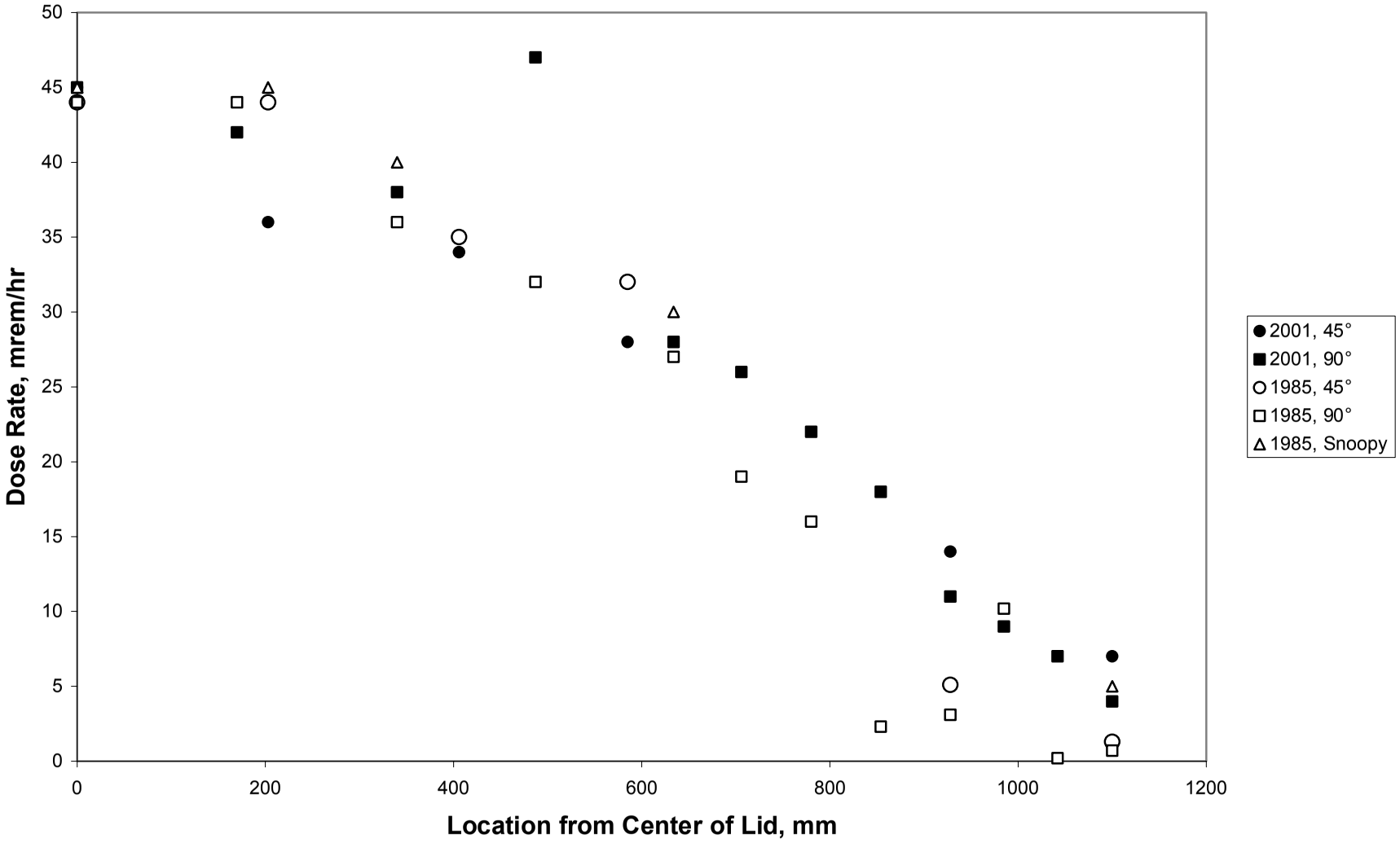

Figure 3-12. Radial neutron dose rate profile on the top surface of the cask. The plot compares the 2001 and 1985 readings at the 45 and 90-degree azimuths.

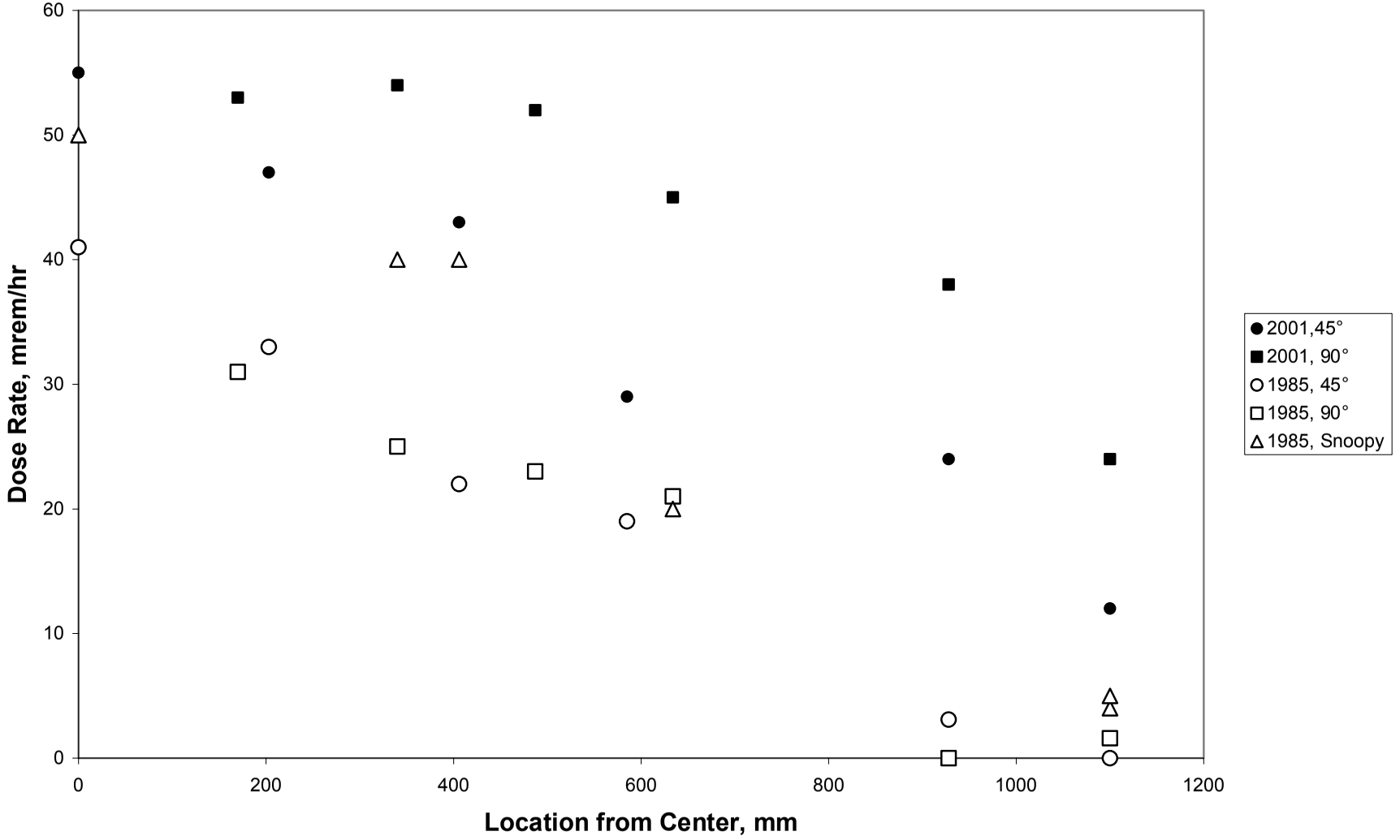

Figure 3-13. Radial neutron dose rate profile on the bottom surface of the cask. The plot compares the 2001 and 1985 readings at the 45 and 90-degree azimuths.

4. GAS SURVEY

4.1 Background

A primary concern of the examination of the CASTOR V/21 cask in late 1999 and early 2000 was the integrity of the cask lid seals and the containment of fission products. Evidence of failure of the cask lid seals may be the loss of the helium backfill and the ingress of ambient air. This condition can cause the corrosion of the spent fuel cladding during long-term storage. As part of the present cask examination, samples of the cover fill gases were analyzed prior to opening the cask and compared with earlier gas analysis results.

The fill gas in the cask was sampled and analyzed several times in 1985 during performance testing of the cask to determine the integrity of the cask lid seals and the spent fuel cladding. Subsequently, the fill gas was sampled and analyzed in 1986 and in 1994 through 1999 prior to opening the cask for the present examination. Gas sample analyses included mass spectroscopy and radiochemical analysis. The results of those analyses are summarized in the following sections. The analyses found primarily helium, indicating satisfactory performance of the cask seals. Further, the absence of fission products in the assay, indicated complete integrity of the fuel cladding for the entire 14-year storage period. Because of the lack of evidence of a fuel breach, no volatile gases or fines were assumed to have been released, so analysis was not done for their presence.

4.2 1985 Data

In 1985, the cask cover gas was sampled several times during cask performance testing to evaluate the integrity of the spent fuel rods and the cask lid seals. Each sample was collected in a separate 500-cc stainless steel cylinder sealed only with quick disconnect-fittings (without bellows-sealed valves). The cylinders were checked for leaks prior to sampling. (PNNL-11576) However, the 1985 cover gas analyses indicated contamination of the samples with air. (EPRI NP-4887) The contamination was probably caused by the quick disconnect-fittings on the sample cylinders and may have occurred during sampling, shipment, or handling prior to analysis at Lawrence Livermore National Laboratory (LLNL). Argon was probably introduced at LLNL when it was necessary for valves to be fitted to the cylinder quick-disconnects in an argon atmosphere to perform the sample analyses. In many cases, the contamination was made more severe by the collection of only small amounts of cask cover gas, presumably due to short equilibration times between the cask and the sample bottle during the gas collection procedure. The end effect of small, diluted samples on the cover gas analyses was to increase detection limits, increase measurement uncertainties, and introduce questions of sample validity. (EPRI NP-4887, PNNL-11576)

The results of the 1985 LLNL gas analyses, originally presented in EPRI NP-4887, are summarized in Table 4-1. The common fixed gases with masses less than 100 were analyzed by mass spectrometry. Only N_2, O_2, He, Ar, and CO_2 are detected at concentrations above 0.01% in any of the samples. Analyses of the other species reported are of marginal reliability. In the EPRI NP-4887 report, water was reported as a contaminant at a level greater than 0.01%. Because the water probably was due to residual physisorbed moisture on sample vessel walls and in the mass spectrometer inlet system, it was omitted in Table 4-1. The accuracy of the mass spectra measurements is noted in Table 4-1. The magnitude and the variations in the N_2 and O_2 gas analysis data clearly indicate that significant amounts of air were introduced in each gas sample.

Table 4-1. 1985 casks gas sample composition (volume percent). (From EPRI NP-4887. Permission to use this copyrighted material is granted by EPRI.)

LLNL Sample No.	He	N_2	O_2	Ar	CO_2	CO	N_2O	H_2
1	89.05	6.02	1.35	3.50	0.05	<0.1	<0.01	<0.01
2	69.30	21.90	5.97	2.80	0.03	<0.01	<0.01	<0.01
3	62.51	25.57	6.69	5.15	0.03	<0.1	<0.01	<0.01
4	59.59	17.59	4.11	18.66	0.05	<0.01	<0.01	<0.01
5	<0.01	95.34	1.18	3.46	0.02	<0.01	<0.01	<0.01
6	<0.01	90.58	6.81	2.58	0.02	<0.01	<0.01	<0.01
7	0.03	68.79	3.13	27.95	0.06	<0.01	0.019	<0.01
8	0.04	70.08	8.43	21.29	0.15	<0.01	<0.01	<0.01
9	70.59	14.23	5.95	9.09	0.06	<0.1	<0.01	0.018
10	32.38	50.55	13.31	3.70	0.05	<0.01	<0.01	<0.01
11	65.59	1.56	0.16	32.58	<0.01	<0.01	<0.01	<0.01
12	<0.01	76.94	20.26	2.75	0.05	<0.01	<0.01	<0.01
13	0.05	74.92	11.44	13.43	0.12	<0.01	0.015	0.016
14	<0.01	73.95	18.77	7.22	0.06	<0.01	<0.01	<0.01
15	0.048	85.63	5.56	8.53	0.06	<0.01	<0.01	0.16
16	0.068	91.06	0.16	8.46	0.04	<0.01	<0.01	0.21

a. Species present in mass spectra at 0.01% or more. Accuracy of these measurements is ± 0.2% of the reported values.

The 1985 gas samples were also analyzed for ^{85}Kr and ^{14}C content. The 1985 report identified that ^{85}Kr concentrations in the samples ranged from <0.02 to 0.4 pCi/cc, which was marginally detectable in the 1985 analyses, while the ^{14}C concentrations ranged from 0.6 to 7.9 pCi/cc. The amounts of ^{85}Kr and ^{14}C are relatively low and are what would be expected to result from crud, not a leaking fuel rod. (EPRI NP-4887)

4.3 1986 Post Cask Performance Test Gas Sampling Data

Post Cask Performance Test Gas Sampling was conducted in 1986. Table 4-2 presents results of the analyses of CASTOR V/21 cask gas samples performed by mass spectrometry and gamma spectrometry (for ^{85}Kr) in 1986. (PNNL-11576)

With the exception of one sample (GN-8A), the analysis results in Table 4-2 (taken from Table 5-3 in reference PNNL-11576) indicate that the cask fill gas consisted primarily of helium with only small amounts of residual air constituents. Sample GN-8A, however, obviously was grossly contaminated with air during sampling or subsequent handling. The scatter in the nitrogen data (excluding GN-8A) is approximately an order of magnitude. The N_2 data scatter indicates that the air contamination is most likely an artifact of the sampling process and is not representative of the cask cover gas composition. Four of the samples in Table 4-2 were also analyzed for H_2 and ^{85}Kr; the ^{85}Kr concentration was less than 0.06 pCi/mL. The relatively low amounts of ^{85}Kr detected indicate that no leaking fuel rods were present.

Table 4-2. 1986 cask gas sample composition (volume percent). (Taken from PNNL-11576)

Sample No.	Sample Date	He	N_2	O_2	Ar	CO_2	H_2	Radionuclide Concentration, pCi/mL ^{85}Kr
GN-3A	3-05-86	99.0	0.82	0.2	≤0.01	≤0.01	—	—
GN-3B	3-05-86	99.7	0.27	0.06	≤0.01	≤0.01	—	—
GN-4A	3-17-86	99.86	0.11	0.03	≤0.01	≤0.01	—	—
GN-4B	3-17-86	99.81	0.15	0.04	≤0.01	≤0.01	—	—
GN-5A	3-24-86	99.84	0.13	0.03	≤0.01	≤0.01	—	—
GN-5B	3-24-86	99.83	0.14	0.03	≤0.01	≤0.01	—	—
GN-8A	6-27-86	65.3	29.1	4.2	0.36	1.1	—	—
GN-9A	8-15-86	99.8	0.05	0.002	0.001	0.001	0.15	<0.027
GN-9B	8-15-86	99.78	0.05	0.006	0.001	0.002	0.16	<0.028
GN-10A	9-26-86	99.8	0.03	<0.01	≤0.01	≤0.01	0.17	<0.024
GN-11A	12-08-86	99.8	0.06	0.01	≤0.01	≤0.01	0.10	<0.057

4.4 1994 Through 1999 Data

The fill gas in the CASTOR V/21 was periodically sampled and analyzed from 1994 through 1999 under the INEEL Spent Fuel Behavior (SFB) Study project beginning in FY 1994. This project was combined with the Long-Term Storage Monitoring (LTSM) Program beginning in FY 1996. The objective of the SFB Study was to provide a database on the behavior of spent nuclear fuel in long-term dry storage through gas sampling to determine the cover gas composition and to infer cladding integrity. The CASTOR V/21 was one of two casks selected for enhanced monitoring in the SFB Study project. This cask was transferred into the SFB Study project in 1994. The CASTOR V/21 Cask was selected because it is fully loaded with intact spent nuclear fuel assemblies that have been undisturbed since July 1985.

Table 4-3 summarizes the results of the mass spectrometric analyses of CASTOR V/21 cask gas samples from 1994 through 1999. Approximately four 300 std-cc of gas samples were taken from the cask for mass spectrometric analysis in each sampling cycle (only two samples were taken after the backfill of fresh helium in 1994). In addition, the samples were also analyzed by gamma spectrometry for ^{85}Kr and by liquid scintillation counting for ^{85}Kr and ^{14}C.

As shown in Table 4-3, the initial analysis of the cover gas in the cask in 1994 indicated that the gas sample consisted of approximately 2% air, with the balance consisting of helium. The introduction of air into the cask was caused by an inadvertent breach during sampling on September 20, 1994. On October 11, 1994, the CASTOR V/21 was refilled with fresh helium. (PNNL-11576) The gas analysis after the fresh helium backfill indicated that the cask cover gas contained 0.5% residual air contamination. Subsequent gas analyses through 1999 suggested slightly rising levels of N_2. The average N_2 and O_2 concentrations in the gas samples, as summarized in Table 4-4, indicated a three-fold increase in the N_2 concentration from an average of 0.4 to 1.4 vol% while the O_2 concentration did not change. The N_2 concentration appeared to increase steadily after the backfill of the cask with fresh helium in 1994 to 1996 and appeared to remain constant thereafter. At first glance, these data suggest a slow air infiltration into the cask. However, the steady N_2 levels from 1996 onwards are not consistent with a continuous leak

Table 4-3. Cask gas sample composition. Values for ^{85}Kr and ^{14}C are in units of nCi/cm^3; values for the remaining gas components are in units of volume percent. Except as noted, ^{85}Kr and ^{14}C were determined by liquid scintillation.

FY 1994 4th Qtr (prior to purging with fresh He)		Cask V/21	Cask V/21	Cask V/21	Cask V/21
	Gas Type	Sample 8A INEEL	Sample VEPCO#24 INEEL	Sample 13D ANL-W	Sample 14A ANL-W
	H2	0.04	0.04	<0.01	<0.01
	He	97.70	97.75	97.84	97.87
	N2	1.83	1.77	1.72	1.69
	O2	0.43	0.41	0.38	0.36
	Ar	0.02	0.02	<0.01	<0.01
	CO2	<0.01	<0.01	<0.01	<0.01
	^{85}Kr	—[a]	—[a]	—[a]	—[a]
	^{14}C	—[b]	—[b]	—[b]	—[b]
FY 1994 4th Qtr (after purging with fresh He)	Gas Type	Sample 14A INEEL	Sample VEPCO#24 INEEL	ANL-W[c]	ANL-W[c]
	H2	<0.01	0.01	—	—
	He	99.4	99.6	—	—
	N2	0.53	0.35	—	—
	O2	0.05	<0.01	—	—
	Ar	<0.01	<0.01	—	—
	CO2	<0.01	<0.01	—	—
	^{85}Kr	—[a]	—[a]	—	—
	^{14}C	—[b]	—[b]	—	—
FY 1995 1st Qtr	Gas Type	Sample 1 INEEL	Sample 2 INEEL	Sample 3 ANL-W	Sample 4 ANL-W
	H2	<0.01	<0.01	<0.01	<0.01
	He	99.11	99.60	99.70	99.60
	N2	0.77	0.39	0.33	0.37
	O2	0.11	0.01	<0.01	0.01
	Ar	<0.01	<01.01	<0.01	<0.01
	CO2	<0.01	<0.01	<0.01	<0.01
	^{85}Kr	—[a]	—[a]	—[a]	—[a]
	^{14}C	—[b]	—[b]	—[b]	—[b]
FY 1995 2nd Qtr	Gas Type	Sample 1 INEEL	Sample 2 INEEL	Sample 3 ANL-W	Sample 4 ANL-W
	H2	<0.01	<0.01	<0.01	<0.01
	He	99.43	99.28	99.37	99.42
	N2	0.56	0.68	0.60	0.56
	O2	<0.01	0.03	0.02	0.01
	Ar	<0.01	<0.01	<0.01	<0.01
	CO2	<0.01	0.01	<0.01	<0.01
	^{85}Kr	0.0067[d]	—[a]	—[a]	—[a]
	^{14}C	—[b]	0.0057[d]	—[b]	—[b]

Table 4-3. (continued).

		Cask V/21	Cask V/21	Cask V/21	Cask V/21
FY 1995 3rd Qtr	Gas Type	Sample 1 INEEL	Sample 2 INEEL	Sample 3 ANL-W	Sample 4 ANL-W
	H2	<0.01	<0.01	0.02	0.02
	He	98.52	99.40	99.40	99.41
	N2	1.28	0.59	0.55	0.55
	O2	0.20	<0.01	0.01	0.01
	Ar	0.01	<0.01	<0.01	<0.01
	CO2	0.01	<0.01	0.01	0.01
	^{85}Kr	$<6 \times 10^{-4}$	—[a]	—[a]	—[a]
	^{14}C	—[b]	0.0108[e]	—[b]	—[b]
FY 1996	Gas Type	Sample 1 INEEL	Sample 2 INEEL	Sample 3 ANL-W	Sample 4 ANL-W
	H2	ND	ND	0.02	0.01
	He	98.51	98.86	98.42	98.93
	N2	1.33	1.07	1.42	1.02
	O2	0.11	0.04	0.10	0.02
	Ar	0.01	0.01	0.01	0.01
	CO2	0.03	0.03	0.02	0.02
	^{85}Kr	$<6 \times 10^{-4}$	—[a]	—[a]	—[a]
	^{14}C	—[b]	0.048[e]	—[b]	—[b]
FY 1997	Gas Type	Sample 1 INEEL	Sample 2 INEEL	Sample 3 ANL-W	Sample 4 ANL-W
	H2	0.01	<.01	<0.01	0.01
	He	98.77	98.83	98.87	98.85
	N2	1.14	1.10	1.07	1.08
	O2	0.02	0.01	<0.01	<0.01
	Ar	0.01	0.01	0.01	0.01
	CO2	0.05	0.05	0.05	0.05
	^{85}Kr	$5.9\ E^{-4}$ [f]	—[a]	—[a]	—[a]
	^{14}C	—[b]	0.061[e]	—[b]	—[b]
FY 1998	Gas Type	Sample 1 INEEL	Sample 2 INEEL	Sample 3 ANL-W	Sample 4 ANL-W
	H2	ND	ND	0.01	0.01
	He	98.48	98.80	98.99	98.98
	N2	1.36	1.11	0.99	1.99
	O2	0.02	0.01	<0.01	<0.01
	Ar	0.01	0.01	0.01	0.01
	CO2	0.07	0.07	0.01	0.01
	^{85}Kr	$<6 \times 10^{-4}$	—[a]	—[a]	—[a]
	^{14}C	—[b]	0.074[g]	—[b]	—[b]

Table 4-3. (continued).

		Cask V/21	Cask V/21	Cask V/21	Cask V/21
FY 1999 (Prior to opening V/21)	Gas Type	Sample 1 INEEL	Sample 2 INEEL	Sample 3 ANL-W	Sample 4 ANL-W
	H2	ND	ND	<0.01	<0.01
	He	98.45	98.82	98.88	98.86
	N2	1.38	1.08	1.03	1.05
	O2	0.08	<0.01	<0.01	<0.01
	Ar	0.01	0.01	0.02	0.02
	CO2	0.08	0.08	0.07	0.08
	^{85}Kr	$<6 \times 10^{-4}$	—[a]	—[a]	—[a]
	^{14}C	—[b]	0.0095[h]	—[b]	—[b]

a. Analyzed by gamma spectroscopy (INEEL) or mass spectroscopy (ANL-W), not by liquid scintillation. Results were below detection limits for gamma spectroscopy (0.3 nCi/cm^3) and mass spectroscopy (0.01 vol%)

b. Not analyzed.

c. There were no gas samples submitted to ANL-W after purging with fresh He.

d. Detection limits not available.

e. Detection limit: 4×10^{-4} nCi/cm^3.

f. Detection limit: 6×10^{-4} nCi/cm^3.

g. Detection limit: 5×10^{-4} nCi/cm^3.

h. Detection limit: 2×10^{-4} nCi/cm^3.

Table 4-4. Summary of the nitrogen and oxygen concentrations in the cask cover gas analyses. Dimensions of values are in volume percent.

	N_2 Content, Vol%		O_2 Content, Vol%	
	Average	Std. Dev.	Average	Std. Dev.
1994, after He purge	0.44	0.13	0.025	0.035
1995, 1st quarter	0.47	0.20	0.032	0.052
1995, 2nd quarter	0.60	0.06	0.015	0.013
1995, 3rd quarter	0.74	0.36	0.055	0.097
1996	1.21	0.20	0.067	0.044
1997	1.10	0.03	0.008	0.010
1998	1.36	0.45	0.008	0.010
1999	1.14	0.16	0.020	0.040

into the cask. The variations in N_2 content from sample to sample in some of the sample sets (see Table 4-3) suggest instead the contamination of the samples during or after the sampling process, possibly by the incomplete removal of residual air from the sample vessel prior to sampling.

The nitrogen to oxygen ratios of the analytical results were consistently higher than the ratio in ambient air, varying from 14 to 180, indicating depletion of the oxygen relative to the nitrogen. The low oxygen results would seem more consistent with air infiltration into the cask than with sample contamination, for the oxygen could be depleted by rapid oxidation of the metal components and possibly the crud (from Fe_3O_4 to Fe_2O_3) within the cask. However, the high nitrogen to oxygen ratios do not preclude contamination of the gas samples. The apparent reduction of oxygen in the gas samples could

instead be an artifact of the mass spectrometric analysis, caused by the oxidation of the rhenium or tungsten filaments and other hot surfaces in the mass spectrometer source.

4.5 C-14 and Kr-85 Data

Table 4-3 presents results of the radiochemical analysis of CASTOR V/21 cask gas samples for the years 1994 through 1999. For all of the samples, krypton was analyzed by mass spectrometry and gamma spectroscopy. However, the detection limits for these methods were 0.01 volume % and 300 pCi/cm^3, respectively. From 1995 through 1999, radiochemical analyses were also performed by liquid scintillation counting, which is approximately 10^3 times more sensitive than gamma counting.

The ^{85}Kr concentration data in Table 4-3 show some inconsistency, with results at or below the detection limits for five of the test periods (3rd quarter 1995, 1996 through 1999) and ten times greater than detection limits for the 2nd quarter of 1995. Of particular interest is the decrease in value from the second to the third quarter of FY 1995. Because krypton is a noble, nonreactive gas, it cannot react with internal components in the cask. Therefore, once krypton is released by a breached fuel rod, its concentration in the backfill gas should remain constant unless it is preferentially physisorbed on the surfaces of the internal components. It is possible that the variations in the krypton results are a result of contamination of the sample containers or inadvertent desorption of krypton from other surfaces during sample processing and analysis. A review of the 1995–1999 data and the method of analysis has substantiated the data in Table 4-3. However, the same review of the krypton analysis method found evidence of low-level cross-contamination of sampling vessels by physisorption of noble gases in other work. At present, the anomalous results in 1995 have not been satisfactorily explained.

The ^{14}C data in Table 4-3 show an order of magnitude increase between 1995 and 1998 to a level that is two orders of magnitude greater than the detection limit, followed by an order of magnitude decrease in the 1999 analysis. A reevaluation of the original data has indicated no significant change in the detection limits or statistics that could account for the variation in the data. There is a possibility that the low values may be an artifact of sample preparation prior to analysis. However, the variation in the results has not been satisfactorily explained yet.

It is likely that the ^{14}C is a real constituent of the cask cover gas. However, the presence of ^{14}C in the cover gas is not a conclusive indicator of breached cladding in the fuel. It is possible that the ^{14}C was generated by neutron capture by an (n,alpha) process from ^{17}O in the crud or other oxides external to the fuel rod cladding, or by an (n,p) process from ^{14}N contamination in the cask cover gas. The absence of a corresponding increase in the ^{85}Kr concentration indicates that the increase in the ^{14}C concentration in the gas samples is not an indicator of cladding failure.

4.6 2000 Data After Refill of CASTOR V/21

Table 4-5 presents results of the mass spectrometric analysis of CASTOR V/21 cask gas samples taken on March 23, 2000, immediately after refill of Cask V/21 with fresh helium of 99.98% purity. In addition to the analysis of helium and air components as shown in the table, the samples were also analyzed for Ne, Kr, and Xe; measurable quantities were not detected. Mass spectrometric data shown as ND (not detected) were interpreted as less than 0.005 mole percent. Detection limits for the ^{85}Kr are based on counting statistics of the gamma spectrometry and are 0.3 nCi/cm^3.

The samples of the helium backfill gas in the cask, which were sampled on the day of completion of the backfill, showed approximately 2% air contamination, comparable to the composition data reported in 1994 and 1996 through 1999. Residual air on the order of 0.7% can be expected for the backfill process consisted of one evacuation to 5 mbar followed by helium backfill to 700 mbar. The observed 2% residual

Table 4-5. Cask gas sample composition (volume mole percent).

FY 2000 March 23	Gas Type	Cask V/21 Sample 1 INEEL	Cask V/21 Sample 2 INEEL
	H_2	ND	ND
	He	98.31	98.19
	N_2	1.31	1.40
	O_2	0.35	0.38
	Ar	0.02	0.02
	CO_2	0.02	0.01
	^{85}Kr	ND	ND
	Xe	ND	ND
ND—Not detected above detection limit of 0.3 nCi/cm^3.			

air may be caused by additional residual air in the sample bottles, which are routinely evacuated to 5–10 mbar prior to taking the sample.

4.7 Conclusion on Gas Survey

The analyses of the cask backfill gases have indicated that there was no air ingress in the 1994–1999 time period and substantiated that the cask lid O-rings were in adequate condition to maintain a good seal. The gas analyses did indicate small amounts of air components, totaling approximately 0.5% after the 1994 helium backfill and as much as 2 vol% air prior to the 1994 backfill with fresh helium and after the 2000 helium backfills. The residual air in the gas samples is most likely an artifact of the backfill process and the sampling process, which used only one evacuation (to approximately 5 mbar) prior to helium backfill. The gas analyses subsequent to the 1994 backfill did not show any significant increase in the total concentration of the air components.

The presence of the residual air appears to have had no detrimental effect on the fuel or cask components, based on visual inspection of the cask internals and the krypton gas analyses. The analytical results for krypton from 1996 through 1999 have been below the detection limits. For the six analyses in the 1995–1999 period, five analyses have resulted in krypton data at or below the detection limits. In the remaining test (2nd quarter of 1995), the krypton concentrations were approximately an order of magnitude greater than the detection limits. Because of the radical variation in the time series of readings, the high krypton results are probably the result of slight contamination of the sample containers or contamination during preparation of the samples for analysis. The krypton results are not consistent with failure of the fuel rod cladding during dry storage.

The $^{14}CO_2$ data also show somewhat erratic behavior. While the ^{14}C results rose by an order of magnitude from 1995 to 1998, the 1999 analysis results were comparable to the 1995 results. The available analysis data do not offer a satisfactory explanation for this behavior. Taken at face value, the erratic results, coupled with the krypton results, are not consistent with failure of fuel rods during dry storage.

5. CONCLUSION

A series of examinations in 1999 and early 2000 to investigate the integrity of the CASTOR V/21 cask were undertaken. The examinations reported in this interim report include:

- Radiation survey of the cask surface and at 1 and 2 m (3 and 6 ft) with comparison to the 1985 radiation survey
- Gas analysis of the internal atmosphere to check for the presence of air ingress into the container past the lid seal and for the presence of fission gases that would suggest cladding failure
- Integrity of the concrete pad upon which the CASTOR V/21 has rested since 1985
- Integrity of the inner and outer O-rings on the lid for signs of corrosion or wear
- Assembly lifting force measurements to see if there is any resistance to pulling the assemblies back out of the cask basket channels due to corrosion or excessive rod bowing
- Visual inspection of the outside of each assembly for indications of additional corrosion, crud spallation or other damage
- Visual inspection of the cask basket welds and internals for indications of additional corrosion or degradation.

There is no evidence of degradation of the CASTOR V/21 cask systems important to safety from the time of initial loading of the cask in 1985 up to the time of testing in 1999. Supporting evidence for this lack of significant degradation are summarized as follows.

The 1999 and 2001radiation survey suggests that doses are generally lower than in 1985—as would be expected. Doses are now well below the 200 mrem/hr contact limit. Due to potential errors or uncertainties in some of the 1985 and 1999 and 2001 measurements, trends in doses between 1985 and 1999 are not always easy to determine, however. Nevertheless, the dose trend is down suggesting that radiation shielding materials in the cask—both gamma and neutron—are maintaining their function.

Gas analyses show neither signs of air ingress into the container nor signs of cladding failure leading to fission product release.

Visual examination of the cask lid O-rings suggest they were, indeed, in adequate condition to maintain a seal.

There was no evidence of major crud spallation from the fuel rod surfaces.

The concrete pad did not show any sign of failure. Strength measurements did not show any evidence of strength loss. Only small cracks typical of a normal, small amount of shrinkage were noticed. Concrete conditions immediately below the cask were similar to that of other areas.

All materials inside the cask—including the assemblies themselves—appeared the same as they did in 1985.

The stitch welds in the triangular air channels appear to be nonstructural welds and were only intended to add additional stability for holding the fuel basket in place during 1985 fuel loading and

vertical and horizontal thermal testing. The 1985 cask heat transfer performance testing (EPRI NP-4887) thermal analysis, concluded that the tightly fitted fuel basket expanded and came in contact with the basket barrel and the fuel barrel came in contact with the inner wall of the cask. The results of the thermal analysis indicated that thermal stresses in the weld joints at the eight crack locations identified in 1985 were well above yield stresses measured during tensile testing of applicable weld samples. Based on these results and speculations, it appears that all new cracks identified in 1999 occurred during the 1985 thermal testing. Further, it is concluded the cracks are not relevant to normal long-term storage and presents no adverse safety implications on the cask or components to perform their safety related function.

The nondestructive and destructive examination of the cladding from assembly T-11 will be reported by others in a later interim or final report.

6. REFERENCES

10 CFR Part 72.122, U.S. Code of Federal Regulations, *Licensing Requirements for the Independent Storage of Spent Nuclear Fuel and High-Level Radioactive Waste*.

Berry, W. E., *Corrosion in Nuclear Applications*, The Electrochemical Society, Inc., John Wiley and Sons, Inc., New York, 1971.

EPRI NP-4887, *The CASTOR-V/21 PWR Spent Fuel Storage Cask: Testing and Analyses*, EPRI NP-4887, PNL-5917, Interim Report, prepared by Virginia Power Company, published by the Electric Power Research Institute, Palo Alto CA, November 1986.

Fisher, L. E., and A. Howe, 1998, *Qualification of Independent Spent Fuel Storage Installation,* Proceedings of the 7th International Symposium on Current Issues Related to Nuclear Power Plant Structures, Equipment and Piping, Raleigh, North Carolina, page IV-5.

General Nuclear System, Inc., *CASTOR Vb Dry Spent Fuel Storage Cask*, GNS Drawing 49001-E-01, sheet 1 of 2.

GNSI, Topical Safety Analysis Report for the CASTOR V/21 Cask Independent Spent Fuel Storage Installation (Dry Storage), Revision 1, General Nuclear Systems, Inc., Avon, Connecticut, January 1985, figures 7.3-5 and -6.

McKinnon, M. A., and A. L. Doherty, *Spent Nuclear Fuel Integrity During Dry Storage-Performance Tests and Demonstrations*, PNNL-11576, Pacific Northwest National Laboratory, Richland, WA, June 1997.

Sandoval, R. P., R. E. Einziger, H. Jordan, A. P. Malinauskas, and W. J. Mings, *Estimate of CRUD Contribution to Shipping Cask Containment Requirements*, SAND88-1358, Sandia National Laboratories, Albuquerque, NM, January 1991.

Appendix A

Dosimeter Radiation Measurements from CASTOR V/21 Cask Performance Test

Appendix A

Dosimeter Radiation Measurements from CASTOR V/21 Cask Performance Test

DOSIMETER RADIATION MESUREMENTS FROM CASTOR V/21 CASK PERFORMANCE TEST

	LOCATION		Dose rates at contact 1985		Dose rate at contact 2001		
	Angle, {a}	Elevation {b} or radius {c}	TLD Dose Rate Gamma	TED Dose Rate Neutron	TLD Gamma	RO-20 Gamma	E-600 Neutron
	Degrees	mm	mR/hr	mR/hr	mR/hr	mR/hr	mR/hr
SIDE	**45**	175	23	2.1	2.6	4	2
		480	140	21 {f}	4.4	2	3
		1048	36	9.7	1.3	1.3	5
		1597	38	11.5	1.3	1.4	7
		2149	38	12	1.6	1.4	6
		2701	37	10.6	1.3	1.5	4
		3298	39	10.3	1.4	1.5	4
		3850	28	7	1	1.2	7
		4350	22	5.3	3	2.5	8
		4400	118	15	8	4	8
		4450	68	9.7	6.2	8	14
		4500	26	7.3	3.8	7	13
		4550	9.4	5.6	2.1	4	8
		4600	4.3	3.8	1.1	2.5	6
		4650	2.5	3.8	0.8	1.5	8
		4700	1.6	2.1	0.5	1	6
		4750	1.1	2.6	0.5	0.6	5
		4800	0.7	1.5	0.3	0.5	4
	60	2701	31	13	1.3	1.4	6
	75	2701	23	11	1.2	1.4	8
	90	175	26	1.5	3.8	6	2
		480	125	3.5	8.1	7	2
		1048	25	8.7	2.2	2	6
		1597	21	15	1.8	1.7	3
		2149	21	12	1.5	1.5	6
		2701	24	16	1.7	1.5	8
		3298	22	13	1.7	1.5	5

	LOCATION		Dose rates at contact 1985		Dose rate at contact 2001		
	Angle, {a}	Elevation {b} or radius {c}	TLD Dose Rate Gamma	TED Dose Rate Neutron	TLD Gamma	RO-20 Gamma	E-600 Neutron
	Degrees	mm	mR/hr	mR/hr	mR/hr	mR/hr	mR/hr
SIDE		3850	70	9.8	4.6	4.5	8
		4350	79	11.5	7.8	8	13
		4400	134	13	11.1	11	8
		4450	81	10	8.5	10	16
		4500	33	4.7	6.4	8	12
		4550	12	6.9	3.2	4.5	8
		4600	5	3.5	1.6	2.7	11
	90	4650	3.1	8.8	1.1	2	9
		4700	1.9	3.8	0.7	1.2	3
		4750	1.3	0.9	0.5	0.8	4
		4800	1.2	0.7	0.4	0.7	3
	105	2701	24	14	1.4	1.3	10
	120	2701	31	9.3	1.1	1.2	6
	72,73	2149	23	15	1.1	1.2	6
	73,74	2149	24	17	1.1	1.2	7
	74,75	2149	23	14	1.1	1.1	7
	75,76	2149	22	11	1.1	1	5
	76,77	2149	25	13	1.1	1	7
	77,78	2149	24	7	1.2	1.3	5
	Top Trunnion, 90	—	19	8.1	2.6	2	10
	Bottom Trunnion, 90	—	42	27	0.9	1.5	11
TOP							
	45	203	32.5	44	0.2	12	36
		406	43	35	3.9	8	34
		585	26	32	3.5	8	28
		928	6.4	5.1	9.8	1	14
		1100	1	1.3	7.2	0.5	7
	90	170	30	44	0.2	6	42
		340	36	36	0.2	6	38
		487	29.5	32	0.3	5	47
		634	29	27	1.8	3.5	28
		706	22	19	2.6	3	26

LOCATION			Dose rates at contact 1985		Dose rate at contact 2001		
	Angle, {a}	Elevation {b} or radius {c}	TLD Dose Rate Gamma	TED Dose Rate Neutron	TLD Gamma	RO-20 Gamma	E-600 Neutron
	Degrees	mm	mR/hr	mR/hr	mR/hr	mR/hr	mR/hr
TOP		780	56	16	2.3	2	22
		854	9.2	2.3	2.7	2.8	18
		928	2.5	3.1 {f}	3.3	1.5	11
		985	3.1	0.2	1.2	1	9
		1042	1.6	0.7	4.2	0.5	7
		1100	1	1.4	5.8	0.5	4
		0	40	44	10.1	90	45
	Fill valve	—	196	30	1	1	1
	Hole at 180	—	32	13	1	1	1
BOTTOM							
	90	0	22	41	6.8	4	55
		170	18	31	6.3	3.8	53
		340	24	25	6.3	3.8	54
		487	22	23	5.5	3.9	52
		634	20	21	4.4	4	45
		928	26	5	0.5	3.5	38
		1100	7	1.6	0.8	2.5	24
	45	203	17.5	33	6.1	4	47
		406	25	22	6	4	43
		585	25	19	5	3.8	29
		928	18	3.1	1.9	2.5	24
		1100	3.4	—	3.4	2	12
2001 Supplemental Cask Side Survey Locations {g}							
SIDE	**0**	4400	—	—	16	12	10
	30	4400	—	—	12	9	14
	60	4400	—	—	12.4	8	14
	120	4400	—	—	12.9	9	9
	150	4400	—	—	15	9	13
	180	4400	—	—	24.7	13	12
	210	4400	—	—	12.3	10	14
	240	4400	—	—	13.9	8	13
	270	4400	—	—	17.3	12	10
	300	4400	—	—	12.6	10	15
	330	4400	—	—	10.1	2.5	7
	0	4298	—	—	1.4	1.8	8

LOCATION		Dose rates at contact 1985		Dose rate at contact 2001		
Angle, {a}	Elevation {b} or radius {c}	TLD Dose Rate	TED Dose Rate	TLD	RO-20	E-600
		Gamma	Neutron	Gamma	Gamma	Neutron
Degrees	mm	mR/hr	mR/hr	mR/hr	mR/hr	mR/hr
30	4298	—	—	0.8	16	9
45	4298	—	—	3.6	2	10
60	4298	—	—	1	2.5	11
90	4298	—	—	18.8	3	13
120	4298	—	—	2.6	2.5	8
150	4298	—	—	1.2	2.2	10
180	4298	—	—	1.3	7	9
210	4298	—	—	1.4	2	10
240	4298	—	—	1.5	2	11
270	4298	—	—	5.7	2.5	12
300	4298	—	—	1.3	2.8	12
330	4298	—	—	0.8	1.5	7
45	4100	—	—	2.5	1.8	9
90	4100	—	—	0.7	1.5	9
45	3370	—	—	1.2	1.4	5
90	3370	—	—	1.5	1.4	8
0	2701	—	—	1.4	1.8	6
30	2701	—	—	1.1	1.4	5
150	2701	—	—	1.3	1.4	6
180	2701	—	—	1.6	1.8	6
210	2701	—	—	1.3	1.8	5
240	2701	—	—	1.5	1.6	6
270	2701	—	—	1.7	2	7
300	2701	—	—	1.2	1.2	5
330	2701	—	—	1	1.3	7
45	2443	—	—	1.4	1.5	6
90	2443	—	—	1.4	2	6

{a} from 0 orientation mark

{b} from exterior bottom of cask

{c} from cask centerline

{f} problem with processing dosimeter

{g} survey locations were not obtained in 1985

Appendix B

Cracked Stitch Welds Identified in Fuel Basket of Castor V/21 Cask Basket

Figure B-1. Top weld crack at location 9 identified in Figure B-19.
(Triangular air channel between fuel tube A7 & B8)

Figure B-2. Bottom weld crack at location 9 identified in Figure B-19.
(Triangular air channel between fuel tube A7 & B8)

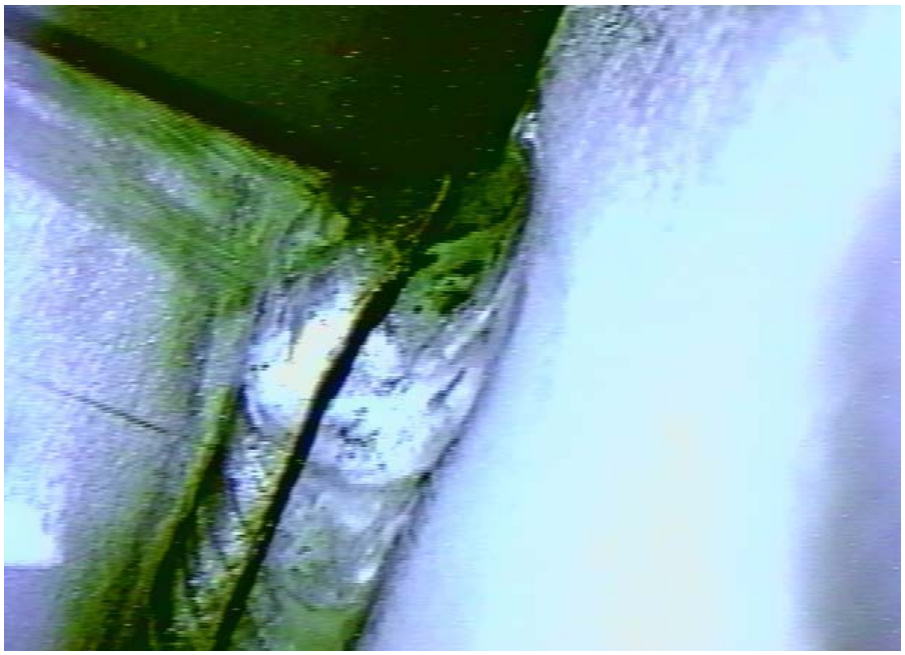

Figure B-3. Top weld crack at location 10 identified in Figure B-19.
(Triangular air channel between fuel tube A3 & A6)

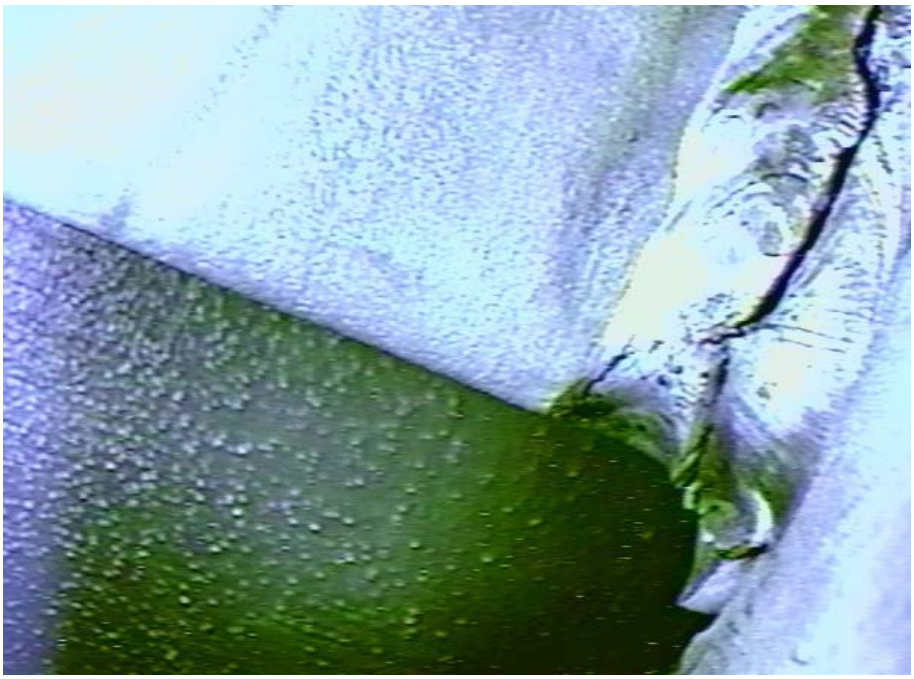

Figure B-4. Bottom weld crack at location 10 identified in Figure B-19.
(Triangular air channel between fuel tube A3 & A6)

Figure B-5. Top weld crack at location 11 identified in Figure B-19.
(Triangular air channel between fuel tube A3 & B6)

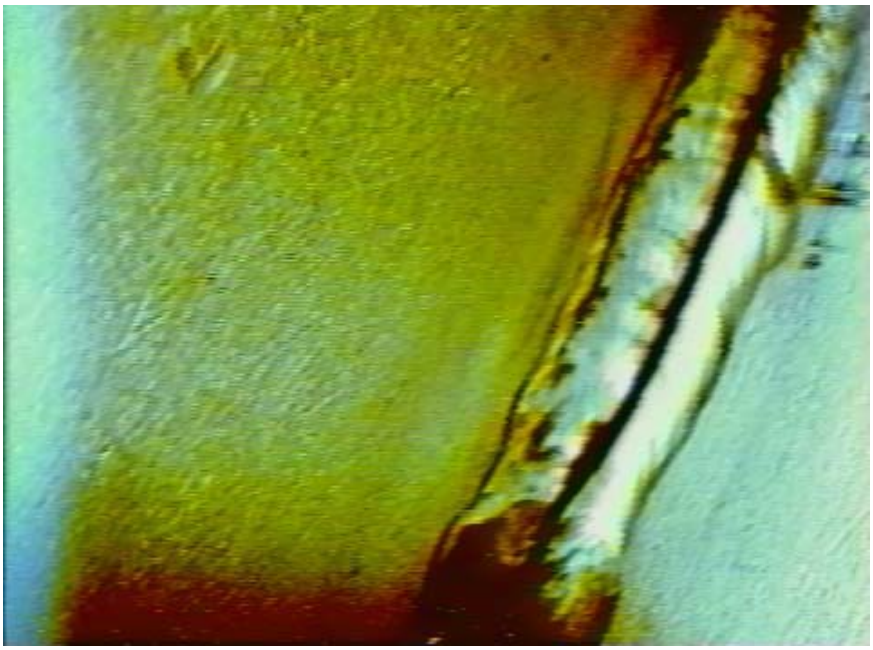

Figure B-6. Bottom weld crack at location 11 identified in Figure B-19.
(Triangular air channel between fuel tube A3 & B6)

Figure B-7. Top weld no crack. Location number 12 identified in Figure B-19.
(Triangular air channel between fuel tube B7 & B8)

Figure B-8. Bottom weld crack at location 12 identified in Figure B-19.
(Triangular air channel between fuel tube B7 & B8)

Figure B-9. Top weld crack (minor) at location 13 identified in Figure B-19.
(Triangular air channel between fuel tube B7 & C8)

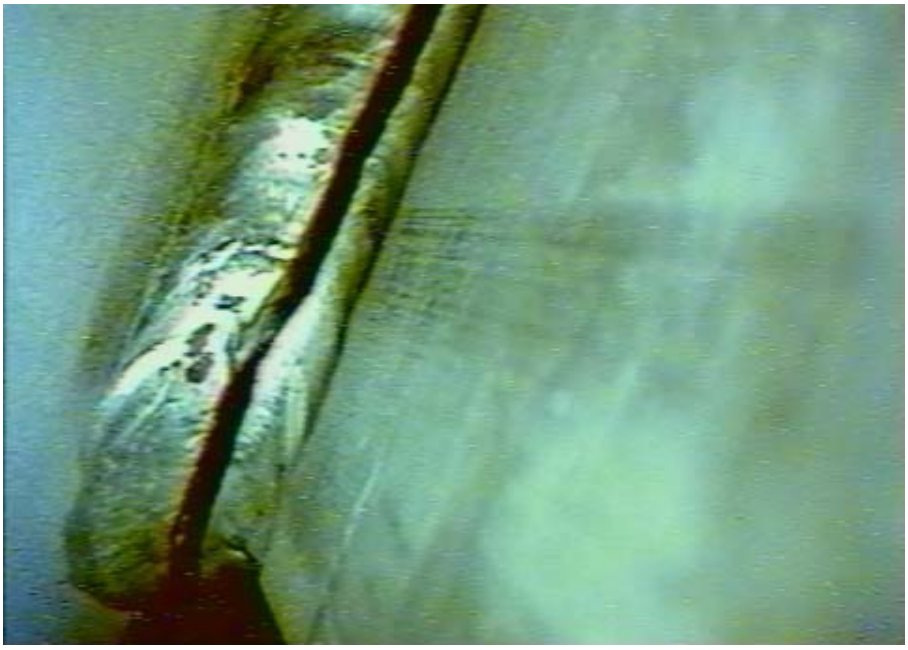

Figure B10. Botton weld crack at location 13 identified in Figure B-19.
(Triangular air channel between fuel tube B7 & C8)

Figure B-11. Top weld crack at location 14 identified in Figure B-19.
(Triangular air channel between fuel tube C6 & D3)

Figure B-12. Botton weld crack at location 14 identified in Figure B-19.
(Triangular air channel between fuel tube C6 & D3)

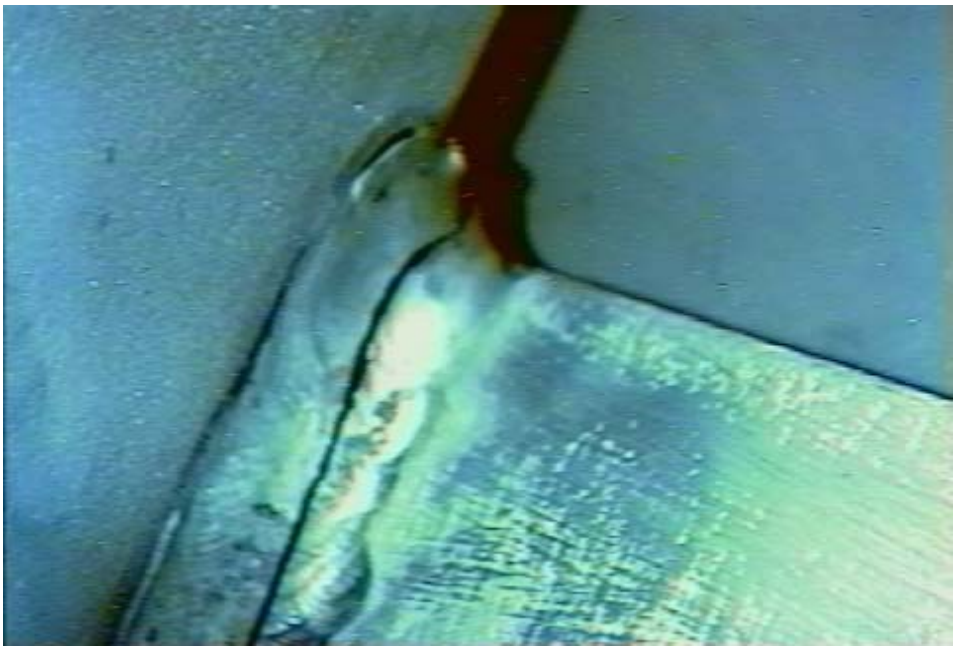

Figure B-13. Top weld crack at location 15 identified in Figure B-1.
(Triangular air channel between fuel tube D3 & D6)

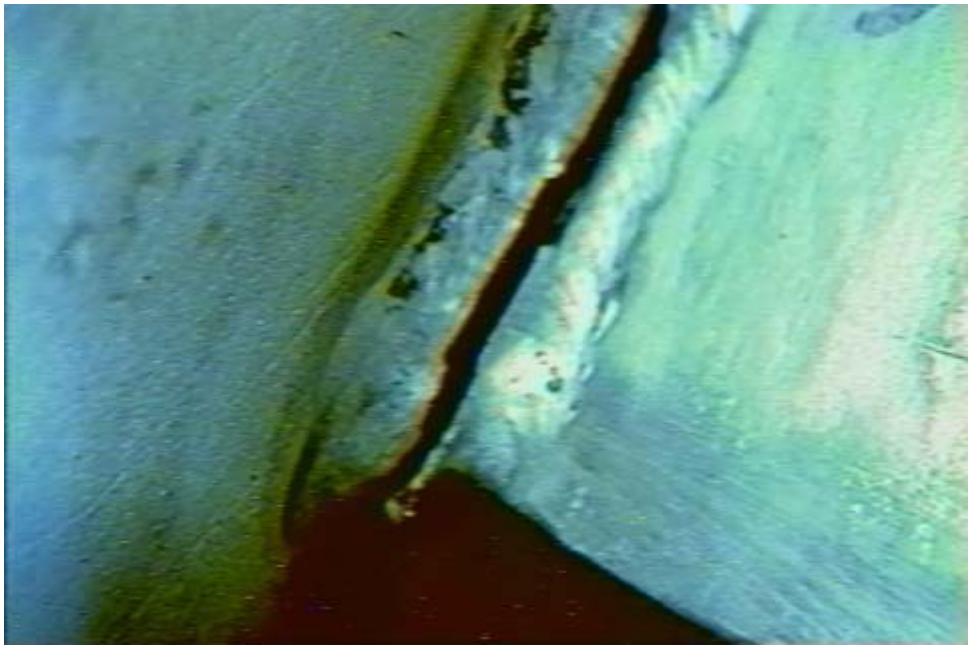

Figure B-14. Bottom weld crack at location 15 identified in Figure B-19.
(Triangular air channel between fuel tube D3 & D6)

Figure B-15. Top weld crack at location 16 identified in Figure B-19.
(Triangular air channel between fuel tube A7 & D8)

Figure B-16. Bottom weld crack at location 16 identified in Figure B-19.
(Triangular air channel between fuel tube A7 & D8)

Figure B-17. Crack in basket weld below weld crack 4 (120°) identified in Figure B-19.

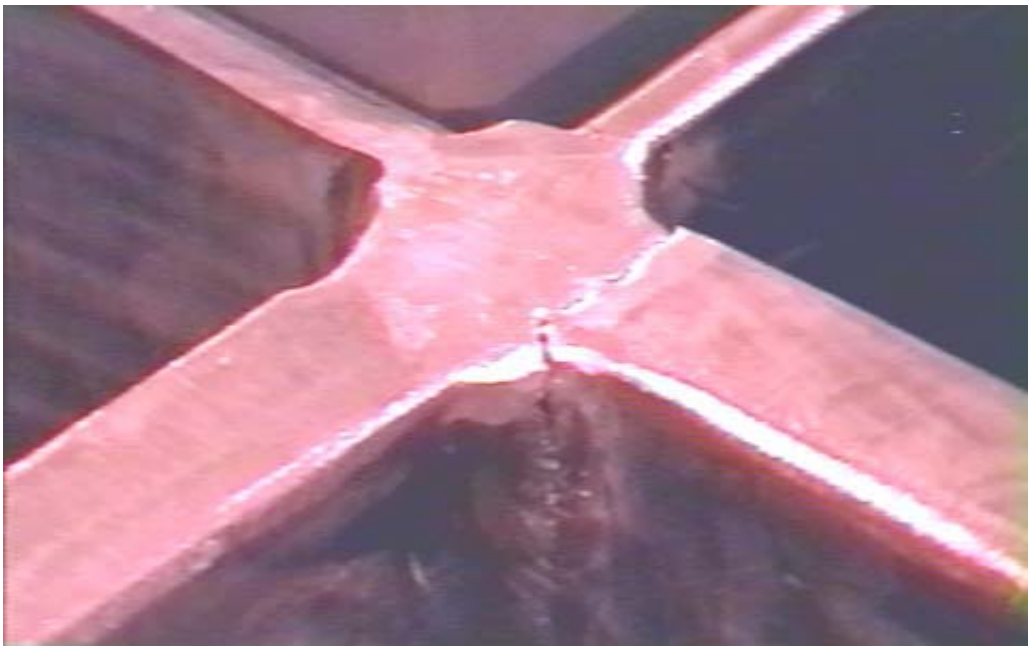

Figure B-18. Same as Figure B-17 with complete view of existing weld crack 4 identified in Figure B-19.

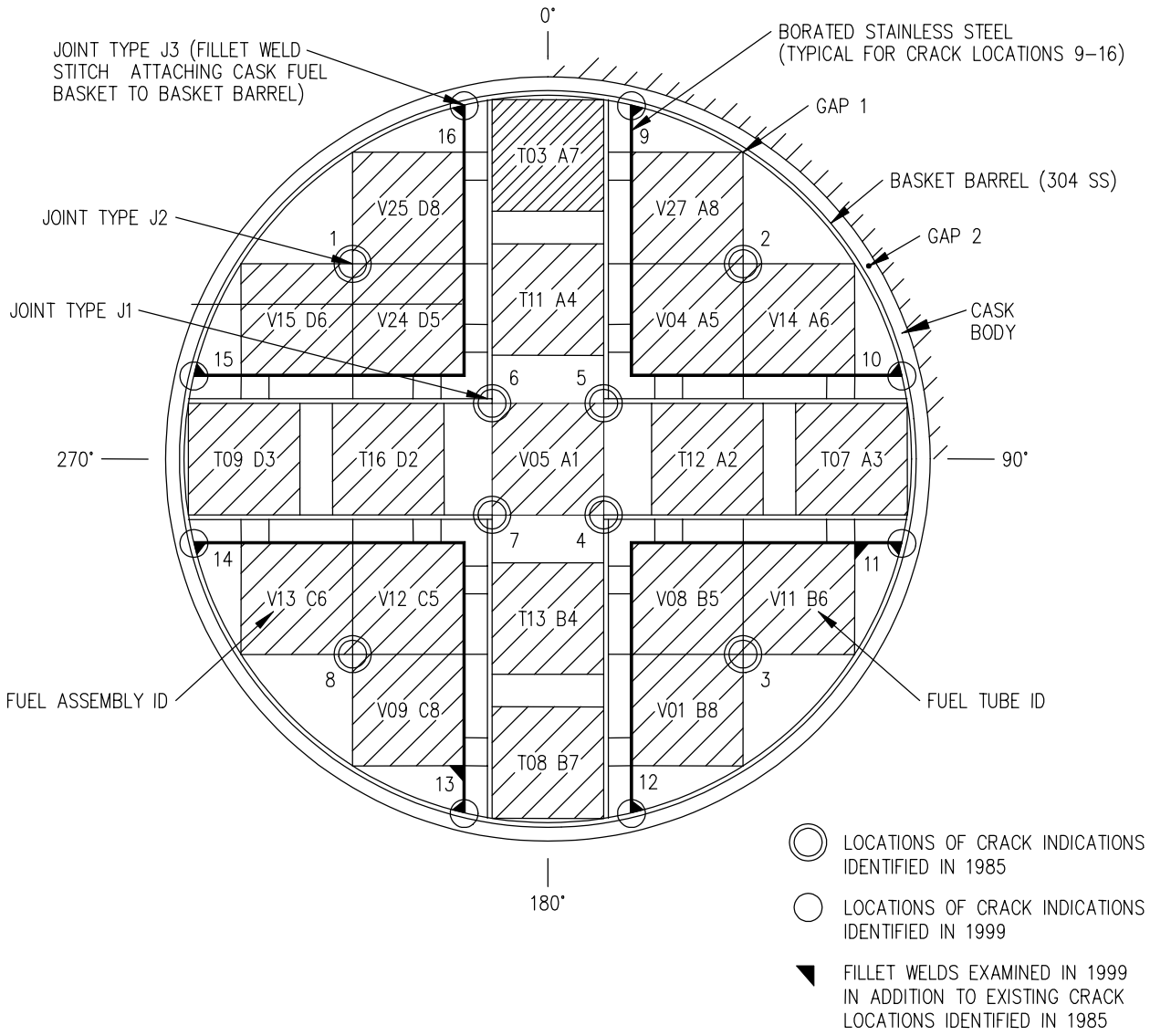

Figure B-19. CASTOR V/21 Basket Crack Indication Locations.

Appendix C

Fuel Assembly Features

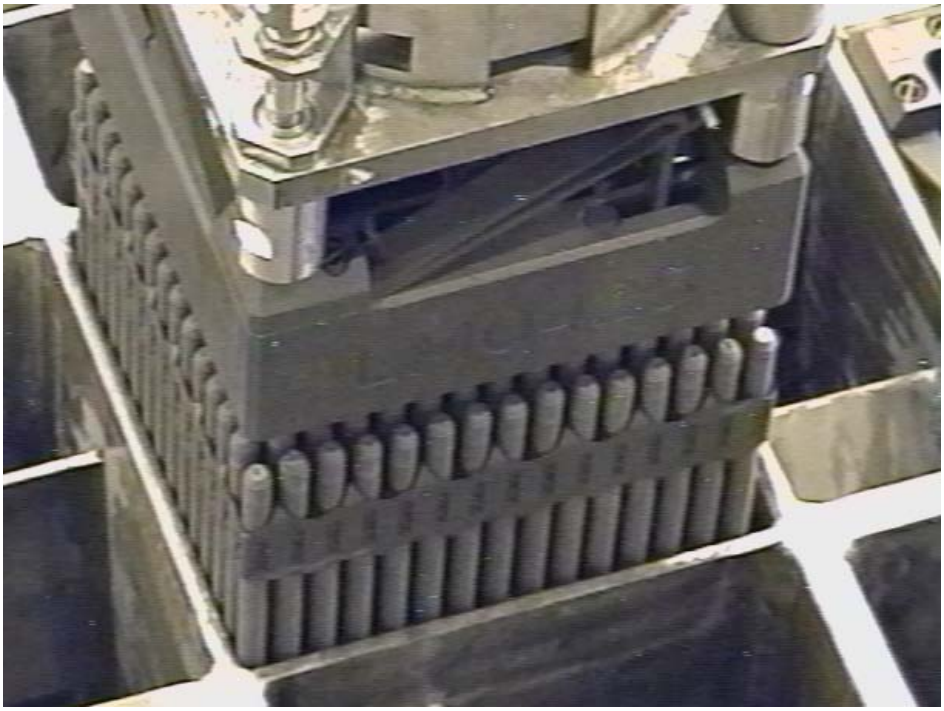

Figure C-1. Westinghouse gropple lifting fuel assembly V-05.

Figure C-2. Top of assembly V-05.

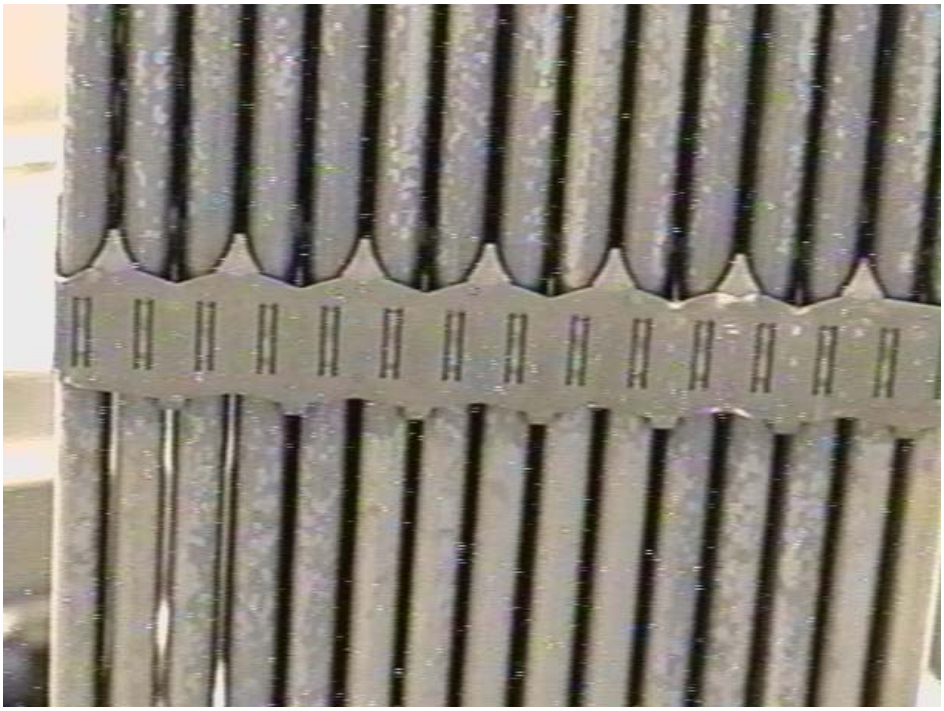

Figure C-3. Oxide mottling noted around spacer #5 on fuel assembly V-05.

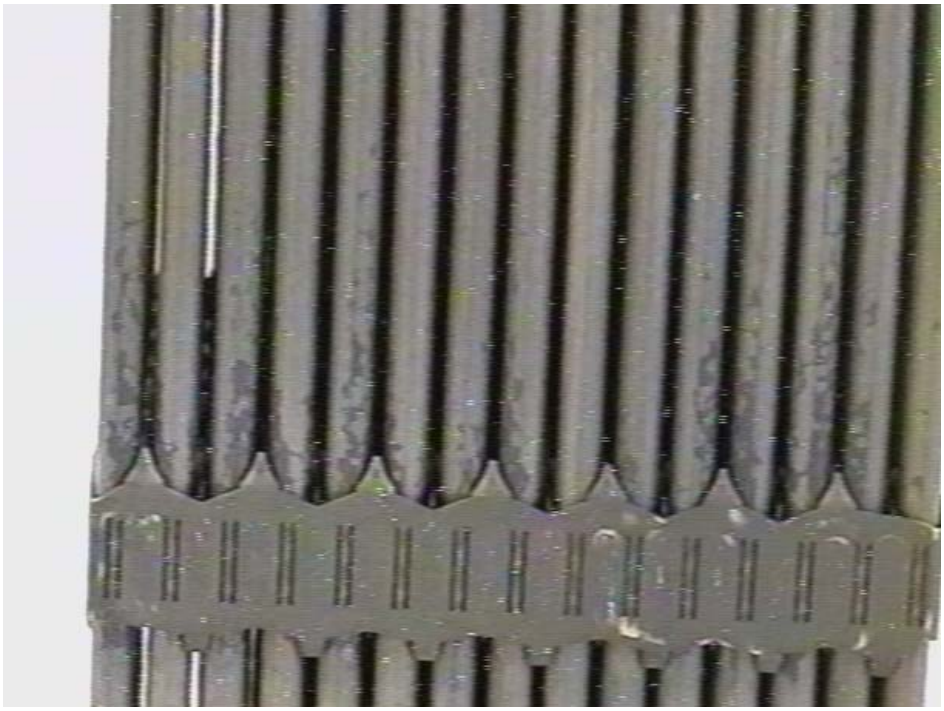

Figure C-4. Oxide mottling noted around grid spacer #6 on V-05.

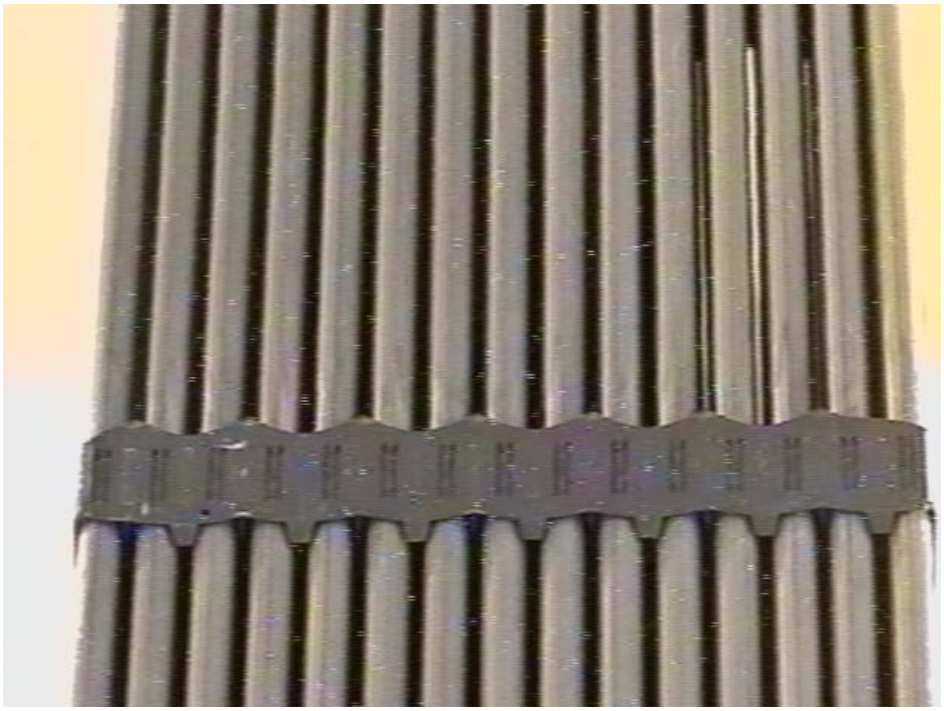

Figure C-5. Fuel assembly V-05—area around upper grid spacer—rods clean and minimal bowing noted.

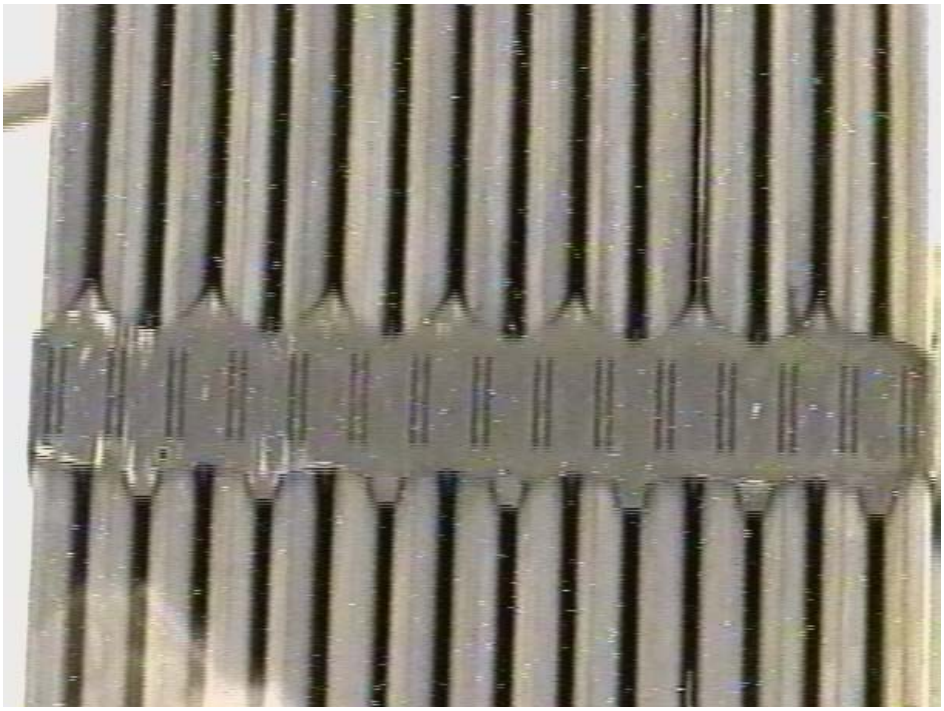

Figure C-6. Fuel assembly V-05 area around third grid spacer—noted light abrasion marking on spacer.

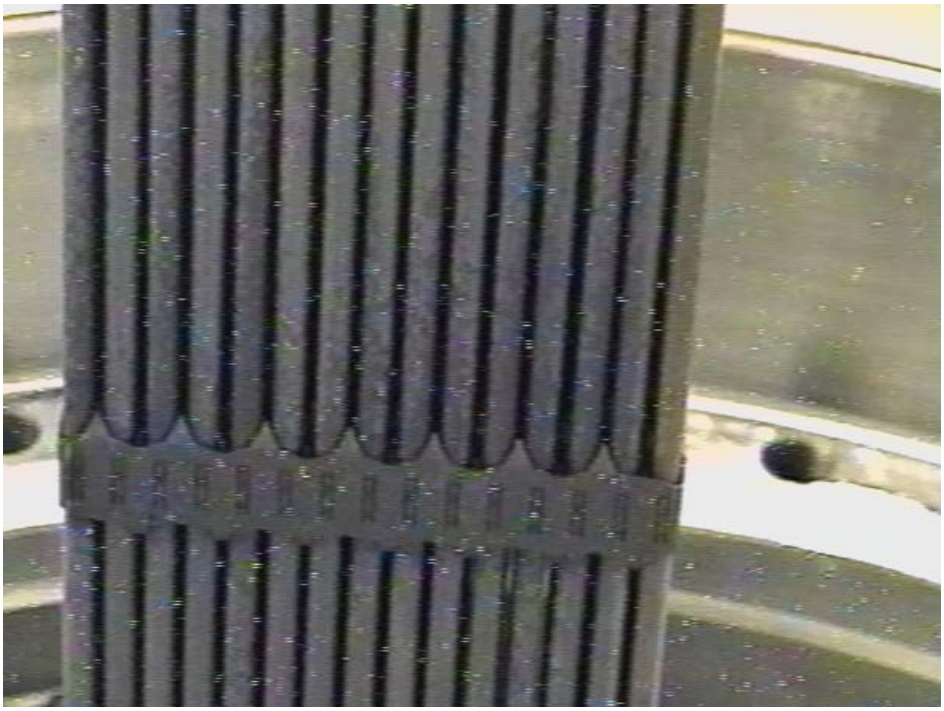

Figure C-7. Fuel assembly V-05 oxide mottling noted around fifth grid spacer.

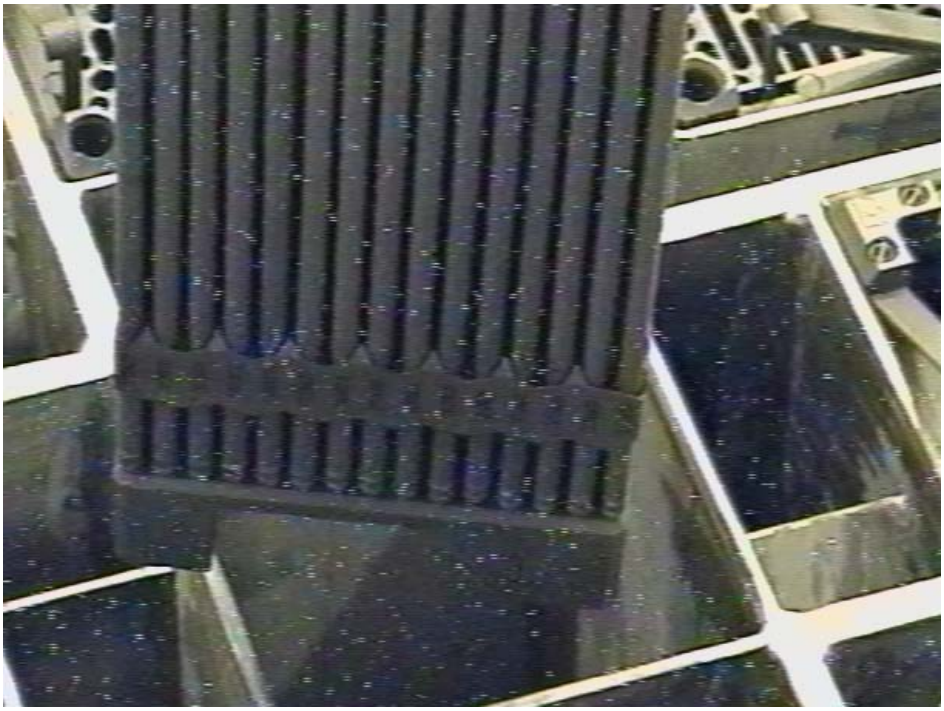

Figure C-8. Fuel assembly V-05 bottom of fuel element V-05—light oxide mottling noted—no loose material seen on rods or top of bottom nozzle.

Figure C-9. Fuel assembly V-05 detail of bottom of element—note oxide rings adjacent to rod end weld.

Figure C-10. Fuel assembly V-05 top of assembly.

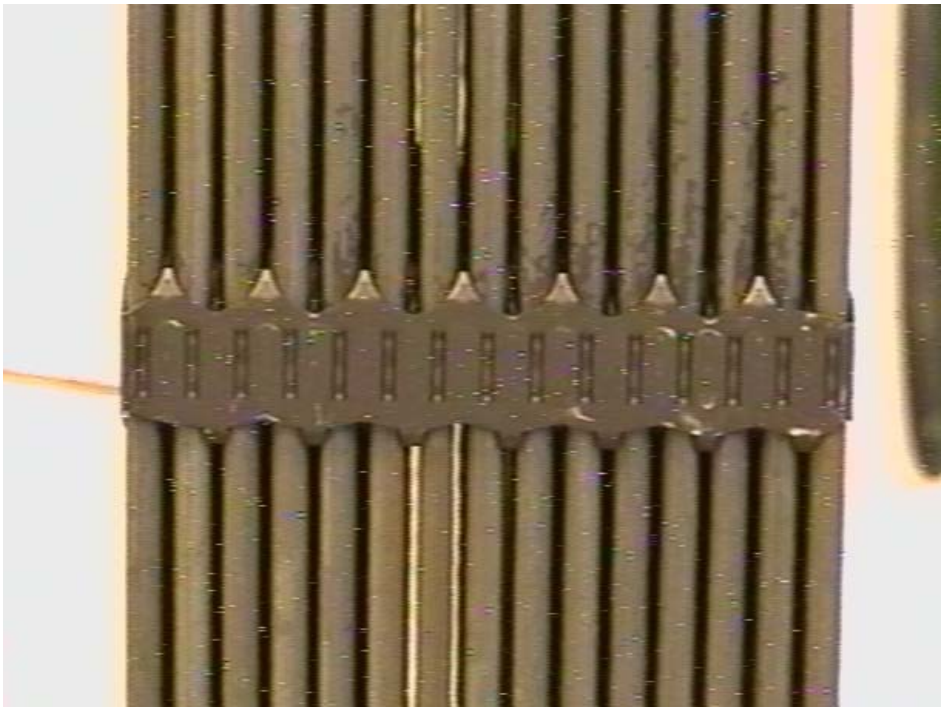

Figure C-11. Fuel assembly V-05 oxide mottling noted around grid spacer 5.

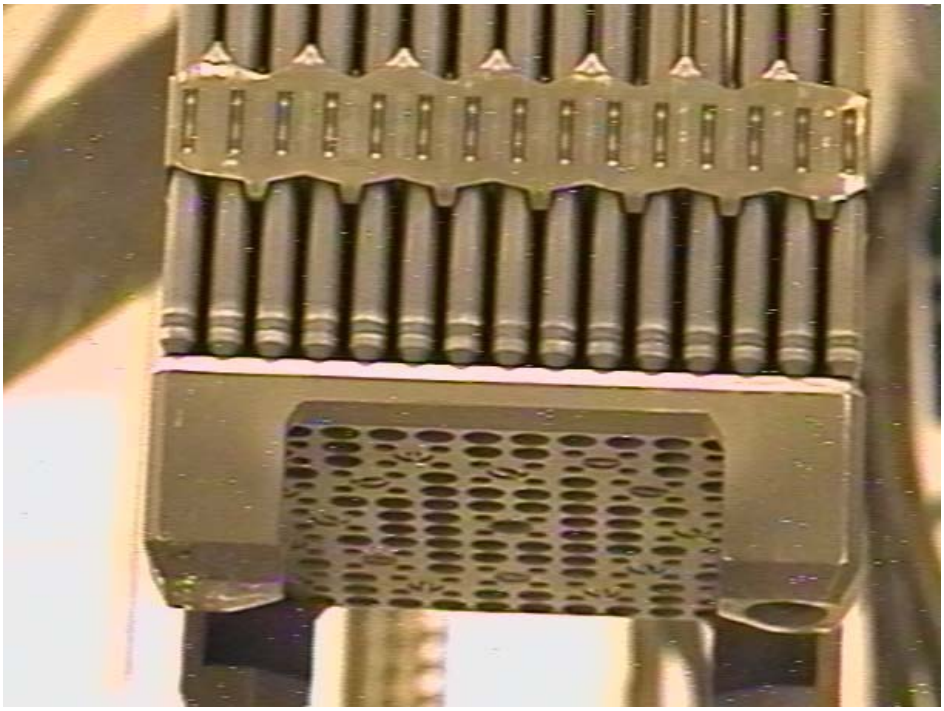

Figure C-12. Fuel assembly V-05—bottom left nozzle—noted mechanical fasteners searing guide tubes.

Figure C-13. Fuel assembly V-05 looking for loose “crud”—non was evident.

Figure C-14. Element T-03 being withdrawn—note fuel rod growth.

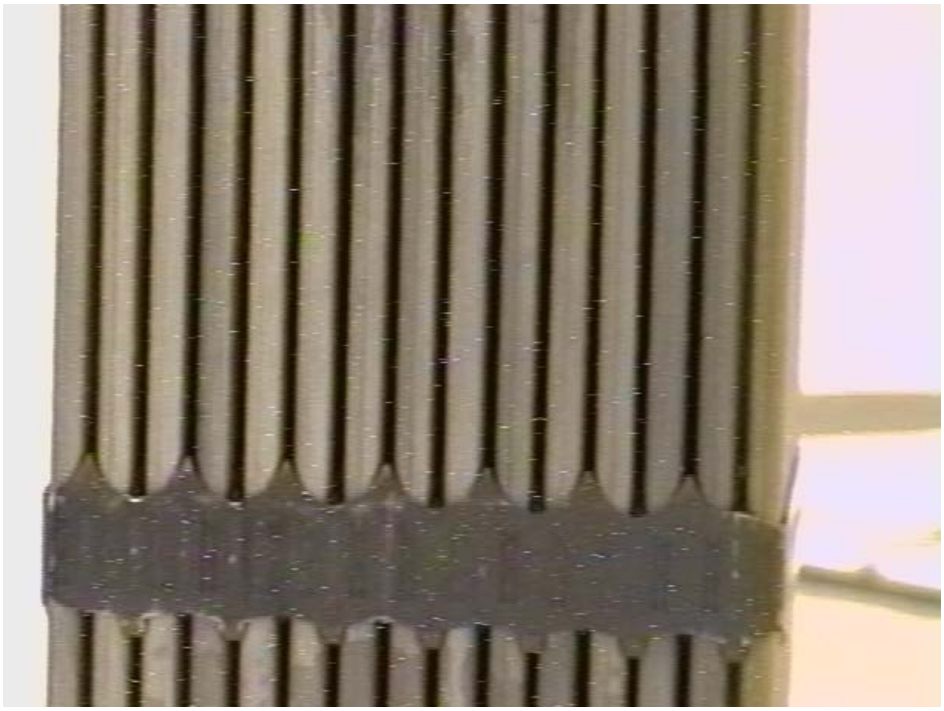

Figure C-15. Element T-03 at intermediate grid spacer—rods appear to be relatively clean with a light oxide coating.

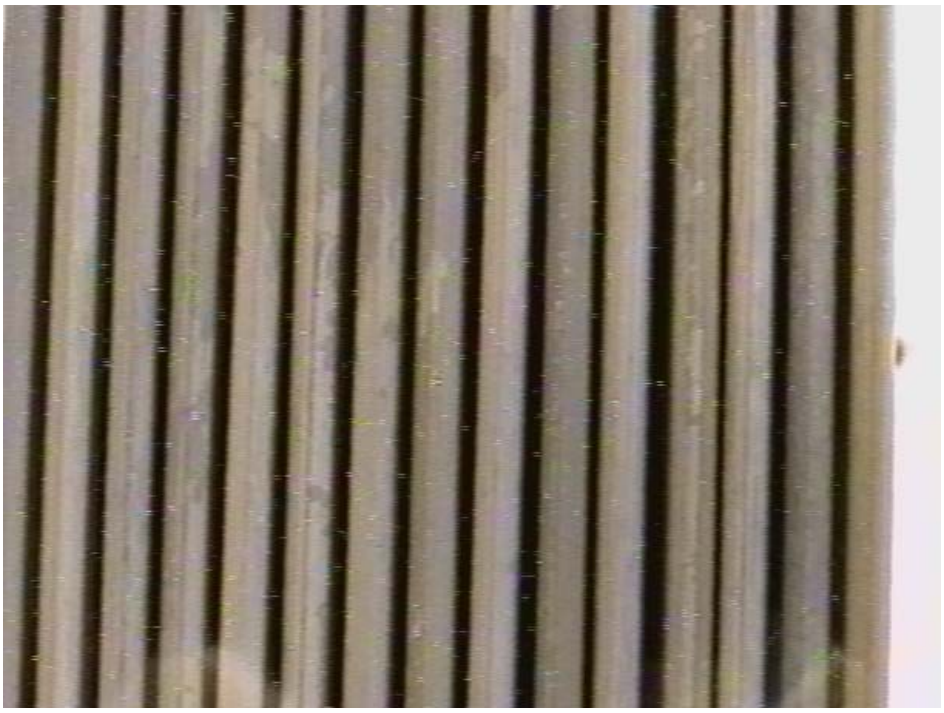

Figure C-16. Element T-03 midpoint of assembly noted oxide density increases as we go lower on the element.

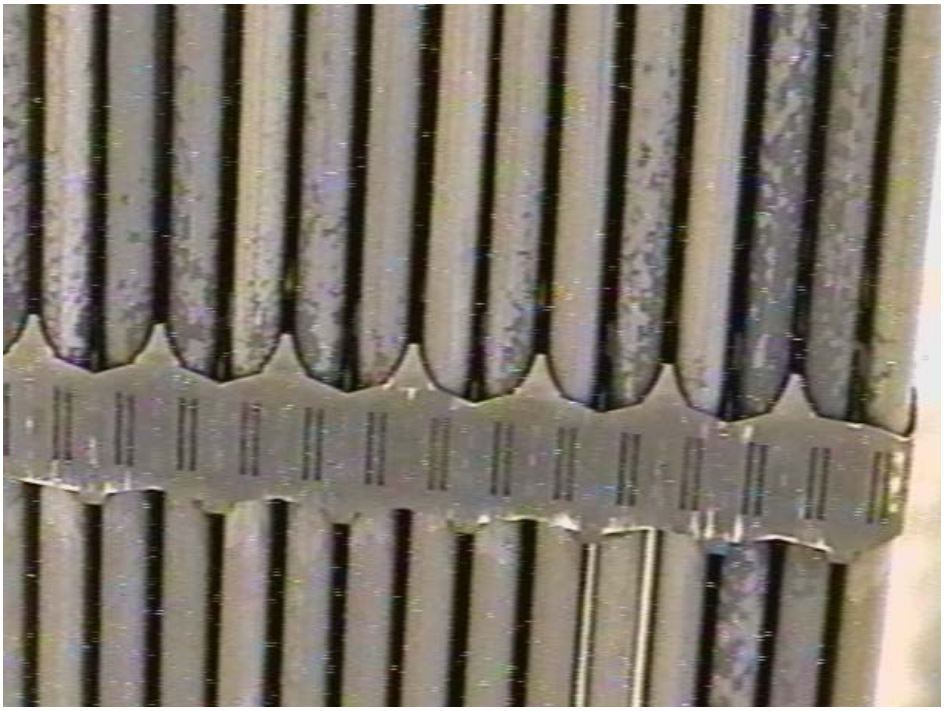

Figure C-17. Element T-03 area adjacent to fifth grid spacer.

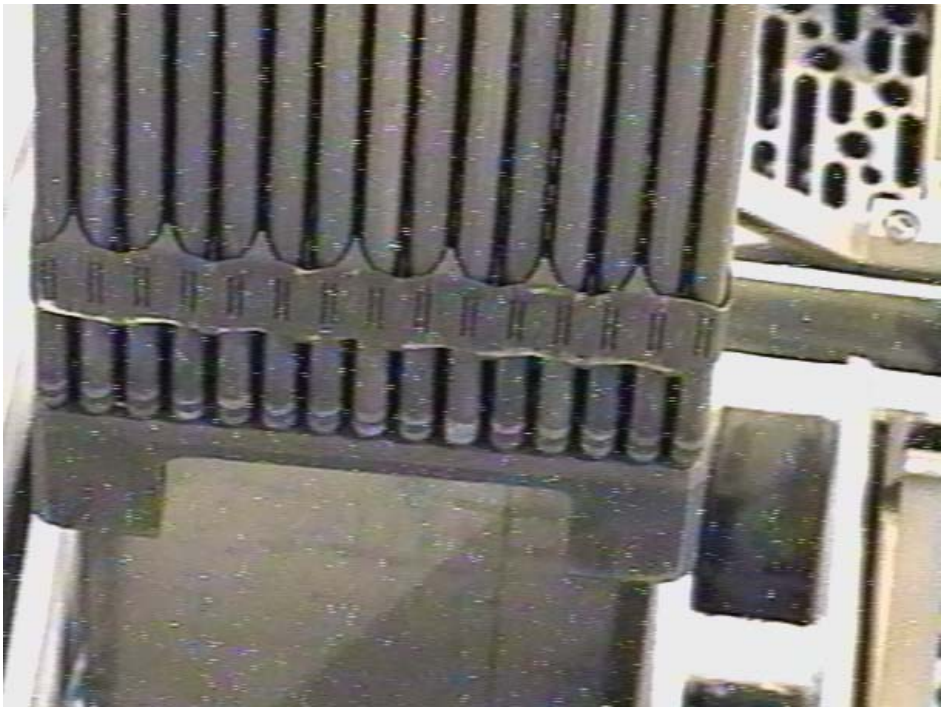

Figure C-18. Element T-03 bottom of fuel element—light oxide—no loose material obvious on surfaces.

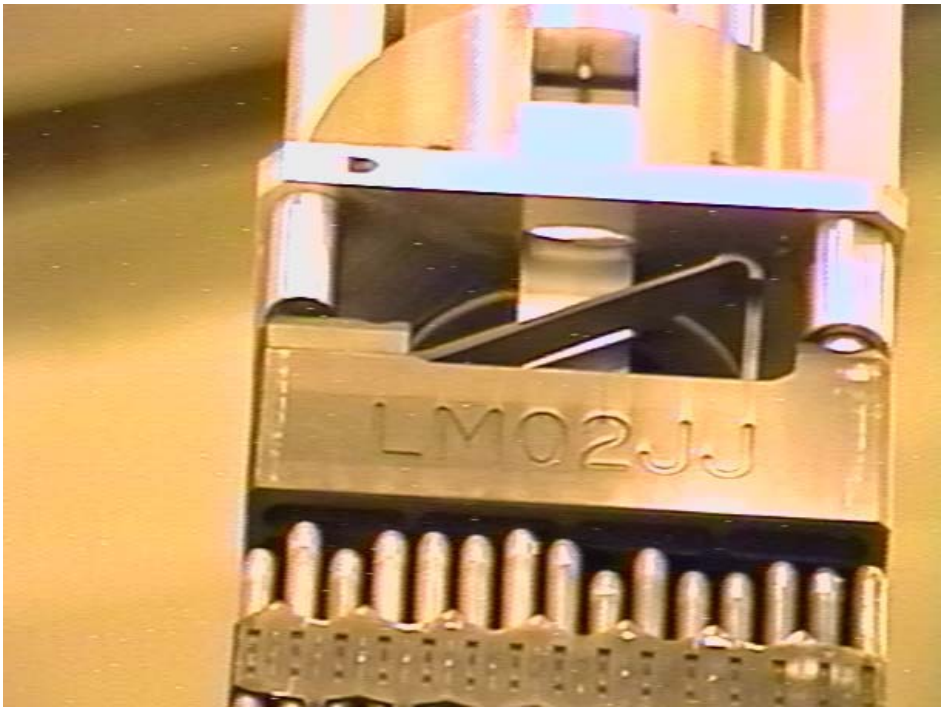

Figure C-19. Fuel element T-03—notes serial number—fuel rod growth evident.

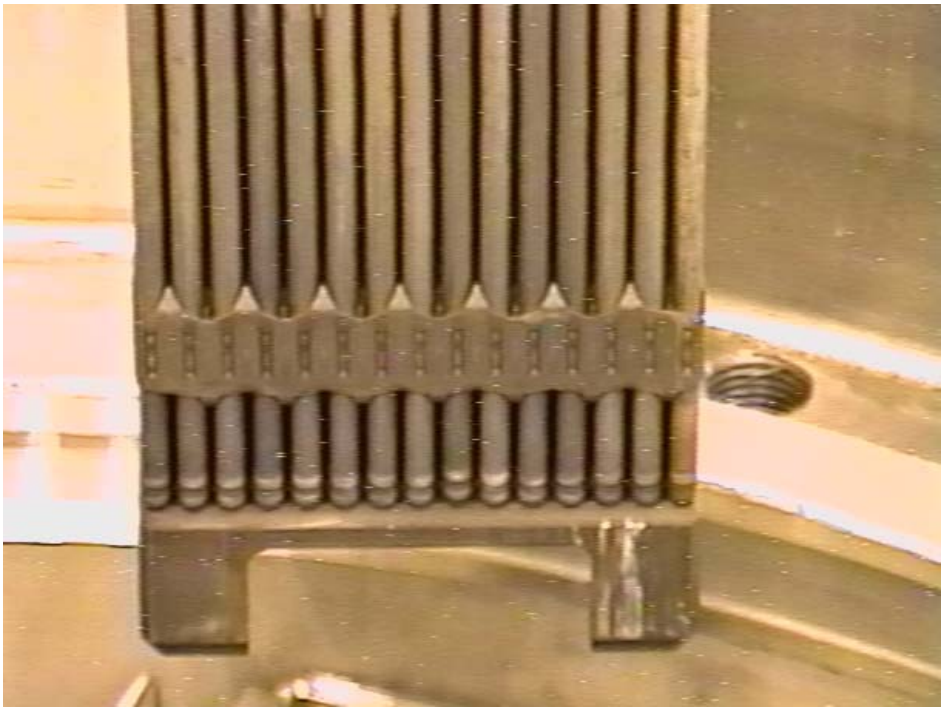

Figure C-20. Fuel element T-03 bottom.

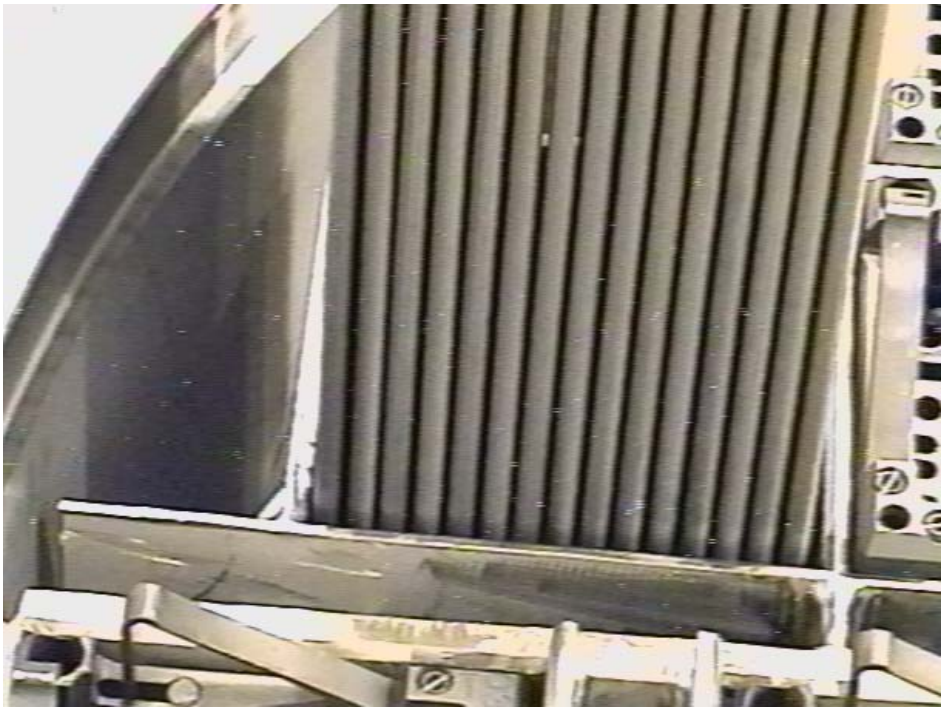

Figure C-21. Fuel assembly V-27 being withdrawn.

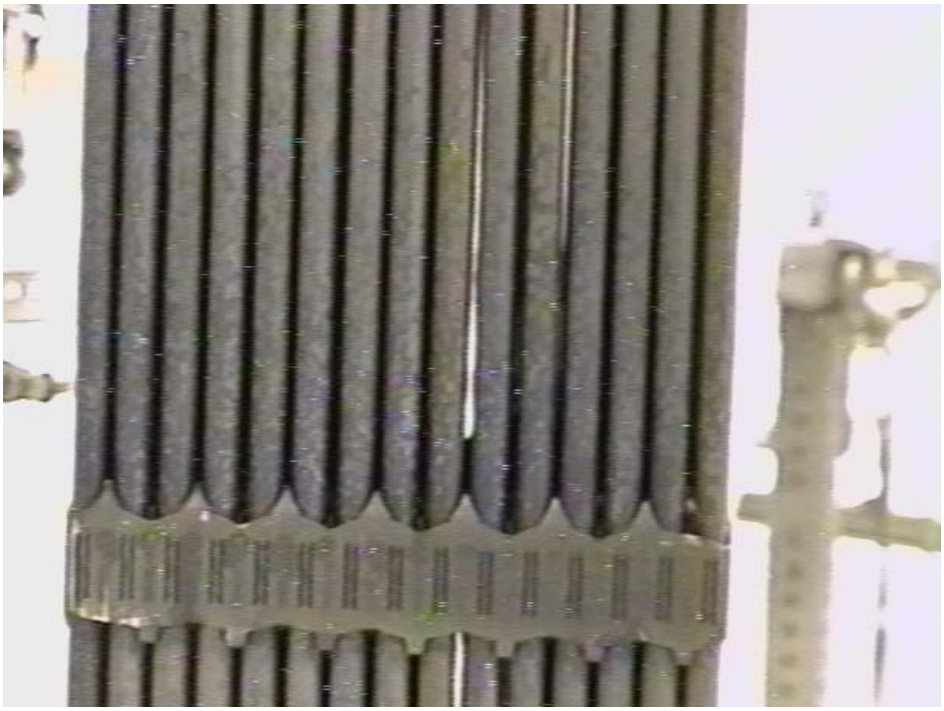

Figure C-22. Fuel assembly V-27 oxide mottling noted.

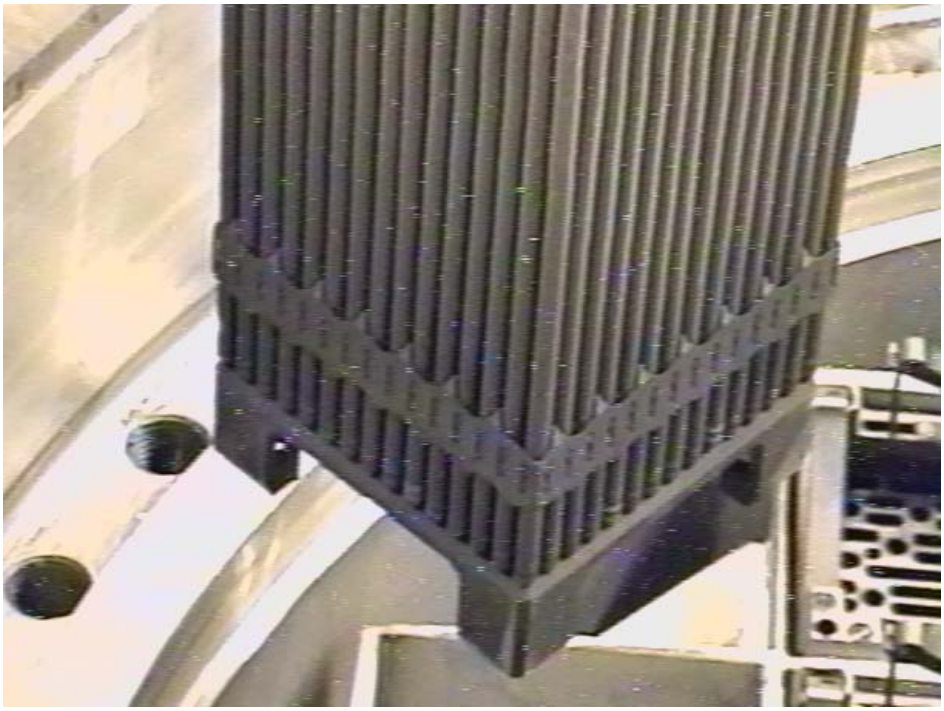

Figure C-23. Fuel assembly V-27 at bottom.

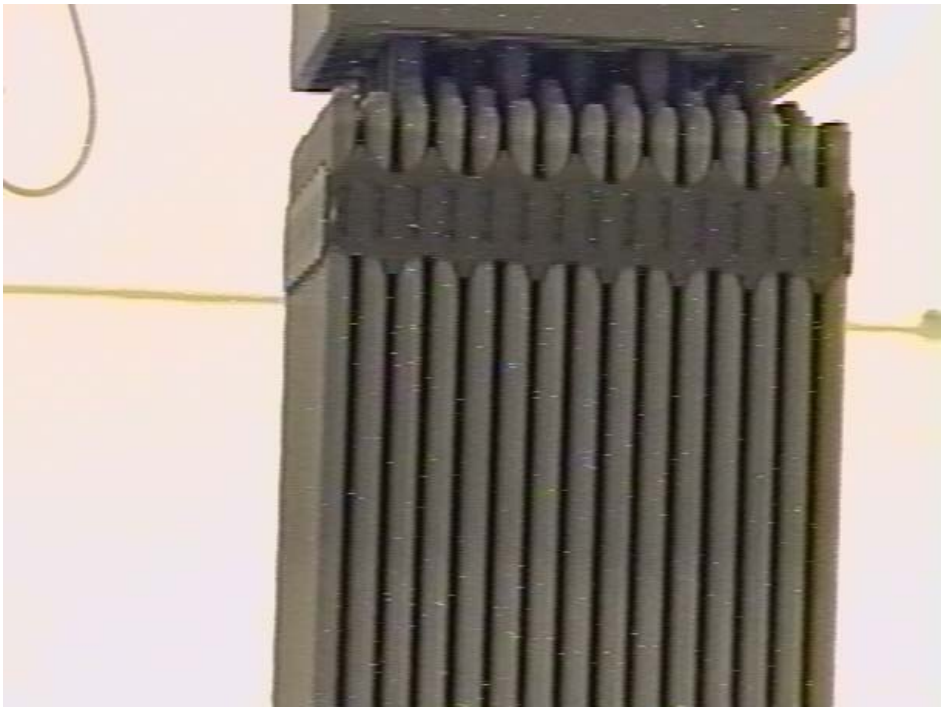

Figure C-24. Fuel assembly V-04.

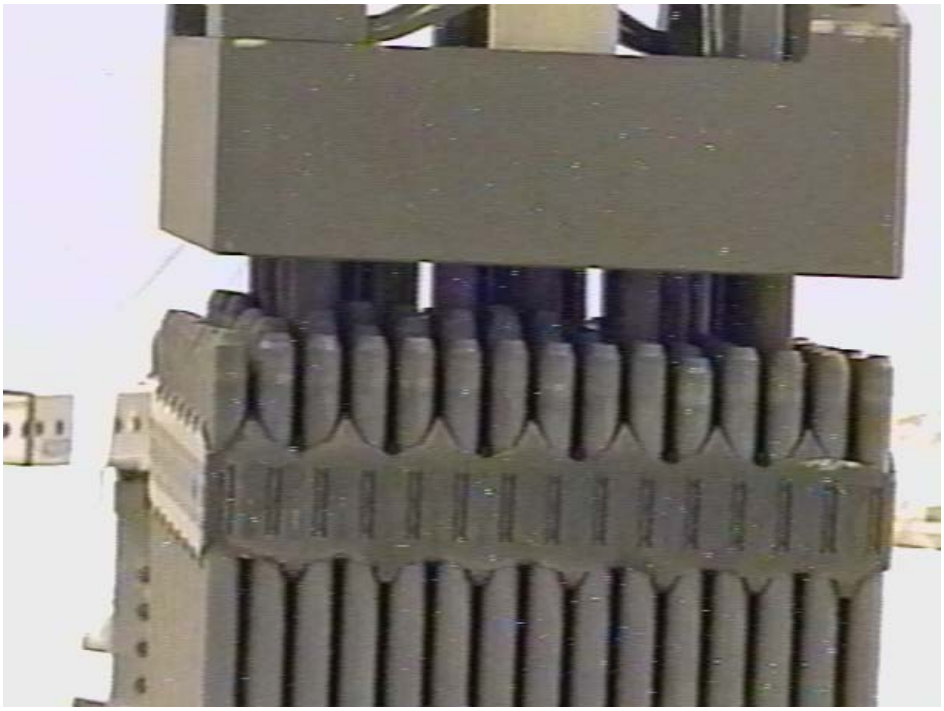

Figure C-25. Fuel assembly V-14.

Figure C-26. Fuel assembly V-14 oxide mottling at fifth grid spacer.

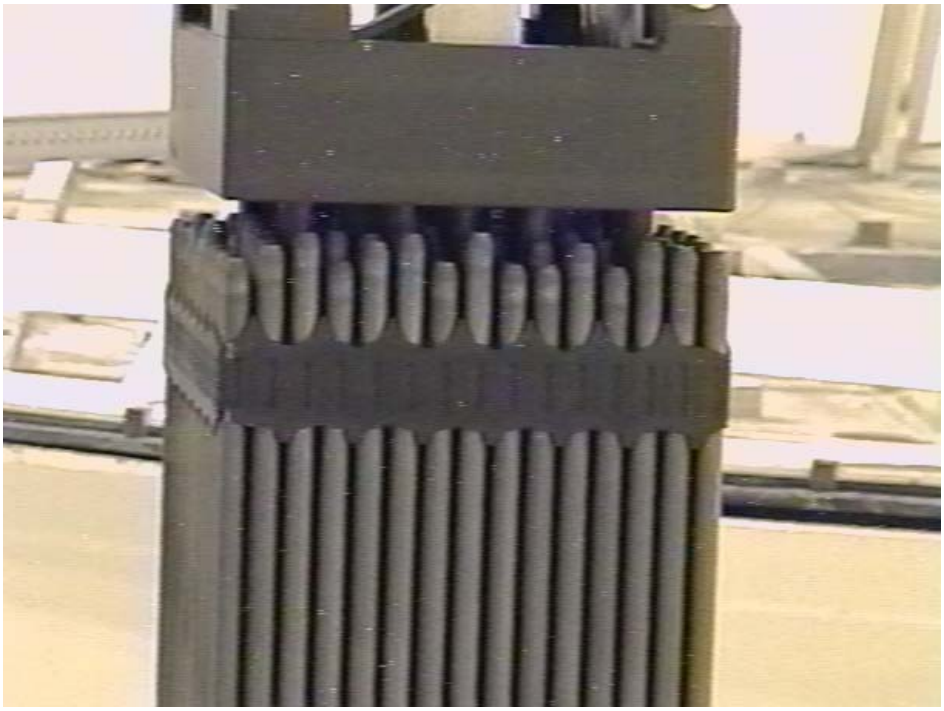

Figure C-27. Fuel assembly T-07 note difference in fuel rod growth.

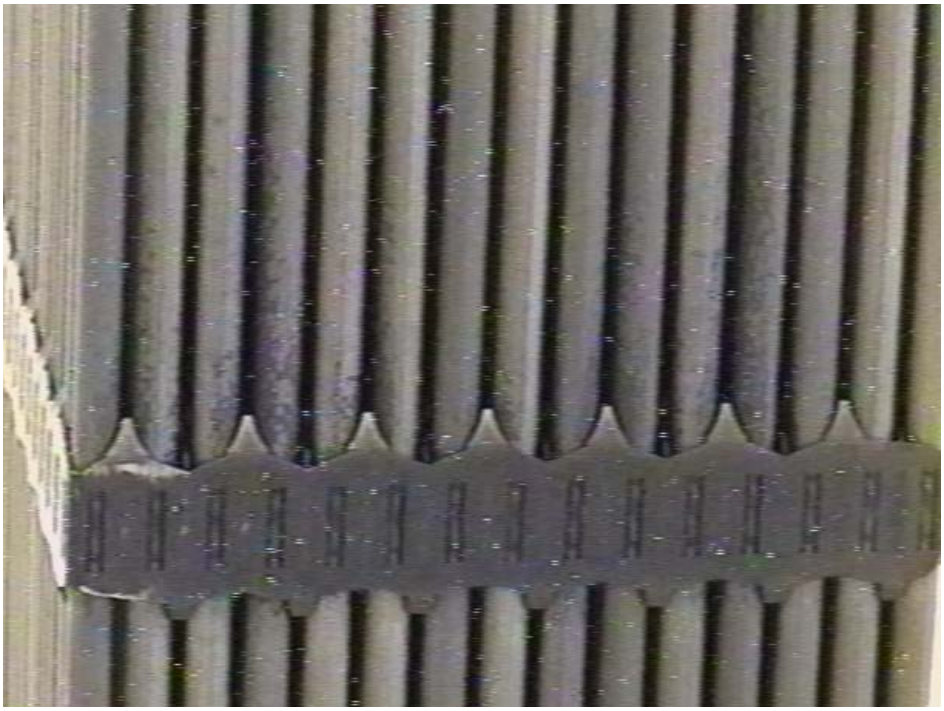

Figure C-28. Fuel assembly T-07 at sixth grid spacer.

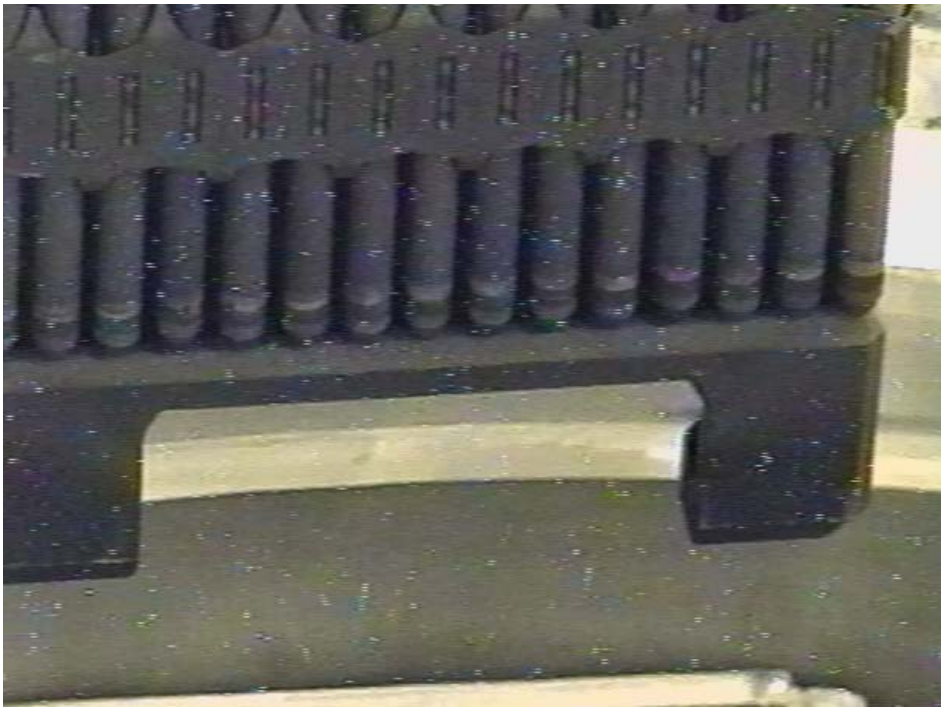

Figure C-29. Fuel assembly T-07 bottom.

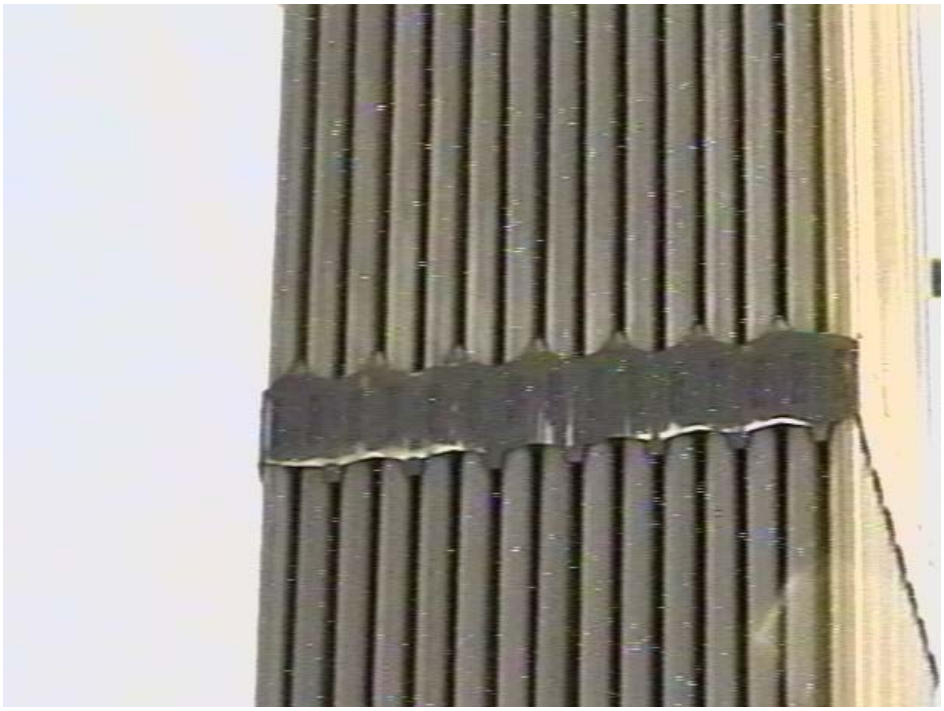

Figure C-30. Fuel assembly T-12 mid point.

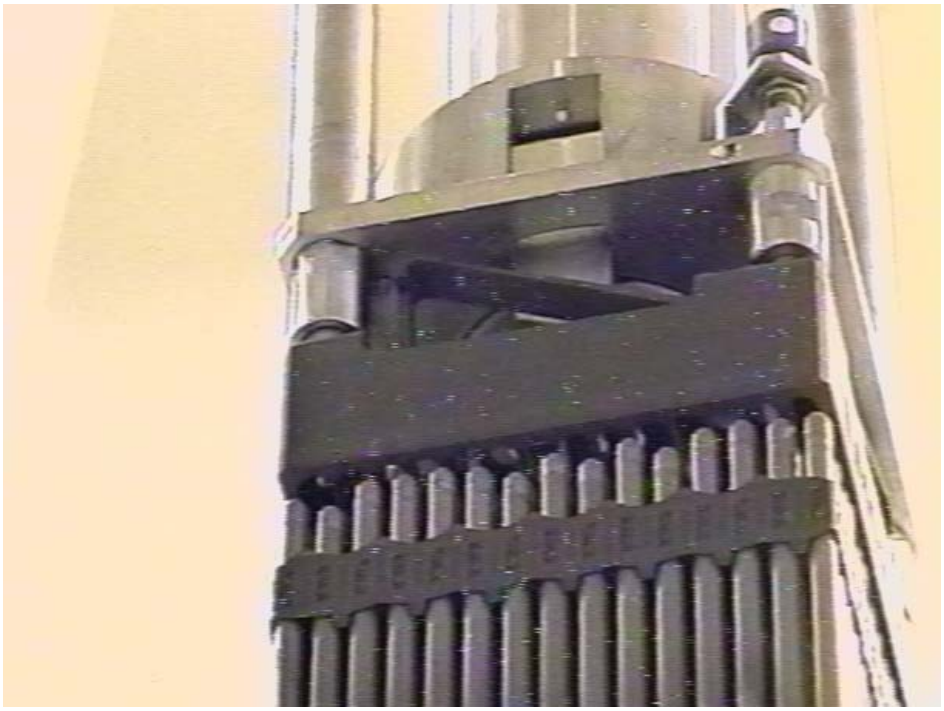

Figure C-31. Fuel assembly T-12.

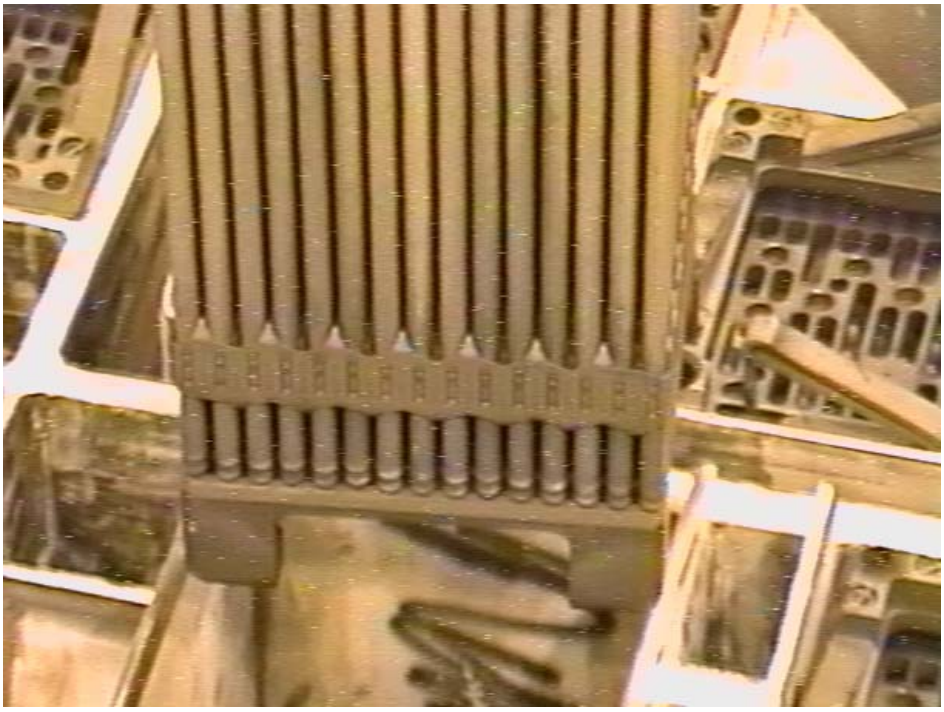

Figure C-32. Fuel assembly T-12.

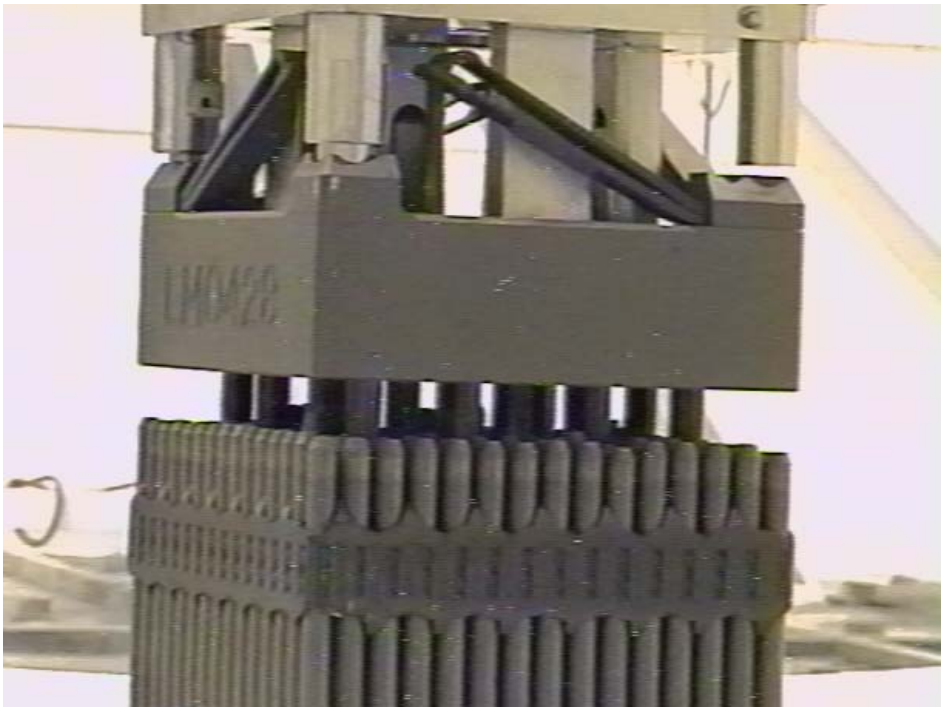

Figure C-33. Fuel assembly V-08 tops of fuel rods appear quite even.

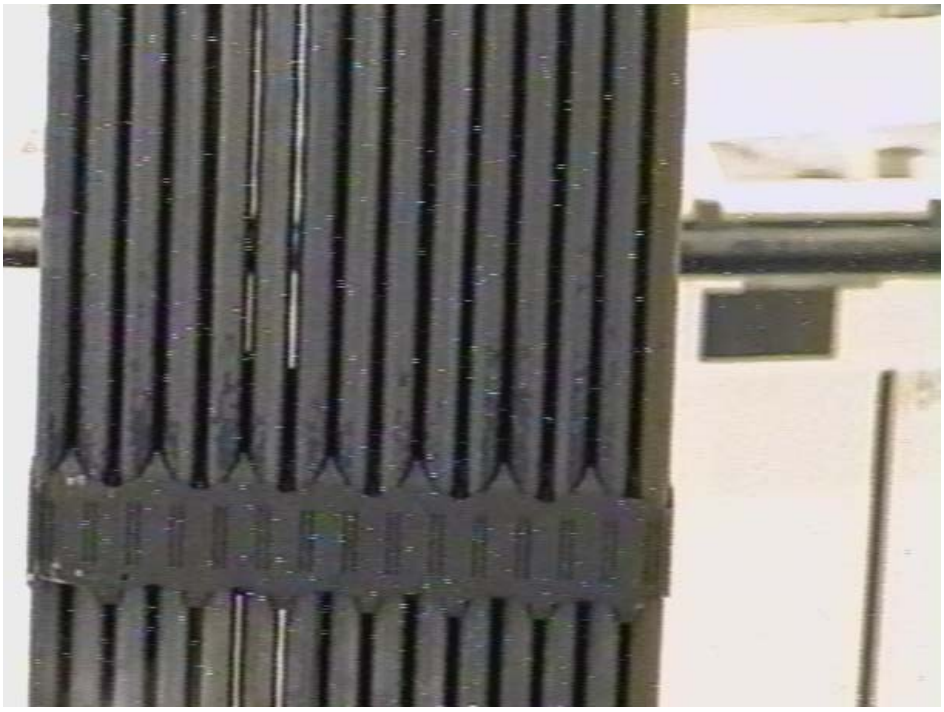

Figure C-34. Fuel assembly V-08 at fifth spacer—noted oxide mottling.

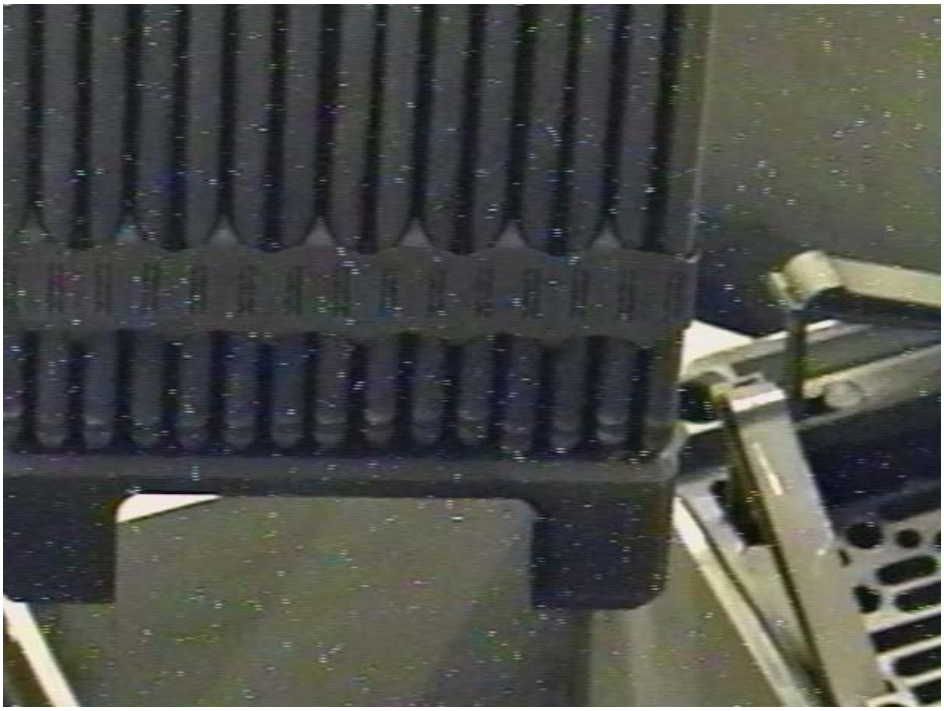

Figure C-35. Fuel assembly V-08.

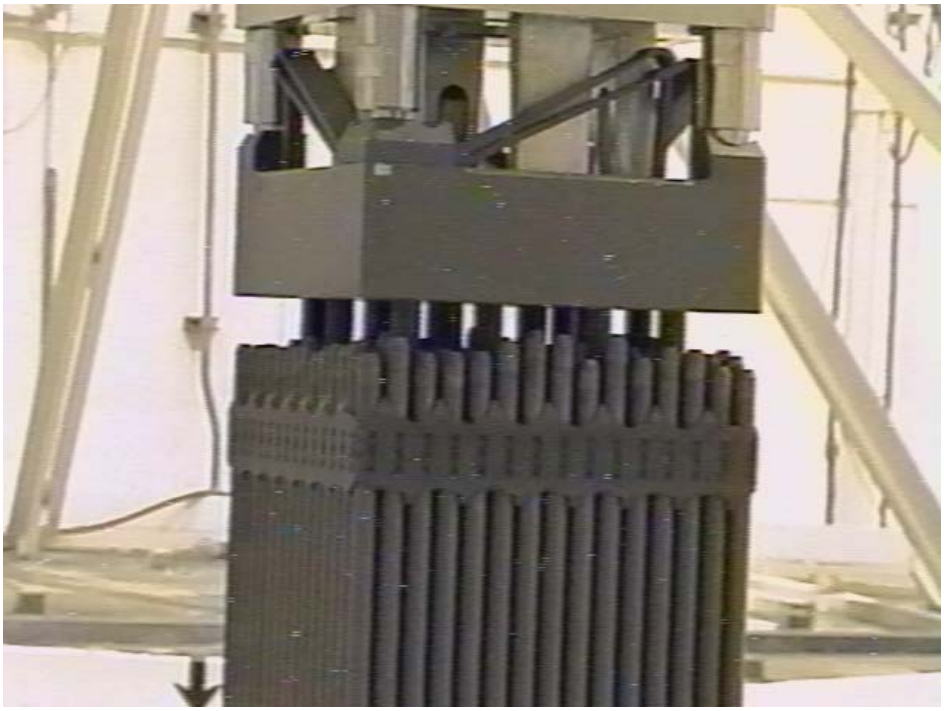

Figure C-36. Fuel assembly V-11.

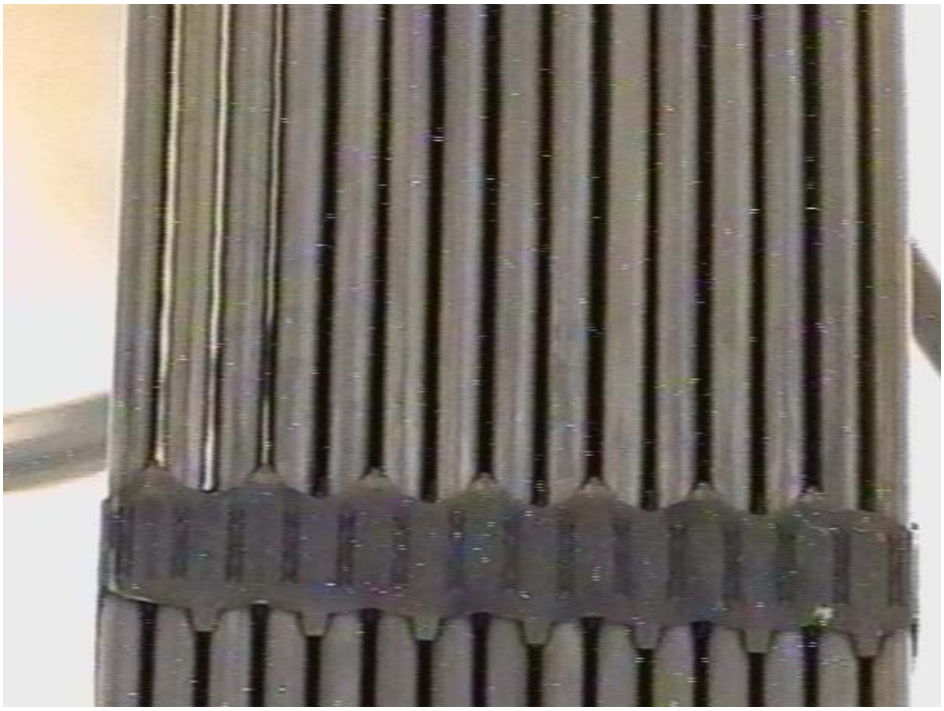

Figure C-37. Fuel assembly V-11 at sixth spacer.

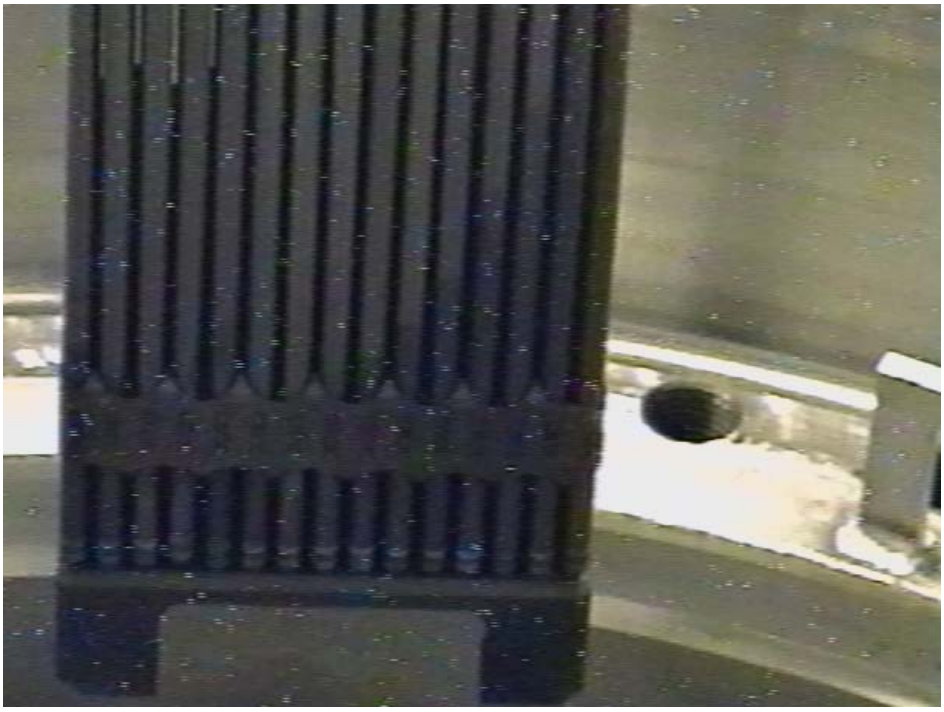

Figure C-38. Fuel assembly V-11.

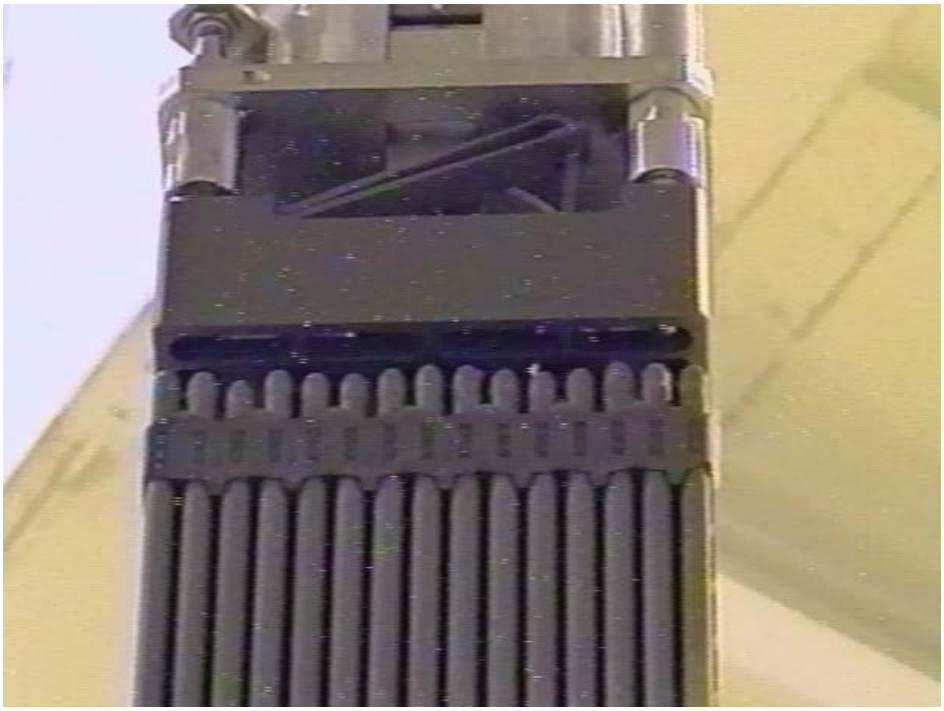

Figure C-39. Fuel assembly V-01.

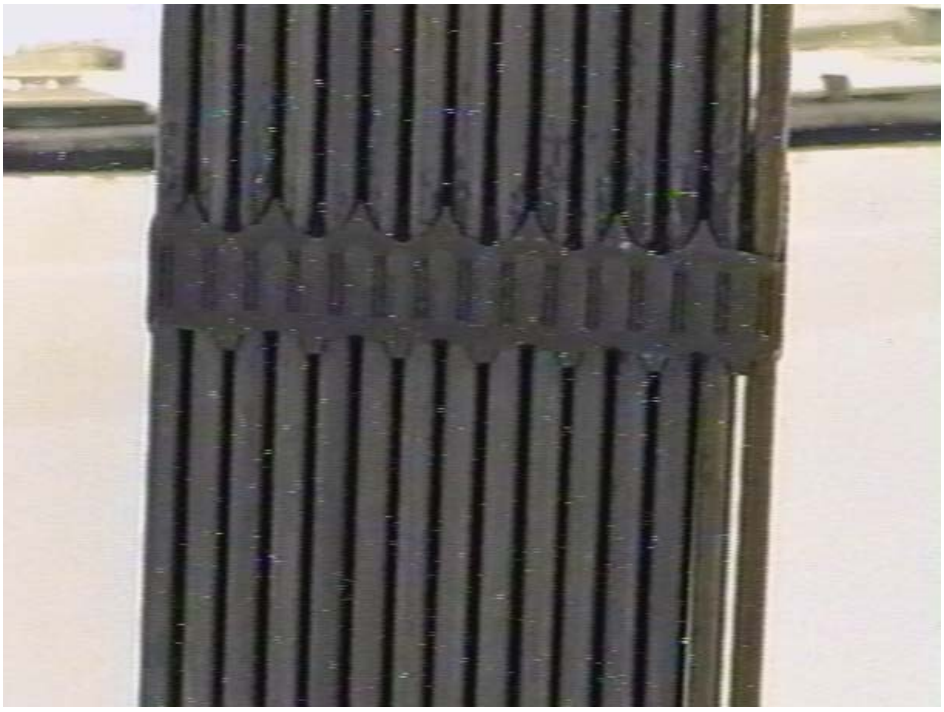

Figure C-40. Fuel assembly V-01 at fifth grid spacer.

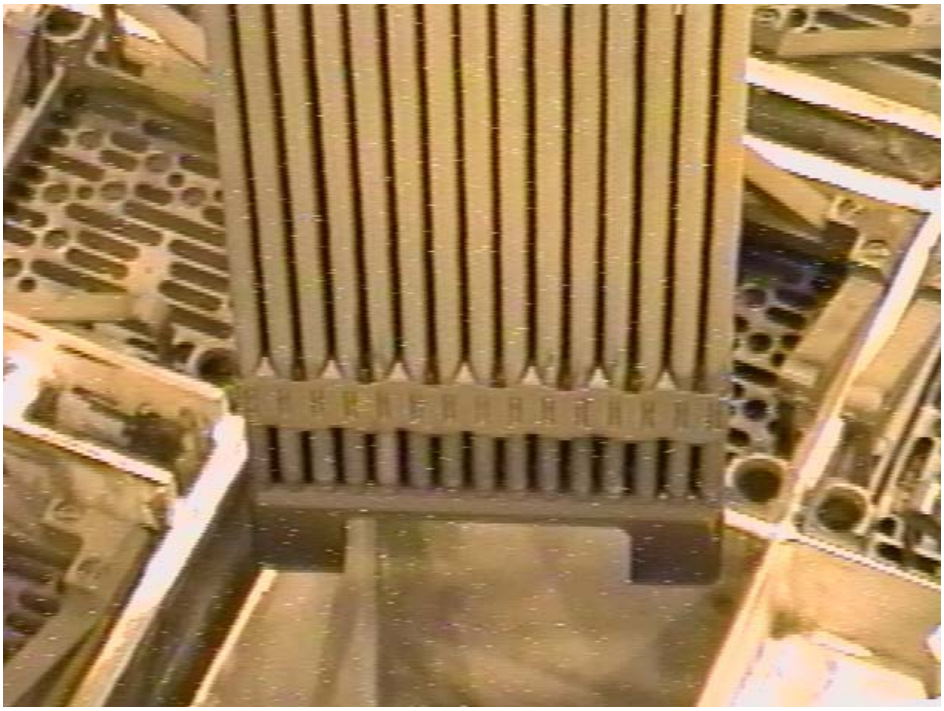

Figure C-41. Fuel assembly V-01.

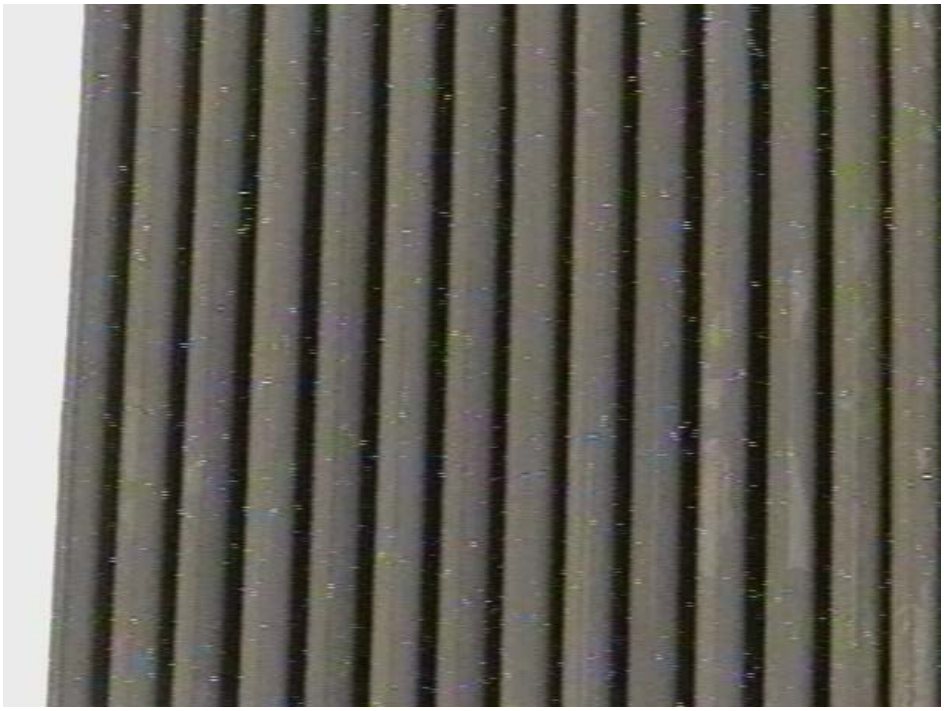

Figure C-42. Fuel assembly T-08 near top.

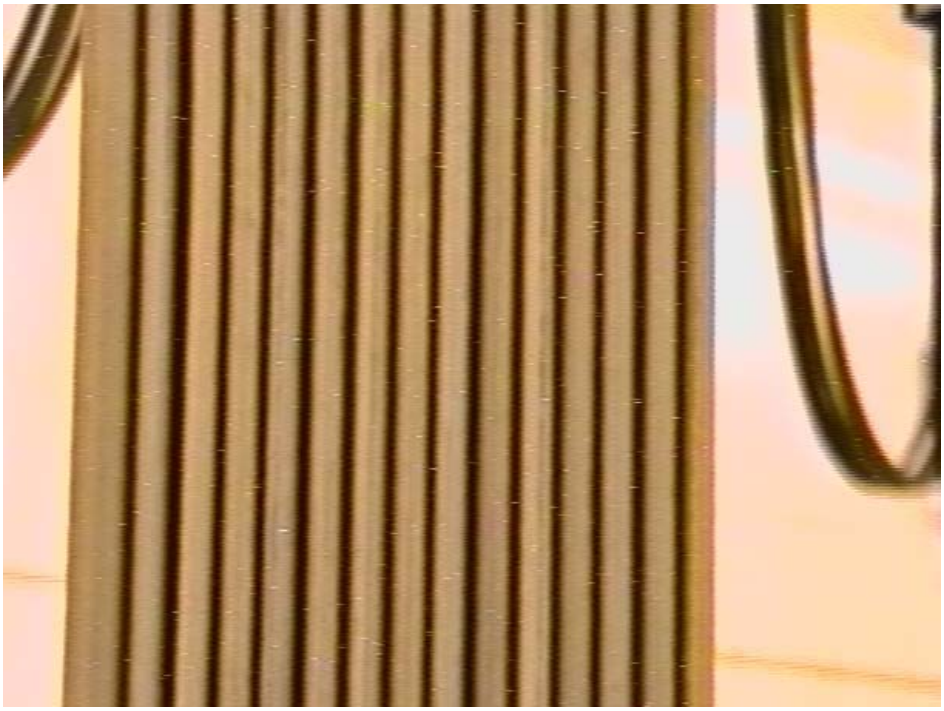

Figure C-43. Fuel assembly T-08 near sixth grid spacer.

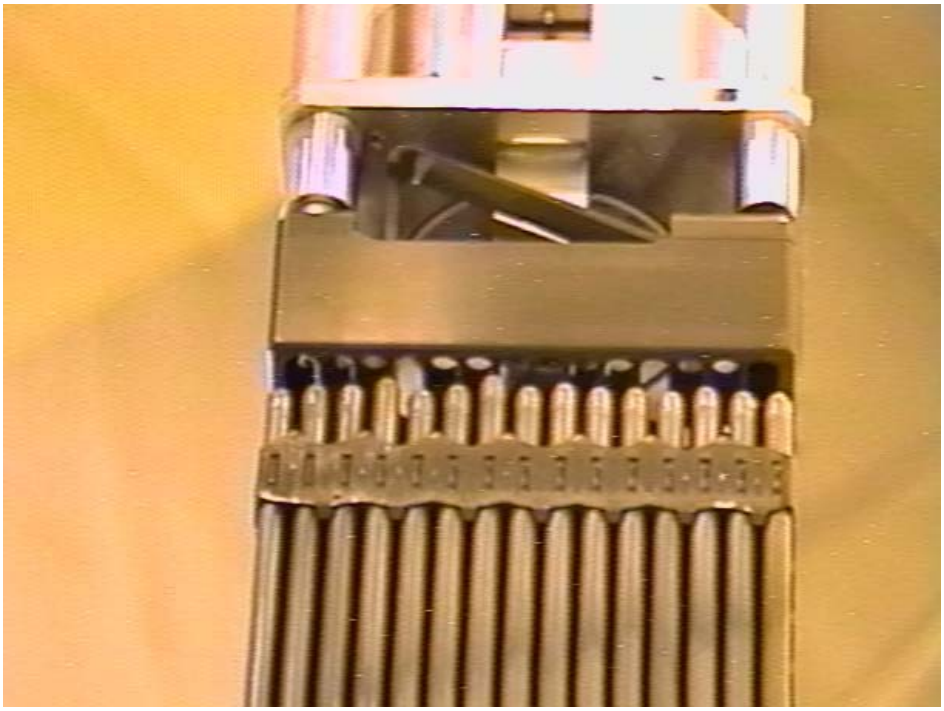

Figure C-44. Fuel assembly T-09—note uneven rods.

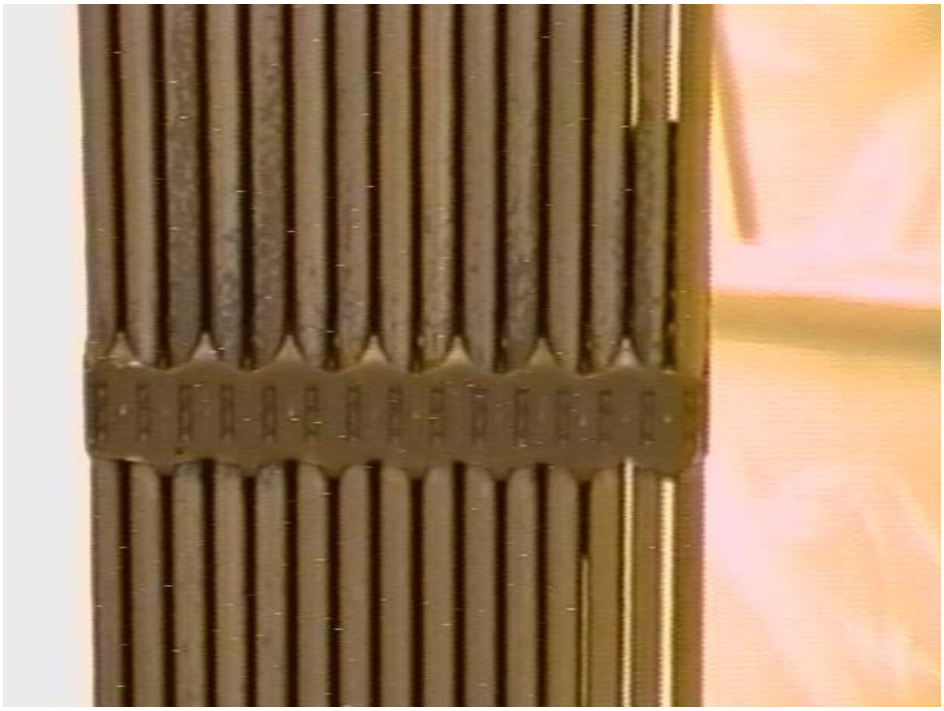

Figure C-45. Fuel assembly T-09 at sixth grid spacer.

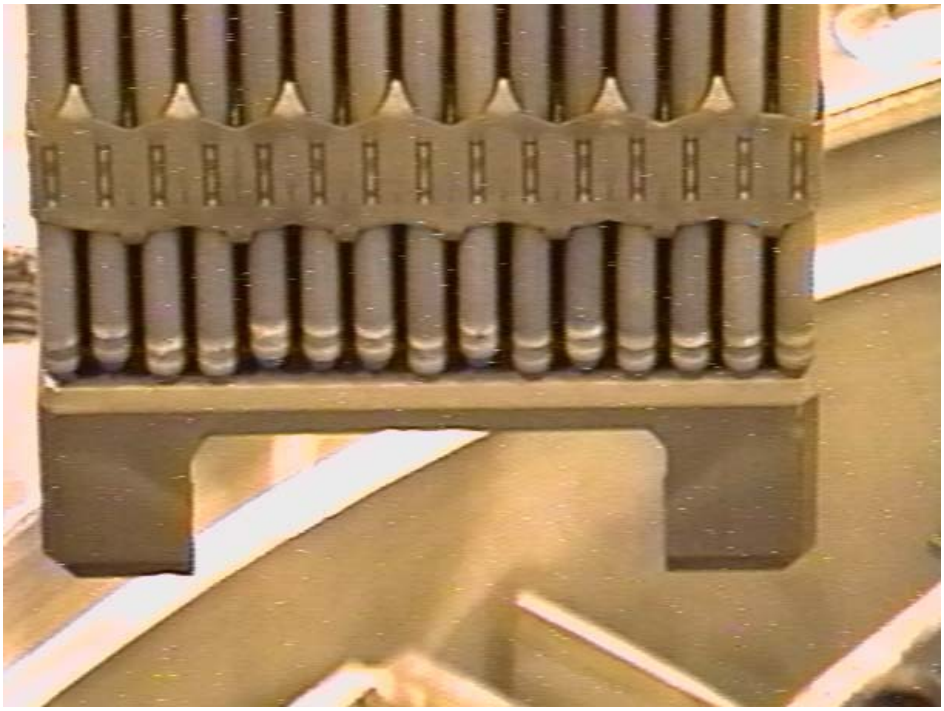

Figure C-46. Fuel assembly T-09.

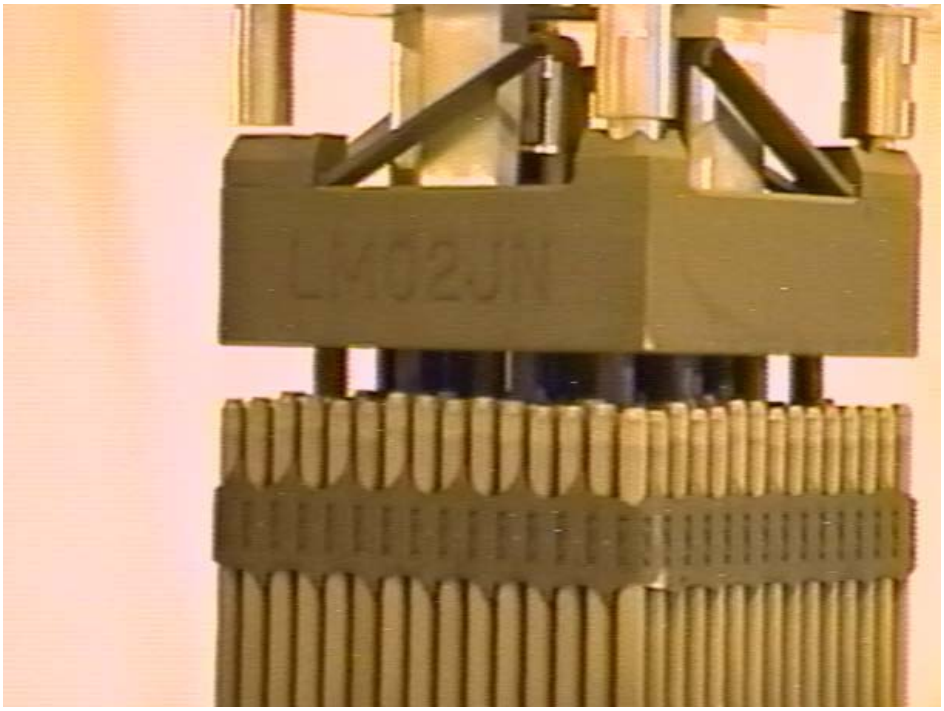

Figure C-47. Fuel assembly T-16.

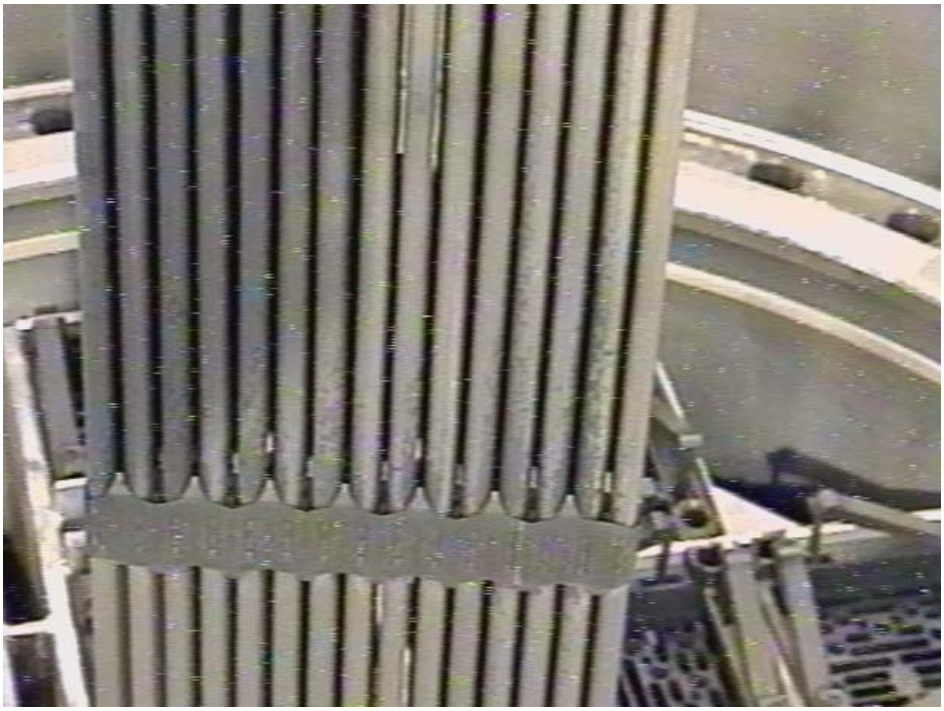

Figure C-48. Fuel assembly T-16 at sixth grid spacer.

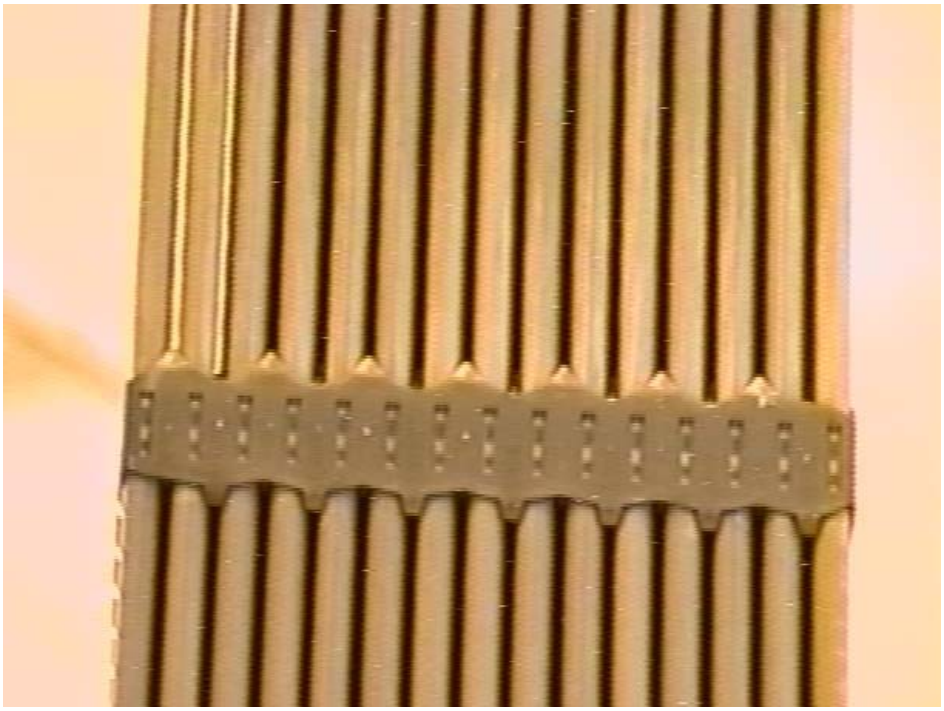

Figure C-49. Fuel assembly T-16.

Figure C-50. Fuel assembly T-16.

Figure C-51. Fuel assembly V-24.

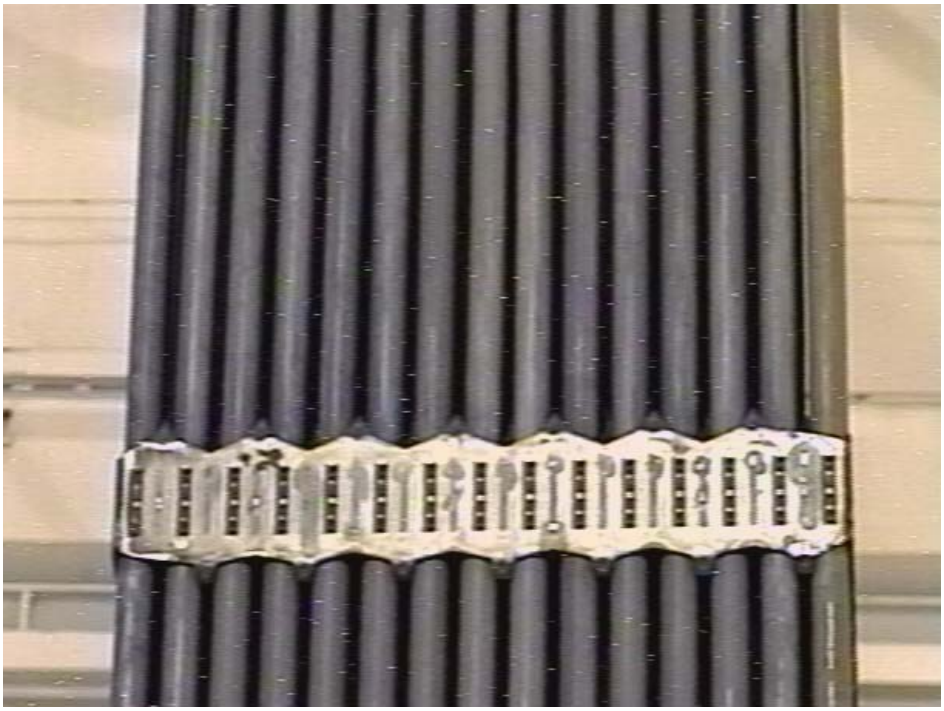

Figure C-52. Fuel assembly V-24 third spacer.

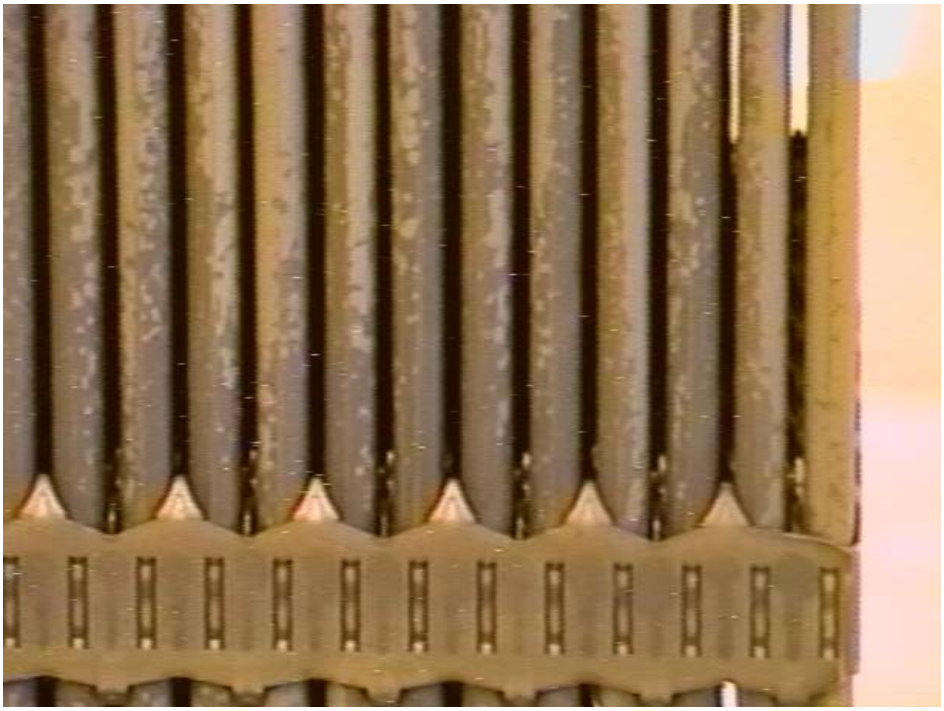

Figure C-53. Fuel assembly V-24 near fifth spacer.

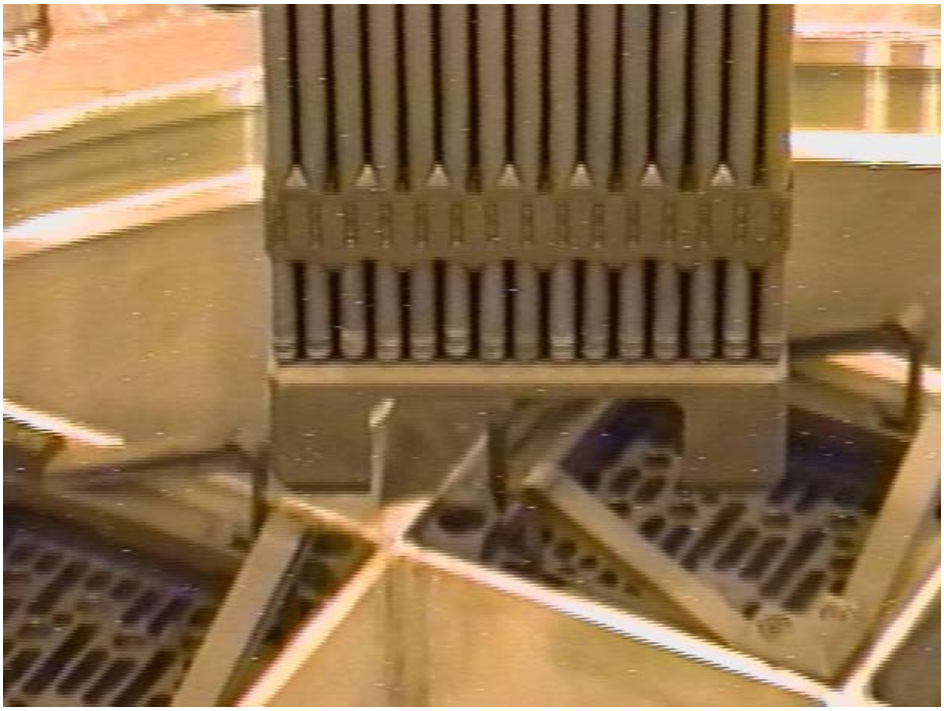

Figure C-54. Fuel assembly V-24.

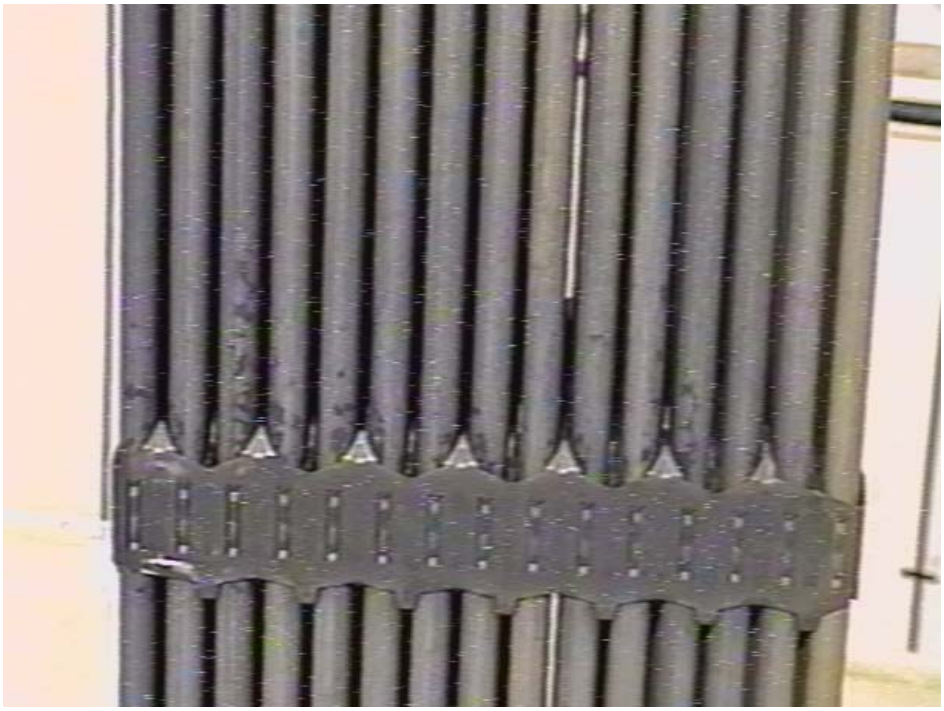

Figure C-55. Fuel assembly V-15 third grid spacer.

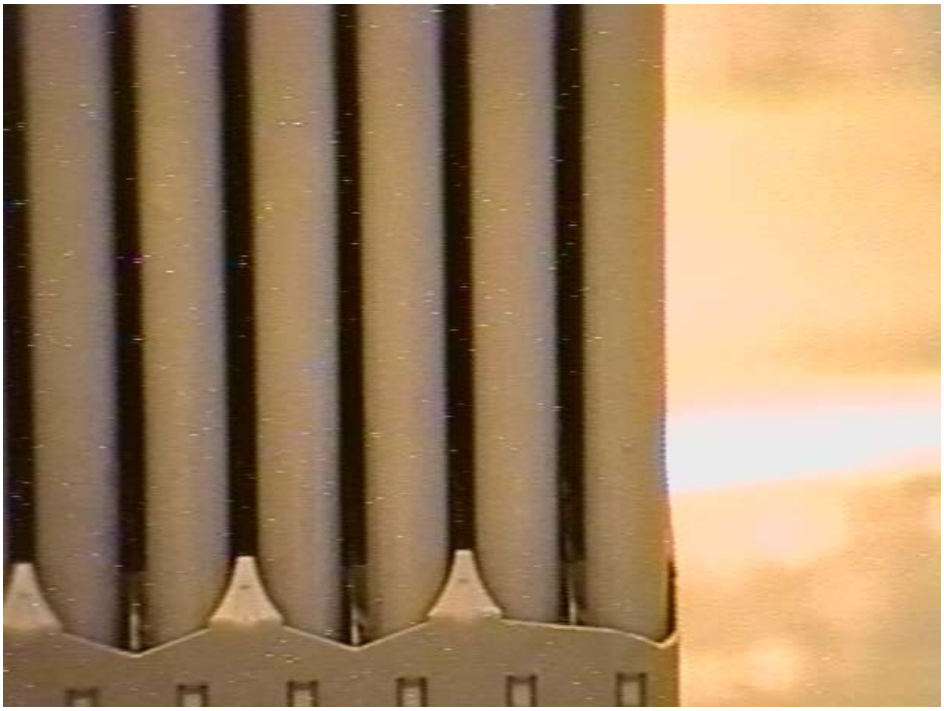

Figure C-56. Fuel assembly V-15 close ups at sixth grid spacer.

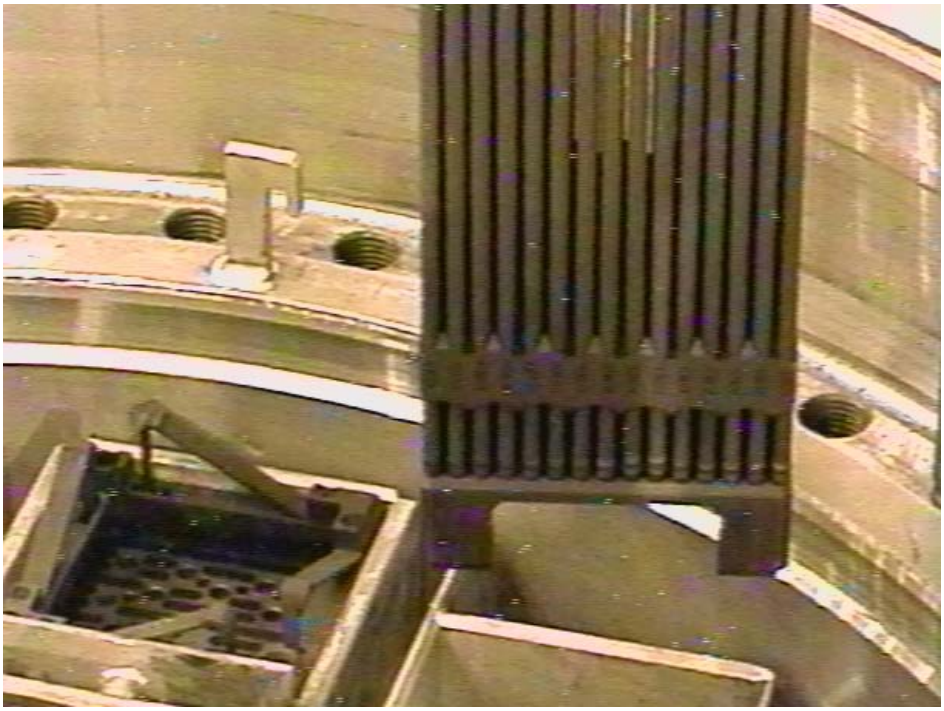

Figure C-57. Fuel assembly V-15.

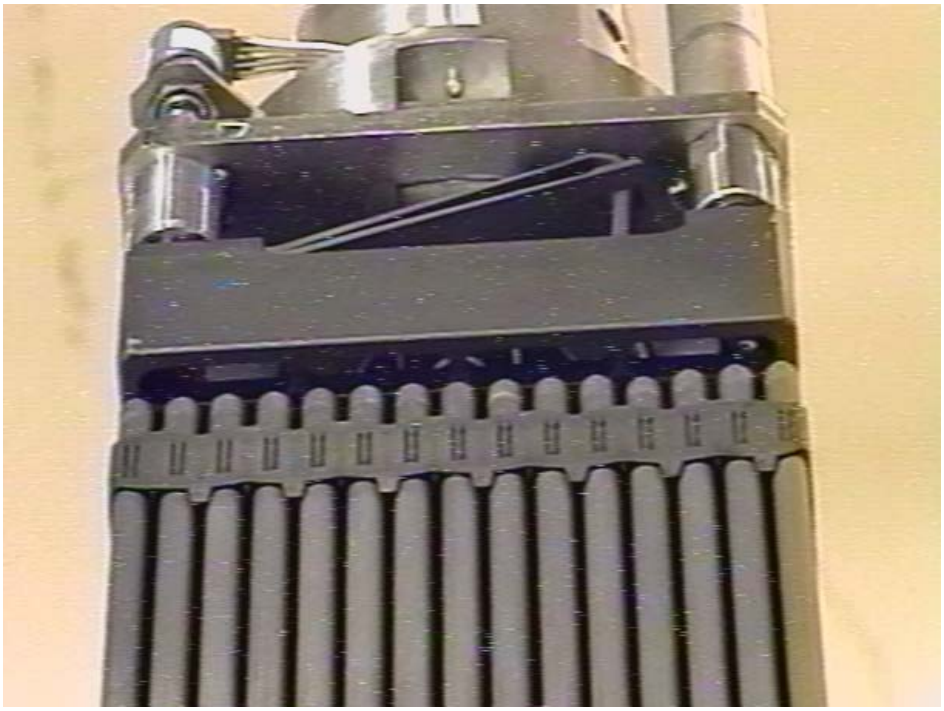

Figure C-58. Fuel assembly V-25.

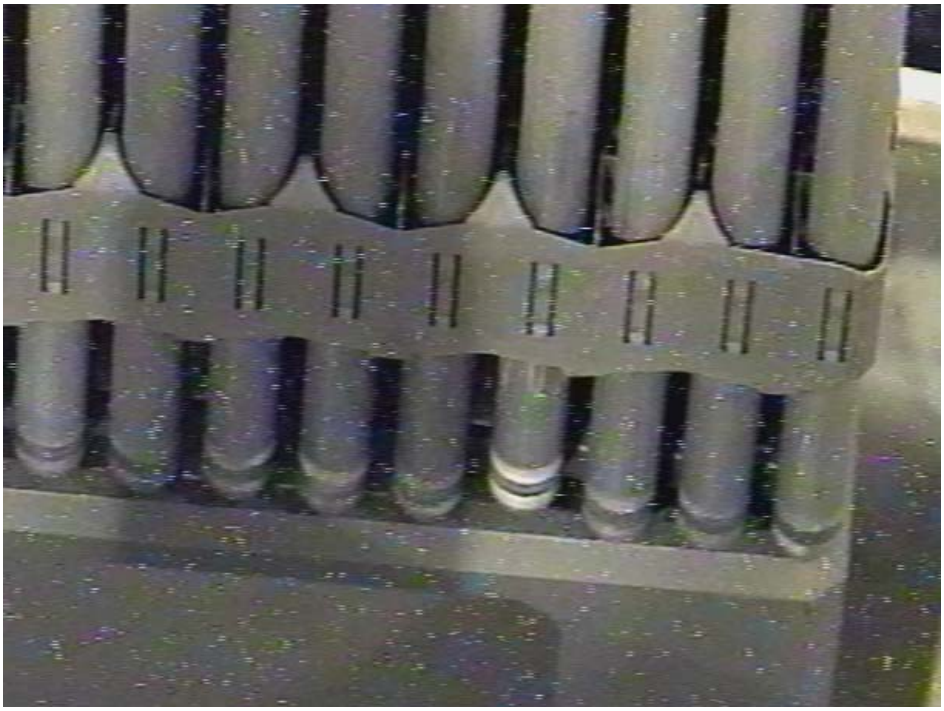

Figure C-59. Fuel assembly V-25.

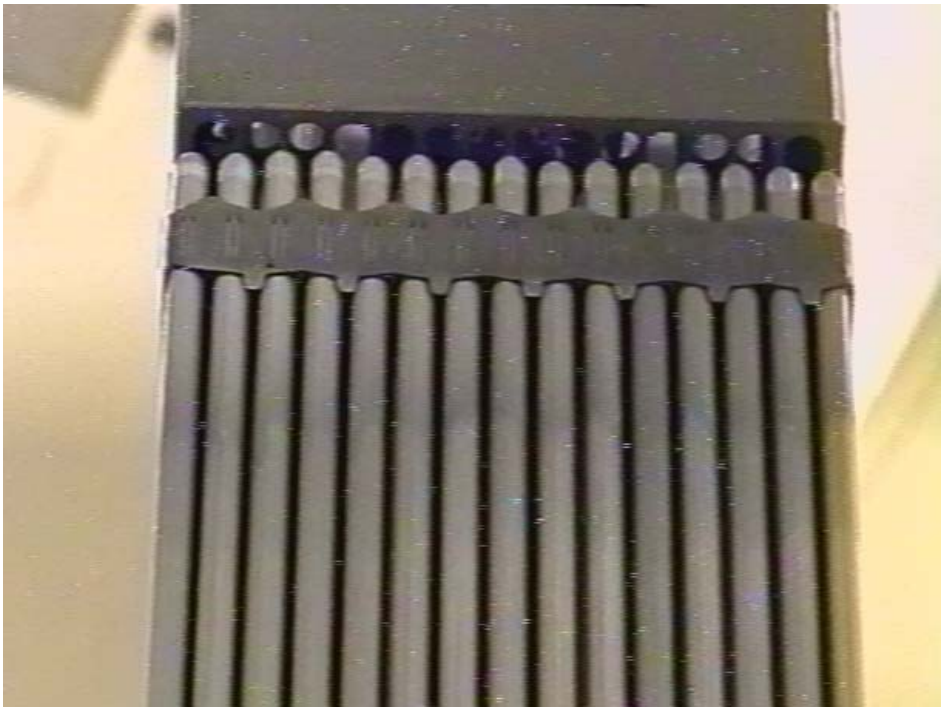

Figure C-60. Fuel assembly T-13.

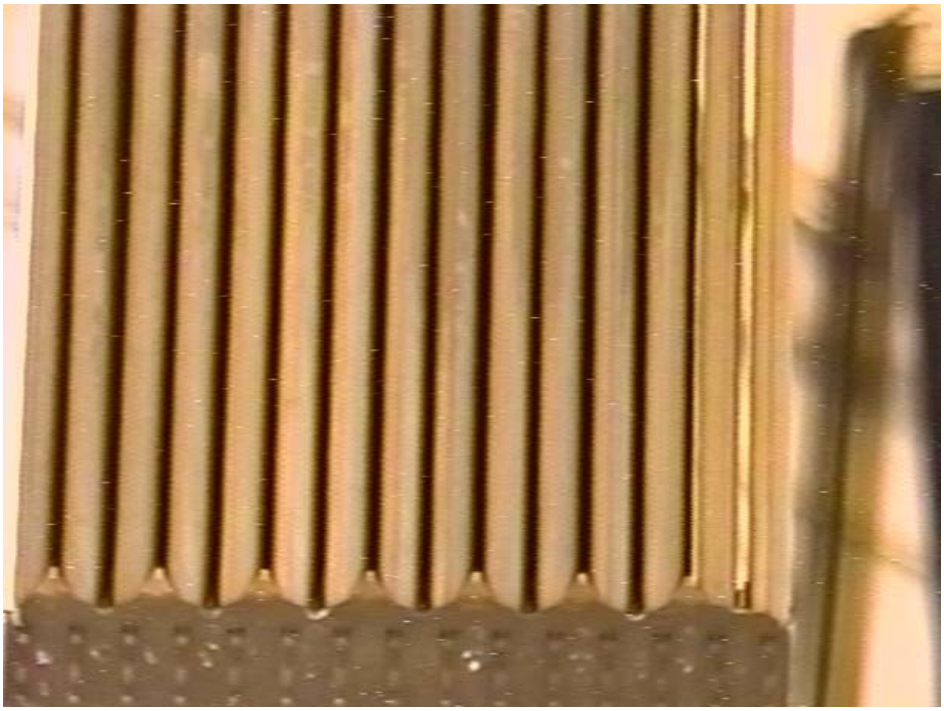

Figure C-61. Fuel assembly T-13 near sixth grid spacer.

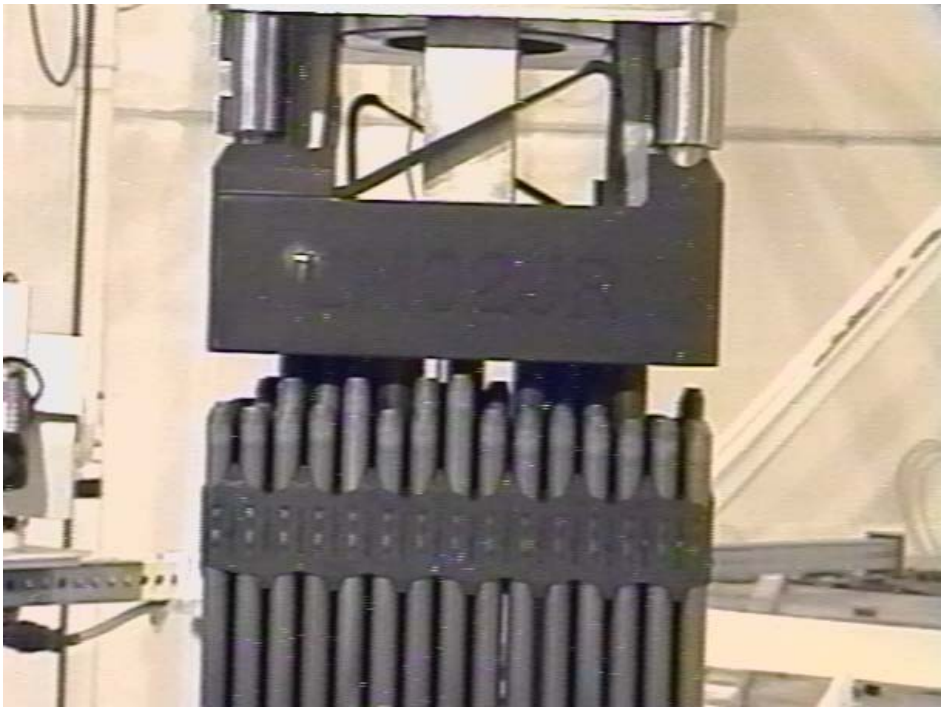

Figure C-62. Fuel assembly T-11.

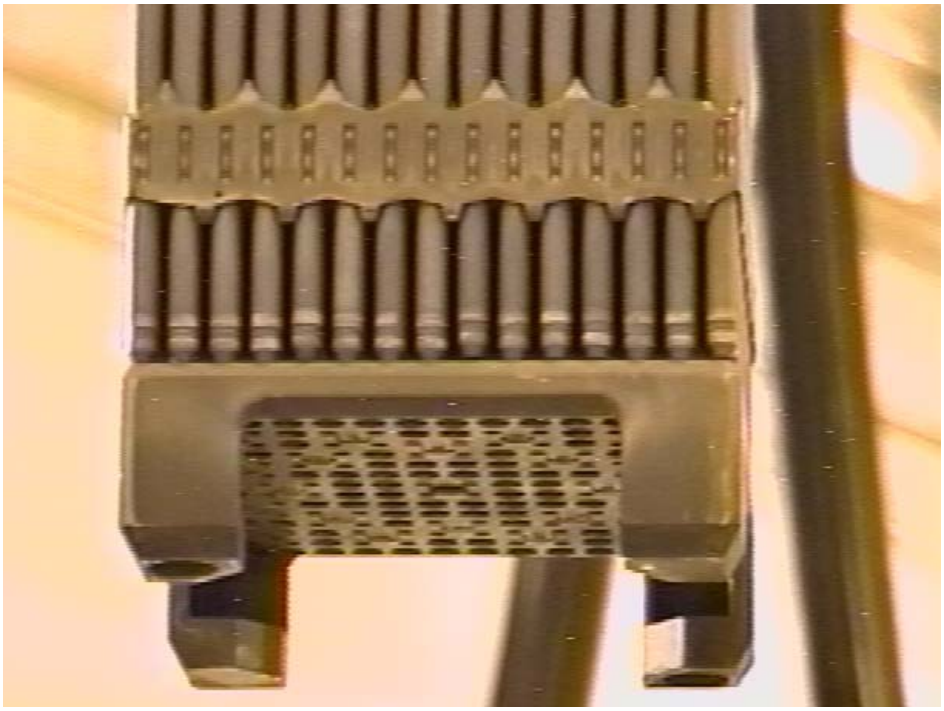

Figure C-63. Fuel assembly T-11.

Figure C-64. Fuel assembly T-11 attempt to obtain loose material.

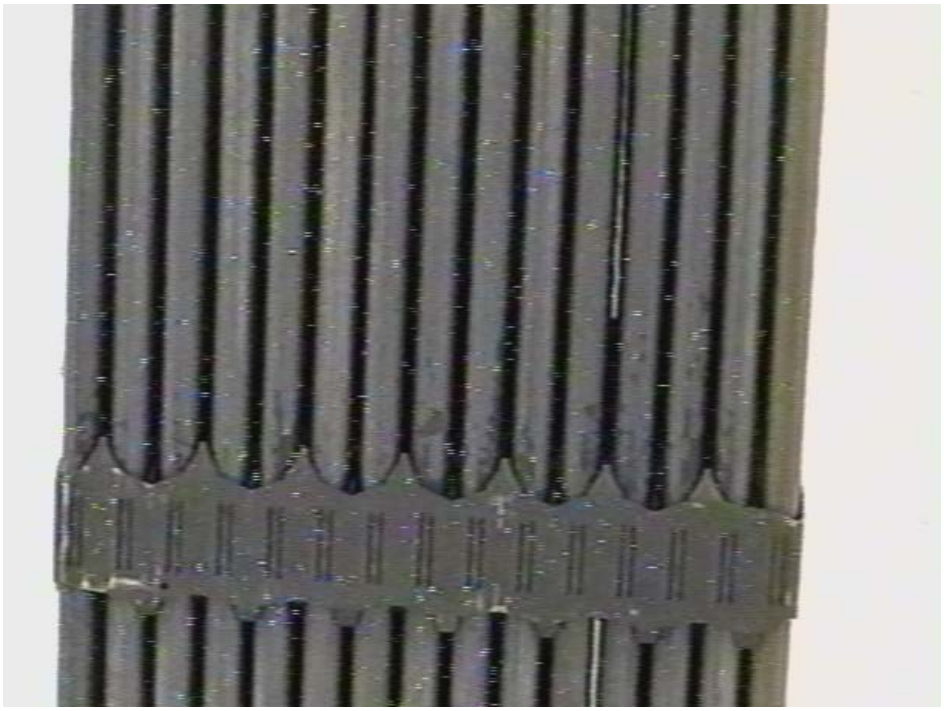

Figure C-65. Fuel assembly V-05 fourth grid spacer oxide mottling noted.

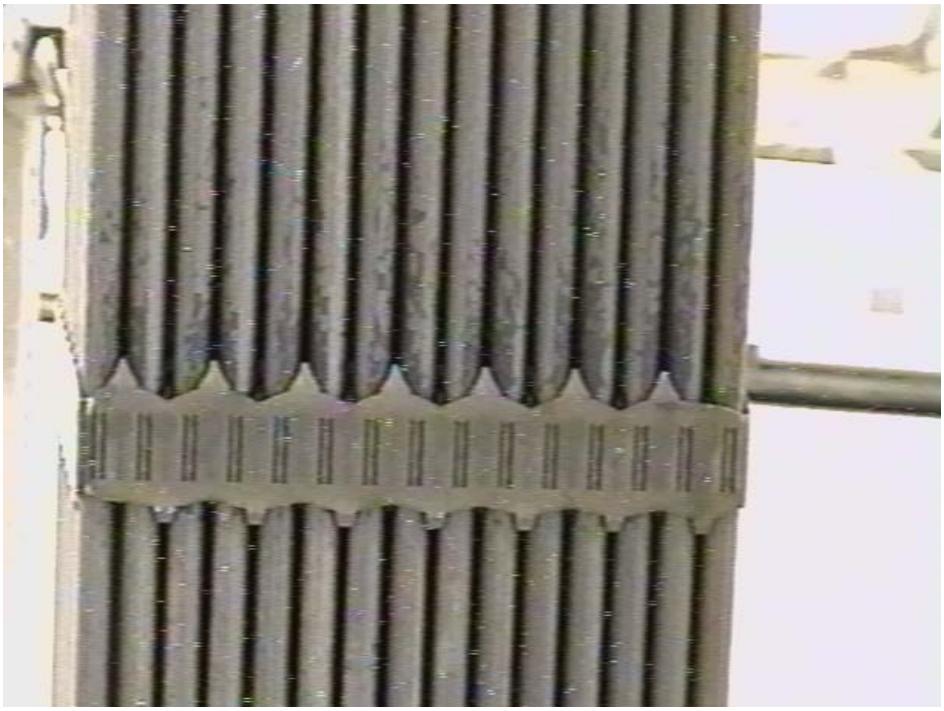

Figure C-66. Fuel assembly V-04 mottling at fifth grid spacer.

Figure 67. Fuel assembly V-04—bottom—rod having greatest indication of oxide appears to be slightly above the nozzle plate—no conclusion made.

Appendix D

Fuel Tubes

Figure D-1. Fuel Tube A-1 top-appears clean. Typical appearance and cleanliness of all fuel tubes.

Figure D-2. Fuel Tube A-1 – Close up of bottom – minor debris noted.

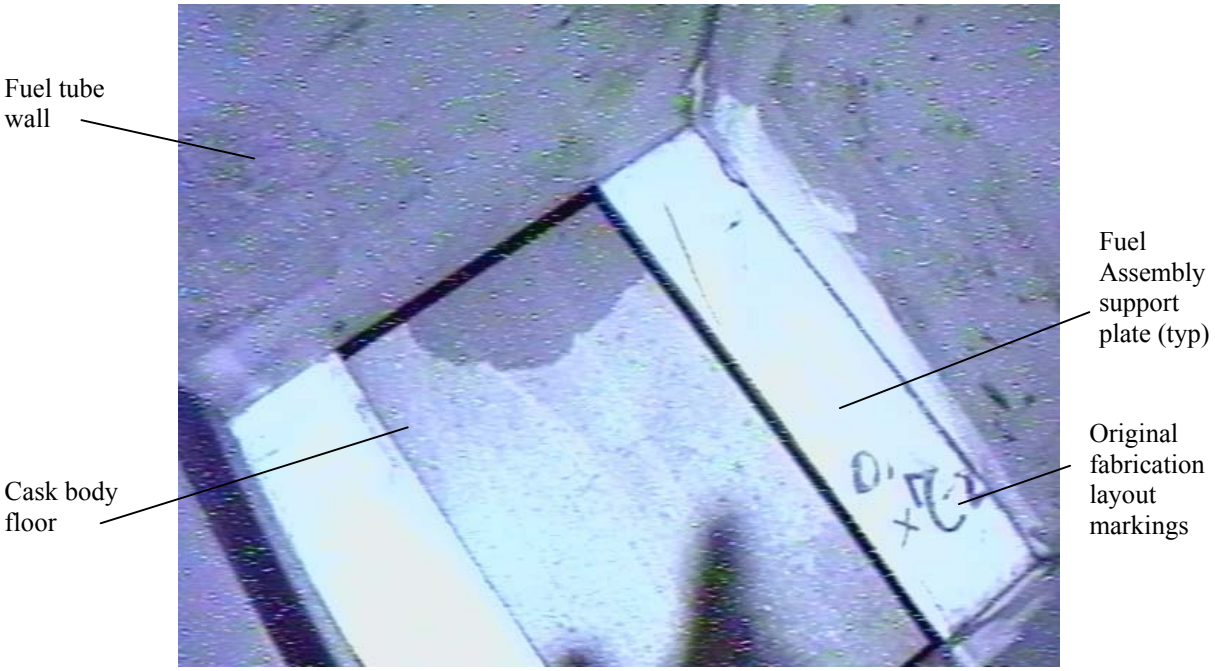

Figure D-3. Fuel tube A-7 – closeup of bottom – noted stain – no conclusion – surfaces are clean and bright. This view approximates condition viewed at the bottom of all fuel tubes.

Figure D-4. Fuel tube A-5 bottom – Noted typical absence of quantities of loose material.

Figure D-5. Fuel tube A-6 bottom.

Figure D-6. Fuel tube A-3 bottom – Surfaces clean and bright.

Figure D-7. Looking down fuel tube B-5.

Figure D-8. Fuel tube B-5 – bottom.

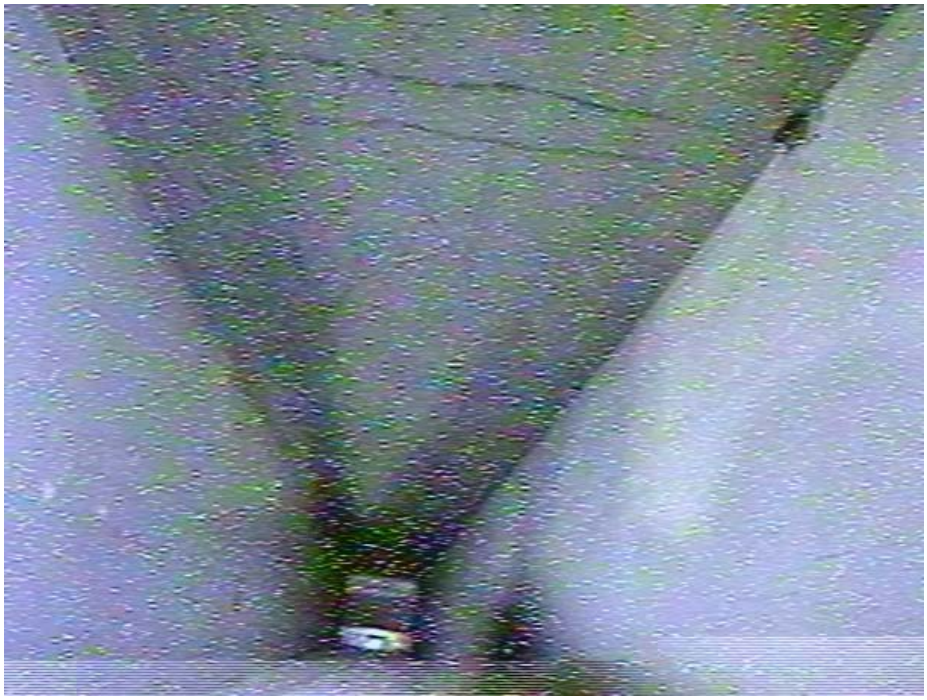

Figure D-9. Fuel Tube B-6.

Figure D-10. Fuel tube B-8 bottom.

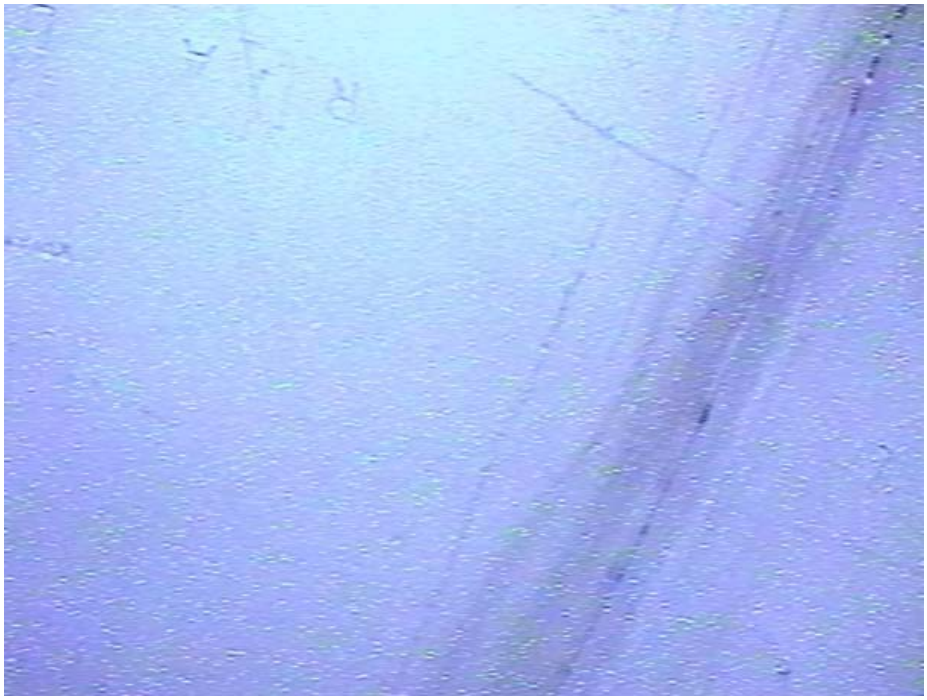

Figure D-11. Inside fuel tube D-5 at the midway of the tube. View as typical of all fuel tubes.

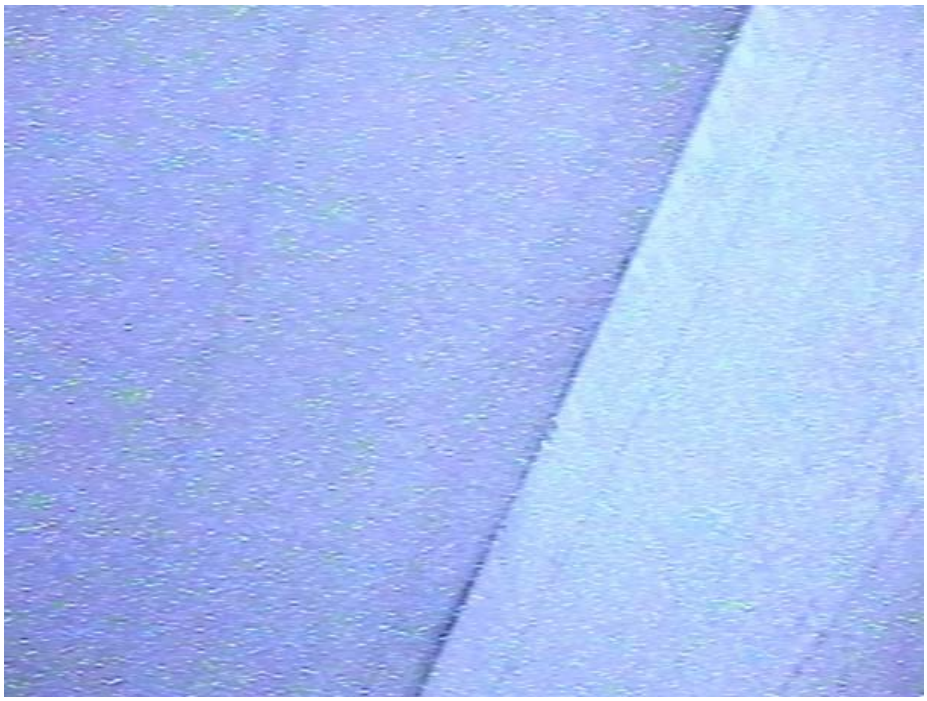

Figure D-12. Midway inside fuel tube D-6.

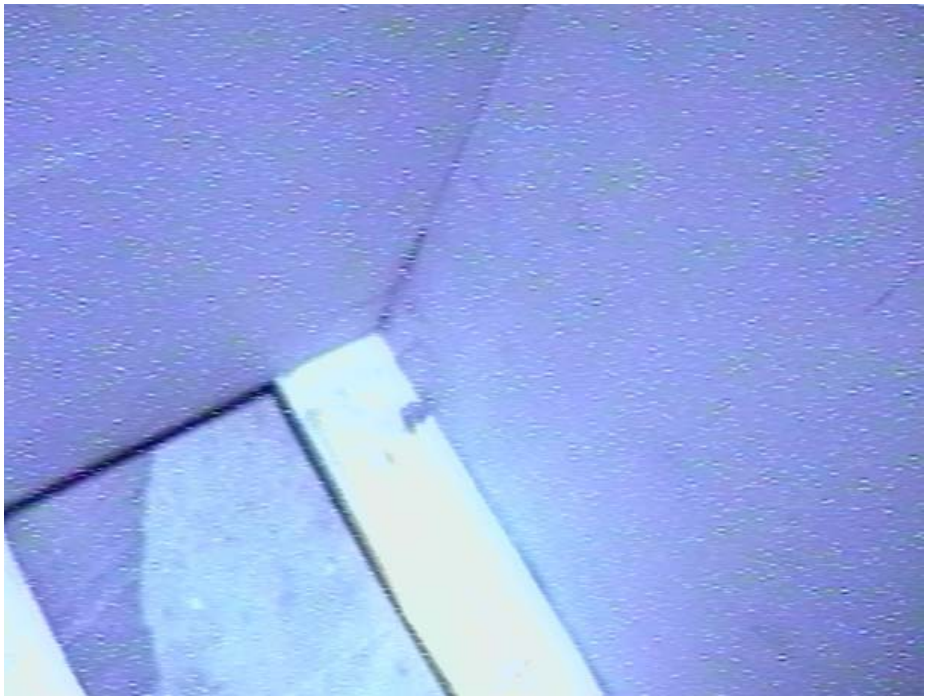

Figure D-13. Fuel tube D-8 – bottom.

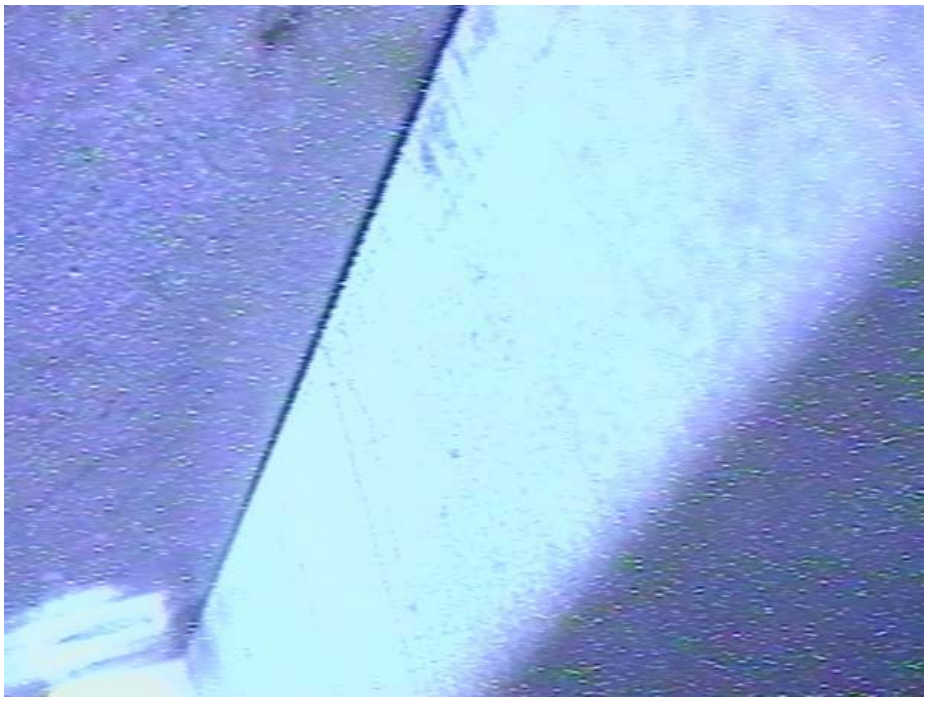

Figure D-14. Fuel tube B-4.

Figure D-15. Fuel tube A-4 bottom.

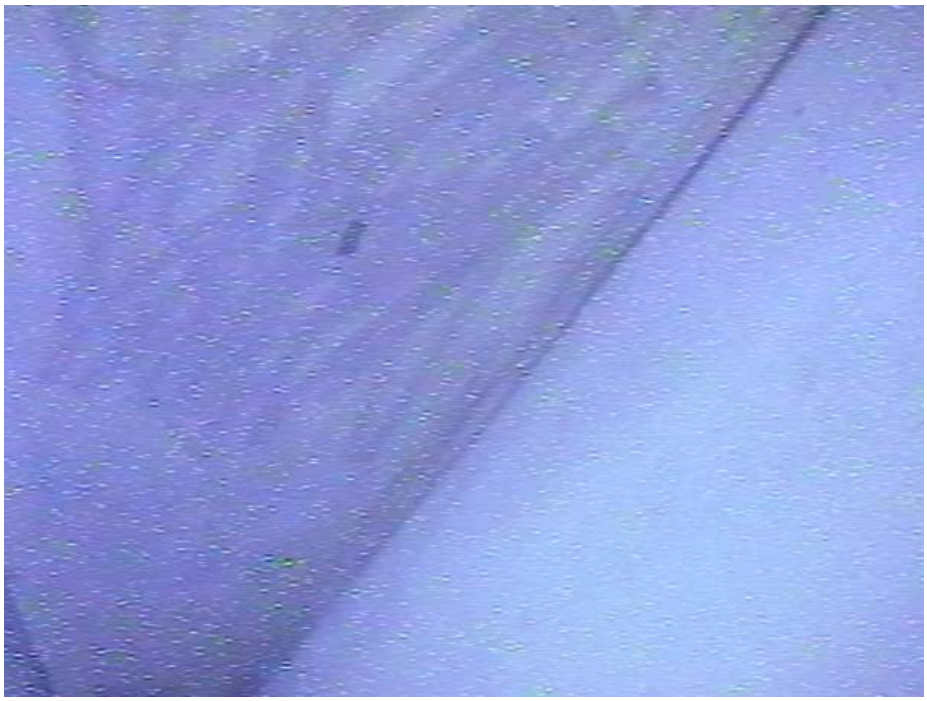

Figure D-16. Fuel tube C-6.

Figure D-17. Fuel tube C-6 – Appeared quite clean.

Figure D-18. Fuel tube D-3 bottom.

Figure D-19. Fuel tube D-2 bottom.

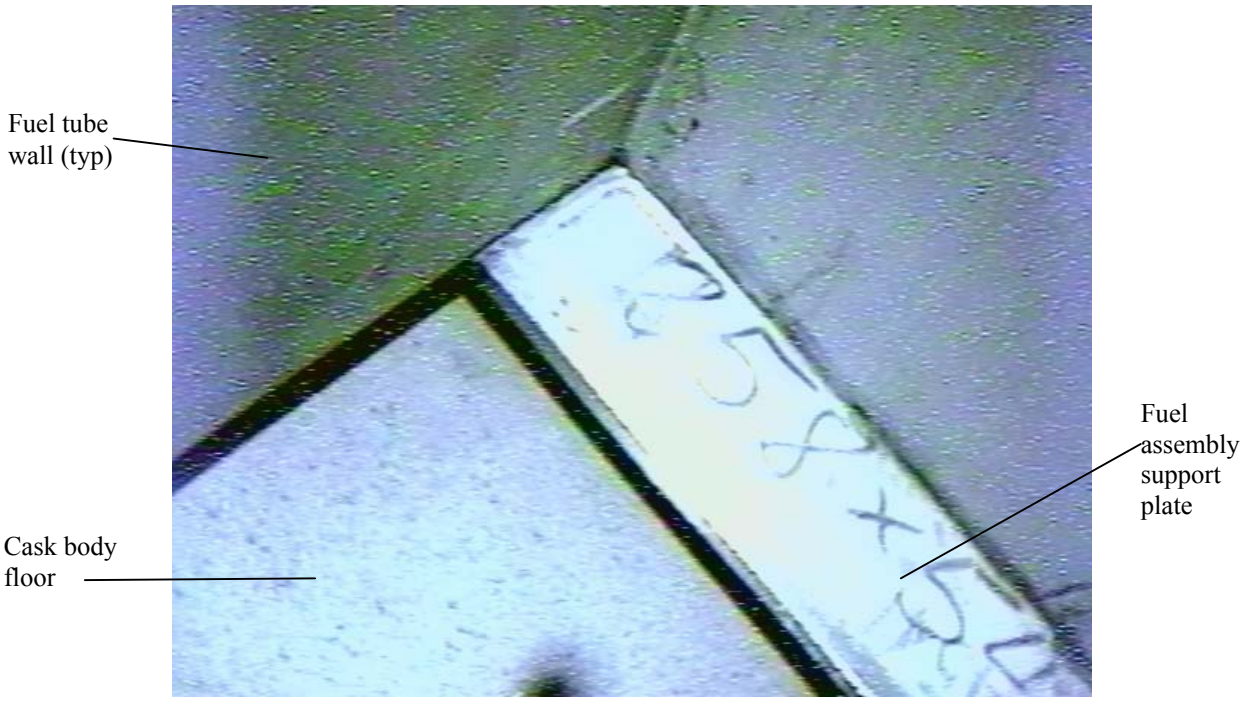

Figure D-20. Fuel tube C-5 reflective surfaces and existence of original fabrication/layout characters.

Figure D-21. Fuel tube C-8, bottom.

Figure D-22. Fuel tube B-7 – near top – showing side plates and basket wall.

Figure D-23. Fuel tube E-7, bottom.

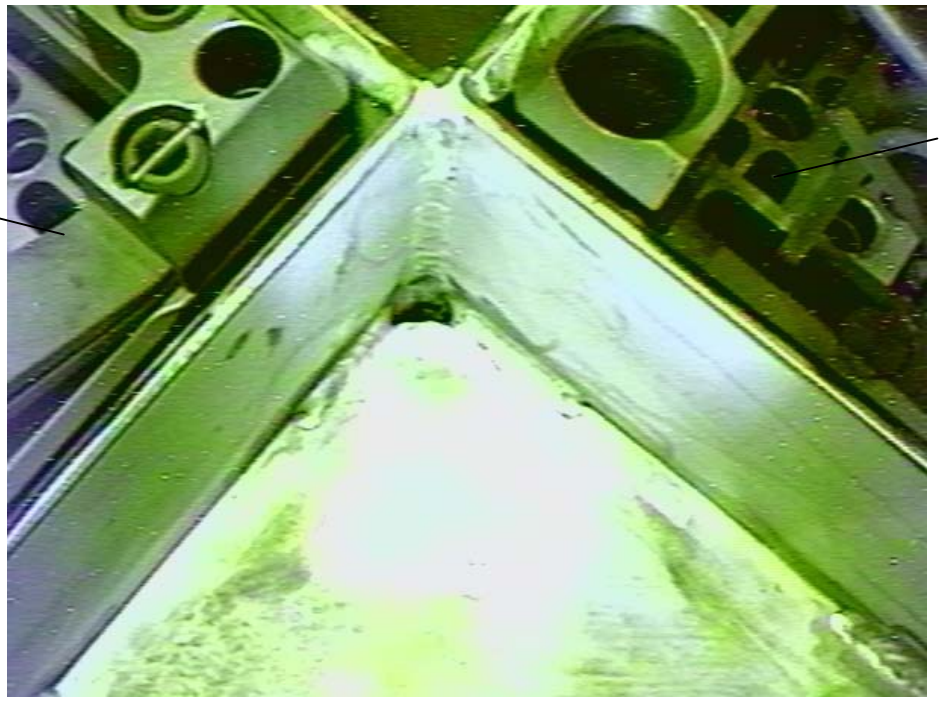

Figure D-24. Tube reinforcement plate and associated welds between A-5, A-6, and A-8.

Figure D-25. Top of fuel tube A-2.

Appendix E

Hot Cell Operation and Removal of Fuel Rods from Fuel Assembly T11

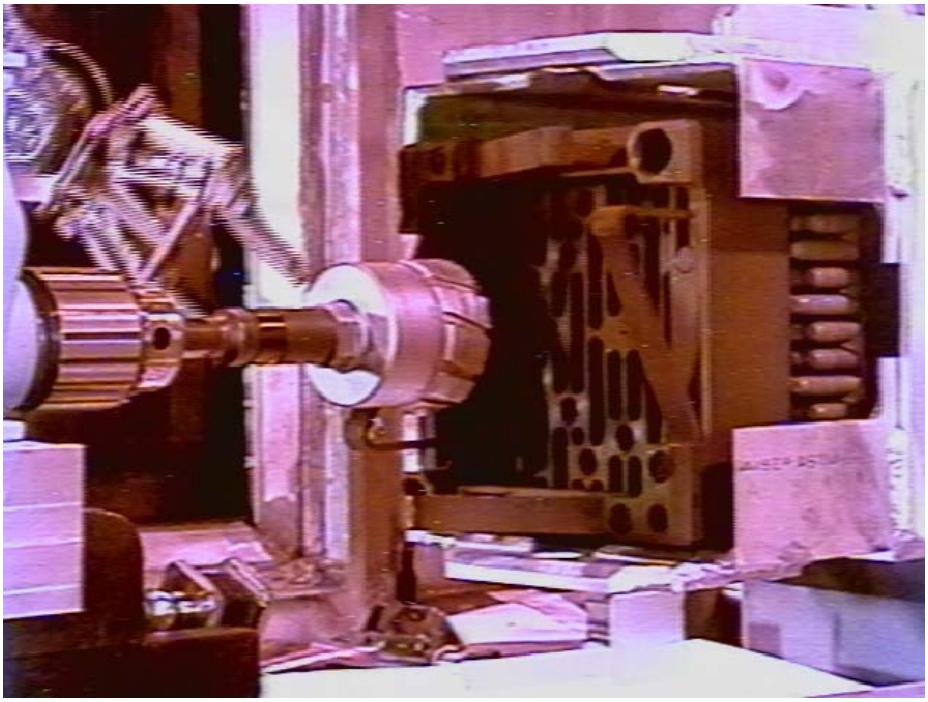

Figure E-1. Fuel assembly and nozzle cutter.

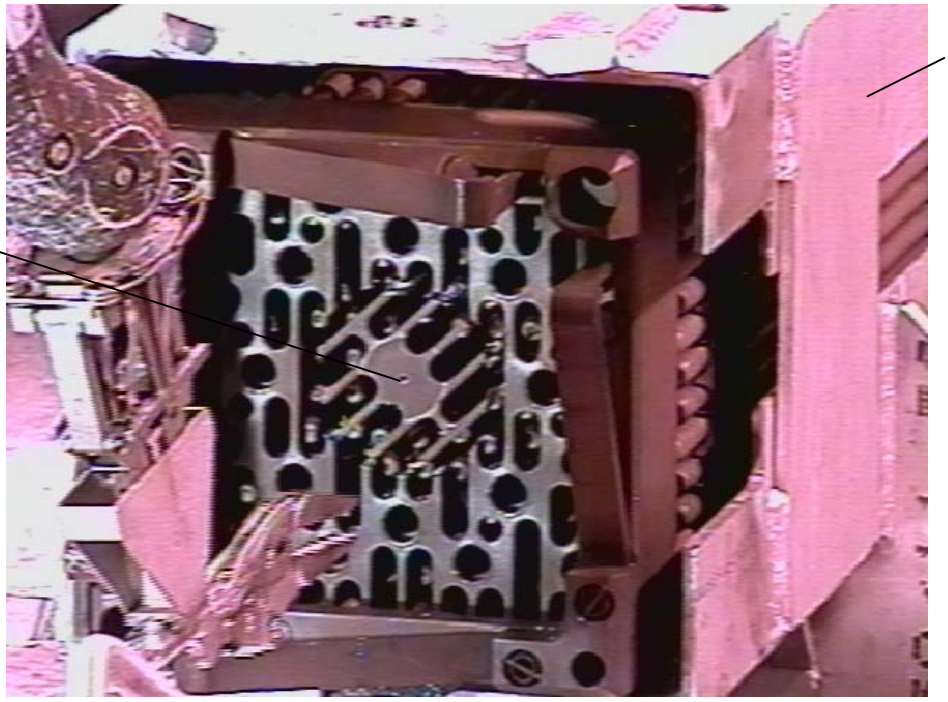

Figure E-2. Fuel assembly T-11—after cutting a 3-inch dia. hole in top nozzle to access rods.

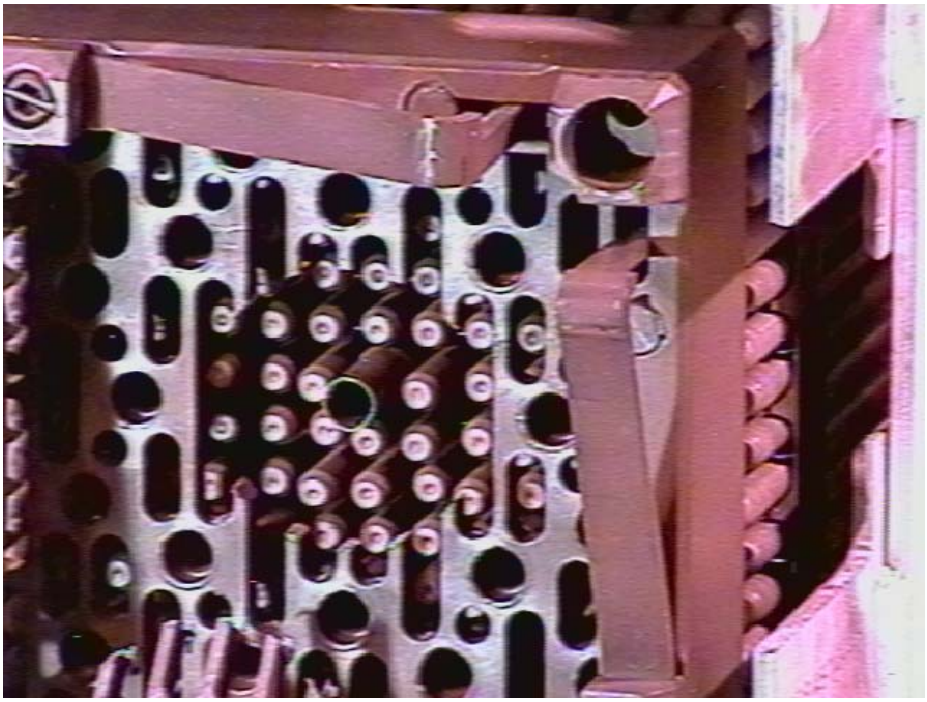

Figure E-3. Fuel assembly T-11—ready to pull fuel rods.

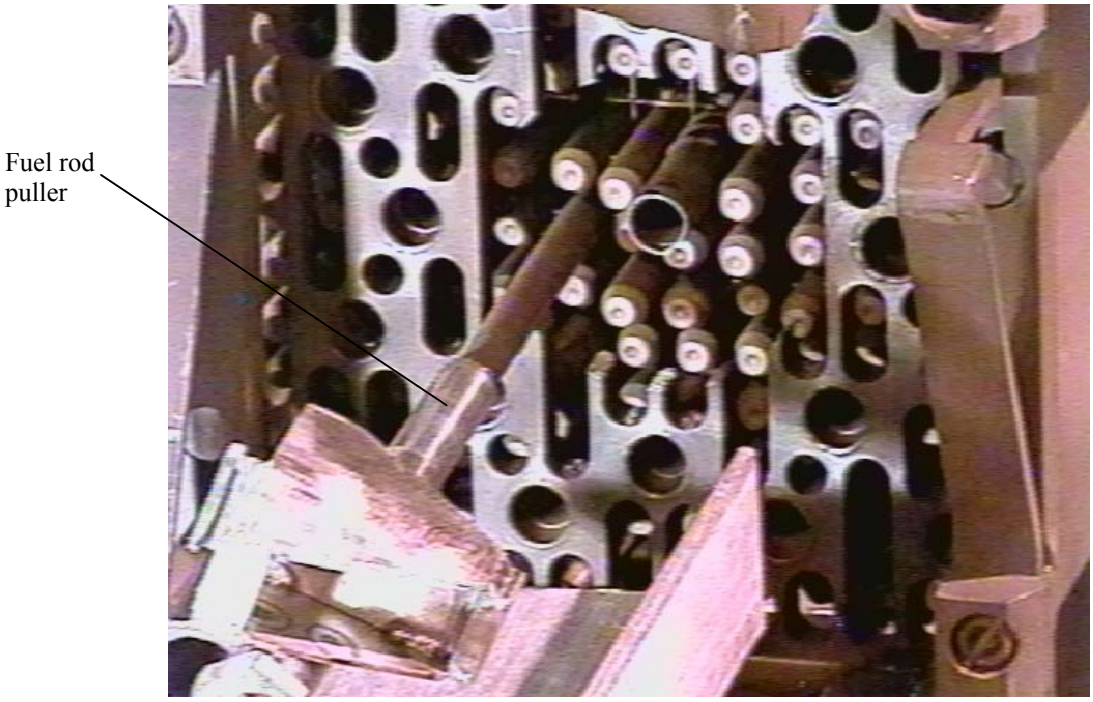

Figure E-4. Fuel rod being pulled from fuel assembly T-11.

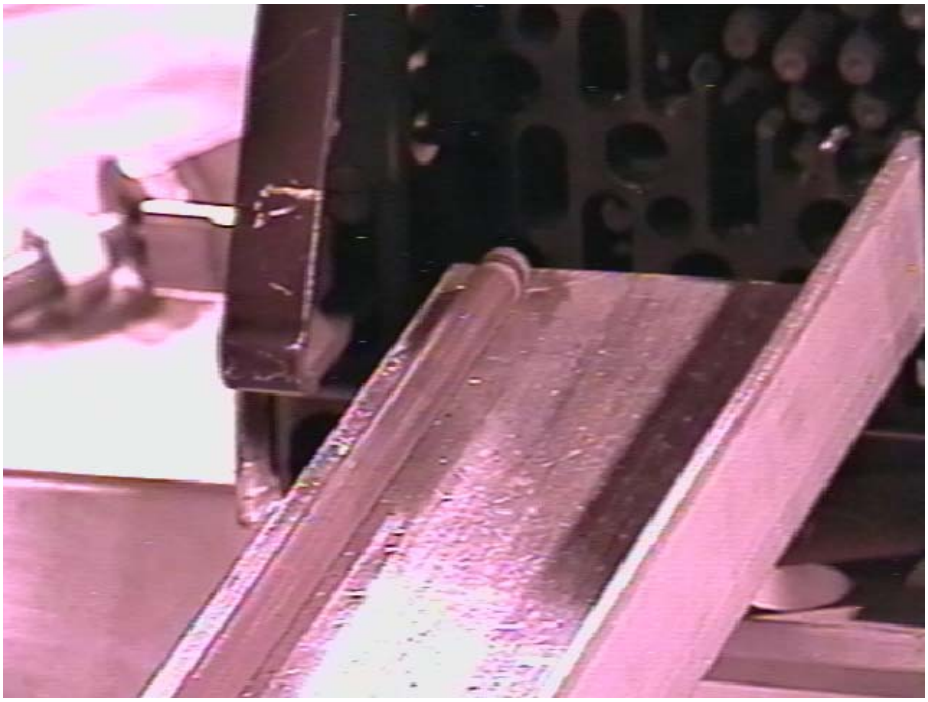

Figure E-5. Fuel rod pulled into inspection tray.

Figure E-6. Oxide mottling on fuel rod.

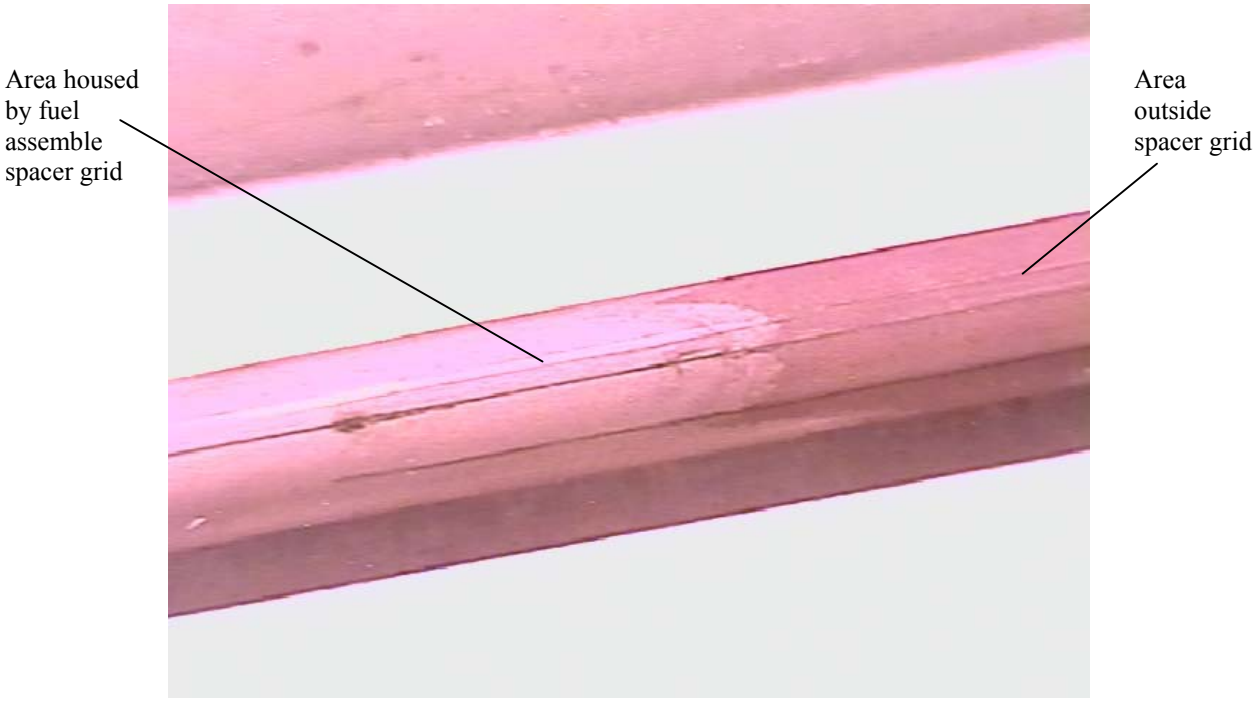

Figure E-7. Condition of fuel rod—light oxide coating minor—scratches believed from moving rod through spacer grids.

Figure E-8. End of fuel rod.

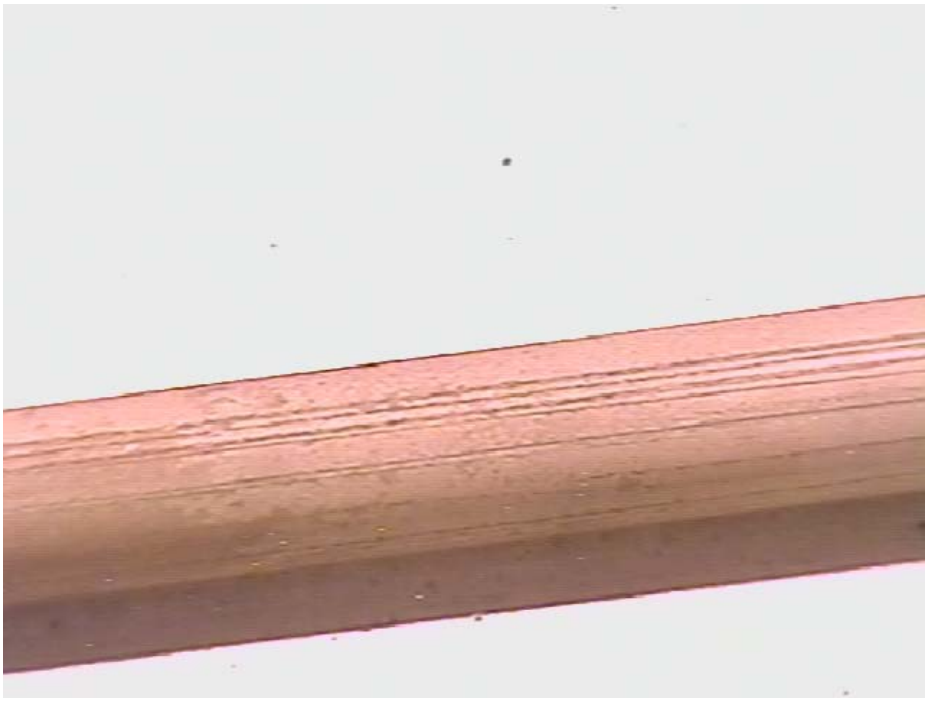

Figure E-9. Fuel rod-linear scratches believed from moving rod through spacer grid plates.

Figure E-10. Fuel rod with linear scratch.

Figure E-11. Fuel rod with linear scratch.

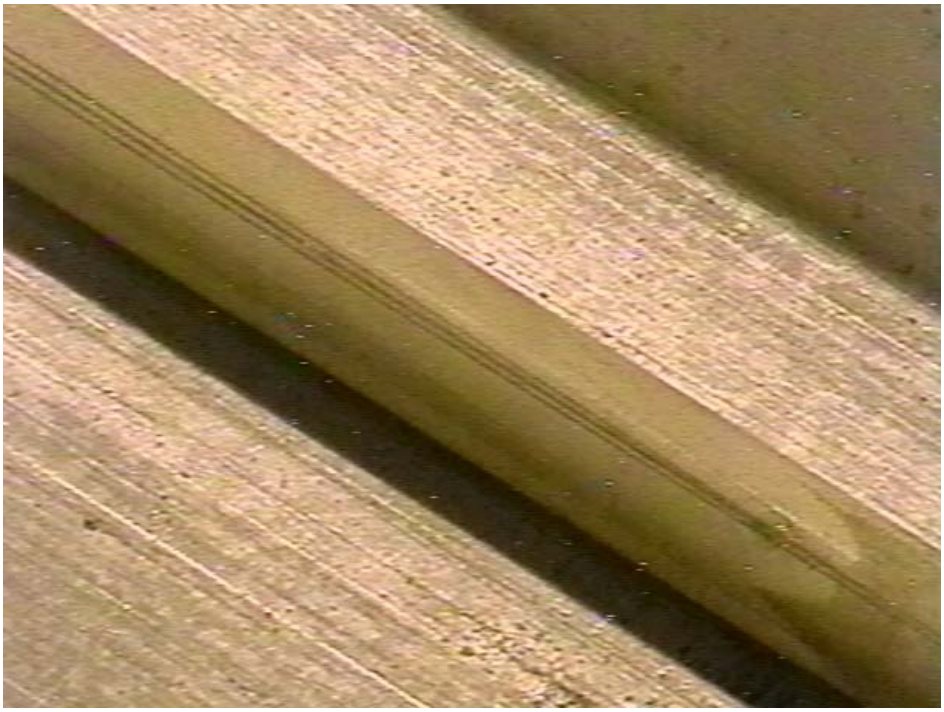

Figure E-12. Fuel rod with linear scratch.

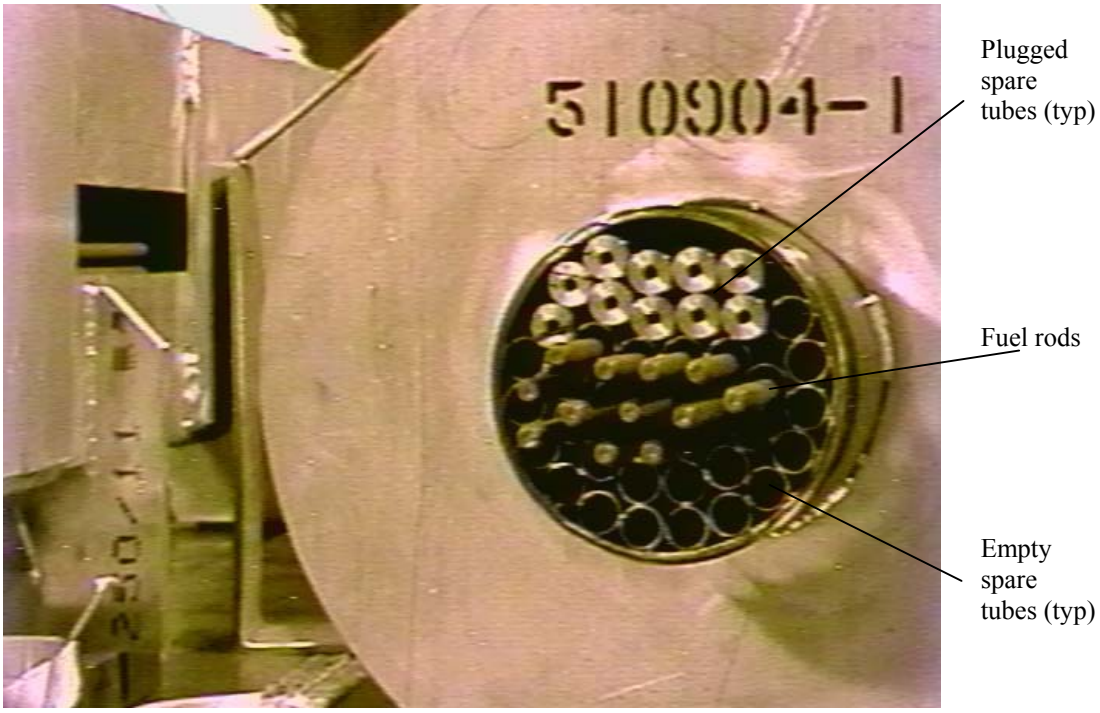

Figure E-13. FSV cask interface shipping tube with the 12 fuel rods.

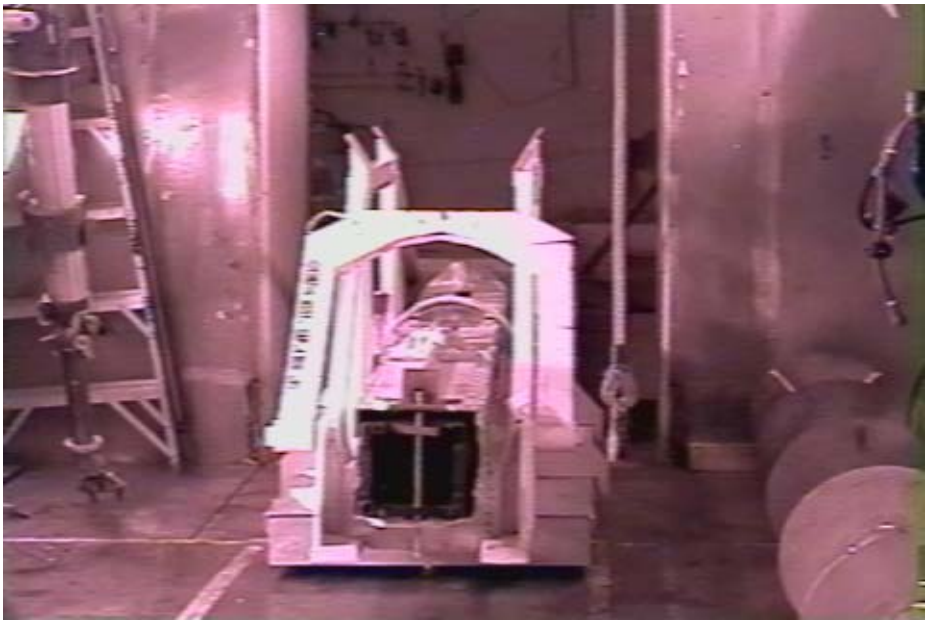

Figure E-14. Fuel assembly being moved from the hot shop into the hot cell.

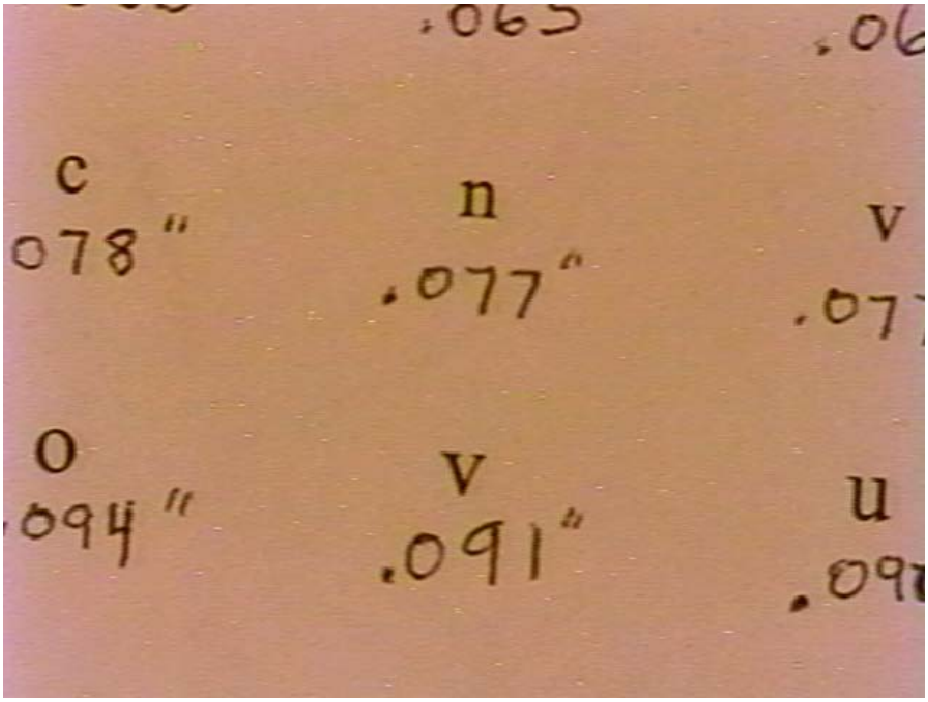

Figure E-15. Camera Resolution Test showing letter size.

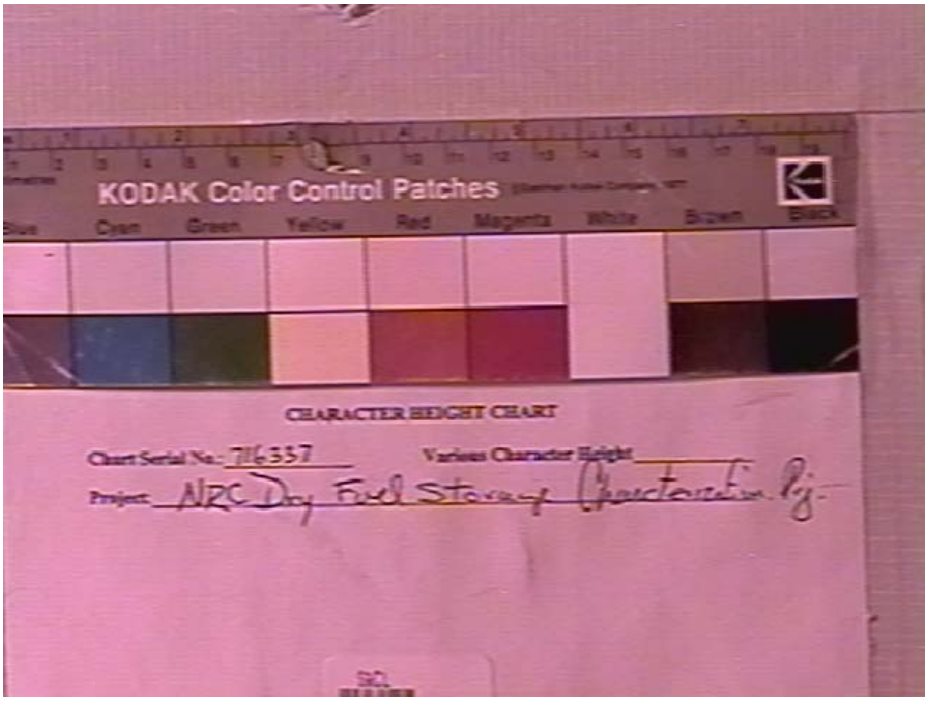

Figure E-16. Typical camera color check.

Appendix F

Cask Interior Wall and Floor

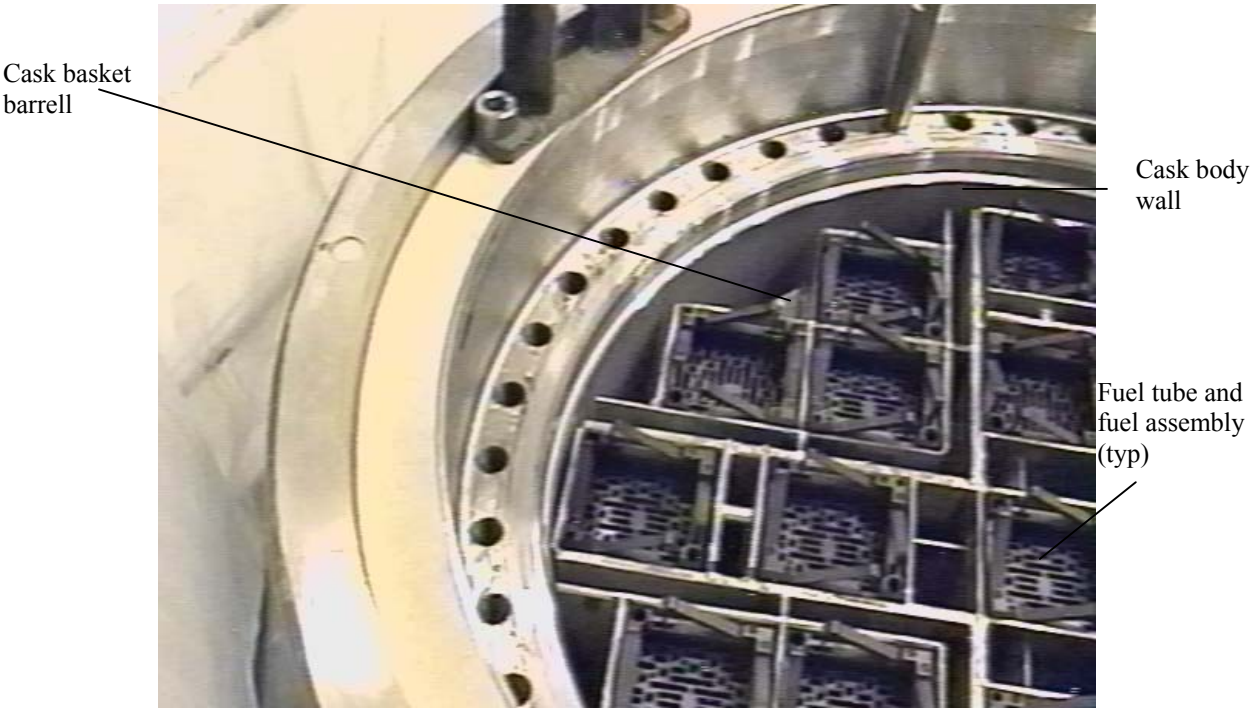

Figure F-1. Castor V/21 configuration with primary lid removed.

Figure F-2. Cask inner wall at top—typical surface condition.

Figure F-3. Cask floor and wall below fuel tube B7.

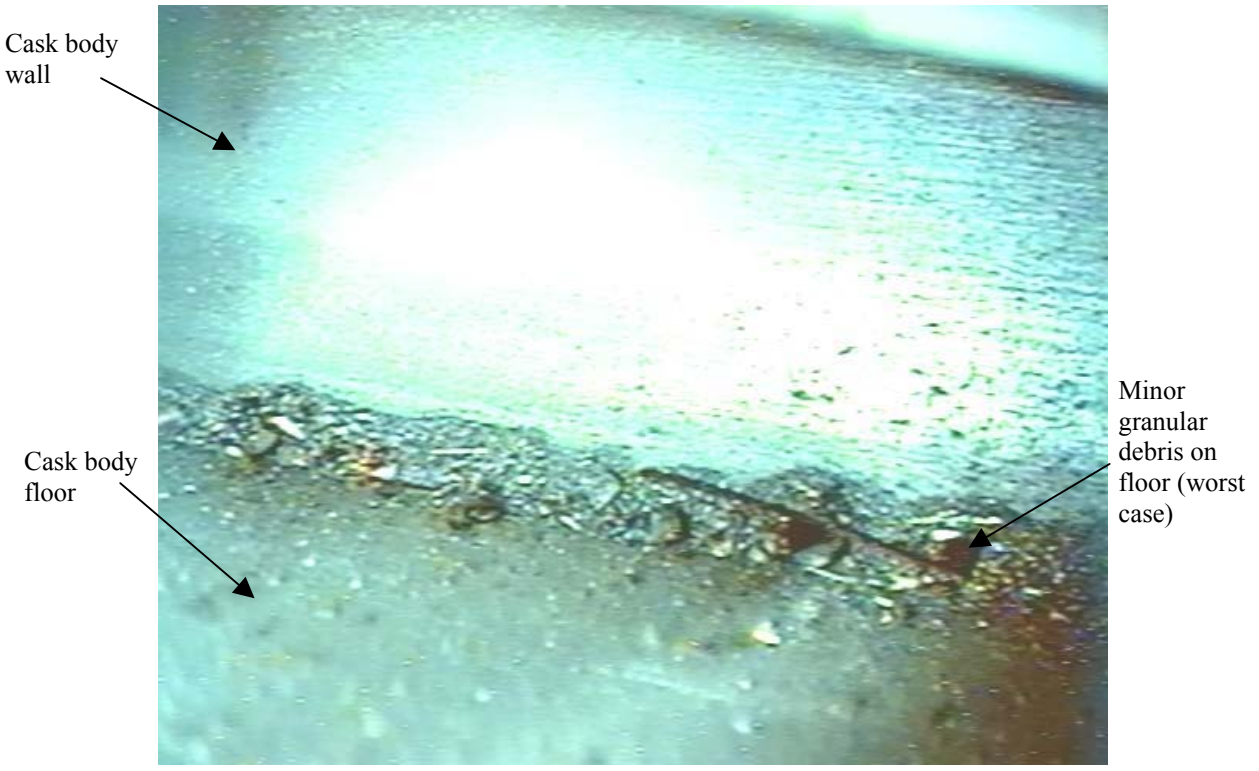

Figure F-4. Cask floor and wall below fuel tube C8—reflective surfaces free of corrosion.

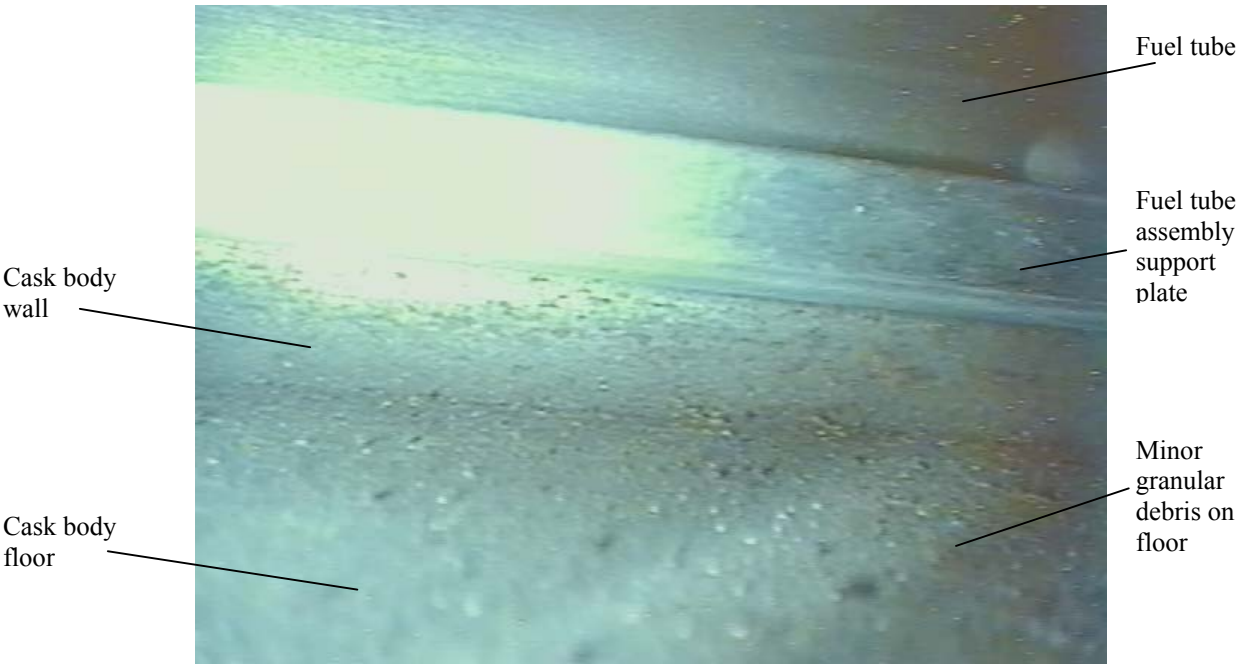

Figure F-5. Cask floor and wall below fuel tube D3—reflective surfaces free of corrosion.

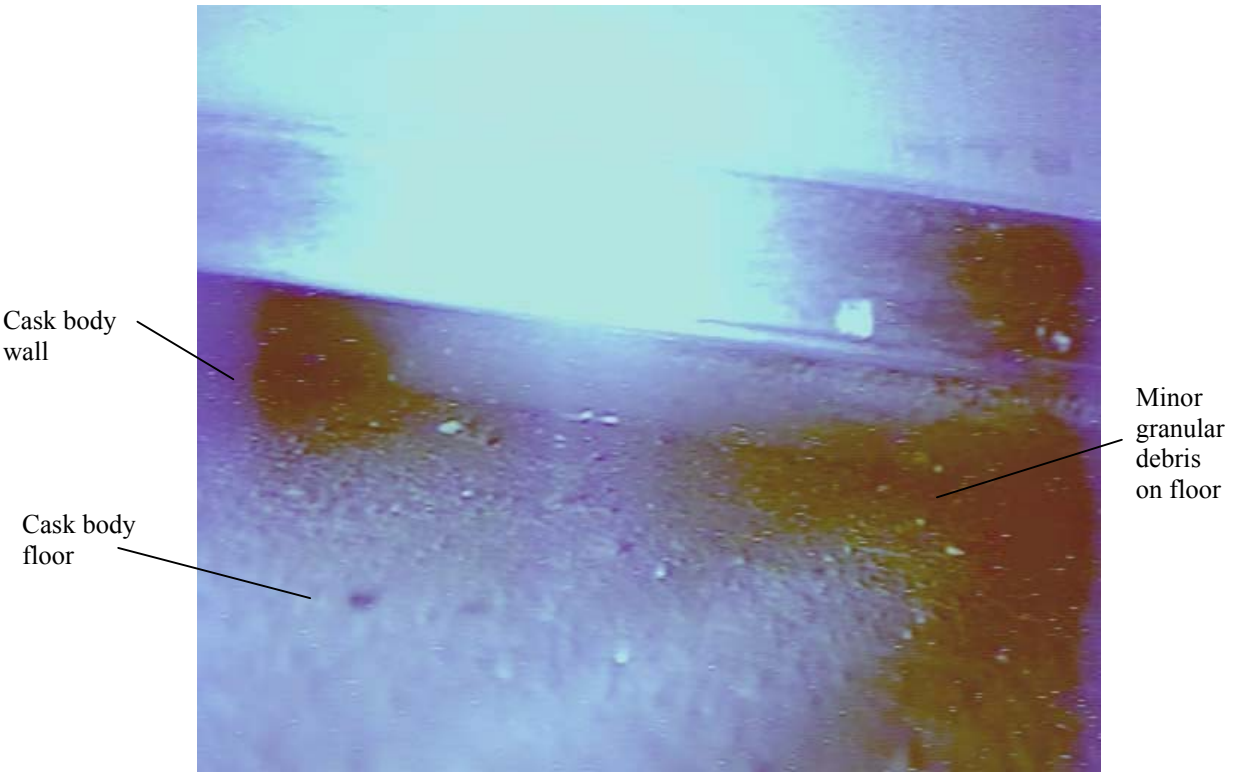

Figure F-6. Cask floor and wall below fuel tube D6—reflective surfaces free of corrosion.

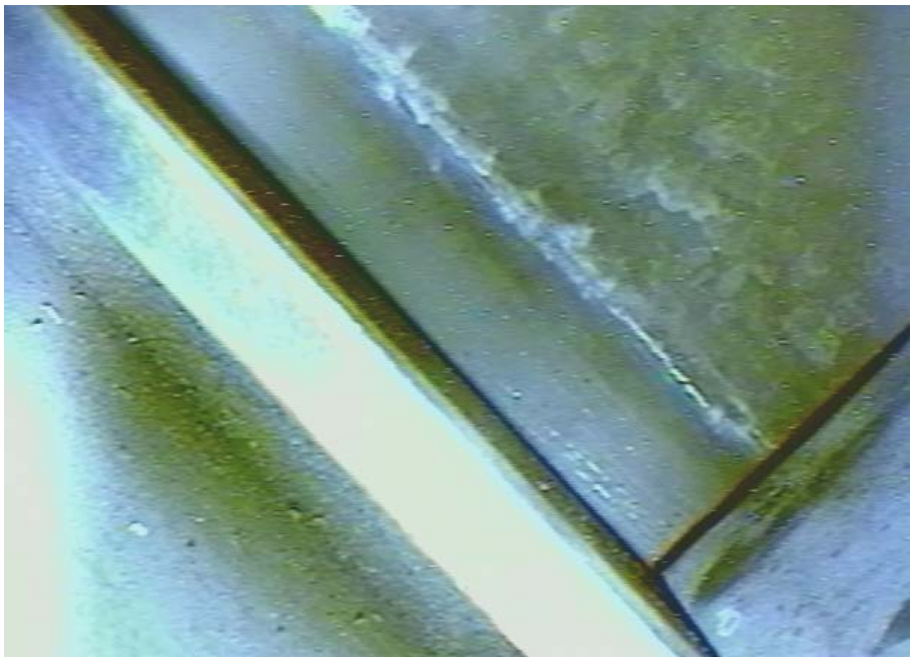

Figure F-7. Cask floor and wall below fuel tube A7—reflective surfaces free of corrosion—minor granular debris on floor.

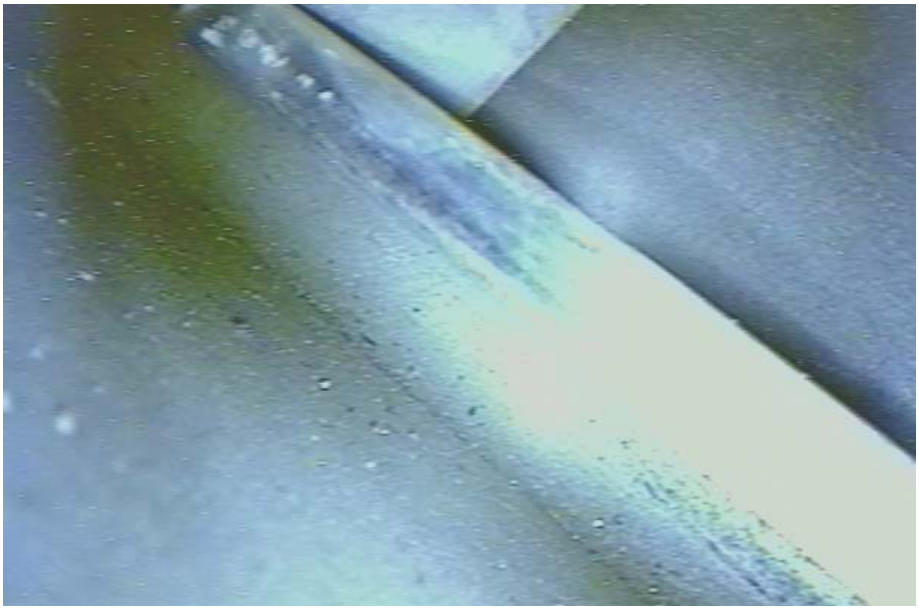

Figure F-8. Cask floor below fuel tube A3—reflective surfaces free of corrosion—minor granular debris on floor.

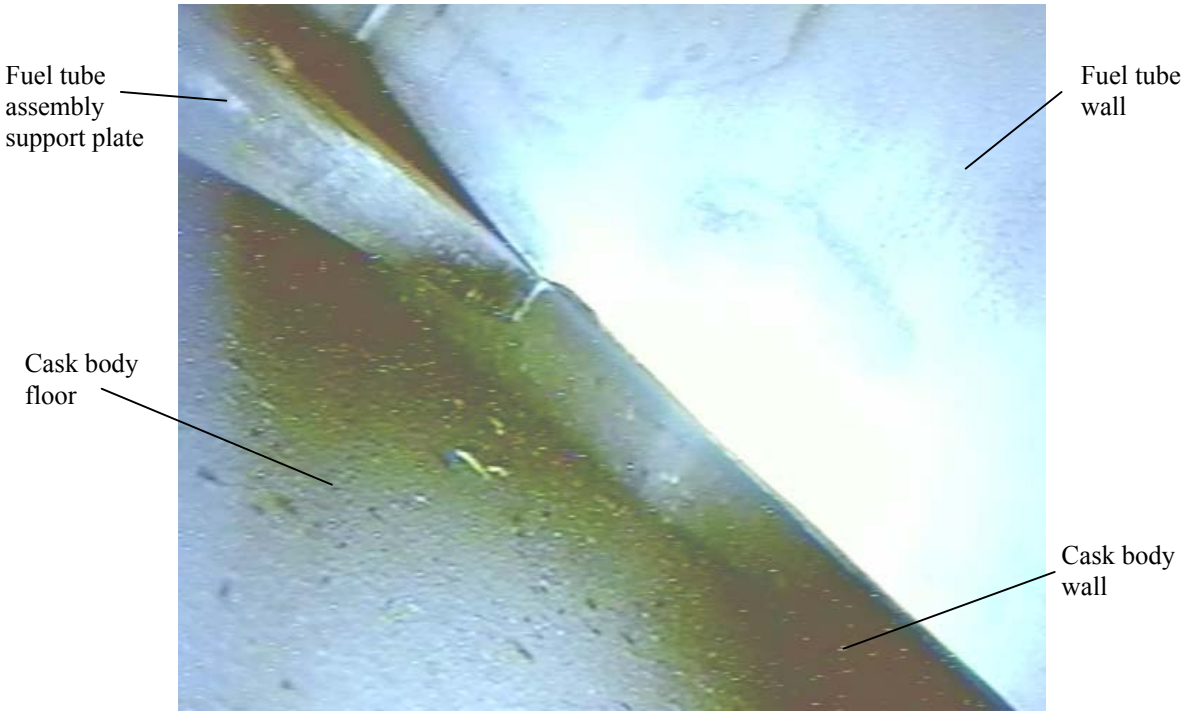

Figure F-9. Cask floor below fuel tube B6—reflective surfaces free of corrosion—minor granular debris on floor.

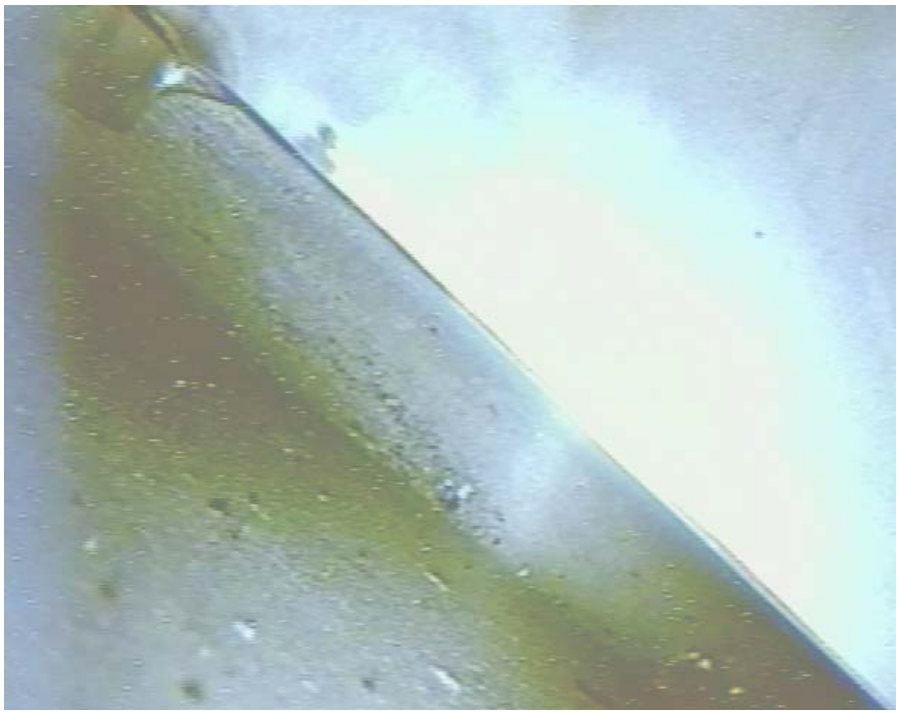

Figure F-10. Cask floor below fuel tube B8—reflective surfaces free of corrosion—minor granular debris on floor.

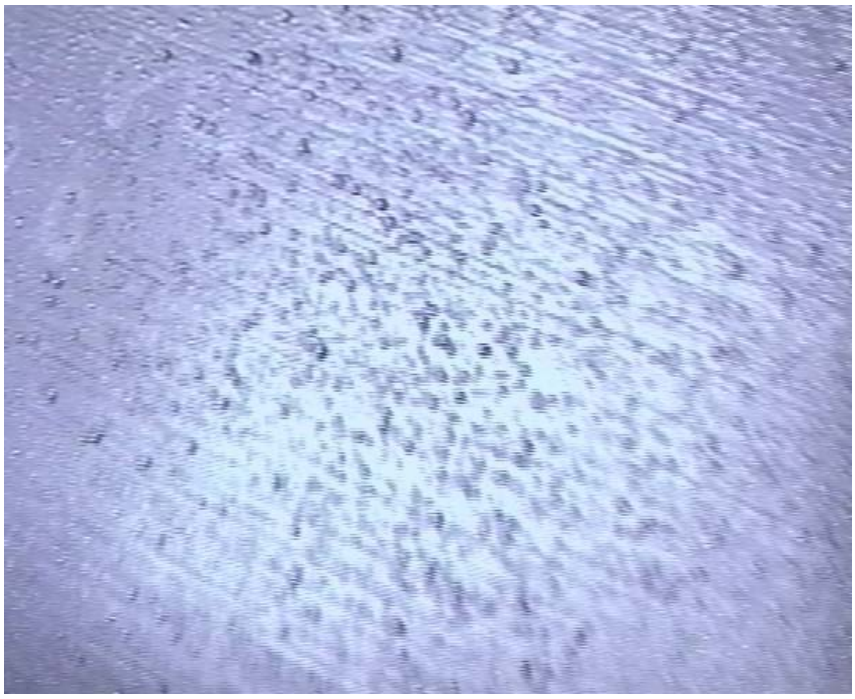

Figure F-11. Cask wall below and between fuel tubeA7 and A8—reflective surface free of corrosion–typical of cask wall condition without mineral stains- nodular ductile cast iron nickel plated.

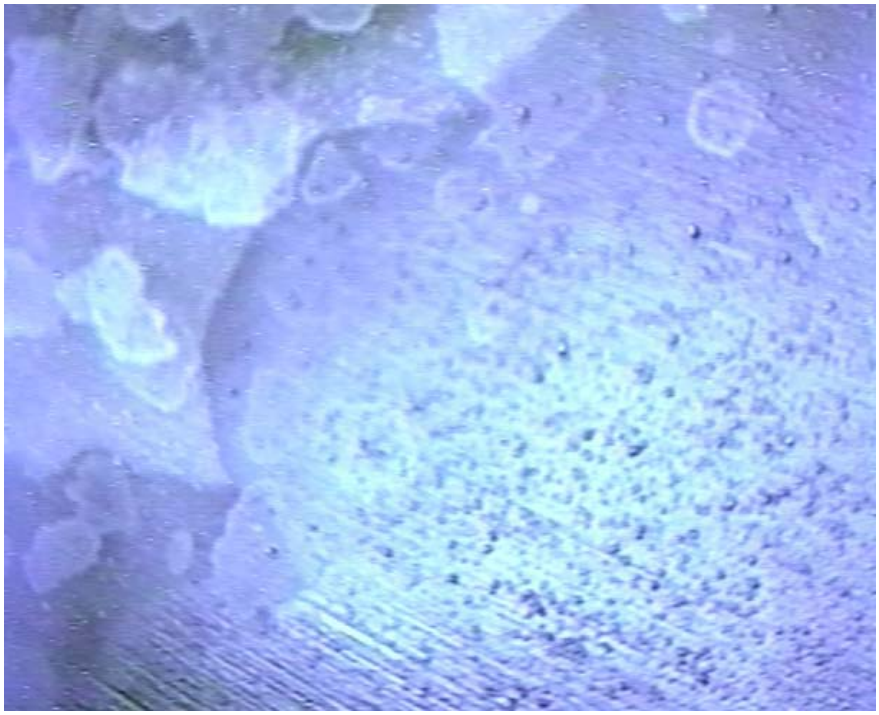

Figure F-12. Cask wall below and between fuel tubeD3 and D6—reflective surface free of corrosion—typical of cask wall condition with mineral stains—nodular ductile cast iron nickel plated.

Appendix G

Condition of Existing Cracked Welds Identified in 1985

Figure G-1. Existing 1985 weld crack at location No. 1 identified in Figure G-9.

Figure G-2. Existing 1985 weld crack at location No. 2 identified in Figure G-9.

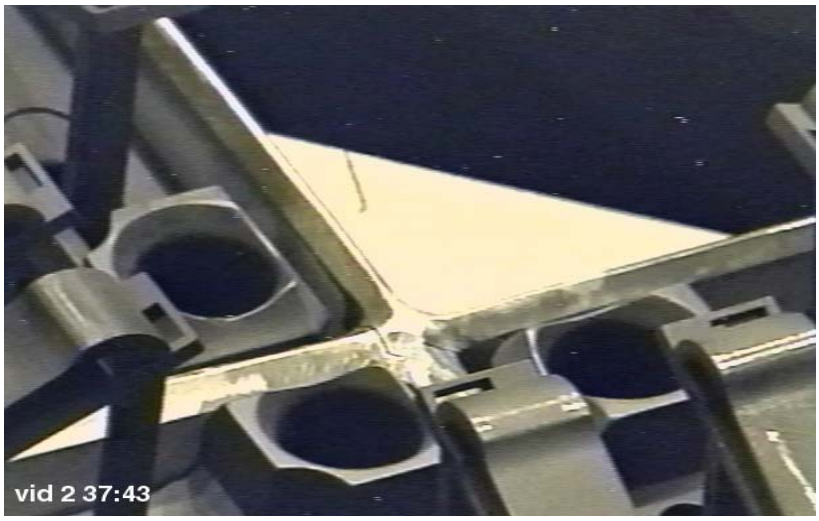

Figure G-3. Existing 1985 weld crack at location No. 3 identified in Figure G-9.

Figure G-4. Existing 1985 weld crack at location No. 4 identified in Figure G-9.

Figure G-5. Existing 1985 weld crack at location No. 5 identified in Figure G-9.

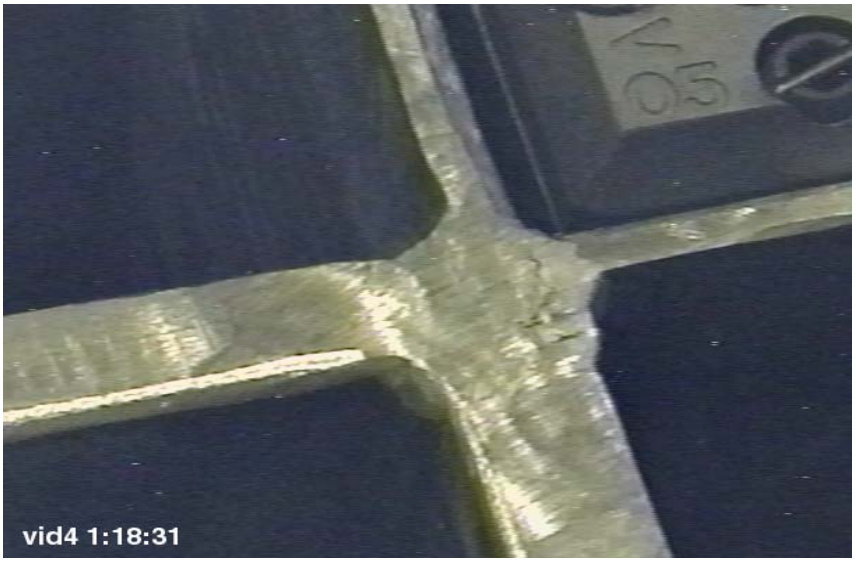

Figure G-6. Existing 1985 weld crack at location No. 6 identified in Figure G-9.

Figure G-7. Existing 1985 weld crack at location No. 7 identified in Figure G-9.

Figure G-8. Existing 1985 weld crack at location No. 8 identified in Figure G-9.

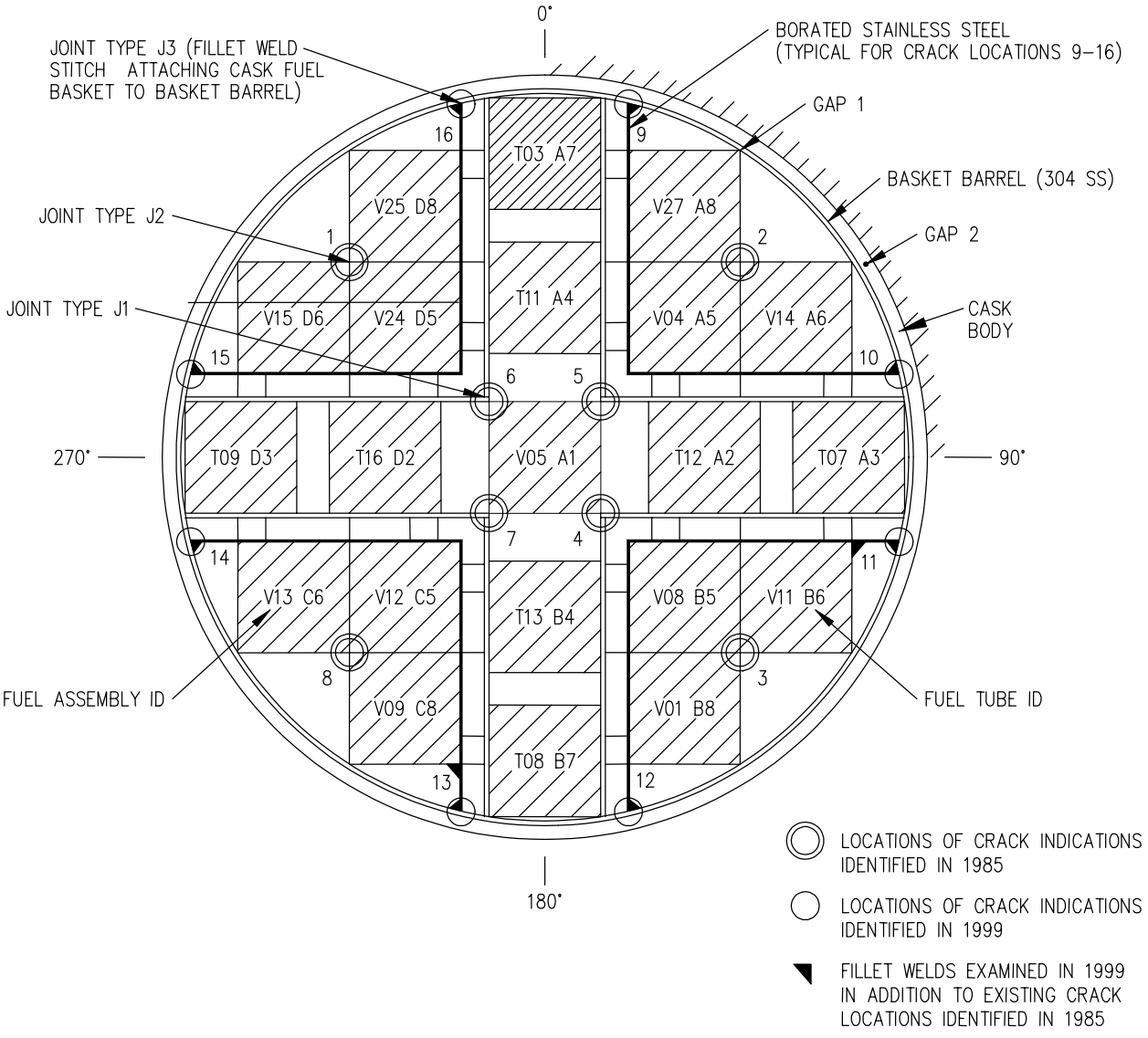

Figure G-9. Castor V/21 basket crack indication location.

Appendix H

Castor V/21 Cask Side Radiation Survey Locations

Appendix H
Castor V/21 Cask Side Radiation Survey Locations

Elevation[a] mm	0°	30°	45°	60°	75°	90°	105°	120°	150°	180°	210°	240°	270°	300°	330°
4886 (192.36")															
[3.39"]															
4800 (188.97")			!			!									
[1.97"]															
4750 (187.00")			!			!									
[1.97"]															
4700 (185.03")			!			!									
[1.96"]															
4650 (183.07")			!			!									
[1.97"]															
4600 (181.10")			!			!									
[1.97"]															
4550 (179.13")			!			!									
[1.97"]															
4500 (177.16")			!			!									
[1.97"]															
4450 (175.19")			!			!									
[1.97"]															
4400 (173.22")	O	O	!	O		!		O	O	O	O	O	O	O	O
[1.97"]															
4350 (171.25")			!			!									
[2.04"]															
4298 (169.21")	O	O	O	O		O		O	O	O	O	O	O	O	O
[7.79"]															
4100 (161.41")			O			O									
[9.84"]															
3850 (151.57")			!			!									
[18.9"]															
3370 (132.67")			O			O									
[2.83"]															
3298 (129.84")			!			!									
[23.5"]															
2701 (106.33")	O	O	!	!	!	!	!	!	O	O	O	O	O	O	O
[10.1"]															
2443 (96.18")			O			O									
[11.5"]															
2149 (84.6")			!			!									
[21.7"]															
1597 (62.8")			!			!									
[21.6"]															
1048 (41.25")			!			!									
[22.4"]															
480 (18.8")			!			!									
[12.0"]															
175 (6.8")			!			!									

[a]Elevation from exterior bottom of cask
! 1985 Radiation survey locations taken on exterior side of cask
O Radiation survey locations to be taken in addition to 1985 locations on exterior side of cask
(--) Inches
[--] Inches between elevation points

WCB 12/00